

# **Lactate and Glucose-Responsive Nanoparticles by Reversible Addition-Fragmentation Chain Transfer (RAFT) Polymerizations**

Harpal Singh Dhiraj

*A thesis submitted in partial fulfilment of the requirements of Kingston  
University for the degree of Doctor of Philosophy*

The logo for Kingston University London, featuring the text "Kingston University London" in white on a black rectangular background.

**Kingston  
University**  
London

Faculty of Science, Engineering and Computing

June 2022

## Table of Contents

<b><i>Declaration.....</i></b>	<b><i>vi</i></b>
<b><i>Abstract.....</i></b>	<b><i>vii</i></b>
<b><i>Acknowledgements.....</i></b>	<b><i>viii</i></b>
<b><i>Abbreviations.....</i></b>	<b><i>ix</i></b>

### **Chapter 1: General Introduction**

<b>1.0 Introduction</b>	<i>page 1</i>
<b>1.1 Diabetes</b>	<i>page 1</i>
<b>1.2 Boronic Acid (BA) and Glucose Chemistry</b>	<i>page 2</i>
<b>1.3 Reversible Deactivation Radical Polymerization (RDRP)</b>	<i>page 6</i>
<b>1.4 Lactic Acid Chemistry and Binding to Boronic Acid (BA)</b>	<i>page 24</i>
<b>1.5 Overall Thesis Aims and Objectives</b>	<i>page 28</i>

### **Chapter 2: Synthesis and RAFT-mediated Polymerization of Boronic Acid and Pinacol Ester Substituted Derivative Monomers using DMP and AIBN**

<b>2.0 Introduction</b>	<i>page 30</i>
<b>2.1 Chapter Aims and Objectives</b>	<i>page 30</i>
<b>2.2 Experimental</b>	<i>page 31</i>
<b>2.2.1 Materials</b>	<i>page 31</i>
<b>2.2.2 Instruments and Measurements</b>	<i>page 32</i>
<b>2.2.3 Preparation of Boronic Acid-Substituted Phenylacrylamides</b>	<i>page 33</i>
<b>2.2.4 Polymerization Procedures</b>	<i>page 42</i>
<b>2.3 Results and Discussion</b>	<i>page 43</i>
<b>2.3.1 Synthesis of Monomers</b>	<i>page 43</i>
<b>2.3.2 RAFT Polymerizations</b>	<i>page 43</i>
<b>2.4 Conclusions and Future Work</b>	<i>page 52</i>

### **Chapter 3: RAFT Dispersion Polymerization Induced Self-Assembly (PISA) Of Boronic Acid-Substituted Acrylamides**

<b>3.1 Introduction</b>	<i>page 53</i>
<b>3.1.1 Heterogeneous Radical Polymerizations</b>	<i>page 53</i>
<b>3.1.2 Polymerization Induced Self-Assembly (PISA)</b>	<i>page 53</i>
<b>3.1.2.1 Overview</b>	<i>page 53</i>
<b>3.1.2.2 Heterogeneous RAFT Polymerizations of BA-Substituted Monomers</b>	<i>page 56</i>
<b>3.2 Chapter Aims and Objectives</b>	<i>page 58</i>
<b>3.3 Experimental</b>	<i>page 59</i>
<b>3.3.1 Materials</b>	<i>page 59</i>
<b>3.3.2 Instrumentation</b>	<i>page 59</i>
<b>3.3.3 Polymerization Procedures</b>	<i>page 59</i>
<b>3.4 Results and Discussion</b>	<i>page 62</i>
<b>3.4.1 Preparation of MacroRAFT Stabilizers</b>	<i>page 62</i>
<b>3.4.2 Solubility studies</b>	<i>page 65</i>
<b>3.4.3 Dispersion Polymerization of 3-BAPhA using Poly(DMA)<sub>28</sub></b>	<i>page 66</i>
<b>3.4.4 Dispersion Polymerization of 3-BAPhA using Poly(DMA)<sub>96</sub></b>	<i>page 68</i>
<b>3.4.5 Dispersion Polymerization of 3-BAEPH A using Poly(DMA)<sub>96</sub></b>	<i>page 73</i>
<b>3.4.6 Dispersion Polymerization of 3-BAEPH A using Poly(DMA)<sub>36</sub></b>	<i>page 75</i>
<b>3.5 Conclusions and Future Work</b>	<i>page 78</i>

### **Chapter 4: Lactate and Glucose-Responsive Block Copolymer Spheres and Worms**

<b>4.1 Introduction</b>	<i>page 79</i>
<b>4.2 Chapter Aims and Objectives</b>	<i>page 81</i>
<b>4.3 Experimental part</b>	<i>page 82</i>
<b>4.3.1 Materials</b>	<i>page 82</i>
<b>4.3.2 Nuclear Magnetic Resonance (NMR) Spectroscopy</b>	<i>page 82</i>
<b>4.3.3 Determination of monomer conversion</b>	<i>page 82</i>
<b>4.3.4 Calculation of the theoretical number fraction of living chains (L)</b>	<i>page 82</i>
<b>4.3.5 Gel Permeation Chromatography (GPC)</b>	<i>page 83</i>

4.3.6 Preparation of GPC Sample (GPC)	<i>page 83</i>
4.4 General polymerization procedure	<i>page 83</i>
4.5 Results and Discussion	<i>page 88</i>
4.5.1 Synthesis of Poly(DMA) <sub>n</sub> - <i>b</i> -(3-BAPhA) <sub>m</sub>	<i>page 88</i>
4.5.2 Synthesis of TBAM-Containing Triblock Copolymers	<i>page 97</i>
4.5.3 Synthesis of Poly(TBAM) <sub>74</sub> - <i>b</i> -(3-BAPhA) <sub>49</sub> - <i>b</i> -(DMA) <sub>79</sub> -TTC	<i>page 102</i>
4.5.4 Self-Assembly	<i>page 106</i>
4.5.4.1 Self-Assembly of poly(DMA) <sub>28</sub> - <i>b</i> -(3-BAPhA) <sub>84</sub> -TTC	<i>page 106</i>
4.5.4.2 Self-Assembly of poly(DMA) <sub>96</sub> - <i>b</i> -(3-BAPhA) <sub>62</sub> -TTC	<i>page 106</i>
4.5.4.3 Self-Assembly of poly(DMA) <sub>36</sub> - <i>b</i> -(3-BAPhA) <sub>49</sub> - <i>b</i> -(TBAM) <sub>46</sub> -TTC	<i>page 107</i>
4.5.4.4 Self-Assembly of poly(TBAM) <sub>74</sub> - <i>b</i> -(3-BAPhA) <sub>49</sub> - <i>b</i> -(TBAM) <sub>79</sub> -TTC	<i>page 108</i>
4.5.5 Glucose and lactate response	<i>page 108</i>
4.5.5.1 Response of poly(DMA) <sub>28</sub> - <i>b</i> -(3-BAPhA) <sub>84</sub> -TTC	<i>page 108</i>
4.5.5.2 Response of Poly(DMA) <sub>96</sub> - <i>b</i> -(3-BAPhA) <sub>62</sub> -TTC	<i>page 110</i>
4.5.5.3 Response of poly(DMA) <sub>36</sub> - <i>b</i> -(3-BAPhA) <sub>49</sub> - <i>b</i> -(TBAM) <sub>46</sub> -TTC	<i>page 112</i>
4.5.5.4 Response of poly(TBAM) <sub>74</sub> - <i>b</i> -(3-BAPhA) <sub>49</sub> - <i>b</i> -(DMA) <sub>79</sub> -TTC	<i>page 114</i>
4.6 Conclusion	<i>page 116</i>

**Chapter 5: Lactate and Glucose-Induced Self-Assembly of Hydrophobic Boronic Acid-Substituted Polymers**

5.1 Introduction	<i>page 117</i>
5.2 Aims and Objectives	<i>page 119</i>
5.3 Experimental	<i>page 121</i>
5.4 General polymerization procedure	<i>page 124</i>
5.4.4 One-pot iterative RAFT polymerizations using VA-044	<i>page 125</i>
5.4.5 Lactate and Glucose-Induced Self-Assembly	<i>page 129</i>
5.4.6 Transmission Electron Microscopy (TEM)	<i>page 130</i>
5.5 Results and Discussion	<i>page 130</i>
5.5.1 Chain extension using AIBN to give poly(3-BAPhA) <sub>79</sub> -TTC	<i>page 130</i>
5.5.2 Polymerization of 3-BAPhA using [3-BAPhA] <sub>0</sub> /[DMP] <sub>0</sub> = 250	<i>page 131</i>



<b>5.5.3 Synthesis using one-pot iterative RAFT polymerizations</b>	<i>page 133</i>
<b>5.6 Lactate and Glucose-Induced Self-Assembly</b>	<i>page 145</i>
<b>5.6.1 Self-assembly of Poly(3-BAPhA)<sub>124</sub>-TTC</b>	<i>page 145</i>
<b>5.6.2 Self-assembly of Poly(3-BAPhA)<sub>91</sub>-<i>b</i>-(TBAM)<sub>35</sub>-TTC</b>	<i>page 146</i>
<b>5.6.3 Self-assembly of Poly(3-BAPhA)<sub>34</sub>-<i>b</i>-(PhA)<sub>131</sub>-TTC</b>	<i>page 147</i>
<b>5.7 Conclusions and Future Work</b>	<i>page 148</i>
<b>6.0 Overall Discussion/Conclusion and Future Work</b>	<i>page 149</i>
<b>7.0 Thesis References</b>	<i>page 151</i>

### **Declaration**

I declare that the work included in this thesis is my own work, except where stated otherwise, and has not been previously submitted for a degree to this or any other academic institution.

---

Harpal Singh Dhiraj

## **Abstract**

Ch. 1 is the background to preparing precision polymers using reversible addition-fragmentation chain transfer (RAFT). Ch. 2-5 describe original primary research.

## **Introduction**

Ch. 2 and 3 overview RAFT homogeneous polymerizations of 3-(acrylamidophenyl)boronic acid (3-BAPhA) and polymerization induced self-assembly (PISA) of free boronic acid (BA) substituted monomers. Ch. 4 rationalizes approaches for the synthesis of glucose and lactate responsive nanoparticles. Ch. 5 reviews the use of BA in polymer morphology transitions.

## **Methods**

Ch. 2 describes the synthesis of 3-BAPhA and its pinacol ester (3-BAEPhA) derivative, along with the *para*-analogue (4-BAEPhA) monomer and compares RAFT with *N*-phenylacrylamide (PhA). Ch. 3 describes the synthesis of poly(*N,N*-dimethylacrylamide) macroRAFT steric stabilizers and protocols for RAFT-mediated dispersion polymerizations of 3-BAPhA. Ch. 4 and 5 describe protocols for one-pot iterative RAFT polymerizations of acrylamides and dialysis approaches to self-assembly.

## **Results**

RAFT polymerizations of 3-BAPhA give similar control/living character to PhA and 3-BAEPhA with 4-BAEPhA polymerizations slower. Ch. 3 describes the first PISA on an unprotected BA-monomer with transitions to higher order morphologies upon dilution with the dispersion solvent. PISA of 3-BAEPhA gave spherical particles, worms, and vesicles. Ch. 4 shows lactate binding at pH = 7.4 leads to comparable effects on morphology to that of glucose binding at pH = 8.7. The first direct formation of pure worms for the self-assembly of free BA polymer was found. Ch. 5 describes lactate and glucose induced self-assembly of solvated hydrophobic polymers containing poly(3-BAPhA) block.

## **Conclusions**

Ch. 2 optimized the conditions for RAFT polymerization of BA-substituted acrylamides. Ch. 3 is published in *Polymer Chemistry* **2022**, *13*, 3750-3755 and achieved new smart nanoparticles, which undergo sphere-to-worm transitions upon hydrolysis of boroxine moieties. Ch. 4 and 5 establishes lactate as a stimulus for self-assembly of amphiphilic and hydrophobic polyacrylamides respectively.

## *Acknowledgements*

*“if ink were never to fail me, and if my pen were able to move like the wind*

*-even so, I could not estimate your value”*, Sri Guru Sahib Ji- Siree Raag.

Reciting your name purifies the mind and sensing your aura is essential to all my successes. Thank you Waheguru, for blessing me with your presence.

I would like to express my sincere gratitude to my First Supervisor, Prof. Fawaz Aldabbagh, for providing me with the opportunity to join his research group. I am eternally grateful for his invaluable support of my research, and relentless dedication to my personal career development.

I am thankful to Prof. Per Zetterlund and Dr Fumi Ishizuka (TEM images), co-authors of my publications, from The University of New South Wales, Australia for invaluable discussions.

Thank you to my Second Supervisor Dr. Amr Elshaer for support throughout my research.

I would like to thank Dr Daniel Keddie (Wolverhampton), Dr Stephen Barton, and Prof. Reem Kayyali for their guidance in the examination process.

I am also grateful to fellow Kingston lab-mates Matteo Zecchini, Darren Conboy, and Gilbert Ampem, for making those long days in the lab significantly more enjoyable. Thank you Siamak Soltani-Khankahdani for his technical assistance with the GPC.

Most importantly, to my wife Amarit Kaur, parents Joginder Singh, Chanchal Kaur, late Amarjit Singh and Jaspal Kaur. Without whom this journey would have not been possible, and this thesis is truly a product of your continuous love and support.

I thank Kingston University for awarding me bursaries for achieving Q1 publication and write-up.

Finally, to Drivetime School of Motoring (West London) for providing employment as a driving instructor, which funded my PhD.

## Abbreviations

$\mathcal{D}$	dispersity
BAPhA	(acrylamidophenyl)boronic acid
$a_h$	interfacial area of the solvophilic chain
$l_c$	length of the solvophobic chain
$\rho$	packing parameter
$V$	volume
ACVA	4,4'-azobis(4-cyanopentanoic acid)
AIBN	2,2'-Azobis(2-methylpropionitrile)
ADP	adenosine diphosphate
ATP	adenosine triphosphate
ATRP	atom transfer radical polymerization
$b$	block
b.p.	boiling point
BA	boronic acid
BBMA	4-pinacolboronylbzyl methacrylate
BDE	bond dissociation energy
BzMA	benzyl methacrylate
$n$ -Bu	$n$ -butyl
$C_{tr}$	chain transfer constant
CLRP	controlled/living radical polymerization
conv.	conversion
CTA	chain transfer agent
DAAM	$N$ -(1,1-Dimethyloxobutyl)acrylamide
DLS	dynamic light scattering
DMA	$N,N$ -dimethylacrylamide
DMP	2-(dodecylthiocarbonothioylthio)-2-methylpropionic acid
DMF	$N,N$ -dimethylformamide
$DP$	degree of polymerization

Et	ethyl
Ac	acyl
ESI	electronic supplementary information
$f$	initiator efficiency
$f_c$	coupling factor
GPC	gel permeation chromatography
h	hour
Hz	hertz
[I]	initiator concentration
$J_{crit}$	critical number-average degree of polymerization
$K$	equilibrium constant
$K_{act}$	rate coefficient for dissociation
$k_\beta$	rate of fragmentation coefficient
$k_d$	decomposition rate coefficient
$k_i$	initiation rate coefficient
$k_p$	propagation rate coefficient
$L$	fraction of living chains or livingness
LAMs	less activated monomers
LCST	lower critical solution temperature
$M_n$	number average molecular weight distribution
MAMs	more activated monomers
Me	methyl
MS	molecular sieves
MW	molecular weight
MWD	molecular weight distribution
NADH	nicotinamide adenine dinucleotide
NIPAM	<i>N</i> -isopropylacrylamide
nm	nano meter
NMP	nitroxide-mediated polymerization

NMR	nuclear magnetic resonance
NP	nanoparticle
Nuc: <sup>o</sup>	nucleophile
PDMS	poly(dimethylsiloxane)
PhA	<i>N</i> -phenylacrylamide
PISA	polymerization induced self-assembly
POEGMA	poly(oligo(ethylene glycol) methacrylate)
ppm	parts per million
PRE	persistent Radical Effect
PTFE	polytetrafluoroethylene
$R_p$	rate of propagation
RI	refractive index
RAFT	reversible addition-fragmentation chain transfer
RDRP	reversible deactivation radical polymerization
scCO <sub>2</sub>	supercritical carbon dioxide
SEC	size exclusion chromatography
St	styrene
$t$	time
T2DM	type 2 diabetes mellitus
TBAM	<i>N</i> - <i>tert</i> -butylacrylamide
TCI	Tokyo Chemical Industry
TEM	transmission electron microscopy
THF	tetrahydrofuran
TFA	trifluoroacetic acid
TMS	tetramethylsilane
TTC	trithiocarbonyl
VA-044	2,2'-azobis[2-(2-imidazolin-2-yl)propane]dihydrochloride

## **Chapter 1: GENERAL INTRODUCTION**

### **1.1 Diabetes<sup>1,2</sup>**

This PhD is concerned with establishing new materials responsive to glucose, and diabetes is a disease characterised by an inability to control blood glucose levels. Diabetes mellitus is typically depicted as an endocrine disease that is characterised by inadequate endogenous insulin secretion, or dysfunctional trans-membrane insulin receptor causing insulin resistance, or possibly as a combination of both. This causes an imbalance in glucose homeostasis, which can progress to hypoglycaemia. Hypoglycaemia leads to mild symptoms such as tachycardia, confusion, perspiration, and can exacerbate to more serious symptoms including fainting and diabetic coma. Hyperglycaemia is an elevated glucose concentration in the bloodstream, which is caused by a lack of glucose uptake by skeletal muscle and adipose tissue. The typical signs and symptoms for hyperglycaemia can be observed as polyuria (frequent urination and large quantities of urine), polyphagia (enlarged appetite) and polydipsia (increased thirst caused by dehydration). Persistent hyperglycaemia leads to manifestations such as micro-vascular and macro-vascular complications *i.e.* kidney failure (nephropathy), blindness (retinopathy), diabetic pain (neuropathy), limb amputations and vascular diseases (cardio and cerebrovascular) which may materialise into a myocardial infraction.

Diabetes Mellitus type 1 is brought about by cellular autoimmune mediated destruction of the  $\beta$ -Islet of Langerhans cells located in the pancreas. The main culprits are the autoantibodies that target  $\beta$ -cells. Type 2 diabetes mellitus (T2DM) accounts for 90% of diagnosed incidents of diabetes, hence it is the most prevalent form of diabetes. This is referred to “adulated-onset diabetes” or “non-insulin dependent”. But in the late stages of T2DM a proportion of patient’s are not able to generate enough endogenous insulin to counteract the hyperglycaemic period. This highlights the non-functionality of the  $\beta$ -islet of Langerhans pancreatic cells. At the extreme spectrum of T2DM disease subjects could experience a diabetic coma. The consensus is that the major risk of contracting T2DM is raised with age and is exacerbated by diminishing physical exercise, epigenetics, and obesity. T2DM is rife amongst women who display gestational diabetes through their pregnancies.

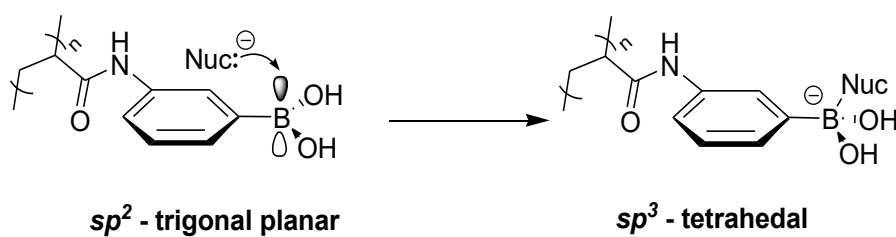


## 1.2 Boronic Acid (BA) and Glucose Chemistry

Sugar sensing has attracted sustained interest, particularly for the treatment of diabetes mellitus.<sup>3,4</sup>

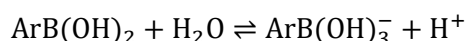
### 1.2.1 General Properties and Reactions of Arylboronic Acids

Arylboronic acids in the neutral form exist with a trigonal planar  $sp^2$ -hybridized boron, with two hydroxyl groups at  $120^\circ$  (Scheme 1.1). Carboxylic acids are acidic by virtue of proton donation, however boronic acid acidity is due to the Lewis acid nature attributed to the empty  $p$ -orbital on the boron atom. Arylboronic acids frequently form complexes with Lewis bases, for instance hydroxide or fluoride anions or electron-donating centres, such as oxygen or nitrogen. The nucleophile ( $\text{Nuc}^-$ ) will add to the vacant  $p$ -orbital of trigonal planar  $sp^2$ -boron to give the  $sp^3$ -hybridized tetrahedral boronate anion.



**Scheme 1.1:** The geometry of arylboronic acid attached to polyacrylamide.

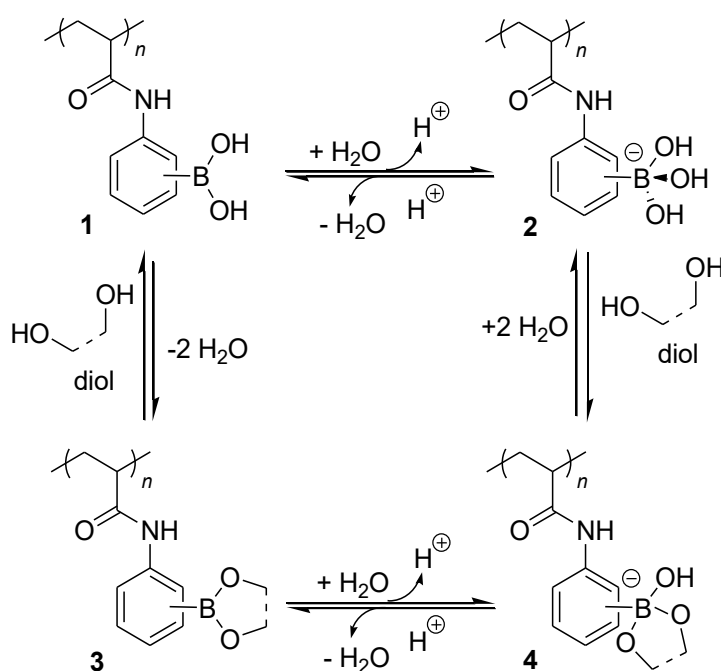
Sugar-response for block copolymers utilizes the dynamic equilibrium for condensation of arylboronic acids with *cis*-diols to give the cyclic ester at slightly basic or neutral conditions.<sup>4-</sup>  
<sup>16</sup>The acidity of arylboronic acid ( $\text{ArB}(\text{OH})_2$ ) is described by the vacant boron  $p$ -orbital, which facilitates the dissociation of water into a proton and hydroxyl ion (Equation 1.1). The hydroxyl ion is nucleophilic and attaches onto the boron, complexing to form the boronate anion. In an alkaline solution the equilibrium favours the boronate anion. ( $\text{ArB}(\text{OH})_2$ ) possesses a  $\text{p}K_a = 8.2$ .<sup>17</sup>



$$K_a = \frac{[\text{H}^+][\text{Ar}(\text{B}(\text{OH})_3)^-]}{[\text{ArB}(\text{OH})_2]}$$

**Equation 1.1:** The association constant ( $K_a$ ) for hydration of arylboronic acid

Acrylamidophenylboronic acid **1** and boronate anion **2** can chelate via a condensation reaction with 1,2- and 1,3-diols, forming boronate ester **3** or hydroxyboronate ester anion (**4**, scheme 1.2). Starichenko and co-workers reported small quantity of arylboronic acid *i.e.* **1** can be deprotonated ( $R(B(OH)O^-)$ ) like a carboxylic acid, facilitating the formation of **3**.<sup>18</sup> However, the equilibrium favours the hydrolysis of **3** to form **1** in a neutral solution. The equilibrium may shift in either direction under the influence of temperature, pH, buffer, etc. The affinity between a diol and arylboronic acid is the greatest when the pH is above the  $pK_a$  of the arylboronic acid species. Springsteen and Wang reported a varying degree of affinity amongst monosaccharide analogues. For instance, the  $pK_a$  of phenylboronic acid more acidic from 8.8 to 6.8 and 4.5 upon formation of boronate ester complexes with glucose and fructose, respectively.<sup>19</sup>

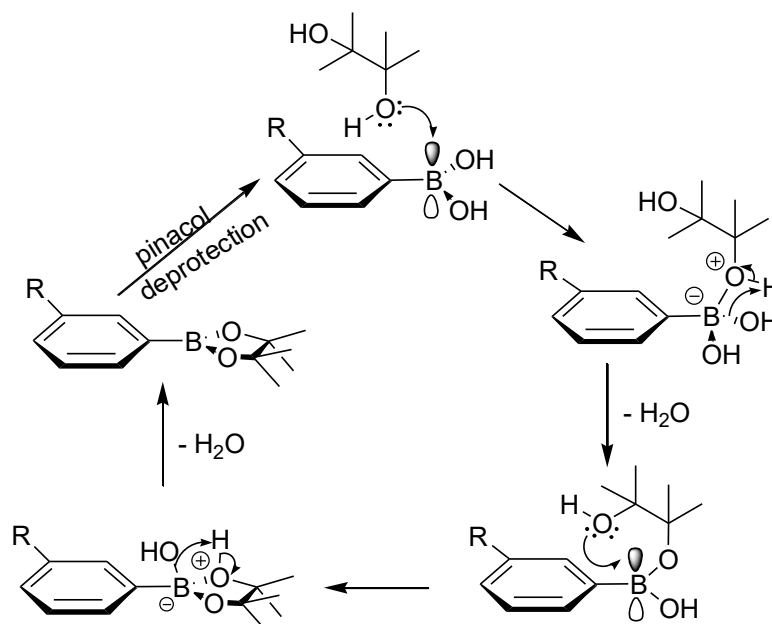


**Scheme 1.2:** Condensation equilibria of arylboronic acid attached to polyacrylamide

### 1.2.2 Pinacol Protection of boronic Acid

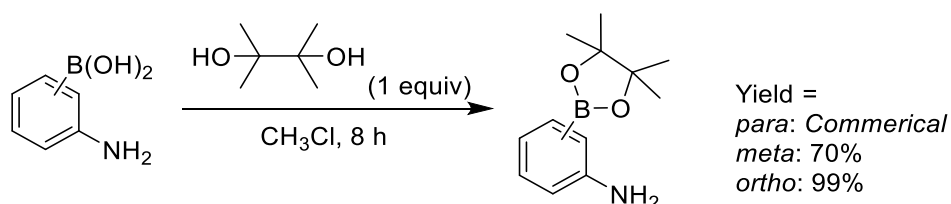
The first pinacol condensation coupling reaction with boronic acid (BA) was published in 1859 by Fittig.<sup>20,21</sup> The advantage of using the pinacol ester protected monomers is the convenience of direct gel permeation chromatography (GPC) analysis.<sup>8</sup> BA is poorly soluble in common organic solvents, including the GPC solvent, DMF. The pinacol protection also facilitates

synthetic functionalisation of the monomer.<sup>7</sup> The lone pair electrons on the hydroxyl groups of the pinacol facilitates a nucleophilic addition on the vacant *p*-orbital of the boron (Scheme 1.3). This addition occurs twice as pinacol is a diol and expels a hydroxide anion on each attack. The hydroxide anions collate with the proton of the hydroxyl group of pinacol and cumulatively form two water molecules.<sup>22</sup>



**Scheme 1.3:** Mechanism for pinacol protection via condensation reaction with BA.

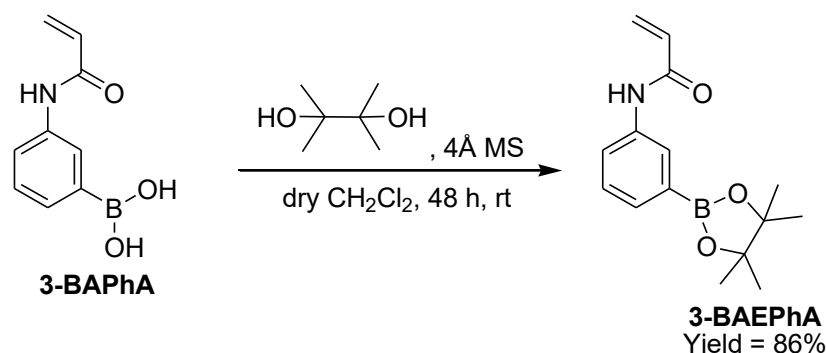
D'Hooge et al. successfully pinacol protected phenylboronic acid aniline in  $\text{CHCl}_3$  with high yields (Scheme 1.4).<sup>23</sup> The reagents were dissolved in chloroform at room temperature and stirred for a duration of 8 h. At the end of the reaction an immiscible water layer was formed, which required separation from the organic layer.



**Scheme 1.4:** D'Hooge *et al.* pinacol protection in  $\text{CHCl}_3$ .<sup>23</sup>

Pinacol protection of 3-aminophenylboronic acid (3-BAPhA) gave 3-aminophenylboronic acid pinacol ester (3-BAEPH), when utilising 4 Å molecular sieves (MS) to absorb the released

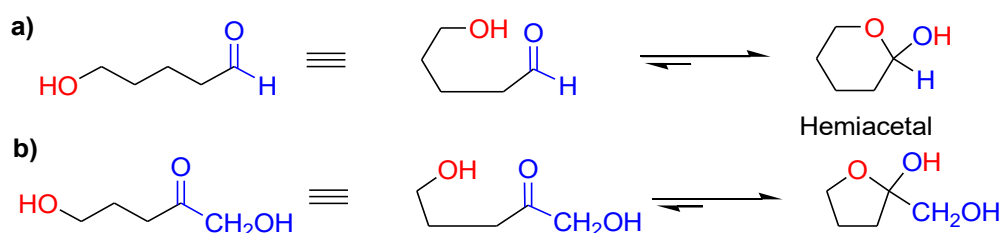
water (Scheme 1.5).<sup>8</sup> This reaction implements Le Chatelier's principle to shift the equilibrium towards 3-BAEPHA.



**Scheme 1.5:** Pinacol protection using molecular sieves (MS).<sup>8</sup>

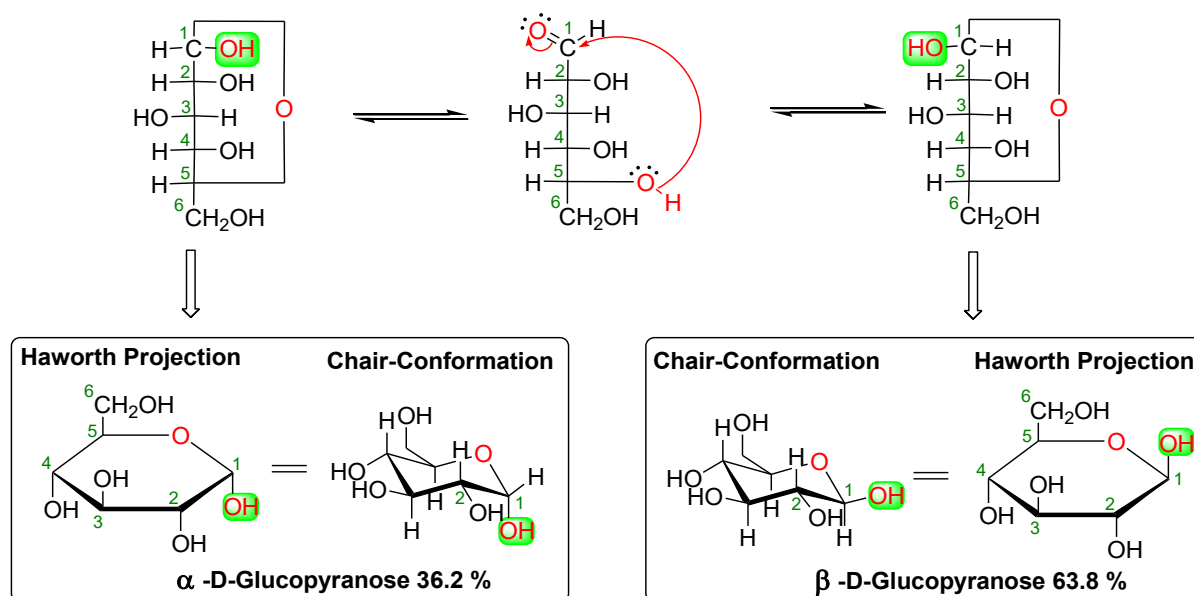
### 1.2.3 Fundamentals of Sugar Chemistry

Monosaccharide acyclic molecules possess both a hydroxyl and aldehyde or carbonyl group and undergo an intramolecular cyclization to give a cyclic hemiacetal (Scheme 1.6). Pyran and furan are six and five-membered rings, respectively. The generalized view is most acyclic monosaccharides exhibit only a minimal presence at equilibrium (<0.01%).



**Scheme 1.6:** Cyclic hemiacetal formation: **(a)** pyran and **(b)** furan

D-Glucopyranose exists as two different stereoisomers with a chiral centre, of  $\alpha$ ,  $\beta$ -anomers, upon pyranose condensation (Scheme 1.7). In  $\beta$ -D-glucopyranose the hydroxyl group is *cis* to the  $\text{CH}_2\text{OH}$  group. The equilibrium established is 2:1 in favour of  $\beta$ -D-glucopyranose (63.8 %) rather than  $\alpha$ -D-glucopyranose (36.2 %).<sup>24</sup> The high stability of the  $\beta$ -pyranose form is due to torsional strain between OH groups at positions C-1 and C-2 in the  $\alpha$ -anomer.

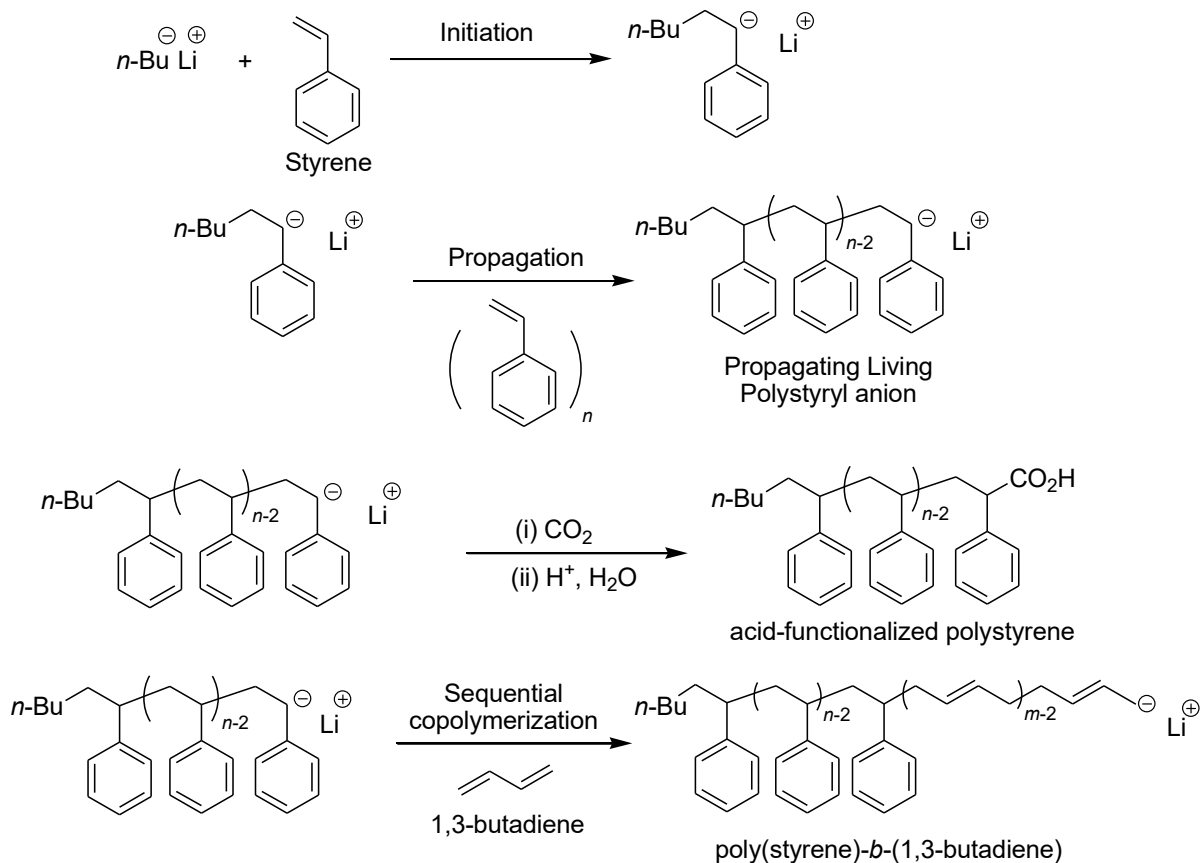


**Scheme 1.7:** D-Glucose: Anomeric Haworth projections with the energy-minimum chair.

### 1.3 Reversible Deactivation Radical Polymerization (RDRP)

#### 1.3.1. Introduction

Szwarc introduced the concept of controlled/living polymerization for the anionic polymerization of styrene in 1956.<sup>25</sup> The polymerization can be initiated/controlled by an organometallic reagent (e.g. *n*-BuLi) and propagating polystyryl chains remain living unless inadvertent termination occurs (Scheme 1.8).<sup>26</sup> Polymer chains are termed “living”, since addition reactions introduce polymer functionality (e.g. carboxylic acid by adding onto CO<sub>2</sub>) or enable block copolymer synthesis (e.g. with 1,3-butadiene). In this controlled/living polymerization the degree of polymerization (*DP*) is predictable by the [Monomer]/[*n*-Bu-Li] ratio.



**Scheme 1.8:** Living anionic polymerization.

However, anionic polymerization has significant disadvantages over radical polymerization for the preparation of addition polymers – 1. Rigorous purification of reagents, anhydrous, and inert atmospheres are required to prevent termination reactions. 2. Applies generally to less activated monomers (*e.g.* (meth)acrylates and (meth)acrylamides) and styrene, and not to acidic monomers (*e.g.* acrylic acid) or more activated monomers, *e.g.* vinyl acetate). Limited to homogeneous polymerization (*e.g.* incompatible with water, a commonly used medium for industrial heterogeneous polymerizations).

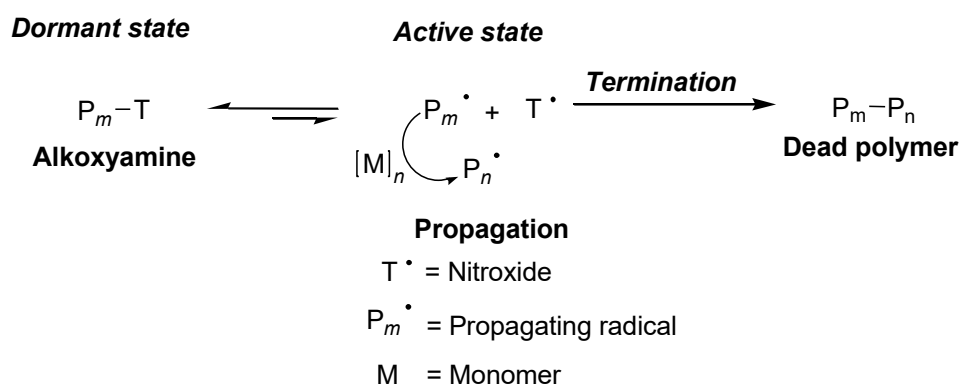
Due to its applicability to all vinyl monomers and less rigorous experimental set-up, the discovery of controlled/living radical polymerizations or reversible deactivation radical polymerization (RDRP) has revolutionized polymer chemistry. There are two main types of RDRP techniques (i) relying on reversible termination: nitroxide-mediated polymerization

(NMP) and atom transfer radical polymerization (ATRP) (ii) degenerative chain transfer processes: reversible addition-fragmentation chain transfer (*e.g.* RAFT).

Control implies governance over the molecular weight distribution (MWD), whereas livingness implies that the end-group is functionalized by the added reagent, and that chain extension can occur. In contrast to conventional (non-living) radical polymerizations, molecular weight or *DP* can be predicted by the  $[\text{Monomer}]_0/[\text{Living Reagent}]_0$  ratio, and block copolymer, other fanciful well-defined architectures are possible, and end-groups can be functionalised.

### 1.3.2 Nitroxide-Mediated Polymerization (NMP)

NMP uses a stable nitroxide free radical ( $\text{R}_2\text{NO}^\bullet$ ), which reversibly traps propagating carbon-centered radicals at elevated temperatures ( $>100\text{ }^\circ\text{C}$  for cyclic nitroxides, *e.g.* commercial TEMPO). At the polymerization temperature, an equilibrium between dormant and active states is set up, with propagation and termination occurring in the active state. An excess of nitroxide over initiating/propagating radicals minimizes termination, and allows a controlled/living polymerization, where all living chains are capped by the nitroxide,  $\text{T}^\bullet$  (Scheme 1.9). *DP* is predictable by  $[\text{Monomer}]_0/[\text{Alkoxyamine}]_0$  ratio.



**Scheme 1.9:** Controlled/living NMP mechanism

The Persistent Radical Effect (PRE) is often used to describe the mechanism of control in NMP.<sup>27</sup> At the start of the polymerization, the propagating radical ( $\text{P}^\bullet$ ) have the same probability to undergo bimolecular termination as to undergo nitroxide ( $\text{T}^\bullet$ ) trapping to give

the dormant alkoxyamine (P-T, Scheme 1.9). The outcome of termination is a rapid buildup in the persistent radical  $T^*$ , and a decline in the relative concentration of propagating (transient) radicals. The excess of  $T^*$  minimizes further termination of  $P^*$  to give dead polymer ( $P_m-P_n$ ) during the polymerization to ensure control/living character. Many other NMP processes begin with a vast excess of nitroxide to azo initiator to minimize termination.<sup>28</sup>

Generally, NMP is only applicable to styrene when using cyclic nitroxides (e.g. TEMPO<sup>29</sup>) but can be applied to a wider range of monomers (e.g. acrylates and acrylamides), when using acyclic nitroxides (e.g. TIPNO<sup>30</sup> and SG1<sup>31</sup>)(Fig. 1.1). This is because the alkoxyamine bond dissociation energy (BDE) is dictated by the nitroxide structure, for a given monomer. Cyclic nitroxides form stronger (C-O) bonds in alkoxyamines, which prevents the sufficient formation of active states for controlled propagation.

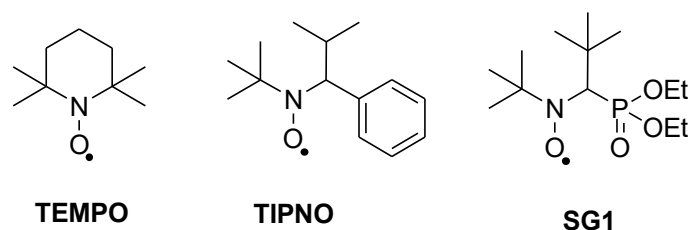
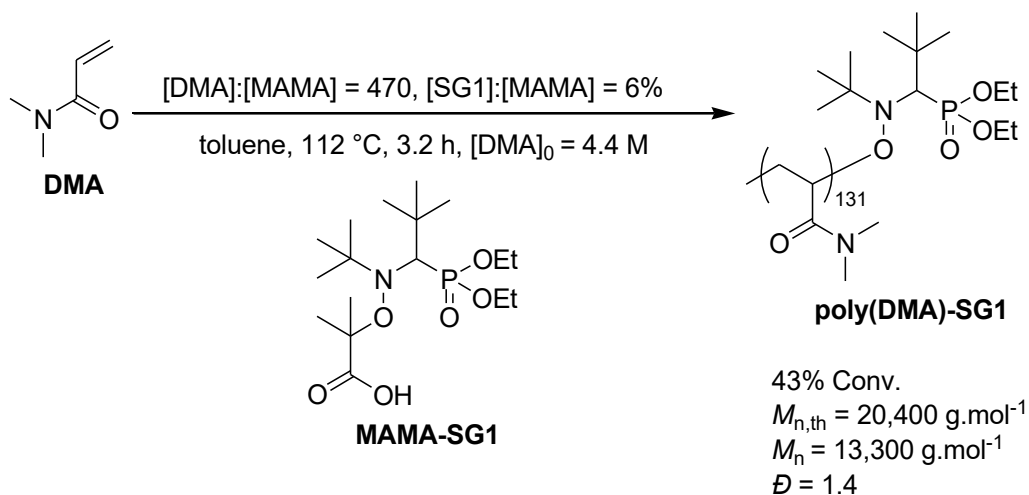


**Figure 1.1:** Nitroxides used in NMP

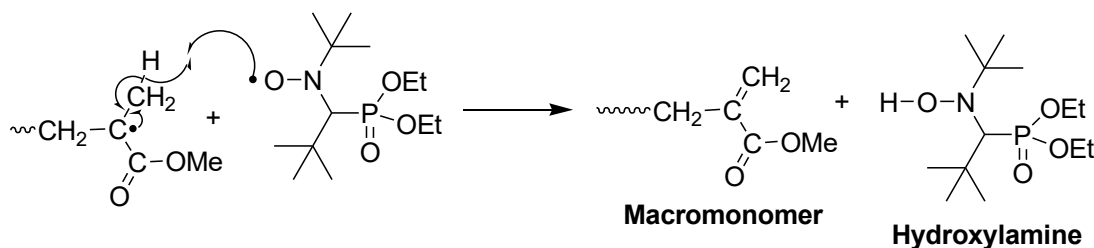
Karaky *et al.* reported a controlled/living NMP of *N,N*-dimethylacrylamide (DMA) using the alkoxyamine MAMA as the initiator, in the presence of 6% excess free SG1 (Scheme 1.10).<sup>32</sup> Poly(DMA) with  $M_n$  of 13,300 g.mol<sup>-1</sup> and  $\bar{D}$  of 1.4 was prepared with the slight excess of SG1 allowing an early on-set of PRE. Higher temperatures are required for NMP compared to RAFT polymerizations of DMA (see later), because of the homolytic fission of MAMA and the polymeric alkoxyamines generated.





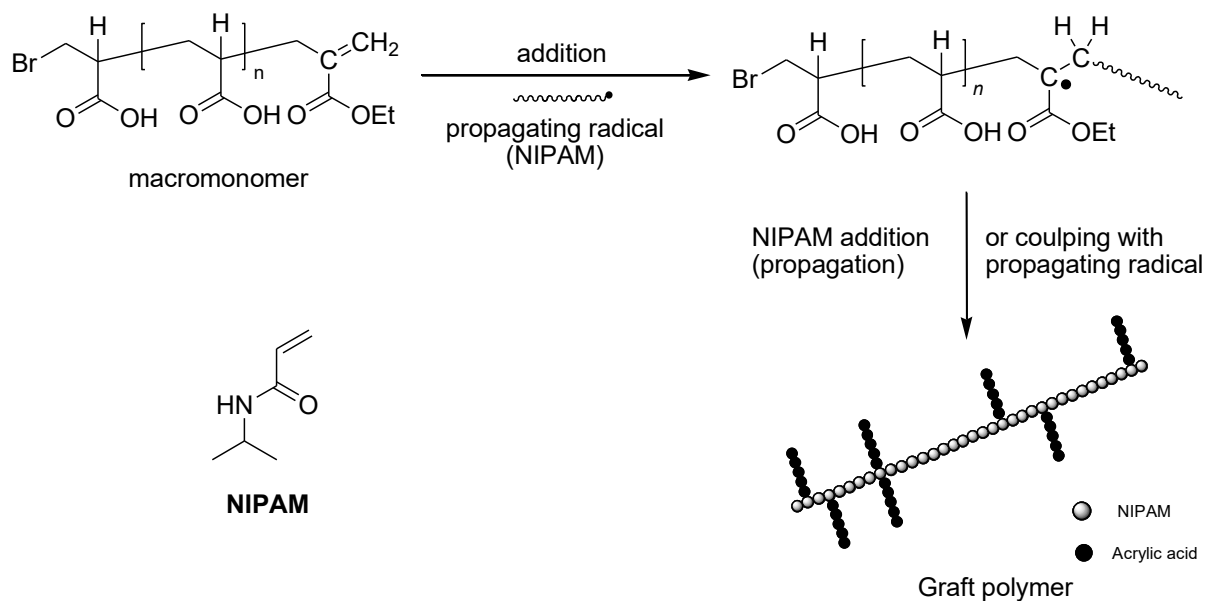
**Scheme 1.10:** An example of NMP of DMA<sup>33</sup>

For methacrylates, hydrogen-abstraction is observed when attempting controlled/living polymerization with NMP (Scheme 1.11).<sup>33</sup> The reaction gives a polymer containing a terminal double bond, called a macromonomer and the hydroxylamine of the nitroxide (*e.g.* SG1).



**Scheme 1.11:** The reason for unsuccessful NMP with methacrylates.<sup>33</sup>

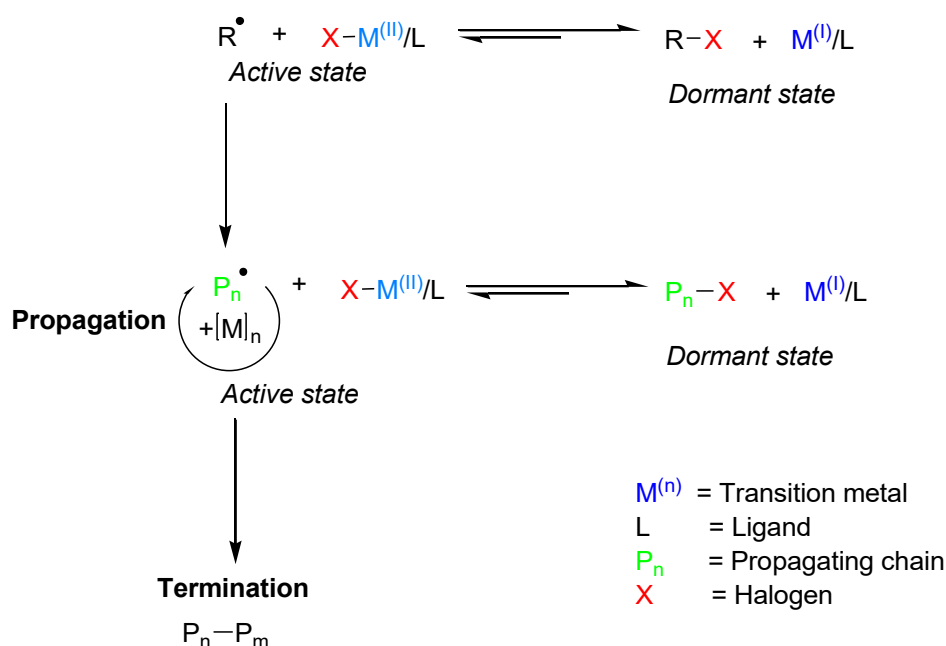
A macromonomer contains a polymerizable group on one chain ( $\omega$ -)end, which can homopolymerize with the same monomer to give a regular comb-polymer or (branched) polymer. A graft copolymer is when monomer is copolymerized with a macromonomer with different monomer units. Aldabbagh *et al.* made a dual responsive - thermoresponsive and pH-responsive graft copolymer by copolymerizing *N*-isopropylacrylamide (NIPAM) with the macromonomer of acrylic acid (Scheme 1.12).<sup>34</sup>



**Scheme 1.12:** Graft copolymer with poly(NIPAM) main chain and poly(AA) branches.<sup>34</sup>

### 1.3.3 Atom Transfer Radical Polymerization (ATRP)

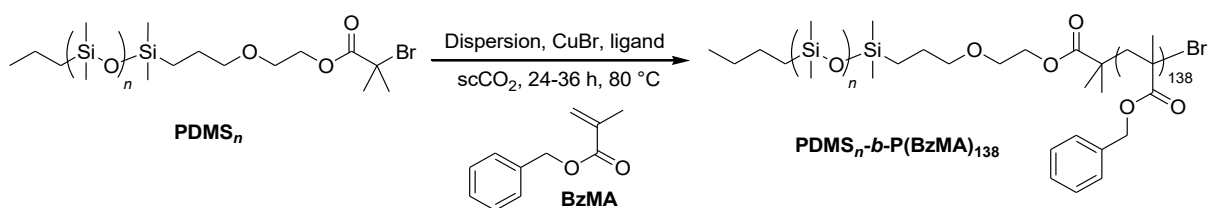
Within a couple of years of the introduction of NMP, ATRP was introduced in 1995, with Matyjaszewski reporting copper-catalysis ( $\text{CuBr}$ )<sup>35</sup> and independently Sawamoto reporting ruthenium-catalysis ( $\text{RuCl}_2(\text{PPh}_3)_3$ ).<sup>36</sup> ATRP requires a multi-reagent system, with monomer, catalyst (a transition metal complex species), an appropriate ligand, and initiator (*i.e.* alkyl halide,  $\text{R-X}$ ). The reversible dissociation mechanism gives active states via reduction of dormant alkyl halides ( $\text{R-X}$ ,  $\text{P}_n\text{-X}$ ) to initiating or propagating radicals (Scheme 1.13). Reversible deactivation occurs upon oxidation of the propagating species by the higher valency metal to give the dormant halide capped polymer chain and lower valency metal.



**Scheme 1.13:** ATRP controlled/living polymerization mechanism.

$DP$  is predictable by  $[\text{Monomer}]_0/[\text{R-X}]_0$ . ATRP, like NMP, also achieves control/living character using the PRE.<sup>27</sup> The initial concentrations of radicals and M(II) halide are zero, when M(I) reacts with the alkyl halide, the concentrations of M(II) halide and  $\text{R}^\bullet$  should remain constant. However, at the early stages, bimolecular termination gives dead polymer ( $\text{P}_n\text{-P}_m$ ), which allows [M(II) halide] to rapidly increase in concentration. The outcome is a sufficiently high concentration of M(II) halide relative to  $\text{P}^\bullet$ , at which point the rate of termination is slow enough for a controlled/living polymerization to occur.

An example of ATRP is the dispersion polymerization of benzyl methacrylate (BzMA), which gave worms and vesicles morphologies via polymerization-induced self-assembly (PISA) in supercritical carbon dioxide ( $\text{scCO}_2$ ) (Scheme 1.14).<sup>37</sup> PISA (described later) achieves control over polymer morphology as well as molecular weight.  $\text{scCO}_2$  is used as the polymerization medium, and poly(dimethylsiloxane) (PDMS-Br) is utilized as a solvophilic *inistab* (initiator + stabilizer) block, which is extended with BzMA, a monomer initially soluble, which forms the solvophobic block. Depending on the relative sizes of the two blocks, different morphologies are achieved.

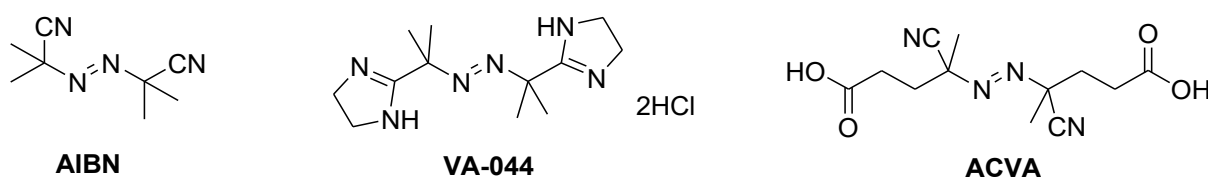


**Scheme 1.14:** ATRP dispersion polymerization of BzMA in  $\text{scCO}_2$ .<sup>37</sup>

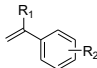
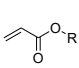
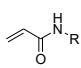
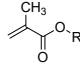
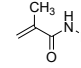
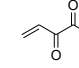
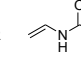
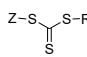
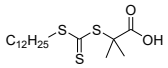
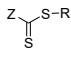
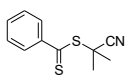
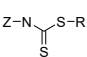
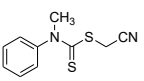
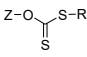
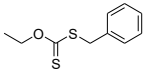
Thus, NMP and ATRP achieve control/living character according to the PRE.<sup>27</sup> The PRE is distinctly different to RAFT (see below), where bimolecular termination does not lead to a loss in living chains, since dead chains are derived from the initiator.

### 1.3.4 Reversible Addition-Fragmentation Chain Transfer (RAFT)<sup>38</sup>

Moad, Rizzardo and Thang *et al.* first reported RAFT-mediated polymerization in 1998.<sup>39</sup> RAFT is distinctive from NMP and ATRP in that it achieves control/living character not by reversible termination but using a degenerative transfer system. Unlike NMP or ATRP, there is no change in the overall number of radicals in the activation-deactivation process, and a source of radicals (the initiator) is required. RAFT agents used include dithioesters, trithiocarbonates, dithiocarbamates or xanthates depending on the monomer type (Table 1.1). The initiator is most often a thermally labile azo initiator (e.g. 2,2'-azobis[2-(2-imidazolin-2-yl)propane]dihydrochloride (VA-044), AIBN, 4,4'-azobis(4-cyanopentanoic acid) (ACVA), etc (Fig. 1.2)).



**Figure 1.2:** Different azo initiators

									
			styrenes	acrylates	acrylamides	methacrylates	methacrylamides	vinyl esters	vinyl amides
Trithiocarbonates			+++	+++	+++	+	+	-	-
Dithioesters			++	+	-	+++	+++	-	-
Dithiocarbamates			-	-	-	-	-	+++	+++
Xanthates			-	-	-	-	-	+++	+++

**Table 1.1:** RAFT agent and monomer compatibility table. The (+) and minuses (-) represent degree of compatibility between monomer classes and a RAFT agent.<sup>42</sup>

RAFT chain transfer agents (CTA) control the radical polymerization process of an array of monomers. The appropriate RAFT CTA to use, is dictated by the type of monomer (Table 1.1). More activated monomers (MAMs) are characterised by double bonds that are conjugated to a carbonyl group (*e.g.* acrylates, CO<sub>2</sub>R, acrylamides, CONR<sub>2</sub>), an aromatic ring (*e.g.* styrenics, Ph), or a nitrile (*e.g.* acrylonitriles, CN). MAMs are traditionally used in anionic addition polymerization. However, the less activated monomers (LAMs) have a double bond which is adjacent to a nitrogen lone pair or an oxygen lone pair (*e.g.* vinyl acetate, OCOCH<sub>3</sub>). LAMs are traditionally used in cationic addition polymerization. MAM polymerizations are better controlled by trithiocarbonates (Z = alkylthio) or dithioesters (Z = aryl, alkyl), while LAM require a RAFT CTA such xanthates or dithiocarbamates (Table 1.1).<sup>40</sup>

The Z group adduct can influence the rate of fragmentation of the intermediate radical (*e.g.* to 2-methylpropan-2-yl in the case of the CTA, 2-(dodecylthiocarbonothioylthio)-2-methylpropionic acid (DMP)). The Z group also determines the rate of addition of propagating radicals (P<sub>n</sub><sup>\*</sup>) to the trithiocarbonyl group, and the solubility of the RAFT CTA or macroRAFT in a particular solvent. In the case of DMP, the twelve-carbon alky-Z group allows amphiphilic self-assembly.<sup>41</sup> The R group is often a good homolytic tertiary radical leaving group (*i.e.* 2-

methylpropan-2-yl for DMP, Fig. 1.3) with respect to a secondary incoming propagating radical  $P_n^\bullet$ . The equilibrium between the active and dormant states is dependent on the fragmentation of the intermediate di- or trisulfur radical adduct, with the forward fragmentation determined by greater radical stability.

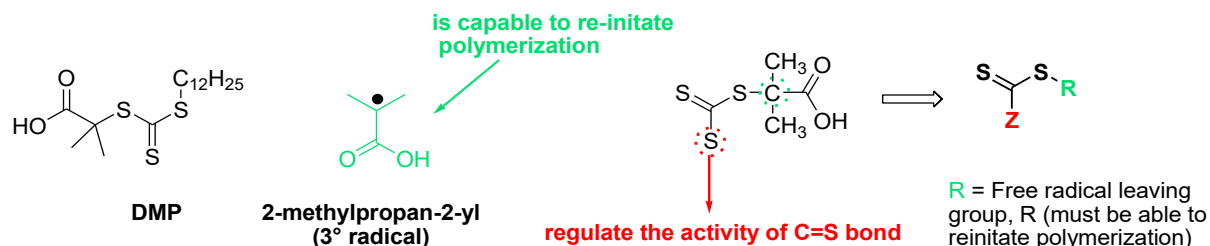


**Figure 1.3:** Shows the important constituents of the RAFT agent and the CTA: DMP.

In this thesis the monomers used are acrylamides and the most suitable RAFT agent is DMP. Scheme 1.15 gives the mechanism for the polymerization of DMA, using DMP and VA-044 as initiator and RAFT agent respectively. This RAFT process was used to prepare hydrophilic poly(DMA) macroRAFT agents for PISA and one-pot iterative chain extensions (described in Chapters 3 and 4 respectively). The first step of the mechanism involves VA-044 thermally decomposing to two initiating 2-(4,5-dihydro-1H-imidazol-2-yl)propan-2-yl radicals (Scheme 1.15). The initiator decomposition is energetically favoured due to the greater stability of the generated tertiary radicals and inert nitrogen gas compared to VA-044. The water-soluble azo initiator VA-044 was chosen due to its high decomposition rate coefficient ( $k_d$ ) allowing completion of each polymerization in 2 h at 70 °C while maximizing livingness.<sup>43</sup> At 70 °C, VA-044 decomposes about 10 times faster than AIBN (Table 1.2), which allows an increase in rate without affecting livingness.

Initiator	$k_d$ (s <sup>-1</sup> )	Solvent
VA-044	$4.30 \times 10^{-4}$	H <sub>2</sub> O/Dioxane (80:20) <sup>43</sup>
ACVA	$2.23 \times 10^{-5}$	H <sub>2</sub> O/Dioxane (80:20) <sup>44</sup>
AIBN	$4.00 \times 10^{-5}$	Toluene <sup>45</sup>

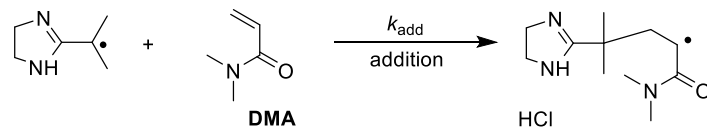
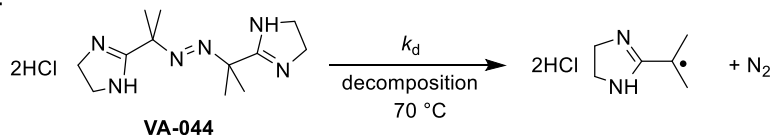
**Table 1.2:** Rate coefficient ( $k_d$ ) for decomposition of common azo initiators at 70 °C.

The second step of initiation is radical addition, which is much faster than initiator decomposition, so the rate of polymerization is expressed as  $R_i = k_d[I]_0$  at a given monomer

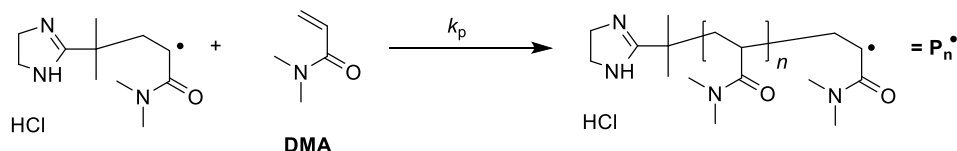
concentration. Since propagation is assumed to occur at the same rate as the initial radical addition, *i.e.*  $k_i = k_p$ , and since chain transfer is faster than propagation, then the rate of a RAFT-mediated polymerization is the same as that in the absence of the RAFT agent. Therefore, RAFT-mediated polymerization should ideally occur at the same rate as a conventional (non-living) radical polymerization. The difference between RAFT and conventional radical polymerization are thus the additional chain transfer steps. The rate of fragmentation ( $k_\beta$ ) should be faster than  $k_p$ , to ensure control/living character without retardation.

A vast excess of RAFT agent (DMP) compared to VA-044 derived radicals, ensures that most chains are living. Control/living character is thus determined by the main chain equilibrium. This allows  $DP$  to equal the ratio of  $[\text{Monomer}]_0/[\text{RAFT}]_0$ , based on the assumption that the number of dead chains is minimal (*i.e.* initiator derived chains or terminated chains is small). The overall outcome is shown in Scheme 1.16, where most poly(DMA) chains contain RAFT CTA (DMP) functionality.<sup>46</sup>

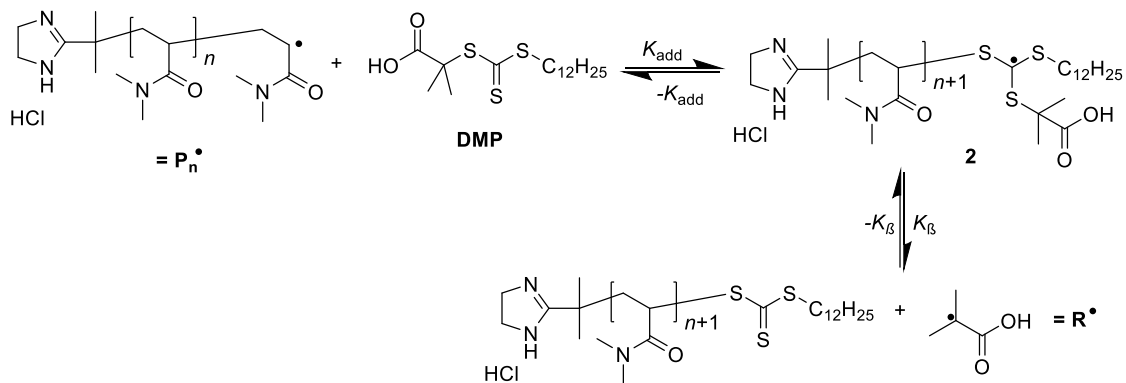
Initiation:



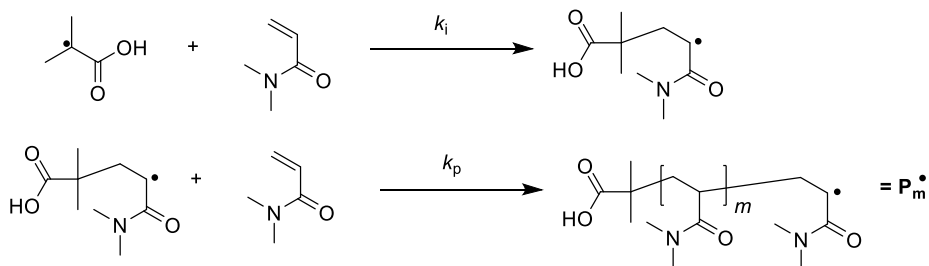
Main Propagation:



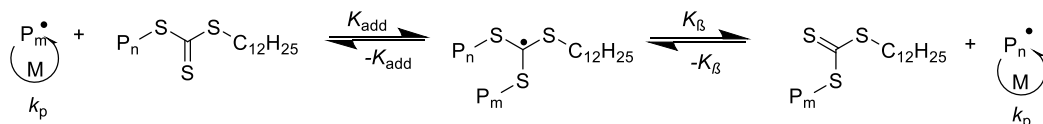
Reversible chain transfer:



Re-initiation:



Main Chain Equilibrium:

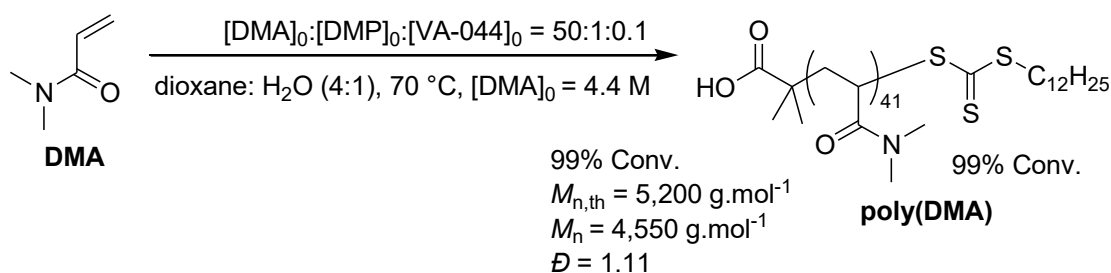


Termination:



**Scheme 1.15: Mechanism for RAFT polymerization of DMA.**



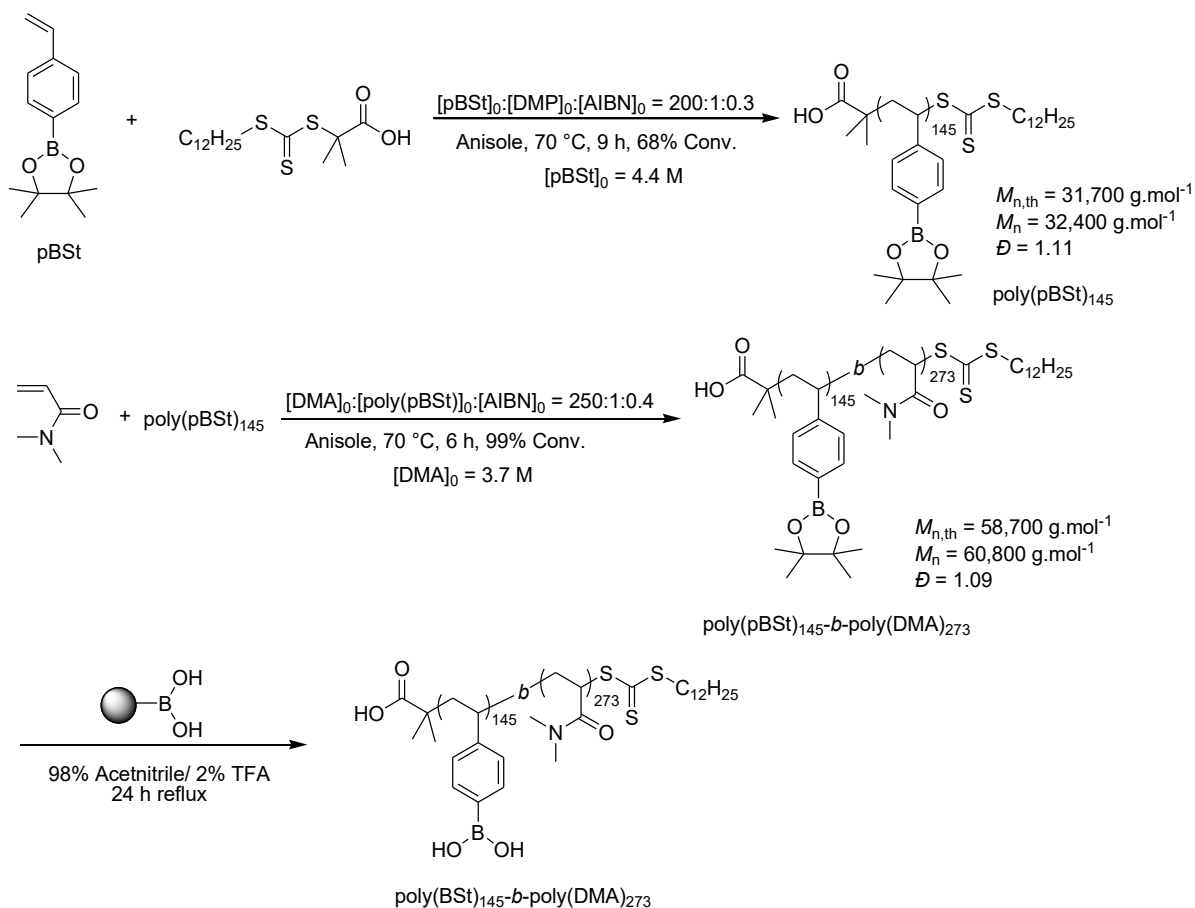


**Scheme 1.16:** RAFT polymerization of DMA.<sup>46</sup>

### 1.3.5 Brief Review of Synthesis of Glucose Responsive Polymers using RAFT

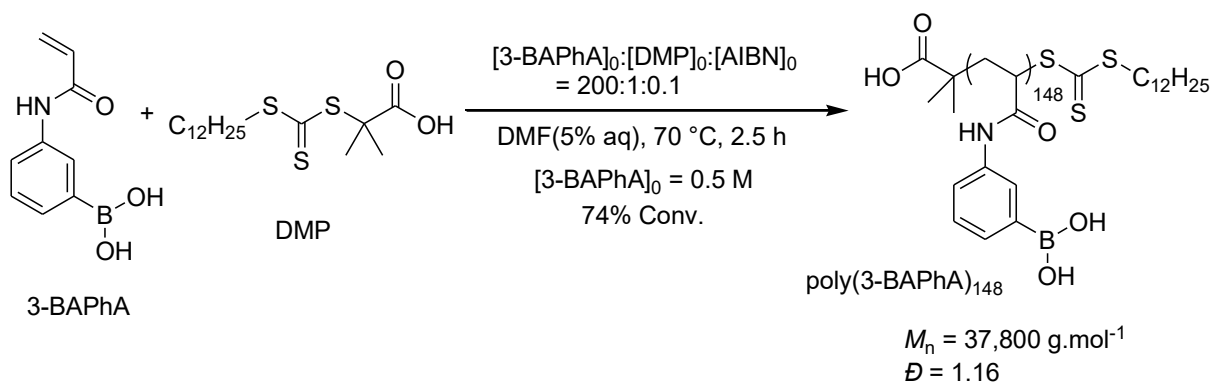
Since 2007,<sup>47</sup> there has been a plethora of reports on the controlled/living RAFT polymerization of BA-substituted acrylamides. The prepared amphiphilic block copolymers become more soluble in water upon BA-binding to glucose. In these reports, insulin is released according to glucose concentration, by binding of the diol to increase the hydrophilicity of the nanoparticle.<sup>4-7,47-49</sup>

Sumerlin pioneered the RAFT polymerization of BA-substituted monomers, beginning with a *para*-styrene (pBSt) derivative (Scheme 1.17).<sup>47</sup> The pinacol ester protected BA-macroRAFT was chain extended with DMA to give water-soluble block copolymer nanoparticles upon deprotection by transesterification with a BA-functionalized polymer in the presence of 2% trifluoroacetic acid (TFA) in acetonitrile.



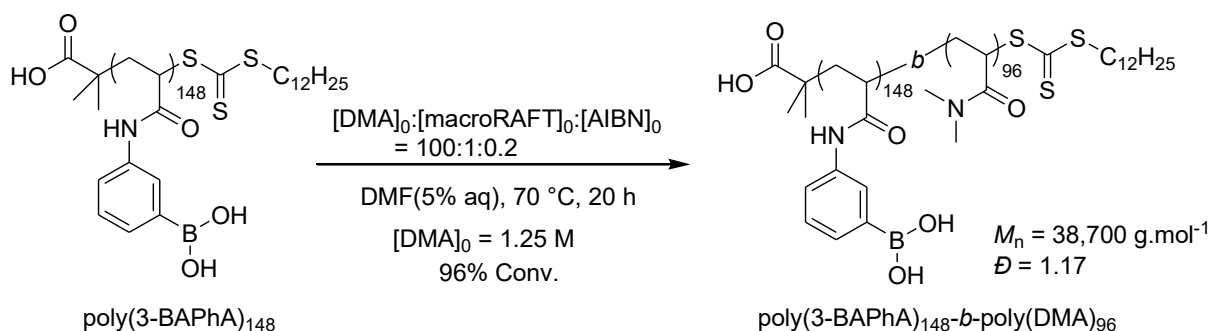
**Scheme 1.17:** RAFT route to water soluble BA-functionalized block copolymers.<sup>47</sup>

3-BAPhA was used by Sumerlin *et al.* to prepare glucose-responsive nanoparticles characterized by dynamic light scattering (DLS). Polymerization of 3-BAPhA in DMF-5% water at 70 °C used DMP and AIBN (Scheme 1.18).<sup>5</sup> The homopolymerizations displayed controlled/living characteristics with  $M_n$  of 37,800  $\text{g}\cdot\text{mol}^{-1}$  and  $\bar{D}$  of 1.16 at  $[\text{3-BAPhA}]_0/[\text{DMP}]_0 = 200$ . Scheme 1.18 uses MWs of the pinacol-protected polymer since the free BA cannot undergo GPC analysis.



**Scheme 1.18:** RAFT block copolymers of 3-BAPhA and DMA.<sup>5</sup>

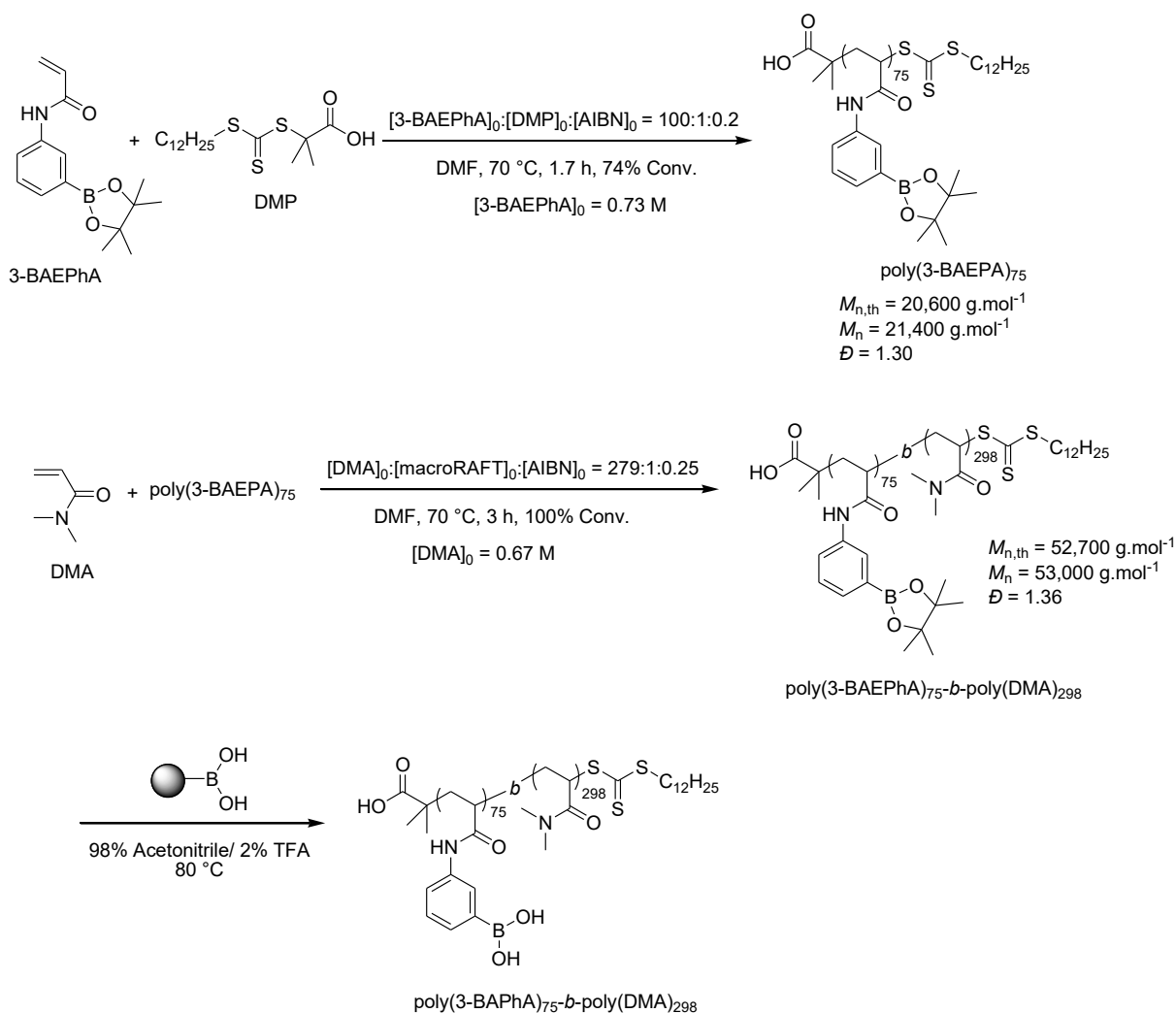
Amphiphilic nanoparticles required chain extension of poly(3-BAPhA) with DMA, as shown in Scheme 1.19, followed by dialysis with water.



**Scheme 1.19:** RAFT block copolymers of 3-BAPhA and DMA.<sup>5</sup>

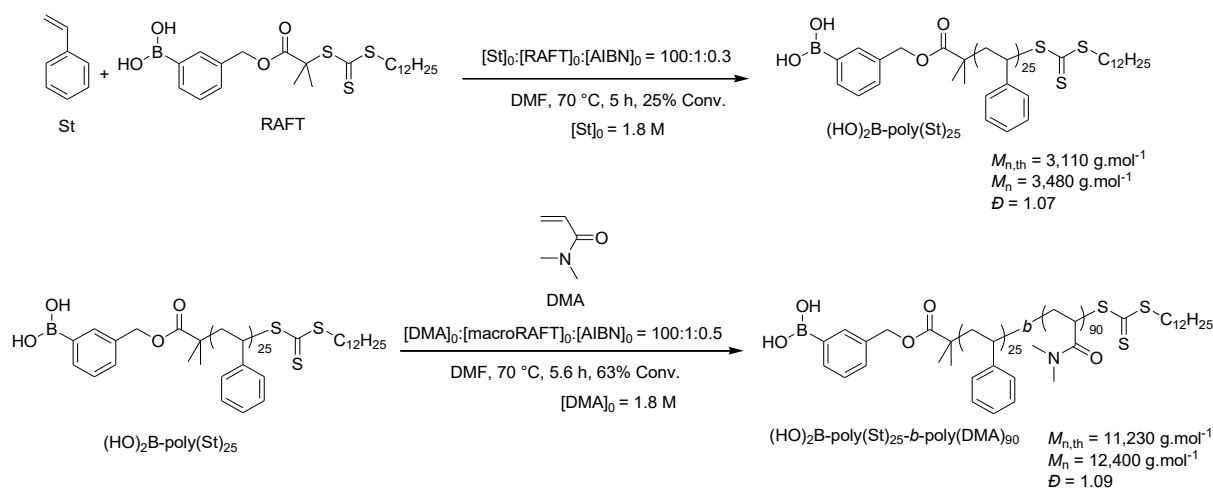
The same approach was used to make poly(3-BAPhA)<sub>81</sub>-*b*-poly(NIPAM)<sub>109</sub>, where poly(3-BAPhA) macroRAFT was chain extended with NIPAM in 90% conversion (Scheme 1.20). NIPAM is interesting because it has lower critical solution temperature (LCST), the block copolymer exists in a solubilized state below LCST but heated above LCST leads to dehydration and aggregation. The LCST of poly(NIPAM) is about 32 °C.<sup>50</sup> Nanoparticles were characterized by DLS at pH = 8.7 ( or at the pKa of 3-BAPhA), with approximately diameter = 55 nm. Glucose response at pH 8.7 caused particles to partially solubilize and the diameter to reduce to 7 nm. When heated to 42 °C at pH ≈11, aggregates with a diameter of 78 nm were detected by DLS, indicating an increase in size of particles above the LCST of poly(NIPAM).





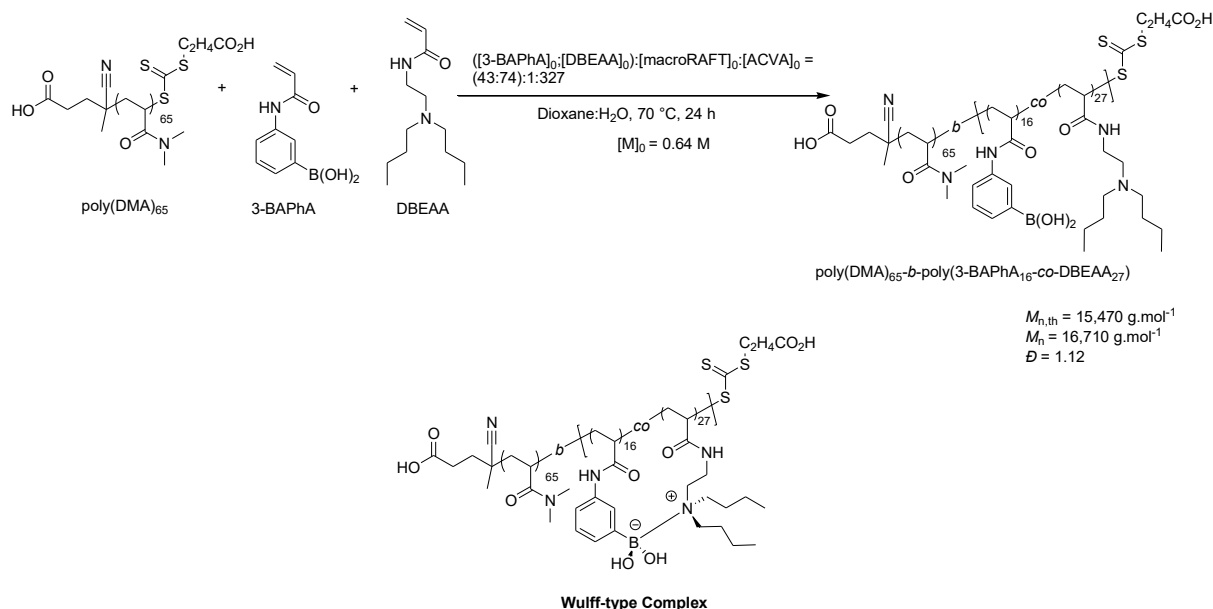
**Scheme 1.21:** RAFT route to water soluble 3-BAEPHA to give block copolymers.<sup>8</sup>

Sumerlin *et al.* also introduced a RAFT agent, which was functionalized with BA for glucose-response.<sup>51</sup> The RAFT agent was called 2-dodecylsulfanylthiocarbonylsulfanyl-2-methylpropionic acid 3-boronic benzyl ester (RAFT) was used to make the macroRAFT of poly(styrene), which was then chain extended with DMA followed by NIPAM, according to Scheme 1.22. The triblock led to self-assembly with boronic acid groups distributed along the corona periphery or within the hydrophobic core. Orange fluorescence emitted from the boronic acid-alizarin complex, demonstrated their availability to form boronic esters with diols. DLS confirmed morphologies of diameter between 23–32 nm at 25 °C.



**Scheme 1.22:** Amphiphilic triblock copolymer with BA-end groups.<sup>51</sup>

Most recently, Prossnitz and Pun produced diblock copolymers by chain extension of poly(DMA) macroRAFT with mixtures of 1:1.7 3-BAPhA: *N,N*-dibutylethylenediamine (DBEDA) at 70 °C using 4,4-azobis(4-cyanovaleric acid) (ACVA), as azo initiator (Scheme 1.23).<sup>52</sup> The Wulff-type complex reduces the  $pK_a$  of the BA moiety allowing response at near-physiological neutral pH towards diols (in this catechol). Drugs were loaded and released upon binding to the diol.



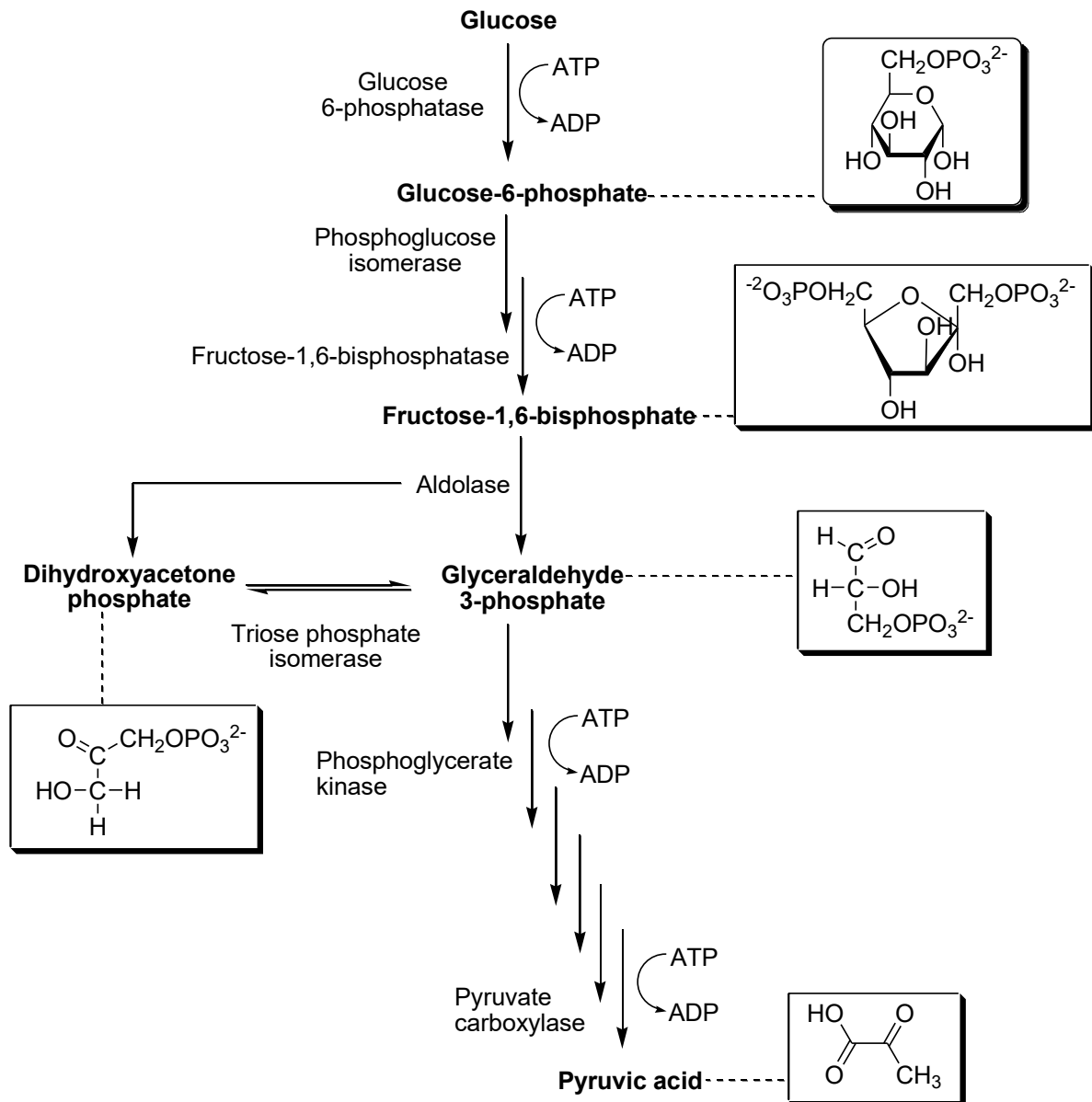
**Scheme 1.23:** Synthesis of Wulff-type complex modulated block copolymers.<sup>52</sup>

## **1.4 Lactic Acid Chemistry and Binding to Boronic Acid (BA)**

### **1.4.1 Glycolysis**

The word “glycolysis” is derived from the Greek “glykys,” meaning “sweet,” and “lysis,” which means “to split.” This refers to the splitting of one glucose molecule into two molecules of pyruvate. Firstly, glucose is converted to fructose-1,6-bisphosphate via a phosphorylation, an isomerization, and a second phosphorylation reaction. The latter pathway consumes two ATP molecules per molecule of glucose.

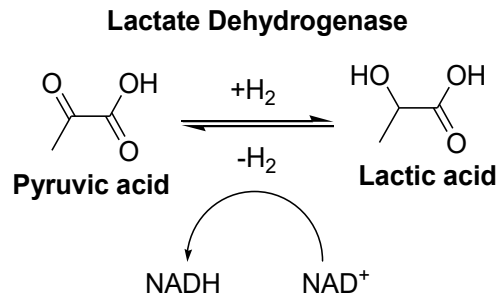
In the second step, fructose-1,6-bisphosphate is cleaved by aldolase into glyceraldehyde 3-phosphate and dihydroxyacetone phosphate. ATP is generated, by glyceraldehyde 3-phosphate being oxidized and phosphorylated producing 1,3-bisphosphoglycerate, an acyl phosphate facilitating the phosphoryl group to transfer ADP to form ATP. A phosphoryl shift and a dehydration form phosphoenolpyruvate, a second intermediate with an increased phosphoryl-transfer potential. Hence, generating another ATP molecule by conversion of phosphoenolpyruvate to pyruvate (Scheme 1.24).



**Scheme 1.24:** Overview of glycolysis.

In the presence of oxygen, pyruvate usually enters the mitochondria where it is oxidized to acetyl-CoA, whereas in the absence of oxygen, pyruvate is reduced into lactate (Scheme 1.25). Lactate is formed from pyruvate in a process called lactic acid fermentation and occurs under anaerobic conditions associated with exercise. The reduction of pyruvate by nicotinamide adenine dinucleotide (NADH) to form lactate is catalyzed by lactate dehydrogenase, which also facilitates the oxidation of lactate to pyruvate in cardiac tissue, which is then used as a fuel by the heart through aerobic metabolism.





**Scheme 1.25:** Reduction and oxidation pyruvic and lactic acid

The Cori cycle prevents lactic acidosis in muscle under anaerobic respiration by conversion of lactate to glucose via pyruvate (Fig. 1.4).<sup>53</sup>

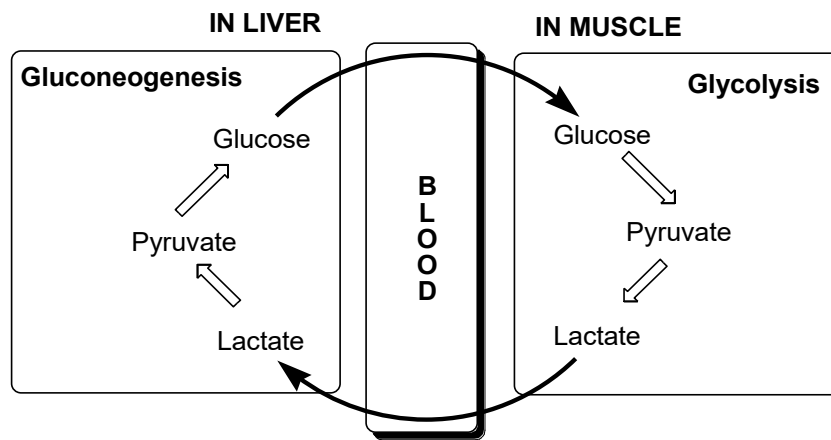


**Figure 1.4:** The Cori cycle

### 1.4.2 Monitoring Lactic Acid with BA

However, L-lactate is also derived from aerobic pathway due to congenital or acquired deficiencies (*e.g.* failure of renal, hepatic system, diabetes, and malignancy, *etc.*).<sup>53</sup> D-Lactate can be exogenously acquired by diet *i.e.*, dairy, or fermented products (Fig. 1.5). D-lactate is endogenously generated from methylglyoxal through the glyoxalase system. The normal blood lactate level in can range from 0.5 to 1.5 mmol.L<sup>-1</sup> at rest and can elevate to 25 mmol.L<sup>-1</sup> during excretion. The monitoring of lactate homeostasis is vital to clinical diagnostics and sports medicine.<sup>54</sup>

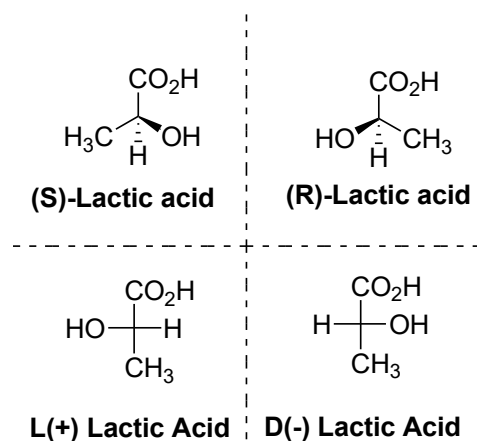
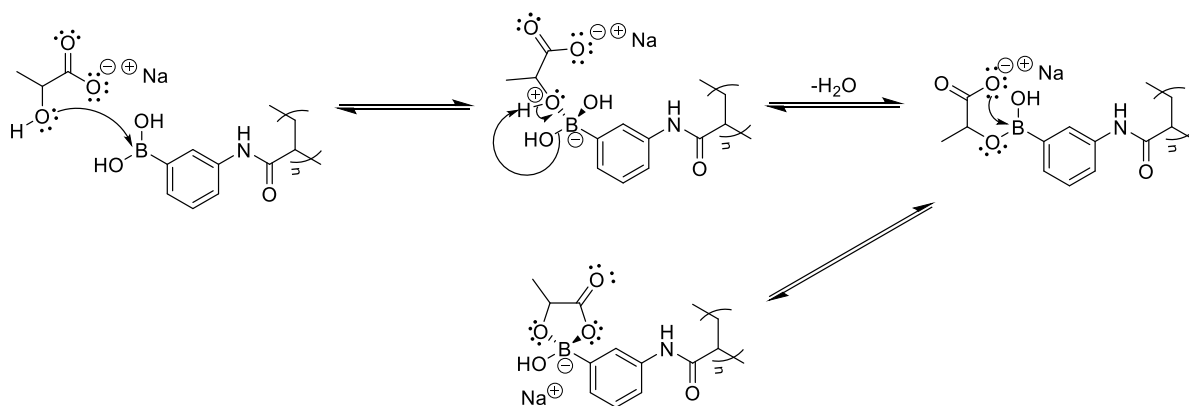


**Figure 1.5:** Stereoisomers of lactic acid with two enantiomers.

Lactate is regarded as bidentate salt, which can reversibly complex with BA at neutral physiological pH. Lactate is carboxylate anion (Lewis Base) at physiological pH, hence favouring the complexation over a diol, such as glucose. Pizer *et al.* was the first to postulate the binding mechanism (Scheme 1.26) by which  $\alpha$ -hydroxy acids reacted with the trigonal planar boronic acid (Lewis acid) through initial attack on the boron empty p-orbital by the hydroxyl oxygen lone pair of electrons, followed by ring closure via dehydration.<sup>55-57</sup>



**Scheme 1.26:** Mechanism for L-lactate binding to poly(3-BAPhA) at pH 7.4

Sartain *et al.* in 2006 found that the incorporation of 3-BAPhA into an acrylamide hydrogel produced the largest response toward L-lactate.<sup>55</sup>  $pK_a$  for 2, 3 and 4-BAPhA is 10.48, 8.87 and 8.93 respectively (Fig. 1.6).<sup>55</sup> A higher affinity to L-lactate was identified in comparison to glucose due to a reduced number of receptor sites at which complexation can occur and the rigid less acidic character of glucose compared to L-lactate. Lowe and co-workers in 2008,

utilized  $^{11}\text{B}$  and  $^1\text{H}$  NMR spectroscopy to verify the addition of L-lactate to 3-BAPhA at pH 7.4.<sup>56</sup>

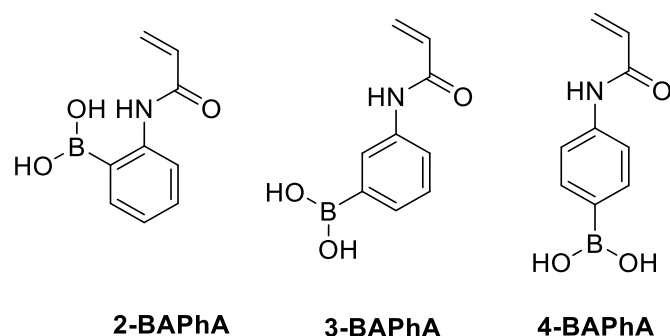


**Figure 1.6:** Substitution of BAPhA

There are two possible structures for 2-BAPhA (Fig. 1.7), which would make controlled/living radical polymerization unfeasible for this monomer, as the ring-closed structure would not stabilize the propagating radical using the acrylamide carbonyl. The internal coordination at neutral and acidic pH is used in self-healing hydrogels.<sup>58</sup>

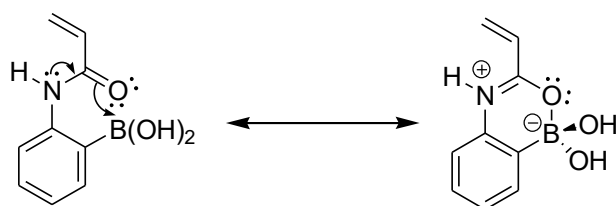


**Figure 1.7:** Resonance structures for 2-BAPhA

### 1.5 Overall Thesis Aims and Objectives

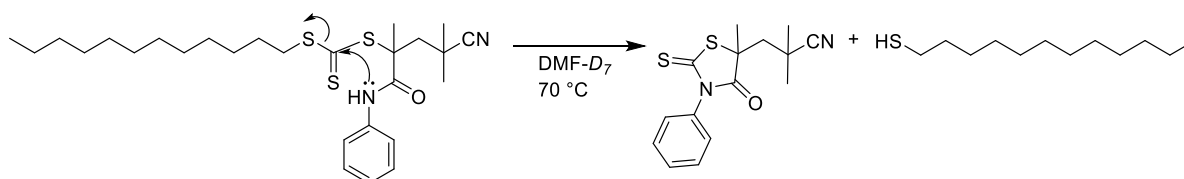
At the start of this PhD, there was no reported polymerization induced self-assembly (PISA) of BA-substituted block copolymers using— see Chapter 3). There were no reports of lactate responsive diblock copolymers. Thus, overall aims were to achieve the first PISA of BA-substituted monomers, as well as develop new synthetic methods for BA-substituted diblock copolymers for use in glucose and lactate response. Lactate (despite its physiological importance) seems to have been overlooked, and aim was to establish response towards nanoparticles under physiological (neutral pH) conditions. The optimizing of RAFT conditions for controlled/living polymerization of a variety of protected and free-BA substituted acrylamides (Chapter 2). The synthetic protocols established in Chapter 2 helped us to

develop the new one-pot iterative RAFT polymerizations of 3-BAPhA in Chapters 4 and 5. The final aim was to use lactate and glucose to induce self-assembly of multi-block hydrophobic block copolymers.

## Chapter 2: SYNTHESIS and RAFT-MEDIATED POLYMERIZATION of BORONIC ACID and PINACOL ESTER SUBSTITUTED DERIVATIVE MONOMERS USING DMP and AIBN

### 2.0 Introduction

Sumerlin *et al.* reported the controlled/living RAFT polymerization of 3-(acrylamidophenyl)boronic acid (3-BAPhA) in DMF (5% aq.) at 70 °C using 2-(dodecylthiocarbonothioylthio)-2-methylpropionic acid (DMP) and 2,2'-azobis(2-methylpropionitrile) (AIBN) (see section 1.3.4).<sup>5,6</sup> RAFT polymerization at 70 °C of *N*-arylmethacrylamides however leads to loss of livingness through degradation of the RAFT end-group. During the RAFT polymerization, Abel and McCormick described an intramolecular cyclization with elimination of the alkylsulfide from the trithiocarbonate end-group (Scheme 2.1).<sup>59</sup> Chalmers *et al.* described the use of acid to quaternize the acrylamide amide-nitrogen and prevent end-group degradation in the RAFT polymerization of *N*-[(cycloalkylamino)methyl]acrylamides at 70 °C.<sup>46</sup>



**Scheme 2.1:** Abel and McCormick degradation of the RAFT end-group

### 2.1 Chapter Aims and Objectives

- To assess control/living character for the RAFT-mediated polymerization of *N*-phenylacrylamide (PhA) at 70 °C using DMP and AIBN, as RAFT agent and azo initiator respectively.
- To compare the RAFT-mediated polymerization of PhA with 3-BAPhA under analogous conditions.
- To compare the RAFT-mediated polymerization of 3-BAPhA with the pinacol ester protected analogue (3-BAEPhA).
- To compare control/living character for RAFT of 3-BAEPhA with the 4-pinacol ester isomer (4-BAEPA).

The monomers, RAFT agent and azo initiator used are displayed in Fig 2.1.

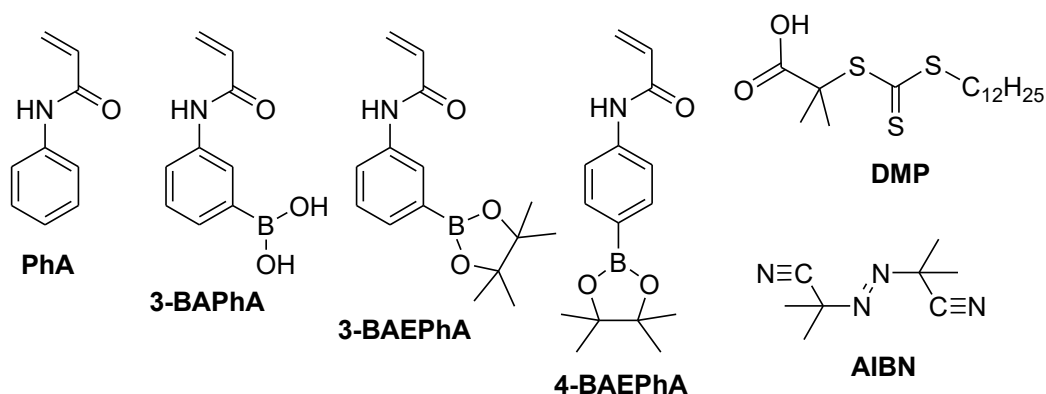
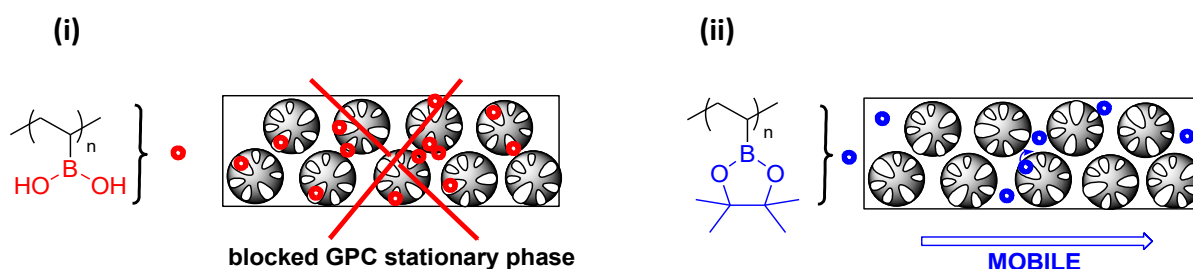


**Fig. 2.1:** Structures of the main chemicals used in this Chapter.

Investigated RAFT polymerization of the pinacol ester protected BAs, because of ease of (direct) GPC analysis, since BA-substituted polymers cannot undergo direct GPC analysis due to binding to the column (Scheme 2.2).<sup>9-11</sup>



**Scheme 2.2:** GPC stationary phase (i) blocked (ii) elution with pinacol-protected polymer

## 2.2 Experimental

### 2.2.1 Materials

2-(Dodecylthiocarbonothioylthio)-2-methylpropionic acid (DMP; TCI, >98%) and 2,2'-azobis(2-methylpropionitrile) (AIBN; Sigma Aldrich, 98%) were used as received. Milli-Q water, ethyl acetate (EtOAc; VWR,  $\geq 99\%$ ), diethyl ether ( $\text{Et}_2\text{O}$ ; Fisher, >99.5%), anisole (TCI, >99%), tetrahydrofuran (THF; Fisher, >99.8%), and *N,N*-dimethylformamide (DMF; VWF, HPLC-grade  $\geq 99.9\%$ ) were used directly as solvents. 3-Aminophenylboronic acid (Fluorochem, 97%), 3-acrylamidophenylboronic acid pinacol ester (Fluorochem, 99%), 4-acrylamidophenylboronic acid pinacol ester (Alfa Aesar, 98%), acryloyl chloride (Alfa Aesar,

96%), NaHCO<sub>3</sub> (Fisher Scientific, >99.7%) and anhydrous Na<sub>2</sub>CO<sub>3</sub> (Alfa Aesar, 99.5%) were used as received. CH<sub>2</sub>Cl<sub>2</sub> (VWR, ≥99.8%) was distilled over CaH<sub>2</sub> (Alfa Aesar, 90-95%).

## 2.2.2 Instruments and Measurements

### 2.2.2.1 General

Melting points were measured on a Stuart Scientific melting point apparatus SMP1.

### 2.2.2.2 Nuclear Magnetic Resonance (NMR) Spectroscopy

NMR spectra were recorded using a Bruker Avance II 400 MHz spectrometer. The chemical shifts are in ppm relative to Me<sub>4</sub>Si. <sup>13</sup>C NMR spectra at 100 MHz are with complete proton decoupling. NMR assignments are supported by distortionless enhancement by polarization transfer (DEPT).

#### 2.2.2.2.1 Conversion Measurements

Conversion was measured using <sup>1</sup>H NMR spectroscopy by comparing the monomer content at 2 h to the monomer content before polymerization. An accurately weighed amount of anisole (~0.350 g) is dissolved in EtOH (for dispersion polymerizations) or in DMF (for solution polymerizations) (10 mL) to make standardized solution. A polymerization sample (20 μl), external standard (anisole standardized, 20 μl), and D<sub>6</sub>-DMSO (460 μl) are mixed in the NMR tube for conversion analysis. Conversion is calculated by comparing the anisole peak integral (representing the standardized solution) at 3.75 ppm (OMe, 3H) to the integral for the monomer (*cis*-vinyl, 1H) at 5.74 (3-BAPhA), 5.76 (3-BAEPPhA) or 5.72 (4-BAEPPhA) ppm. Theoretical number average molecular weight ( $M_{n,th}$ ) was calculated according to Eq. (2.1):

$$M_{n,th} = \left[ \left( \frac{[Monomer]_0}{[RAFT\ Agent]_0} \right) \times MW_{Monomer} \times conversion \right] + MW_{[RAFT\ Agent]} \quad (2.1)$$

#### 2.2.2.3 Gel Permeation Chromatography (GPC)

Molar mass distributions were measured using Agilent Technologies 1260 Infinity liquid chromatography system with Agilent GPC/SEC Software for Windows (version 1.2; Build 3182.29519) using a Polar Gel-M guard column (50 × 7.5 mm) and two Polar Gel-M columns (300 × 7.5 mm). DMF containing LiBr (0.01 molL<sup>-1</sup>) was used as eluent at 1.0 mL·min<sup>-1</sup> at 60 °C. Twelve narrow polydispersity poly(styrene, St) standards (Agilent, 580-301,600 gmol<sup>-1</sup>, *D* = 1.05) were used to calibrate the GPC system. Samples were dissolved in the eluent and

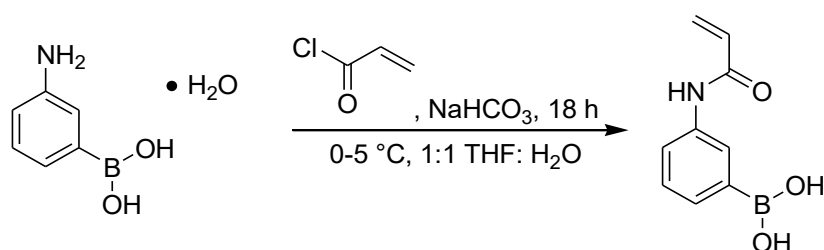
filtered through a PTFE membrane with 0.22  $\mu\text{m}$  pore size before injection (100  $\mu\text{L}$ ). Number average molecular weight ( $M_n$ ) values are not absolute, but relative to linear poly(St) standards (as above).

#### 2.2.2.4 Preparation of GPC sample

Molecular sieves (MS, Alfa Aesar, 3  $\text{\AA}$ , 0.800 g) were activated three times by microwave (Toshiba ER-7620 650 W) for 2 min periods at medium power, with 30 s swirling aeration intervals.<sup>60</sup> Pinacol (TCI, >98%, 0.148 g, 1.250 mmol) in  $\text{CHCl}_3$  (Fisher, >99.8%, 5.00 mL) and the polymerization sample (20  $\mu\text{L}$ ) were added to the activated MS, and stirred for 24 h, at room temperature. MS were removed using gravity filtration, and the solution evaporated to a residue, which was dissolved in 1 mL of the GPC eluent.

### 2.2.3 Preparation of Boronic Acid-Substituted Phenylacrylamides

#### 2.2.3.1 Preparation of 3-(acrylamidophenyl)boronic acid (3-BAPhA): *N*-acryloyl-3-aminophenylboronic acid



**Scheme 2.3:** Synthesis of 3-BAPhA

Acryloyl chloride (3.4 mL, 3.77 g, 41 mmol) was added to 3-aminophenylboronic acid monohydrate (3.16 g, 20 mmol) and sodium bicarbonate (3.36 g, 40 mmol) in a 1:1 THF:H<sub>2</sub>O (80 mL) at 0–5 °C. The solution was stirred at room temperature for 18 h (Scheme 2.3) and the organic solvent evaporated, and the aqueous residue filtered using a sinter funnel. The residue was stirred in EtOAc (50 mL) for 2 h. The organic layer was washed with water (50 mL), saturated sodium bicarbonate solution (50 mL), water (50 mL) and brine (50 mL). The combined organic layers were dried ( $\text{MgSO}_4$ ), evaporated to dryness and the brown residue recrystallized twice from hot water and the needles dried under vacuum, 3-BAPhA (mp 146 - 148 °C, mp<sup>61</sup>148 °C). Isolated = 3.195 g (82%) (Fig. 2.2).



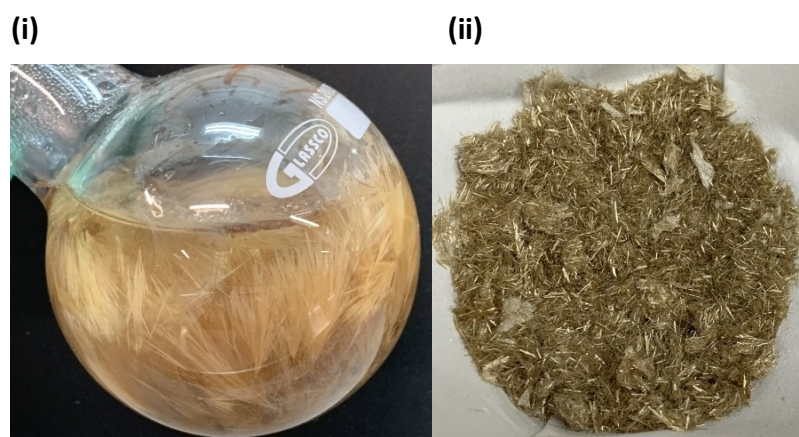


**Figure 2.2:** Prepared 3-BAPhA (i) recrystallization in hot water (ii) needles of purified product

$^1\text{H}$  NMR spectrum of 3-BAPhA:  $\delta_{\text{H}}$  (400 MHz) ( $D_6$ -DMSO)  $\delta$  = 5.74 (dd,  $J$  = 10.1, 2.0 Hz, 1H, *cis*-H), 6.25 (dd,  $J$  = 17.0, 2.0 Hz, 1H, *trans*-H), 6.46 (dd,  $J$  = 17.0, 10.1 Hz, 1H), 7.29 (t,  $J$  = 7.7 Hz, 1H), 7.49 – 7.52 (m, 1H), 7.81 – 7.83 (m, 1H), 7.89 (s, 1H, 2-H), 8.01 (s, 2H, B-OH), and 10.06 (s, 1H, NH).  $^{13}\text{C}$  NMR spectrum of 3-BAPhA:  $\delta_{\text{C}}$  (100 MHz) ( $D_6$ -DMSO), 121.8 (CH), 125.8 (CH), 127.1 ( $\text{CH}_2$ ), 128.2 (CH), 129.8 (CH), 132.5 (CH), 135.4 (C), 138.6 (C), and 163.5 (C=O) (Fig. 2.3).

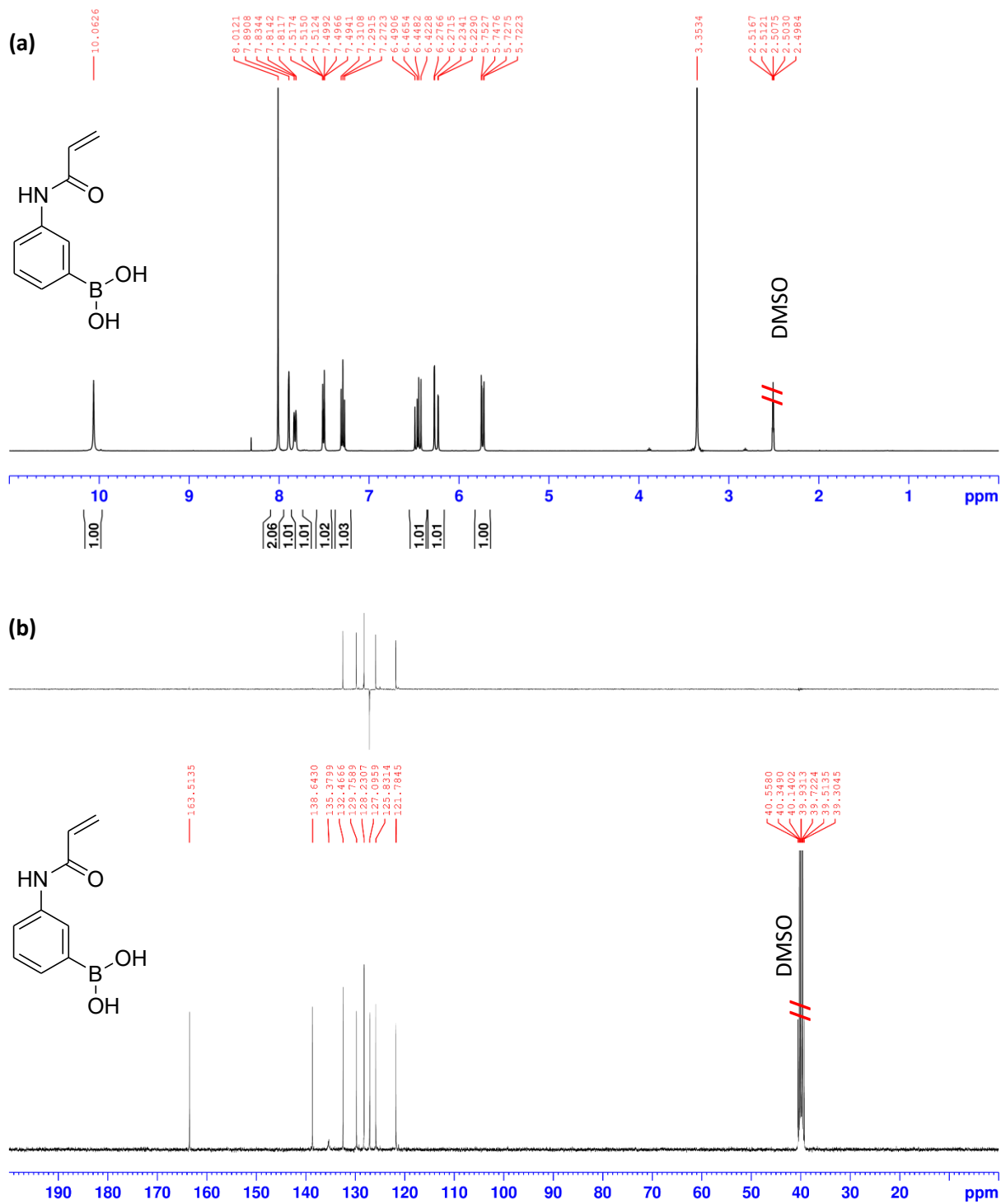
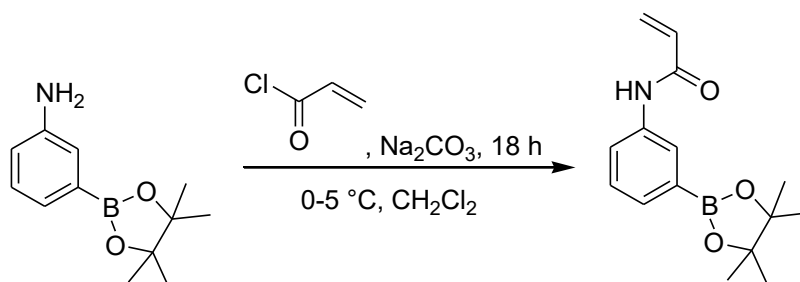


Figure 2.3: (a)  $^1\text{H}$  NMR and (b)  $^{13}\text{C}$  NMR of 3-BAPHA in  $\text{DMSO-}D_6$

### 2.2.3.2 Preparation of 3-(acrylamidophenyl)boronic acid pinacol ester (3-BAEPhA): *N*-(3-(4,4,5,5-tetramethyl-1,3,2-dioxaborolan-2-yl)phenyl)acrylamide



**Scheme 2.4:** Synthesis of 3-BAEPhA

Acryloyl chloride (2.7 mL, 3.00 g, 33 mmol) was added to 3-aminobenzeneboronic acid pinacol ester (6.04 g, 28 mmol) and anhydrous Na<sub>2</sub>CO<sub>3</sub> (3.51 g, 33 mmol) in dry CH<sub>2</sub>Cl<sub>2</sub> (470 mL) at 0–5 °C. The solution was left to stir at room temperature for 18 h (Scheme 2.4). The organic layer was washed with water (50 mL), saturated sodium bicarbonate solution (50 mL), water (50 mL) and brine (50 mL). Organic layer was separated, dried (MgSO<sub>4</sub>), and evaporated to dryness. The residue was dissolved in the minimum amount of EtOAc and precipitated from cold hexane to give off-white crystals. 3-BAEPhA (mp = 166 – 168 °C). *R*<sub>f</sub> = 0.47 (3:1 Pet. Ether: EtOAc); Isolated = 4.560 g (60%) (Fig. 2.4).

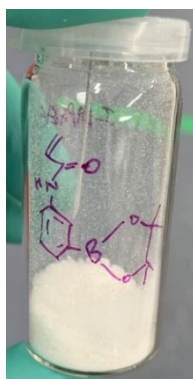


**Figure 2.4:** Recrystallized and dried 3-BAEPhA

<sup>1</sup>H NMR spectrum of 3-BAEPhA:  $\delta_{\text{H}}$  (400 MHz) (*D*<sub>6</sub>-DMSO), 1.30 (s, 12H), 5.76 (dd, *J* = 10.0, 2.1 Hz, 1H, *cis*-H), 6.27 (dd, *J* = 17.0, 2.1 Hz, 1H, *trans*-H), 6.43 (dd, *J* = 17.0, 10.1 Hz, 1H, *vicinal*-H), 7.33 – 7.38 (m, 2H), 7.85 – 7.87 (m, 1H), 7.80 (d, *J* = 2.1 Hz, 1H, 2-H), and 10.17 (s, 1H, NH).

$^{13}\text{C}$  NMR spectrum of 3-BAEPhA:  $\delta_{\text{C}}$  (100 MHz) ( $D_6$ -DMSO), 25.2 ( $\text{CH}_3$ ), 84.2 (C), 122.7 (CH), 125.8 (CH), 127.4 ( $\text{CH}_2$ ), 128.9 (CH), 129.8 (CH), 132.3 (CH), 139.1 (C), and 163.6 (C=O)(Fig. 2.5). A melting point for 3-BAEPhA could not be found in the literature, but is commercially available from TCI Chemicals: CAS 8743634-18-5 Product Number: T3826 with mp = 158-162 °C.

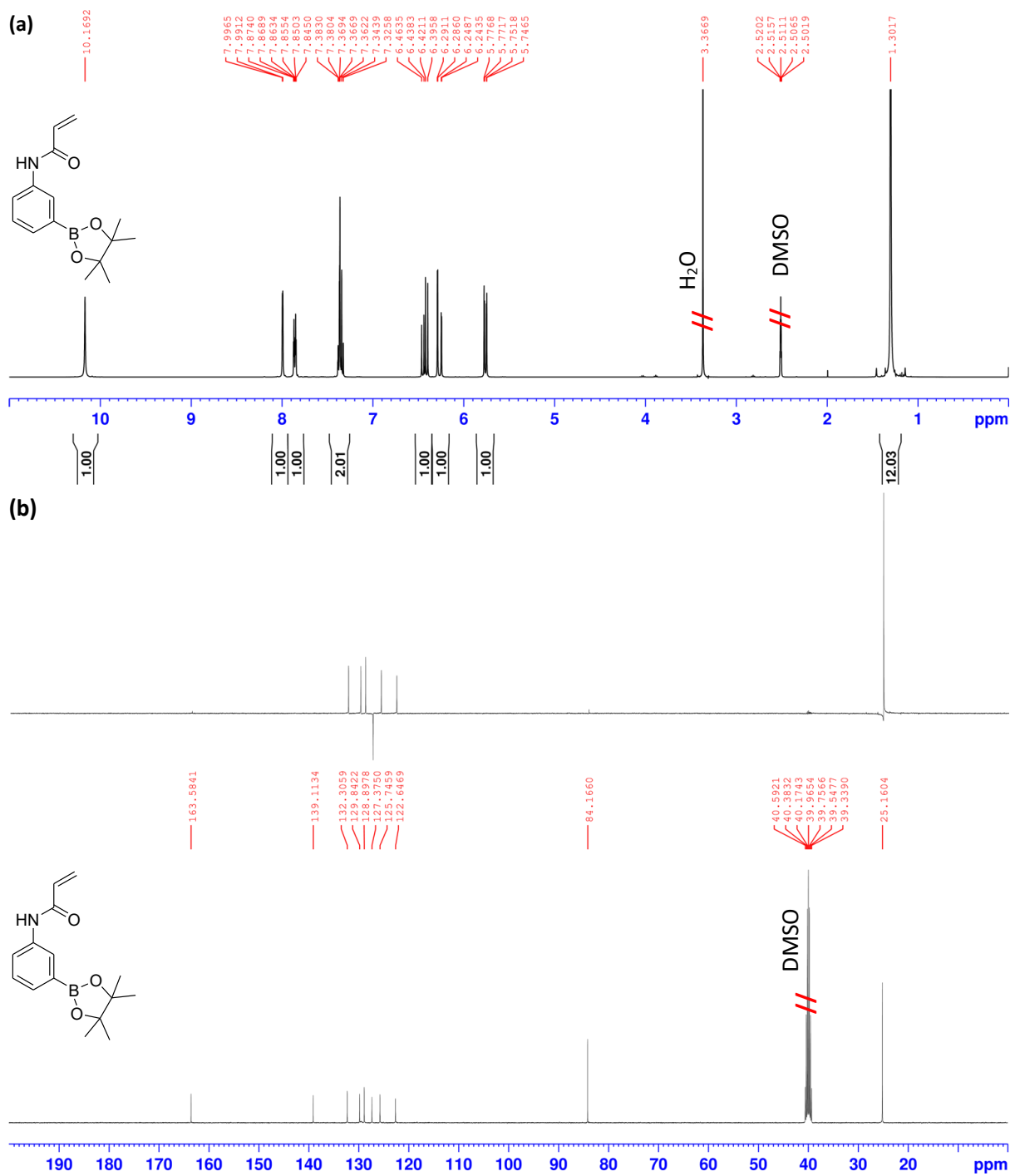
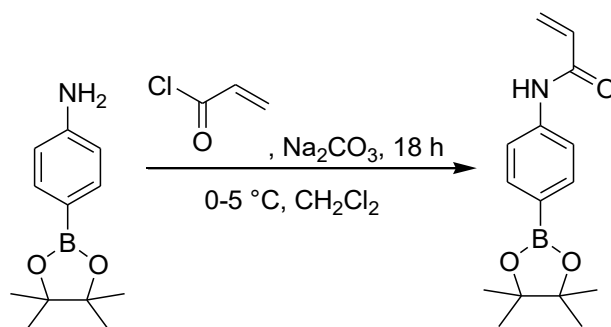


**Figure 2.5:** (a)  $^1\text{H}$  NMR and (b)  $^{13}\text{C}$  NMR of 3-BAEPHa in  $\text{DMSO-}D_6$

### 2.2.3.3 Preparation of 4-(acrylamidophenyl)boronic acid pinacol ester (4-BAEPhA): *N*-(4-(4,4,5,5-tetramethyl-1,3,2-dioxaborolan-2-yl)phenyl)acrylamide



**Scheme 2.5:** Synthesis of 4-BAEPhA

Acryloyl chloride (2.7 mL, 3.00 g, 33 mmol) was added to 4-aminobenzeneboronic acid pinacol ester (6.05 g, 28 mmol) and anhydrous Na<sub>2</sub>CO<sub>3</sub> (3.50 g, 33 mmol) in dry CH<sub>2</sub>Cl<sub>2</sub> (470 mL) at 0–5 °C. The solution was left to stir at room temperature for 18 h (Scheme 2.5). The organic layer was washed with water (50 mL), saturated sodium bicarbonate solution (50 mL), water (50 mL) and brine (50 mL). Organic layer was separated, dried (MgSO<sub>4</sub>), and evaporated to dryness. The residue was dissolved in the minimum amount of EtOAc and precipitated from cold hexane to give off-white crystals. 4-BAEPhA (mp = 148 – 150 °C; mp<sup>62</sup> 157.5 – 158.5 °C). *R*<sub>f</sub> = 0.71 (3:1 Pet. Ether: EtOAc); Isolated = 4.181 g (55%) (Fig. 2.6).



**Figure 2.6:** Recrystallized and dried 4-BAEPhA

<sup>1</sup>H NMR spectrum of 4-BAEPhA:  $\delta_{\text{H}}$  (400 MHz) (CDCl<sub>3</sub>), 1.33 (s, 12H, Pinacol CH<sub>3</sub>), 5.72 (dd, *J* = 1.4 Hz, 10.0 Hz, 1H, *cis*-H), 6.29 (dd, *J* = 10.0 Hz, 16.9 Hz, 1H, *trans*-H), 6.41 (dd, *J* = 1.4 Hz, 16.9 Hz, *vicinal*-H), 7.61 (d, *J* = 8.0 Hz, 2H), 7.76 (d, *J* = 8.4 Hz, 2H), 8.05 (s, 1H, NH). <sup>13</sup>C NMR

spectrum of 4-BAEPhA:  $\delta_{\text{C}}$  (100 MHz) ( $\text{CDCl}_3$ ), 24.9 ( $\text{CH}_3$ ), 83.8 (C), 118.9 (CH), 128.0 ( $\text{CH}_2$ ), 131.2 (CH), 135.8 (CH), 140.5 (C) and 163.8 (C=O) (Fig. 2.7).

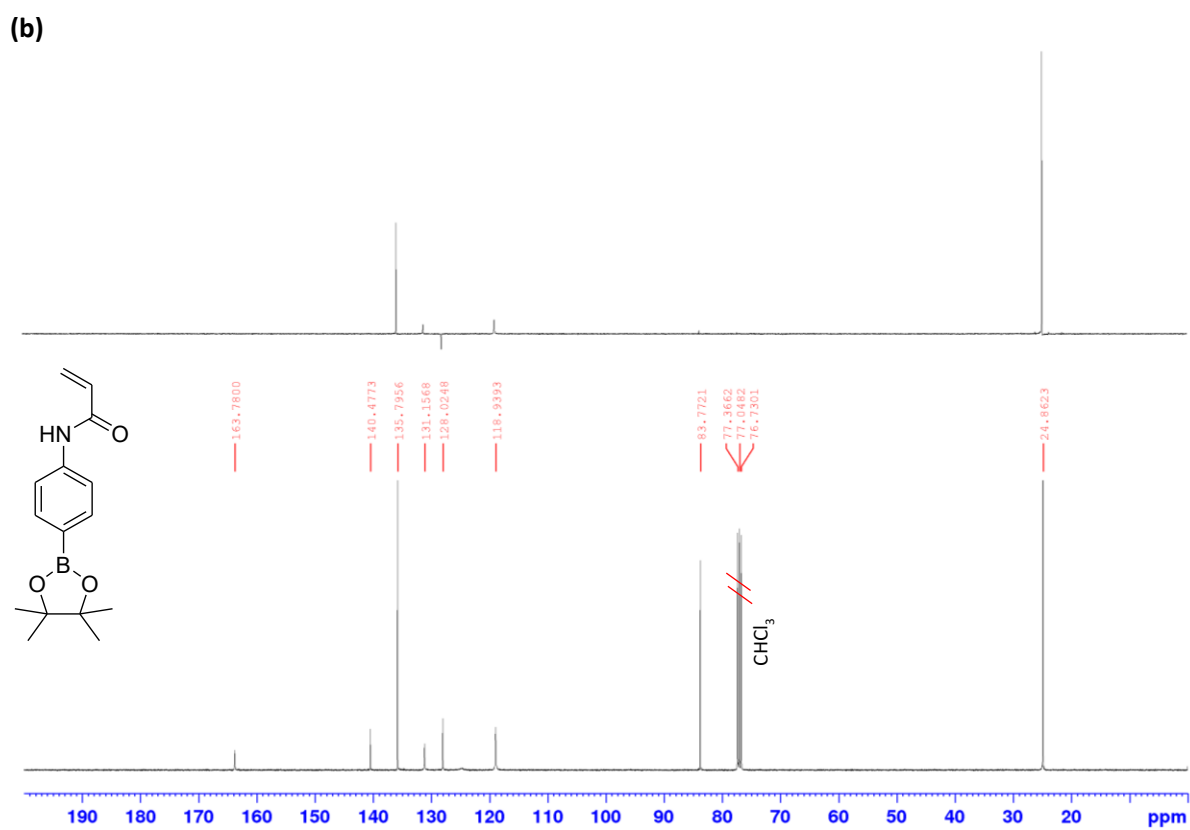
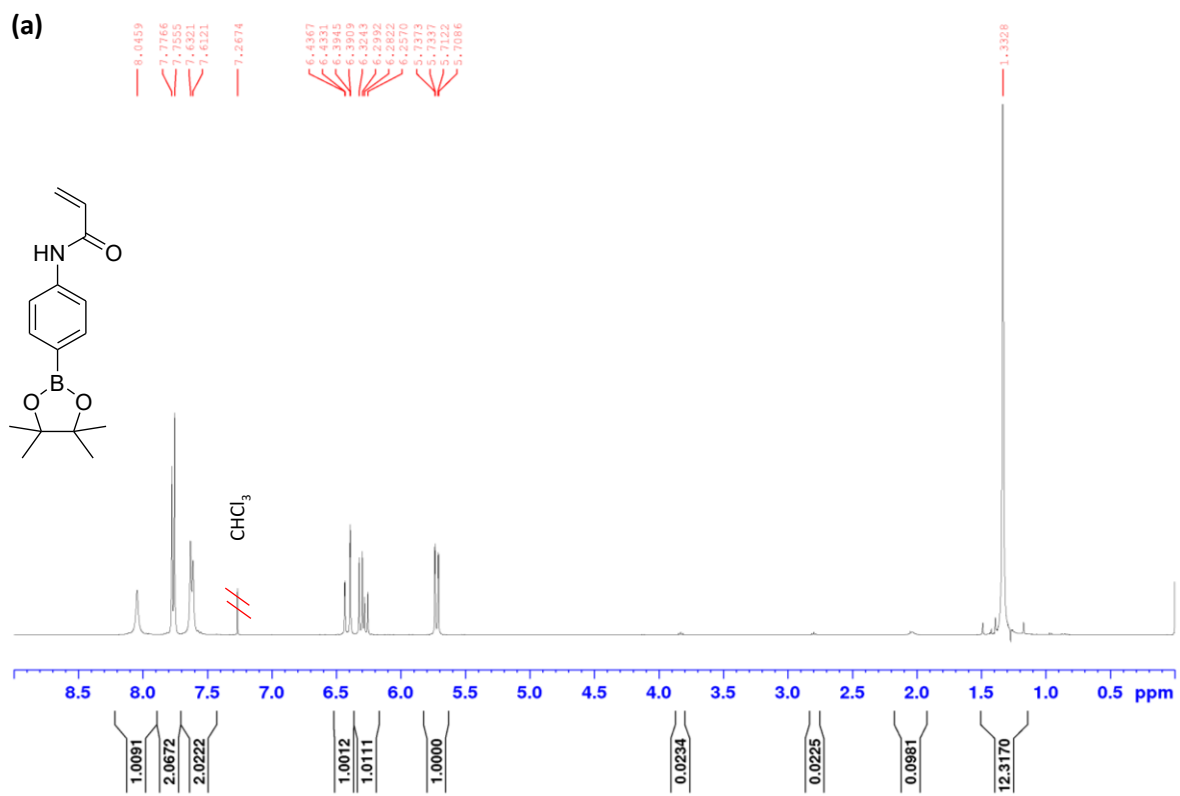


Figure 2.7: (a) <sup>1</sup>H NMR and (b) <sup>13</sup>C NMR of 4-BAEPHa in CDCl<sub>3</sub>



## 2.2.4 Polymerization Procedures

### 2.2.4.1 Polymerization Equipment

All polymerization solutions were added to test tubes (Biotage microwave tubes 10 mL 100 x 18 mm), placed in a constant temperature aluminum heating block at 70 °C. Test tubes were sealed with rubber septum containing a nitrogen balloon. Polymerization were stopped by quenching in an ice-water bath.

### 2.2.4.2 RAFT Polymerizations of 1 M PhA

For the  $[\text{PhA}]_0/[\text{DMP}]_0/[\text{AIBN}]_0 = 150/1/0.22$ : A standardized solution of AIBN and DMP ( $1.48 \times 10^{-3} \text{ molL}^{-1}$  and  $6.66 \times 10^{-3} \text{ molL}^{-1}$ , respectively) in a volumetric flask was prepared using serial dilution. AIBN (61 mg, 0.37 mmol) was diluted 25 times with DMF and 1 mL was added to DMP (24.2 mg, 0.066 mmol), and topped up to 10 mL with DMF in a volumetric flask. The latter standardized solution (1 mL) was added to PhA (0.147 g, 1.00 mmol). The polymerization was sampled (20  $\mu\text{L}$ ) for conversion (NMR at time = 0), and the reaction heated at 70 °C for 3 h with periodic sampling (20  $\mu\text{L}$ ) for conversion and GPC measurements (Fig. 2.8).

For  $[\text{PhA}]_0/[\text{DMP}]_0/[\text{AIBN}]_0 = 100/1/0.15$  and  $50/1/0.075$ , only the amount of DMP is varied.

For  $[\text{PhA}]_0/[\text{DMP}]_0/[\text{AIBN}]_0 = 100/1/0.15$ , DMP (36.3 mg, 0.099 mmol) gave a concentration of DMP =  $9.96 \times 10^{-3} \text{ mmol}$ .

For  $[\text{PhA}]_0/[\text{DMP}]_0/[\text{AIBN}]_0 = 50/1/0.075$ , DMP (72.6 mg, 0.20 mmol) gave a concentration of DMP =  $0.0199 \text{ mmol}^{-1}$ .

### 2.2.4.3 RAFT Polymerizations of 1 M 3-BAPhA

The serial dilution used AIBN (61 mg, 0.37 mmol) dissolved in 5% aq. DMF (25 mL), from which 1 mL is taken and added to DMP (37 mg, 0.1 mmol) to make a 5% aq. DMF solution (10 mL). A solution polymerization of 3-BAPhA (0.191 g, 1.00 mmol), DMP ( $0.01 \text{ molL}^{-1}$  from serial dilution), AIBN ( $1.48 \times 10^{-3} \text{ molL}^{-1}$  from serial dilution) in 5% aq. DMF (1.00 mL) was heated at 70 °C for specific times (Fig. 2.9). Conversion was determined by  $^1\text{H}$  NMR (see RAFT of PhA) and GPC required pinacol protection (see section 2.2.2.4).

### 2.2.4.4 RAFT Polymerizations of 1 M 3-BAEPPhA

The serial dilution used AIBN (61 mg, 0.37 mmol) dissolved in DMF (25 mL), from which 1 mL is taken and added to DMP (37 mg, 0.1 mmol) to make a DMF solution (10 mL). A solution

polymerization of 3-BAEPHA (0.273 g, 1.00 mmol), DMP ( $0.01 \text{ molL}^{-1}$  from serial dilution), AIBN ( $1.48 \times 10^{-3} \text{ molL}^{-1}$  from serial dilution) in DMF (1.00 mL) were heated at 70 °C for specific times (Fig. 2.10). Conversion was determined by  $^1\text{H}$  NMR and GPC analysis does not require pinacol ester protection.

#### 2.2.4.5 Polymerizations of 2.5 M Monomers

The serial dilution used AIBN (61 mg, 0.37 mmol) dissolved in DMF (25 mL), from which 1 mL is taken and added to DMP (37 mg, 0.1 mmol) to make a DMF solution (10 mL). Stock solutions of AIBN and DMP at 250-fold and 10-fold dilution were used. A solution polymerization of PhA (0.367 g, 2.5 mmol), 3-BAEPHA or 4-BAEPHA (0.367 g, 2.5 mmol) with DMP (0.049 mmol) and AIBN ( $1.48 \times 10^{-3} \text{ mmol}$ ) in DMF (1.00 mL) were heated at 70 °C for set times. The test tube was placed on ice to quench the polymerization prior to NMR and GPC analysis (see in section 2.2.2.4).

## 2.3 Results and Discussion

### 2.3.1 Synthesis of Monomers

3-BAPhA was prepared using acryloyl chloride, 3-aminophenylboronic acid monohydrate and sodium bicarbonate (3.36 g, 40 mmol) in a 1:1 THF:H<sub>2</sub>O (Scheme 2.3).<sup>11</sup> For the pinacol-protected monomers, 3-BAPhA and 4-BAPhA, 3 and 4-aminobenzeneboronic acid pinacol esters were respectively used with acryloyl chloride, but anhydrous conditions were employed in order to prevent hydrolysis of the protecting group (Schemes 2.4 and 2.5). Anhydrous Na<sub>2</sub>CO<sub>3</sub> replaced NaHCO<sub>3</sub> as the base in the condensation reaction, according to the procedure reported by Sumerlin *et al.*<sup>5</sup> 3-BAPhA was the easiest to prepare in 82% yield, while 3-BAPhAE and 4-BAPhAE were prepared in 60 and 55% yield respectively.

### 2.3.2 RAFT Polymerizations

#### 2.3.2.1 RAFT of PhA

Initial investigations examined the polymerization of 1 M *N*-phenylacryamide (PhA) in DMF at 70 °C using DMP and AIBN as the RAFT agent and azo initiator respectively. Three different degree of polymerization *D*P<sub>s</sub> (= 50, 100 and 150) were targeted (Fig 2.8). All three polymerization systems proceed at similar rates, indicating that the chain transfer is faster than propagation, even at the highest RAFT agent concentration. In a degenerative chain

transfer system, such as RAFT, the amount of dead chains is determined by the amount of initiator decomposed throughout the polymerization,<sup>63</sup> so as you increase  $DP$ , the relative fraction of AIBN-derived chains increases, so increasing the size of the low MW tail at high conversion (noticeable at  $DP = 150$ ). It follows that molecular weight distributions were narrowest at the lowest  $DP$ , but in all cases dispersity,  $\mathcal{D}$  increased almost linearly with conversion. At the lowest targeted,  $DP = 50$ ,  $M_n$  values were as predicted by the  $[\text{PhA}]_0/[\text{DMP}]_0$  ratio up to 81% conversion, but the polymerizations for  $DP = 100$  and  $150$ , deviated from the  $M_{n,\text{th}}$  line towards lower values at intermediate conversions. This is due to an increase in the number of low MW (dead) chains, lowering the  $M_n$ .

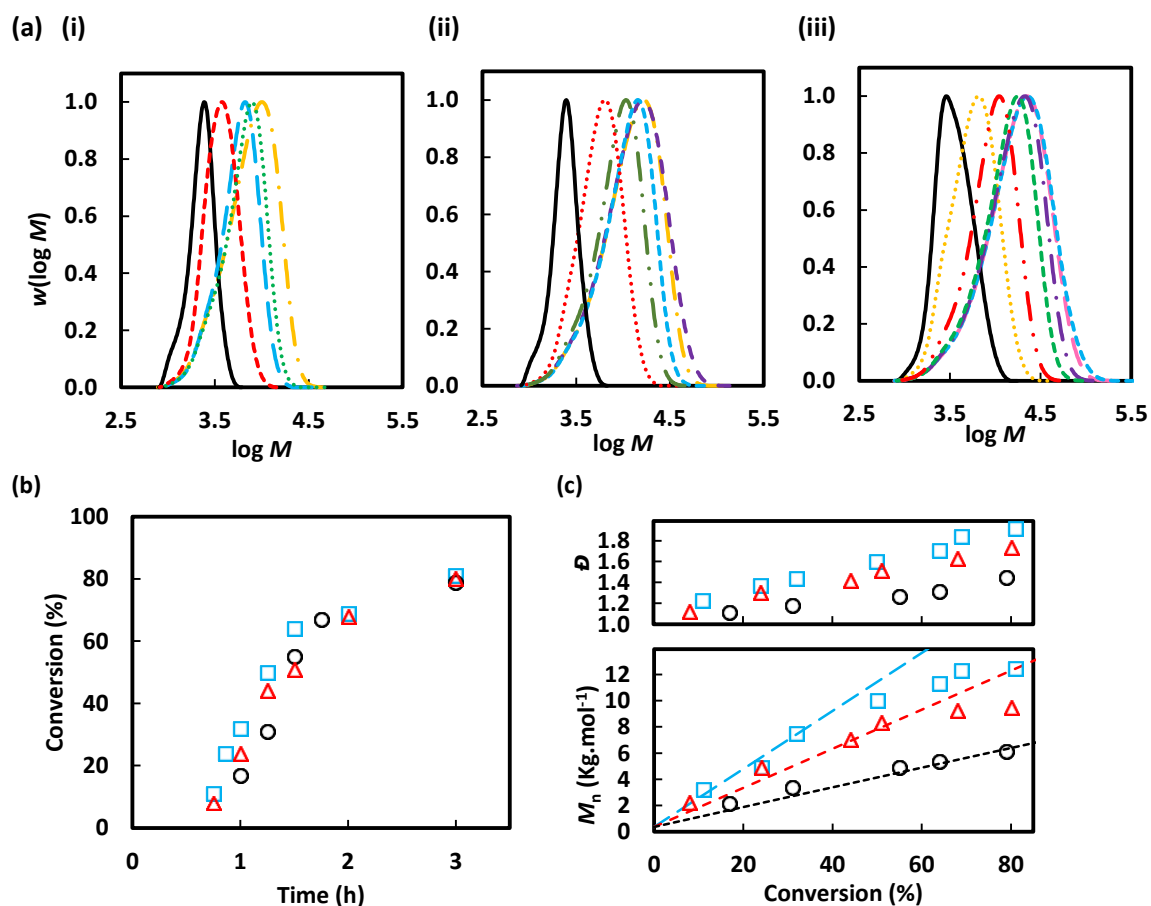


**Figure 2.8.** RAFT polymerization at 70 °C of 1 M PhA in DMF with  $[\text{PhA}]_0/[\text{DMP}]_0/[\text{AIBN}]_0 = 50/1/0.075$  (circles),  $100/1/0.15$  (triangles) and  $150/1/0.22$  (squares). **(a)** MWDs for  $DP = 50$ , 100 and 150 respectively and correspond to conversions at **(i)** 17% (1 h), 31% (1.25 h), 55% (1.5 h), 67% (1.75 h) and 79% (3 h) **(ii)** 8% (0.75 h), 24% (1 h), 44% (1.25 h), 51% (1.5 h), 68% (2 h) and 80% (3 h), and **(iii)** 11% (0.75 h), 24% (0.87 h), 32% (1 h), 50% (1.25 h), 64% (1.5 h), 69% (2 h) and 81% (3 h). **(b)** Conversion versus time plot. **(c)**  $M_n$  and  $\bar{D}$  vs. conversion with  $M_{n,\text{th}}$  lines calculated according to Eq (1).

### 2.3.2.2 Comparing the RAFT polymerization of 3-BAPhA to PhA

3-BAPhA and PhA were polymerized using  $[3\text{-BAPhA}]_0/[DMP]_0/[AIBN]_0 = 100/1/0.15$  with the 3-BA substituted monomer polymerizing faster reaching 93% conversion, while PhA reached 80% conversion in the same time period (of 3 h) (Fig. 2.9). MWDs appeared broader for the polymerization of 3-BAPhA ( $\mathcal{D} = 1.35\text{-}1.75$ ) compared to PhA (1.11-1.22), with some bimodality up to 42% conversion, and  $\mathcal{D}$  lowering at the highest conversions for the polymerizations of 3-BAPhA. The bimodality at low conversions, may be due to some polymer chains residing at the pre-equilibrium stage, while others are at main equilibrium (RAFT mechanism, Scheme 1.15).<sup>64</sup> Thereafter  $M_n$  increased linearly with conversion for 3-BAPhA, but were significantly lower than theoretical values predicted by Eq 1. In contrast the poly(PhA)  $M_n$  values were close to the  $M_{n,\text{th}}$  line, signifying GPC calibration error against linear polystyrene standards was more significant for the 3-BA substituted monomer. Note that GPC analysis is after pinacol protection to convert poly(3-BAPhA) to poly(3-BAEPHA).

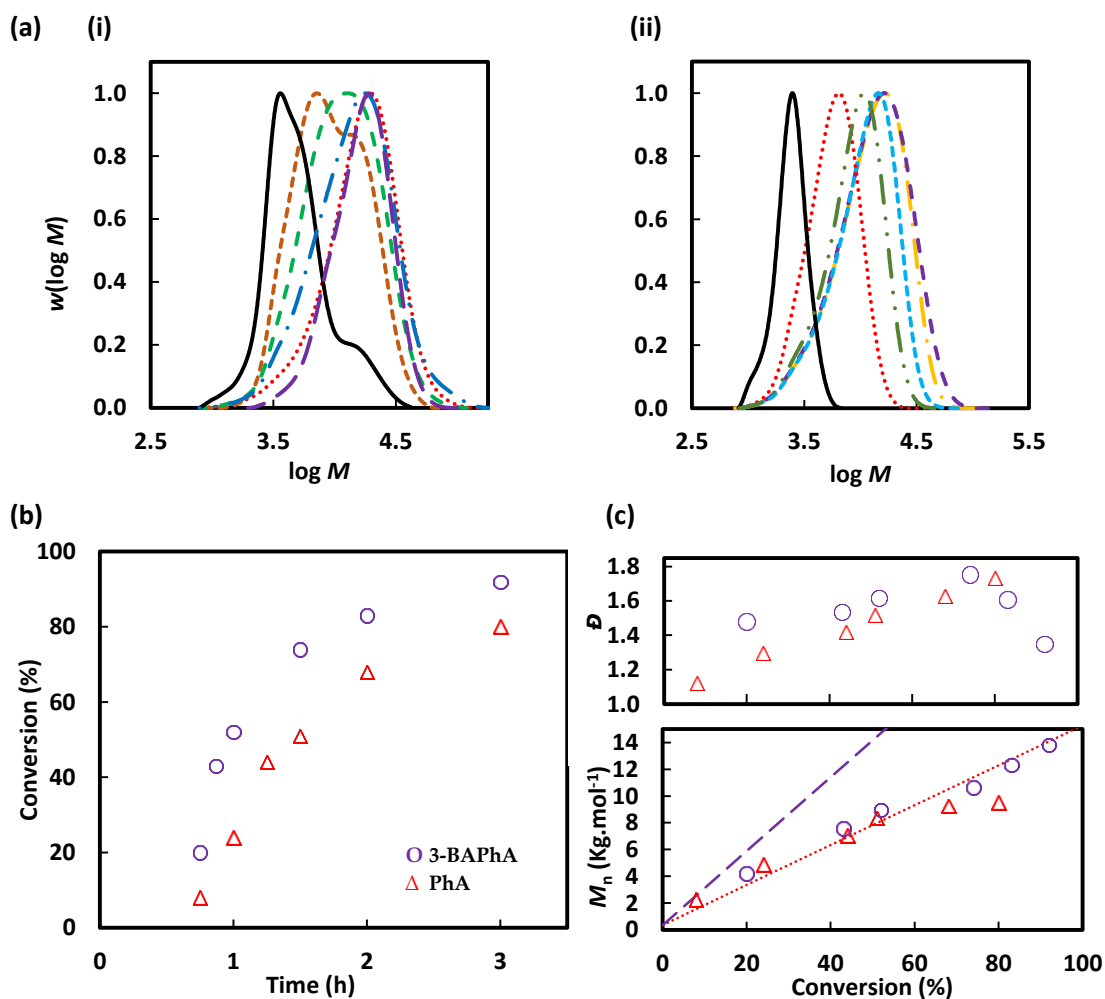


**Figure 2.9:** RAFT polymerization at 70 °C of 1 M 3-BAPhA (circles) and PhA (triangles) in DMF with  $[\text{Monomer}]_0/[\text{DMP}]_0/[\text{AIBN}]_0 = 100/1/0.15$  (a) MWDs correspond to conversions for 3-BAPhA and PhA respectively, at (i) 8% (0.75 h), 24% (1 h), 44% (1.25 h), 51% (1.5 h), 68% (2 h) and 80% (3 h), and (ii) 20% (0.75 h), 43% (0.87 h), 52% (1 h), 74% (1.5 h), 83% (2 h) and 92% (3 h). (b) Conversion versus time plot. (c)  $M_n$  and  $\bar{D}$  vs. conversion with  $M_{n,th}$  lines for 3-BAPhA and PhA (dashed and dotted line respectively) calculated according to Eq (1).

### 2.3.2.3 Comparing the RAFT polymerization of 3-BAPhA to 3-BAEPhA

The pinacol-protected BA (3-BAEPhA) monomer was investigated with the advantage of direct GPC analysis of the resultant polymer. The RAFT polymerization at 70 °C of 3-BAPhA was compared with 3-BAEPhA using  $[\text{Monomer}]_0/[\text{DMP}]_0/[\text{AIBN}]_0 = 100/1/0.15$  (Fig. 2.10). The outcome was overlapping time versus conversion and  $M_n$  versus conversion data, indicating similar rates of polymerization and similar control/living character. However, the 3-BAPhA polymerization MWDs were consistently broader ( $\mathcal{D} = 1.48\text{-}1.61$ ) than for the pinacol derivative ( $\mathcal{D} = 1.13\text{-}1.14$ ). This indicates that protection of the BA moiety allows marginally better control/living character, possibly due to boroxine formation with 3-BAPhA despite 5% water in DMF use as the polymerization solvent (see Chapter 3).

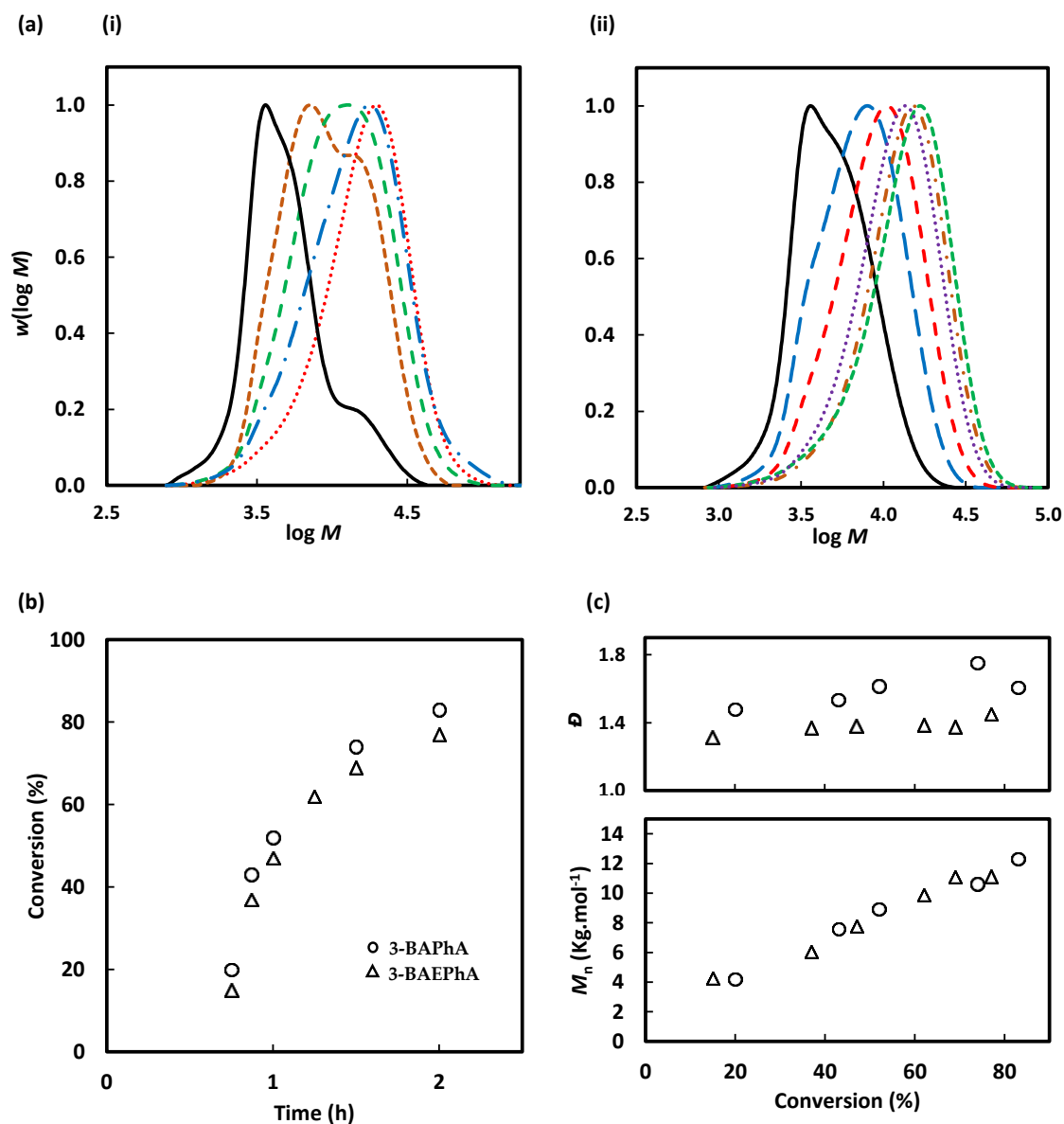


**Figure 2.10:** RAFT-mediated homogeneous polymerizations at 70 °C of 3-BAPhA and 3-BAEPhA (1 M) in 5% aqueous DMF and DMF, respectively, using  $[\text{Monomer}]_0/[\text{DMP}]_0/[\text{AIBN}]_0 = 100/1/0.15$ . **(a)** MWDs correspond to conversions at **(i)** 3-BAPhA: 20% (0.75 h), 43% (0.87 h), 52% (1 h), 74% (1.5 h) and 83% (2 h), and **(ii)** 3-BAEPhA: 15% (0.75 h), 37% (0.87 h), 47% (1 h), 62% (1.25 h), 69% (1.5 h), and 77% (2 h). **(b)** Conversion versus time plot, and **(c)**  $M_n$  and  $\bar{D}$  (after pinacol protection for 3-BAPhA) vs. conversion. Note that points represent individual experiments at different times (not sampling of polymerizations).



#### 2.3.2.4 Comparing the RAFT polymerization of pinacol esters (3-BAEPhA and 4-BAEPhA)

RAFT polymerizations were carried out using 2.5 M monomer concentrations in DMF using  $[\text{Monomer}]_0/[\text{DMP}]_0 = 50$  (Fig. 2.11). Each data point represents a separate polymerization reaction. The RAFT polymerization of 3-BAEPhA proceeds at the same rate as PhA, reaching 92% conversion in 3 h. The RAFT polymerization of 4-BAEPhA is about five times slower reaching 18% in 3 h and 72% conversion after 24 h. This difference in rate for isomers of the BA pinacol ester monomer (BAEPhA) is independent of the RAFT process. This was inferred by carrying out conventional radical polymerizations (in the absence of the RAFT agent) for 3-BAEPhA and 4-BAEPhA, which demonstrated the same trend in rate. The RAFT of 3-BAEPhA ( $\mathcal{D} = 1.19\text{-}1.21$ ) produced wider MWDs than 4-BAEPhA ( $\mathcal{D} = 1.06\text{-}1.18$ ) and PhA ( $\mathcal{D} = 1.13\text{-}1.19$ ), although all three polymerizations gave approximately linear  $M_n$  increases with conversion.

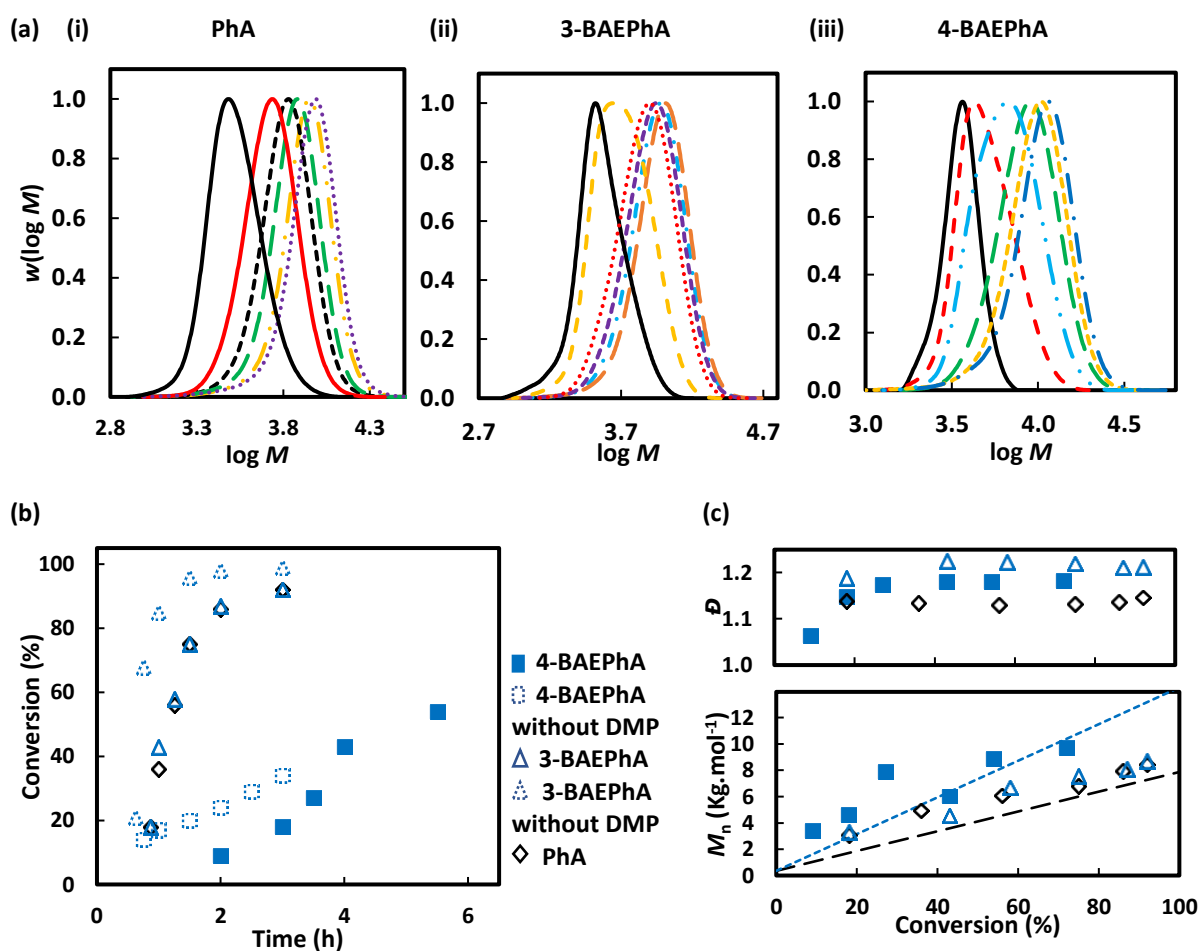


**Figure 2.11.** RAFT polymerization of 2.5 M PhA, 3-BAEPhA and 4-BAEPhA in DMF at 70 °C, using  $[\text{Monomer}]_0/[\text{DDMAT}]_0/[\text{AIBN}]_0 = 50/1/0.03$ . **(a)** MWDs correspond to conversions at **(i)** 18% (0.87 h), 43% (1 h), 56% (1.25 h), 70% (1.5 h), 86% (2 h) and 92% (3 h), **(ii)** 18% (0.87 h), 43% (1 h), 58% (1.25 h), 75% (1.5 h), 87% (2 h) and 92% (3 h), and **(iii)** 9% (2 h), 18% (3 h), 27% (3.5 h), 43% (4 h), 54% (5.5 h) and 72% (24 h). **(b)** Conversion versus time plot (24 h omitted). **(c)**  $M_n$  and  $\bar{D}$  vs. conversion with  $M_{n,th}$  lines (long dashed for PhA and short dashed for 3-BAEPhA and 4-BAEPhA) calculated according to Eq (1).

## **2.4 Conclusions and Future Work**

4-BAEPHA polymerizes much slower than the 3-isomer, so is not pursued in further RAFT polymerizations in this thesis. 3-BAEPHA polymerizes faster than PhA, with comparable control/living character. However, the pinacol ester-protected monomers are more difficult to prepare (reactions require anhydrous conditions and difficult recrystallizations), so 3-BAPHA was chosen for subsequent RAFT polymerizations for the synthesis of sugar-responsive polymers. In this case, pinacol protection of the polymer was established based on a literature procedure.<sup>23</sup>

## **CHAPTER 3: RAFT DISPERSION POLYMERIZATION INDUCED SELF-ASSEMBLY (PISA) OF BORONIC ACID-SUBSTITUTED ACRYLAMIDES**

### **3.1 Introduction**

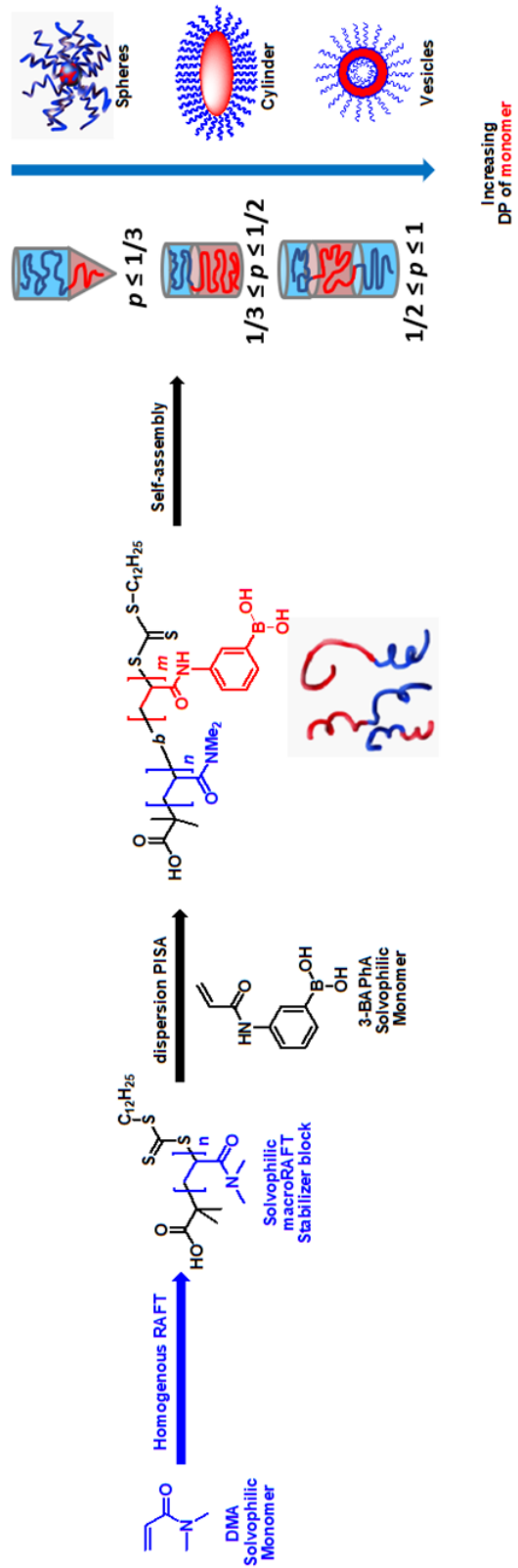
#### **3.1.1 Heterogeneous Radical Polymerizations<sup>65,66</sup>**

A heterogeneous polymerization typically employs water or an alcohol as the reaction solvent in the presence of a stabilizer and the resultant polymer is insoluble. A suspension polymerization is usually composed of a liquid matrix and monomer droplets. The monomer and initiator are insoluble in the liquid phase, and monomer/polymer droplets can be generated within the liquid matrix and suspended as the viscosity increases under continuous mechanical agitation. In dispersion and precipitation polymerization the monomer is soluble in the continuous phase, but the resulting polymer is not. In a dispersion a colloidal suspension with aid of a stabilizer and aqueous/organic solvent is achieved. The resultant polymer in a precipitation falls out of the continuous (aqueous) phase and forms agglomerate *i.e.* hydrophilic monomer but the resultant polymer is hydrophobic. An emulsion system differs from a dispersion polymerization, in that the monomer is insoluble and is commonly composed of a continuous phase and a dispersed phase which is stabilized by the emulsifiers located at the interface.

#### **3.1.2 Polymerization Induced Self-Assembly (PISA)**

##### **3.1.2.1 Overview**

Polymerization induced self-assembly (PISA) is a RDRP (see section 1.3) dispersion or emulsion polymerization. PISA allows control of polymer microstructure (narrow MWD block copolymers) and macrostructure (morphology). Firstly, a solvophilic block is prepared using a homogeneous polymerization (Scheme 3.1). The solvophilic block is a macroinitiator (in NMP)<sup>67</sup> or macroRAFT agent (in this thesis),<sup>68</sup> which also acts as a steric stabilizer in the PISA process. Chain extension of the solvophilic block with monomer (soluble in a dispersion) (or insoluble in an emulsion) forms an insoluble block, which initiates self-assembly beginning at  $J_{crit}$  (critical degree of polymerization at which particle nucleation occurs).  $J_{crit}$  or particle nucleation is varied by monomer loading and solvent composition.<sup>69</sup>



**Scheme 3.1:** PISA using poly(DMA) macroRAFT as steric stabilizer and 3-BAPhA monomer

PISA in water achieves colloidal stabilization, where the hydrophilic block becomes the corona, and the hydrophobic block is at the core. For any specific heterogeneous system, the morphology of the core-shell particle is determined by the relative fraction of the two blocks, with higher order morphologies (worms and vesicles) achieved by increasing the relative size of the hydrophobic block. The packing parameter  $P$  rationalizes the morphological size variation during PISA<sup>70</sup> in Eq. (3.1):

$$p = V/(a_h l_c) \quad (3.1)$$

Eq. (3.1) estimates  $p$ , where  $V$  is the volume of the solvophobic chains,  $a_h$  is the interfacial area of the solvophilic chain,  $l_c$  is the length of the solvophobic chain (Fig. 3.1). Spherical micelles are favoured when  $p \leq 1/3$ , cylindrical micelles when  $1/3 \leq p \leq 1/2$ , and generating an enclosed membrane structures *i.e.* vesicles when  $1/2 \leq p \leq 1$ .

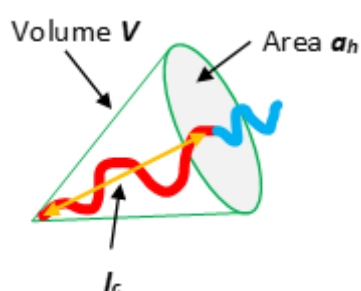
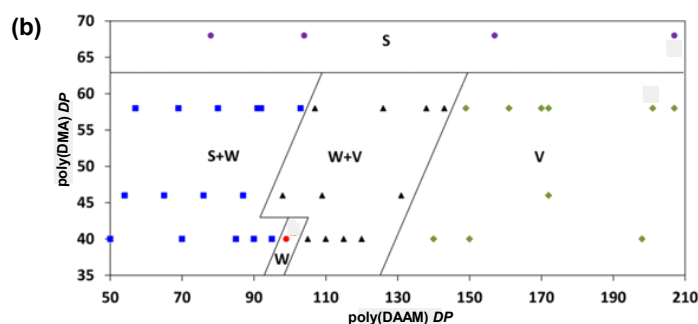
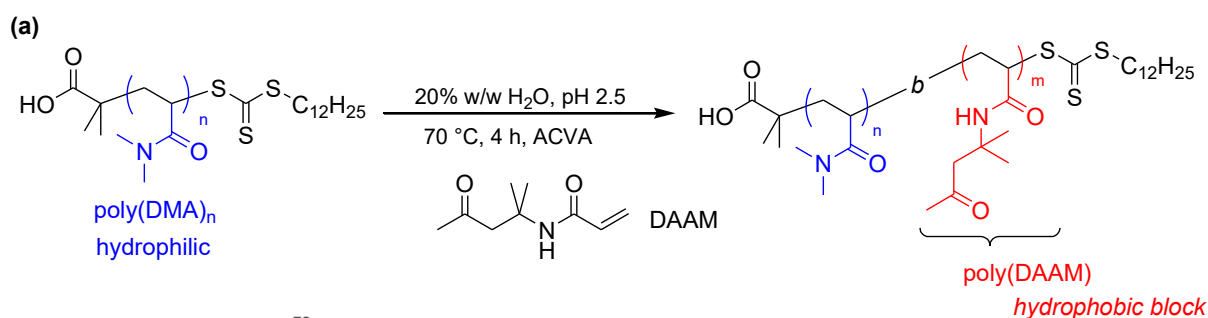


**Figure 3.1:** Packing parameter of a PISA block copolymer amphiphile

Byard *et al.* reported the aqueous dispersion polymerization of diacetone acrylamide (DAAM, 20% w/w) at 70 °C using poly(DMA) macroRAFT at various  $DP$ s as the steric stabilizer giving amphiphilic diblock copolymer (Scheme 3.2(a)).<sup>71</sup> DAAM has high water solubility and forms a water-insoluble block at  $DP$ s as low as 50, while poly(DMA) is hydrophilic, allowing PISA to be carried out in water. DAAM forms polymers sensitive to temperature and enables postpolymerization crosslinking at the carbonyl group. A phase diagram (Scheme 3.2(b)) is used to predict morphology according to  $DP$  of the two different polyacrylamide blocks (poly(DMA) and poly(DAAM)) with spheres formed when the hydrophilic (poly(DMA)) block is long, and when the hydrophobic (poly(DAAM)) block is much longer than the stabilizer block, vesicles are formed. A pure worm phase (red dot in the phase diagram) occurs at a small region, when the diblock = poly(DMA)<sub>40</sub>-*b*-poly(DAAM)<sub>99</sub>.



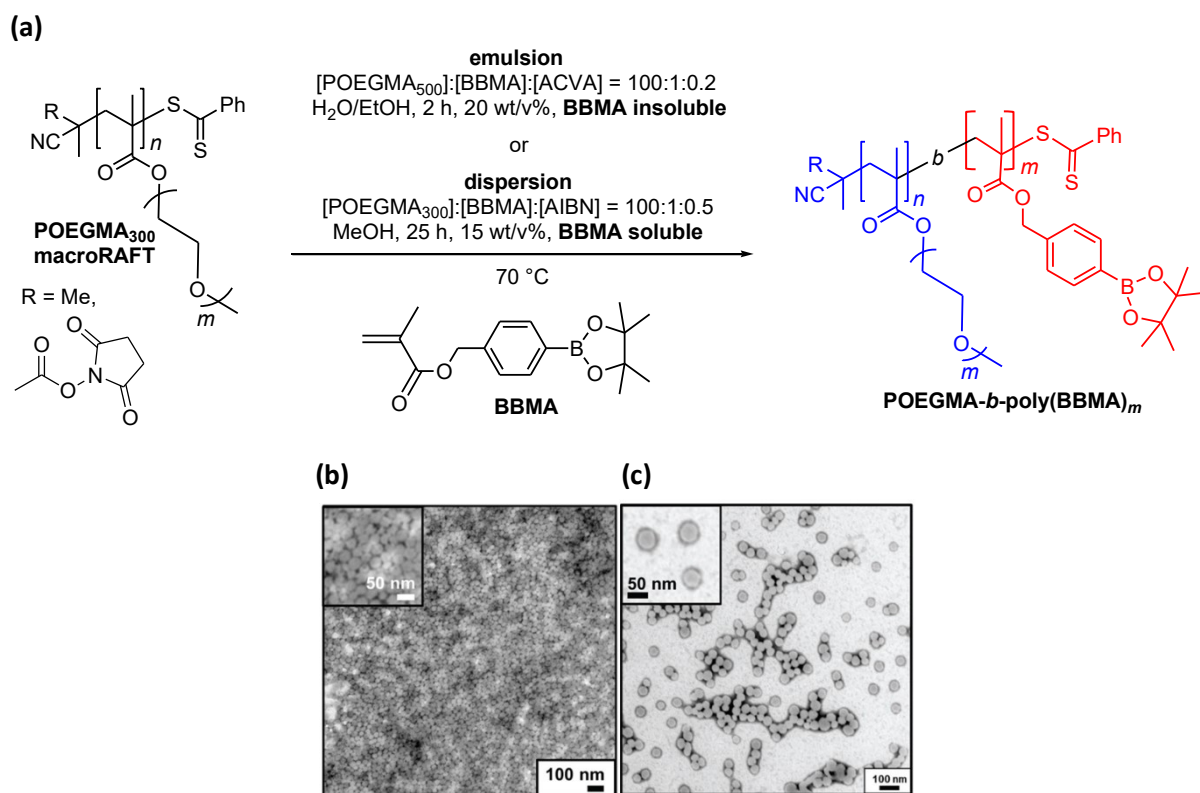
**Scheme 3.2:** Dispersion of DAAM (b) phase diagram showing morphology, where S = spheres, W = worms and V = vesicles.<sup>71</sup>

The advantage of PISA is the rapid production of high concentrations of nano-objects, without the requirement for polymer processing (e.g. in this thesis, 20 w/v% monomer/polymer is used). Traditional core-shell nanoparticle synthesis is a two-step process, with polymer synthesis followed by a slow dialysis process (less than 1 w/v% of polymer), so producing very low concentrations of nanoparticles.<sup>72</sup>

### 3.1.2.2 Heterogeneous RAFT Polymerizations of BA-Substituted Monomers

Hsu and Delaittre *et al.* reported the emulsion and dispersion RAFT polymerization of 4-pinacolboronylbenzyl methacrylate monomer (BBMA) using poly(oligo(ethylene glycol) methacrylate) (POEGMA) attached to dithiobenzoate-based as the macroRAFT agent and steric stabilizer block (Scheme 3.3).<sup>73</sup> The authors proposed applications for the boron-rich nanoparticles, where is at the core in boron-neutron capture therapy.<sup>74</sup> The emulsion polymerization reached 94% conversion in 2 h when using  $DP = 100$  giving spheres of about 50 nm, but there was a coagulant. The dispersion polymerization at  $DP = 100$  reached 94% conversion after 25 h giving spheres of about 50 nm in diameter. The coagulation observed is

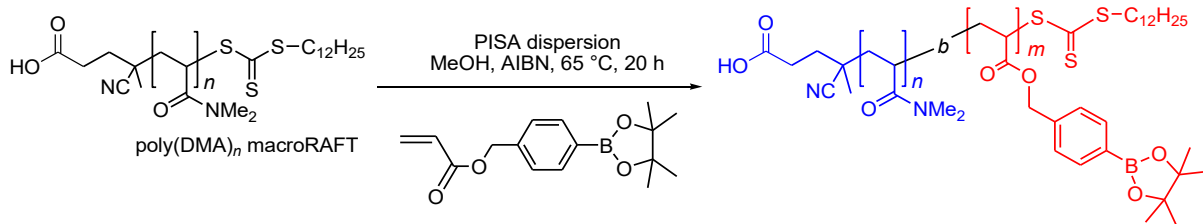
probably due to cleavage of the pinacol protecting group leading to boroxine formation from the free BA (not discussed by these authors but tackled later in this Chapter).



**Scheme 3.3:** Hsu and Delaitre *et al.* **(a)** dispersion or emulsion polymerization with **(b)** TEM of emulsion and **(c)** TEM of dispersion.<sup>73</sup>

Fan and Thang *et al.* reported the dispersion polymerization of the acrylate analogue of BBMA 4-pinacolboronylbenzyl acrylate monomer also in MeOH, using poly(DMA) macroRAFT agents as the steric stabilizer block (Scheme 3.4).<sup>75</sup> In this case, a range of higher order polymer objects were achieved, including with cubic and hexagonal mesophases, and oxidative removal of the BA group led to disassembly by converting the hydrophobic BA block into a hydrophilic acrylic acid block.

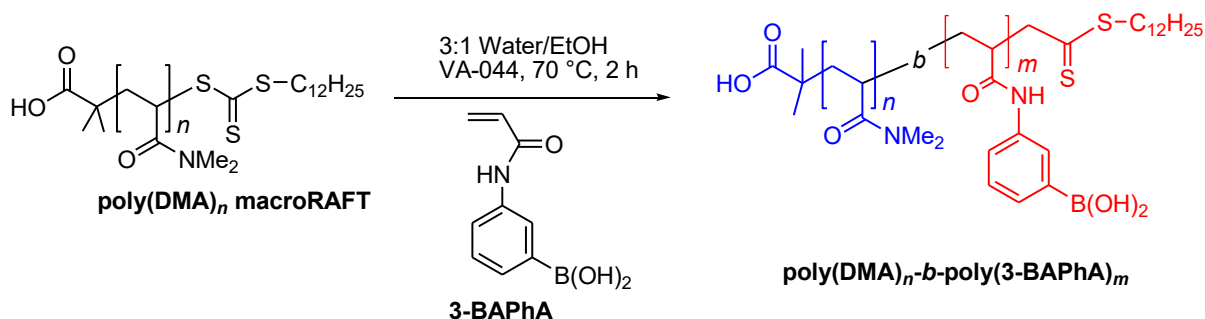




**Scheme 3.4:** Thang *et al.* dispersion polymerization of the acrylate analogue of BBMA.<sup>75</sup>

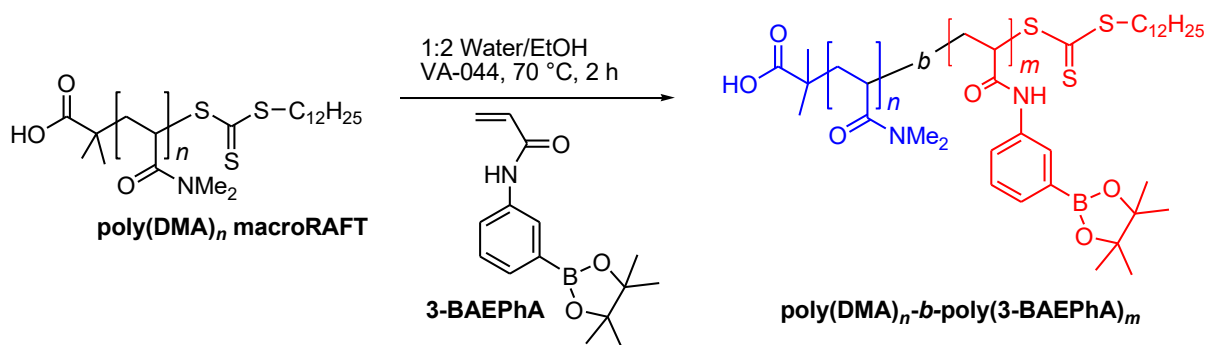
### 3.2 Chapter Aims and Objectives

- To achieve the first PISA with an unprotected boronic acid monomer (i.e. 3-BAPhA) (Scheme 3.5)



**Scheme 3.5:** Dispersion PISA with 3-BAPhA

- To carry out PISA of 3-BAPhA with a protected boronic acid monomer (i.e. 3-BAEPHA), in order to achieve higher order morphologies using poly(DMA) as the macroRAFT and steric stabilizer block (Scheme 3.6)



**Scheme 3.6:** Dispersion PISA with 3-BAEPHA

### 3.3 Experimental

#### 3.3.1 Materials

2-(Dodecylthiocarbonothioylthio)-2-methylpropionic acid (DMP; TCI, >98%), 2,2'-azobis[2-(2-imidazolin-2-yl)propane]dihydrochloride (VA-044; Wako, 97%), and 2,2'-azobis(2-methylpropionitrile) (AIBN; Sigma Aldrich, 98%) were used as received. Milli-Q water, ethanol (EtOH; VWR, ≥99%), ethyl acetate (EtOAc; VWR, ≥99%), diethyl ether (Et<sub>2</sub>O; Fisher, >99.5%), dioxane (Fluorochem >99%), anisole (TCI, >99%), and *N,N*-dimethylformamide (DMF; VWF, HPLC-grade ≥99.9%) were used directly as solvents. *N,N*-Dimethylacrylamide (DMA; TCI, 98%) was passed through a column of basic alumina (Acros Organics 40 – 300 μm, 60 Å) to remove the inhibitor prior to use.<sup>76</sup> 3-(Acrylamidophenyl)boronic acid (3-BAPhA) was prepared according to the literature,<sup>11</sup> from 3-aminophenylboronic acid monohydrate (Fluorochem, 97%), acryloyl chloride (Alfa Aesar, 96%), and sodium bicarbonate (Alfa Aesar 99.5%) in 1:1 tetrahydrofuran (THF; Fisher, >99.8%):water. Please refer to section 2.2.2.3.1 for more information on 3-BAPhA. *N*-[3-(4,4,5,5-tetramethyl-1,3,2-dioxaborolan-2-yl)phenyl]prop-2-enamide (3-BAEPH) was prepared according to the literature,<sup>8</sup> from 3-acrylamidophenylboronic acid pinacol ester (Fluorochem, 99%), acryloyl chloride, and anhydrous sodium carbonate in CH<sub>2</sub>Cl<sub>2</sub> (VWR, ≥99.8%, distilled over CaH<sub>2</sub>, Alfa Aesar, 90-95%). Please see section 2.2.3.2 for on 3-BAEPH and 2.2.3.3 for 4-BAEPH preparation.

#### 3.3.2 Instrumentation

Please see chapter 2.2.2.

##### 3.3.2.1 Transmission Electron Microscopy (TEM)

Micrographs were obtained at an accelerating voltage of 100 keV (JEOL-1400). Neat samples were deposited onto carbon-coated copper grids (Ted Pella, Redding CA). Excess solvent was drained using filter paper. The samples were subsequently stained with uranyl acetate for 2 min at room temperature. Images were recorded digitally using a Phurona CCD Camera (Emsis) and radius imaging software (Emsis). TEM analysis was conducted by Dr Fumi Ishizuka of The University of New South Wales, UNSW, Sydney, Australia.

#### 3.3.3 Polymerization Procedures

##### 3.3.3.1 Preparation of MacroRAFT agents

##### 3.3.3.2 Preparation of poly(DMA)<sub>28</sub>

The initiator serial dilution used VA-044 (36.34 mg, 0.11 mmol) diluted 250 times with 20% aq. dioxane. DMP (0.163 g, 0.45 mmol), DMA (2.212 g, 22.32 mmol) and VA-044 ( $4.50 \times 10^{-4}$  molL<sup>-1</sup> from serial dilution) in 20% aq. dioxane (5.00 mL) were heated at 70 °C for 2 h. The polymer was precipitated in Et<sub>2</sub>O, filtered, and dried at room temperature under vacuum for 24 h to give poly(DMA)<sub>28</sub> macroRAFT,  $M_n = 3,100$  g.mol<sup>-1</sup>,  $\bar{D} = 1.12$ , isolated = 1.951 g, Yield = 82% (Figure 3.2).

### 3.3.3.3 Preparation of poly(DMA)<sub>36</sub>

The initiator serial dilution used VA-044 (36.34 mg, 0.11 mmol) diluted 250 times with 20% aq. dioxane. DMP (0.163 g, 0.45 mmol), DMA (2.212 g, 22.32 mmol) and VA-044 ( $4.50 \times 10^{-4}$  molL<sup>-1</sup> from serial dilution) in 20% aq. dioxane (5.00 mL) were heated at 70 °C for 2 h. The polymer was precipitated in Et<sub>2</sub>O, filtered, and dried at room temperature under vacuum for 24 h to give poly(DMA)<sub>36</sub> macroRAFT,  $M_n = 3,900$  g.mol<sup>-1</sup>,  $\bar{D} = 1.10$ , isolated = 2.114 g, Yield = 89% (Figure 3.3).

### 3.3.3.4 Preparation of poly(DMA)<sub>39</sub>

The initiator serial dilution used VA-044 (36.34 mg, 0.11 mmol) diluted 250 times with 20% aq. dioxane. DMP (0.163 g, 0.45 mmol), DMA (2.212 g, 22.32 mmol) and VA-044 ( $4.50 \times 10^{-4}$  molL<sup>-1</sup> from serial dilution) in 20% aq. dioxane (5.00 mL) were heated at 70 °C for 2 h. The polymer was precipitated in Et<sub>2</sub>O, filtered, and dried at room temperature under vacuum for 24 h to give poly(DMA)<sub>39</sub> macroRAFT,  $M_n = 4,200$  g.mol<sup>-1</sup>,  $\bar{D} = 1.10$ , isolated = 2.004 g, Yield = 82% (Figure 3.4(dashed black line)).

### 3.3.3.5 Preparation of poly(DMA)<sub>96</sub>

The initiator serial dilution used VA-044 (25 mg, 0.08 mmol) diluted 250 times with 20% aq. dioxane. Poly(DMA)<sub>39</sub> (1.284 g, 0.30 mmol), DMA (1.501 g, 15.14 mmol) and VA-044 ( $3.20 \times 10^{-4}$  molL<sup>-1</sup> from serial dilution) in 20% aq. dioxane (5.00 mL) were heated at 70 °C for 2 h. The polymer was precipitated in Et<sub>2</sub>O, filtered, and dried at room temperature under vacuum for 24 h to give poly(DMA)<sub>96</sub> macroRAFT,  $M_n = 9,900$  g.mol<sup>-1</sup>,  $\bar{D} = 1.17$ , isolated = 2.088 g, Yield = 75% (Figure 3.4 (solid red line)).

### 3.3.3.6 Attempted preparation of the longer stabilizer block by a single RAFT polymerization

The initiator serial dilution used VA-044 (45 mg, 0.14 mmol) diluted 625 times with 20% aq. dioxane. DMP (81.5 mg, 0.22 mmol), DMA (2.212 g, 22.32 mmol) and VA-044 ( $2.23 \times 10^{-4} \text{ molL}^{-1}$  from serial dilution) in 20% aq. dioxane (5 mL) were heated at 70 °C for 2 h.  $M_n = 6,800 \text{ g.mol}^{-1}$ ,  $D = 1.15$ ; Conv. = 72% (measured by NMR, see above) (Fig. 3.5).

#### 3.3.3.6.1 Preparation of poly(3-BAPhA) homopolymer for solubility studies

The initiator serial dilution used VA-044 (39 mg, 0.12 mmol) diluted 100 times with 20% aq. DMF. 3-BAPhA (0.573 g, 3.000 mmol), DMP (21.86 mg, 0.060 mmol), and VA-044 ( $1.19 \times 10^{-3} \text{ molL}^{-1}$  from serial dilution) in 20% aq. DMF (1.00 mL) were heated at 70 °C for 2 h. The polymer was precipitated in Et<sub>2</sub>O, filtered, and dried at room temperature under vacuum for 24 h to give poly(3-BAPhA),  $M_n = 9,400 \text{ g.mol}^{-1}$ ,  $D = 1.16$  (after pinacol protection), Isolated = 0.395 g, Yield = 66% (Fig. 3.6).

#### 3.3.3.6.2 Preparation of poly(3-BAEPPhA) homopolymer for solubility studies

The initiator serial dilution used AIBN (61 mg, 0.37 mmol) diluted 250 times with DMF. 3-BAEPPhA (0.683 g, 2.497 mmol), DMP (17.87 mg, 0.049 mmol), and AIBN ( $1.48 \times 10^{-3} \text{ molL}^{-1}$  from serial dilution) in DMF (1.00 mL) were heated at 70 °C for 2 h. The polymer was precipitated in Et<sub>2</sub>O, filtered, and dried at room temperature under vacuum for 24 h to give poly(3-BAEPPhA),  $M_n = 8,700 \text{ g.mol}^{-1}$ ,  $D = 1.31$ , Isolated = 0.264 g, Yield = 38% (Fig. 2.10).

#### 3.3.3.6.3 Dispersion polymerization of 3-BAPhA using poly(DMA)<sub>28</sub>

The initiator serial dilution used VA-044 (42 mg, 0.13 mmol) diluted 250 times with 3:1 Water/EtOH. 3-BAPhA (0.400 g, 2.094 mmol), poly(DMA)<sub>28</sub> (0.044 ( $5.20 \times 10^{-4} \text{ molL}^{-1}$  from serial dilution) in 3:1 Water/EtOH (2.00 mL) were heated at 70 °C, while stirring at 1000 rpm with a magnetic stirrer bar for 2 h. The visual appearance at the end of the polymerizations is in Fig. 3.7(b). The upper free-flowing white suspension was separated upon cooling and manipulated as described in Fig. 3.7. Conversion was by <sup>1</sup>H NMR (2.2.2.2.1) and GPC required pinacol protection.

#### 3.3.3.7 Dispersion polymerization of 3-BAPhA using poly(DMA)<sub>96</sub>

The initiator serial dilution used VA-044 (42 mg, 0.13 mmol) diluted 250 times with 3:1 Water/EtOH. 3-BAPhA (0.400 g, 2.094 mmol), poly(DMA)<sub>96</sub> (0.416 g, 0.042 mmol), and VA-044

( $5.20 \times 10^{-4} \text{ molL}^{-1}$  from serial dilution) in 3:1 Water/EtOH (2.00 mL) were heated at 70 °C, while stirring at 1000 rpm with a magnetic stirrer bar for 2 h. The visual appearance at the end of the polymerizations is in Fig. 3.8. The upper free-flowing white suspension was separated upon cooling and manipulated as described in Fig 3.10. Conversion was by  $^1\text{H}$  NMR and GPC required pinacol protection.

#### **3.3.3.8 Dispersion polymerization of 3-BAEPHA using poly(DMA)<sub>96</sub>**

The initiator serial dilution used VA-044 (24 mg, 0.07 mmol) diluted 250 times with 1:2 Water/EtOH. 3-BAEPHA (0.400 g, 1.464 mmol), poly(DMA)<sub>96</sub> (0.291 g, 0.029 mmol), and VA-044 ( $2.80 \times 10^{-4} \text{ molL}^{-1}$  from serial dilution) in 1:2 Water/EtOH (2.00 mL) were heated at 70 °C, while stirring at 1000 rpm with a magnetic stirrer bar for 2 h. The visual appearance at the end of the polymerization is in Fig. 3.12. Conversion was by  $^1\text{H}$  NMR (2.2.2.2.1) and GPC.

#### **3.3.3.8 Dispersion polymerization of 3-BAEPHA using poly(DMA)<sub>36</sub>**

The initiator serial dilution used VA-044 (24 mg, 0.07 mmol) diluted 250 times with 1:2 Water/EtOH. 3-BAEPHA (0.400 g, 1.464 mmol), poly(DMA)<sub>36</sub> (0.115 g, 0.029 mmol), and VA-044 ( $2.80 \times 10^{-4} \text{ molL}^{-1}$  from serial dilution) in 1:2 Water/EtOH (2.00 mL) were heated at 70 °C, while stirring at 1000 rpm with a magnetic stirrer bar for 2 h. The visual appearance at the end of the polymerizations is in Fig. 3.13. Conversion was by  $^1\text{H}$  NMR (2.2.2.2.1) and GPC.

### **3.4 Results and Discussion**

#### **3.4.1 Preparation of MacroRAFT Stabilizers**

Preparation of poly(DMA)<sub>28</sub> used a targeted  $DP = 50$  using DMP and VA-044 as RAFT agent and azo initiator respectively (Fig. 3.2).

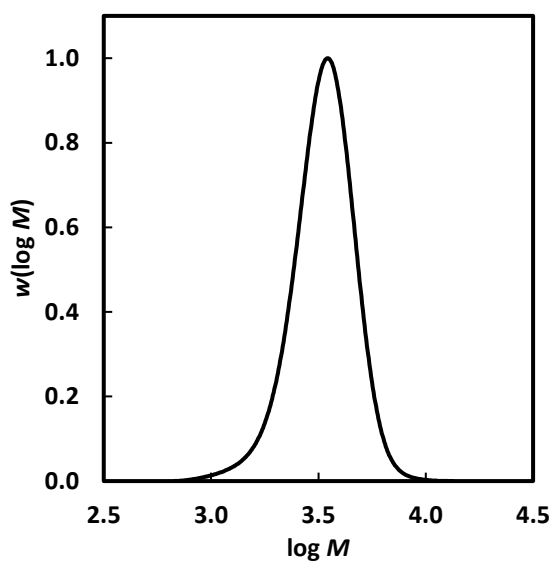


**Figure 3.2:** MWD of macroRAFT stabilizer poly(DMA)<sub>28</sub>  $M_n = 3,100 \text{ g}\cdot\text{mol}^{-1}$  and  $\mathcal{D} = 1.12$ .

The same reaction conditions were used to prepare poly(DMA)<sub>36</sub> (Fig. 3.3) and poly(DMA)<sub>39</sub> (Fig. 3.4), which proceeded to the same conversion of 82%, as the preparation of poly(DMA)<sub>28</sub>. The difference in MW is due to experimental error.

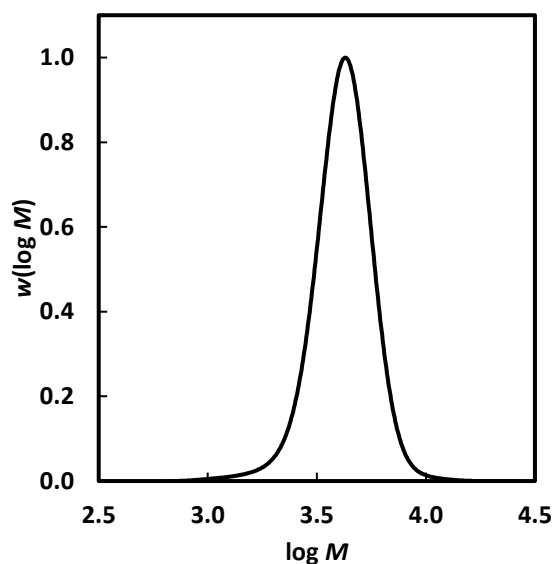


**Figure 3.3:** MWD of macroRAFT stabilizer poly(DMA)<sub>36</sub>  $M_n = 3,900 \text{ g}\cdot\text{mol}^{-1}$  and  $\mathcal{D} = 1.10$ .

Preparation of the poly(DMA)<sub>96</sub> involved two RAFT polymerizations of DMA at targeted  $DP = 50$ . Thus poly(DMA)<sub>96</sub> is equiv. to poly(DMA)<sub>39</sub>-*b*-poly(DMA)<sub>57</sub>, where  $DP$  is calculated from

$M_n$  using GPC. The preparation of the poly(DMA)<sub>96</sub> by chain extension of poly(DMA)<sub>39</sub> ( $M_n = 4,200 \text{ g mol}^{-1}$ ,  $\mathcal{D} = 1.10$ ) occurred in 88% conversion (Fig. 3.4).

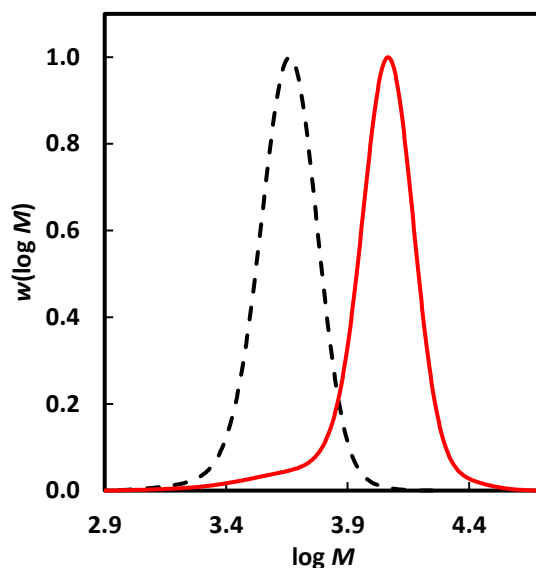


**Figure 3.4:** MWDs of macroRAFT stabilizer poly(DMA)<sub>39</sub>  $M_n = 4,200 \text{ g.mol}^{-1}$  and  $\mathcal{D} = 1.10$  (dashed black line), which was chain extended to poly(DMA)<sub>96</sub>  $M_n = 9,900 \text{ g.mol}^{-1}$  and  $\mathcal{D} = 1.17$  (solid red line).

Note attempted preparation of this longer stabilizer block in a single RAFT polymerization of DMA at 70 °C with  $[\text{DMA}]_0/[\text{DMP}]_0 = 100$ , resulted in lower conversion (72%) and thus shorter stabilizer, poly(DMA)<sub>65</sub> ( $M_n = 6,800 \text{ g.mol}^{-1}$ ,  $\mathcal{D} = 1.15$ ) (Fig. 3.5).

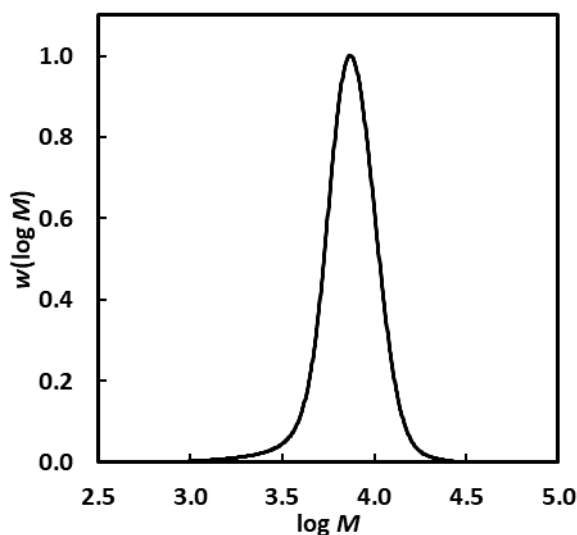


**Figure 3.5.** Attempted preparation of poly(DMA) using one RAFT polymerization with  $[DMA]_0/[DMP]_0 = 100$  ( $M_n = 6,800 \text{ gmol}^{-1}$ ,  $D = 1.15$ ).

### 3.4.2. Solubility studies

3-BAPhA and 3-BAEPHA require a solvent concoction that can accommodate a 20 wt/vol% monomer loading, but to meet the requirements for dispersion polymerization, the polymer needs to be insoluble. This was achieved through the addition of ethanol with 3:1 water/EtOH, providing soluble monomer and insoluble poly(3-BAPhA) at 70 °C. Although the medium was different (1:2 water/EtOH as opposed to 3:1 water/EtOH) for PISA of 3-BAEPHA. The greater proportion of ethanol allowed solvation of the more hydrophobic monomer 3-BAEPHA, while maintaining insolubility of the derived polymer. The water-soluble azo initiator VA-044 and the macroRAFT poly(DMA) steric stabilizers are hydrophilic, hence the requirement for 20% water. Poly(3-BAPhA) was prepared by RAFT of 3-BAPhA using DMP and VA-044 (Fig. 3.6) and poly(3-BAEPHA) was prepared using RAFT of 3-BAEPHA using DMP and AIBN (Fig 2.10).



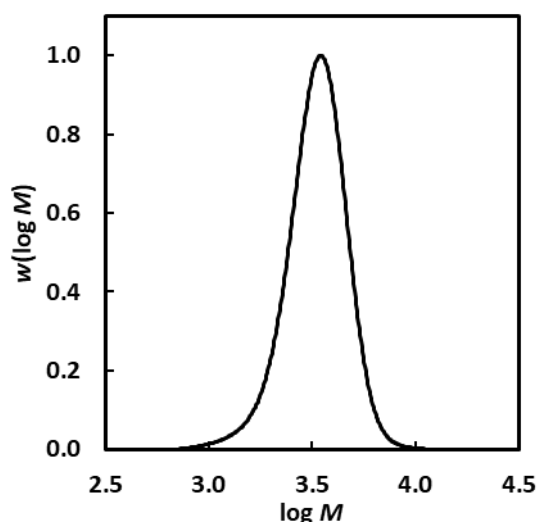


**Figure 3.6.** GPC of poly(3-BAPhA) homopolymer ( $M_n = 9,400 \text{ g mol}^{-1}$ ,  $\mathcal{D} = 1.16$ ) homopolymer for preliminary solubility studies.

### 3.4.3 Dispersion Polymerization of 3-BAPhA using Poly(DMA)<sub>28</sub>

Initial studies involved optimizing the initiator concentration ( $[\text{VA-044}]_0$ ) for the 2 h dispersion polymerization of 3-BAPhA (20 wt/vol%) using poly(DMA)<sub>28</sub> as macroRAFT agent at 70 °C. Three different initiator concentrations at  $[\text{poly(DMA)}_{28}]_0/[\text{VA-044}]_0 = 70, 57$  and 45 were investigated, at a targeted degree of polymerization of  $[\text{3-BAPhA}]_0/[\text{poly(DMA)}_{28}]_0 = 50$  (Fig. 3.7). For the lowest  $[\text{VA-044}]_0$ , the solution remained transparent and conversion was low (23%, Run 1; Table 3.1), with the low rate of polymerization ( $R_p$ ) attributed to the absence of particle nucleation. After nucleation, monomer swell the formed micelles, leading to a relatively high local monomer concentration, and thus rate enhancement.<sup>77,78</sup> Considerably higher conversion (70%) was obtained for  $[\text{poly(DMA)}_{28}]_0/[\text{VA-044}]_0 = 57$ , with relatively good control/livingness ( $M_n = 14,600 \text{ g mol}^{-1}$ ;  $M_{n,\text{th}} = 12,700 \text{ g mol}^{-1}$ ;  $\mathcal{D} = 1.35$ ) (Run 2, Table 3.1). Note that the GPC data are recorded after the pinacol-protection of BA moieties to give poly(3-BAEPPhA) and is subject to calibration error against linear polystyrene standards. Near-complete conversion (91%, Run 3) was obtained at the highest VA-044 concentration, but with a broad molecular weight distribution (MWD,  $\mathcal{D} = 1.80$ ), with  $M_n$  ( $19,500 \text{ g mol}^{-1}$ ) higher than  $M_{n,\text{th}}$  ( $15,700 \text{ g mol}^{-1}$ ).

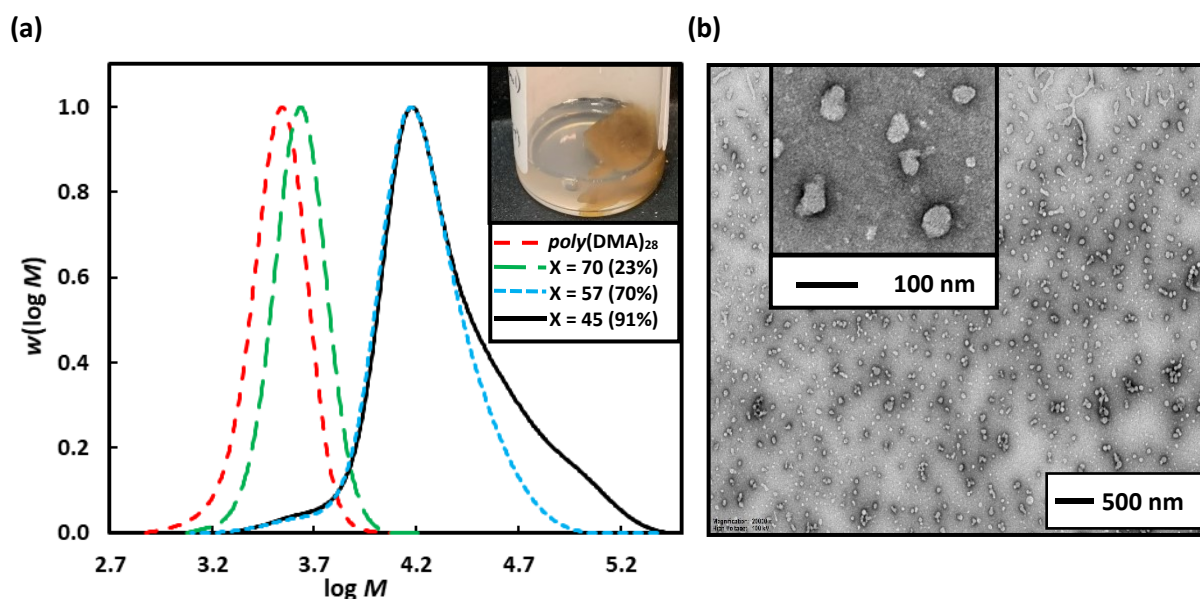


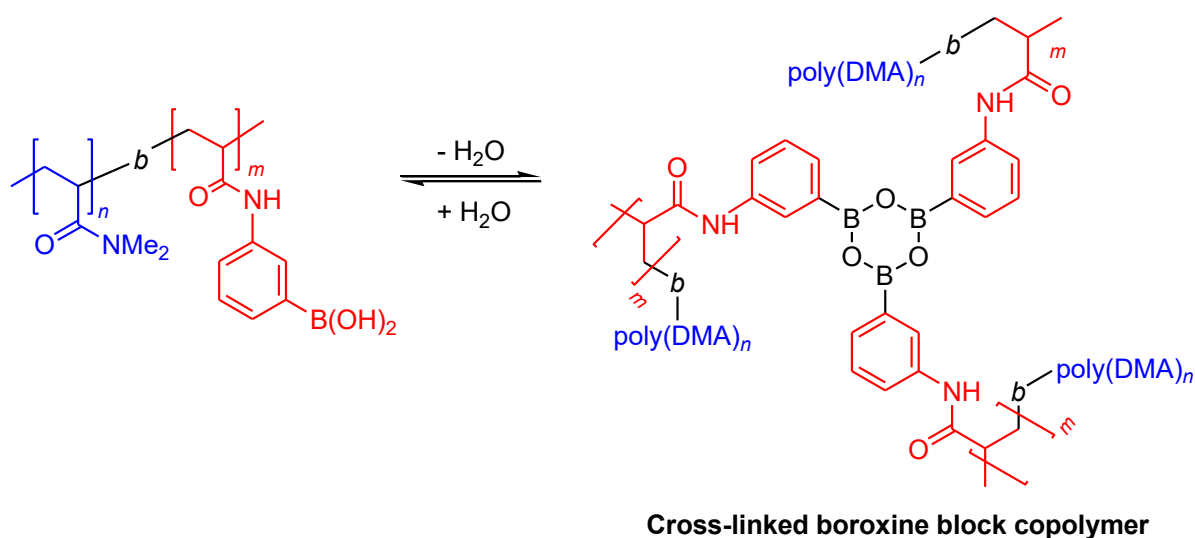
**Figure 3.7:** Varying the initiator concentration  $[\text{VA-044}]_0$  for the 2 h RAFT dispersion polymerization of 3-BAPhA (20 wt/vol%) in 3:1 Water/EtOH at 70 °C using  $[\text{3-BAPhA}]_0/[\text{poly(DMA)}_{28}]_0 = 50$ , with  $[\text{poly(DMA)}_{28}]_0/[\text{VA-044}]_0 = X$  (Run 1-3). (a) MWDs after pinacol protection (with conv.) and visual appearance of polymerization for  $X = 45$ ; (b) Sample image for PISA at  $X = 45$  (additional images see ESI<sup>4</sup>).

**Table 3.1.** Experimental results for dispersion PISA of 3-BAPhA using  $\text{poly(DMA)}_{28}$  and  $\text{poly(DMA)}_{96}$  macroRAFT agents.

Run <sup>a</sup>	$[\text{M}]_0/[\text{poly(DMA)}]_0$	Polymer <sup>b</sup>	Conv. (%) <sup>c</sup>	$M_{n,\text{th}}$ <sup>d</sup>	$M_n$ <sup>e</sup>	$\bar{D}$ <sup>e</sup>
1	50	$\text{poly(DMA)}_{28}\text{-}b\text{-poly(3-BAPhA)}_{12}$	23	6,400	4,000 <sup>f</sup>	1.10 <sup>f</sup>
2	50	$\text{poly(DMA)}_{28}\text{-}b\text{-poly(3-BAPhA)}_{35}$	70	12,700	14,600 <sup>f</sup>	1.35 <sup>f</sup>
3	50	$\text{poly(DMA)}_{28}\text{-}b\text{-poly(3-BAPhA)}_{46}$	91	15,700	19,500 <sup>f</sup>	1.80 <sup>f</sup>
4	50	$\text{poly(DMA)}_{96}\text{-}b\text{-poly(3-BAPhA)}_{50}$	99	23,600	24,500 <sup>f</sup>	1.27 <sup>f</sup>

<sup>a</sup>See Fig. 3.7 and Fig. 3.8 for dispersion polymerization conditions and conversions. <sup>b</sup> $DP$  of the stabilizer block is calculated from  $M_n(\text{GPC})$   $\text{poly(DMA)}_{28}$  (3100 g mol<sup>-1</sup>,  $\bar{D} = 1.12$ ) or  $\text{poly(DMA)}_{96}$  (9900 g mol<sup>-1</sup>,  $\bar{D} = 1.17$ ) and the  $DP$  of the  $\text{poly(3-BAPhA)}$  block is based on conversion. <sup>c</sup>Measured by <sup>1</sup>H NMR see SI. <sup>d</sup>Theoretical ( $M_{n,\text{th}}$ ) is calculated from  $\text{poly(3-BAEPPhA)}$   $DP$  added to the  $\text{poly(DMA)}$   $M_n(\text{GPC})$ . <sup>e</sup>g mol<sup>-1</sup> and <sup>f</sup>GPC for the polymerization of 3-BAPhA is after pinacol protection to  $\text{poly(3-BAEPPhA)}$ .

The two polymerizations of 3-BAPhA at high conversions led to significant agglomeration, which visibly increases upon cooling. This brown coagulum is assumed to be boroxine, which is the anhydride of BA formed in the solid state,<sup>79</sup> and is in equilibrium in solution.<sup>80</sup> Boroxine (Scheme 3.7) is favored at the locus of polymerization (within the monomer-rich particles), where the concentration of water is low, in contrast to the dispersion medium. Part of the highest conversion sample (Run 3) could however be re-suspended on shaking, with TEM analysis indicating irregularly shaped near-spherical sub-100 nm solid particles (Fig. 3.7(b)).



**Scheme 3.7:** Reversible formation of boroxine moieties

#### 3.4.4 Dispersion Polymerization of 3-BAPhA using Poly(DMA)<sub>96</sub>

Attempts to circumvent the formation of coagulum by carrying out the dispersion polymerization of 3-BAPhA using poly(DMA)<sub>28</sub> macroRAFT at lower monomer loadings resulted in low  $R_p$ , agglomeration and inferior control/living character. The use of a longer hydrophilic macroRAFT agent was investigated - this would lead to a significant delay in the on-set of particle nucleation, but the longer stabilizer block may improve colloidal stability. Thus dispersion polymerization of 3-BAPhA (20 wt/vol%) was carried out using poly(DMA)<sub>96</sub> macroRAFT agent (as opposed to poly(DMA)<sub>28</sub>); a free-flowing colloidal dispersion formed, as indicated by a cloudy-white layer, which separated from the lower brown agglomeration upon cooling (Fig. 3.8). The polymerization reached completion (99% conv., Run 4), with excellent control/living character demonstrated by  $M_n$  (24,500 g mol<sup>-1</sup>) in close agreement

with  $M_{n,th}$  (23,600 g mol<sup>-1</sup>), and a narrow MWD ( $\mathcal{D} = 1.27$ ) (Table 3.1). TEM analysis of the white dispersion layer showed mainly small spherical NPs (Fig. 3.8(b)), but with some short rods, and large well-defined up to 200 nm spherical particles.

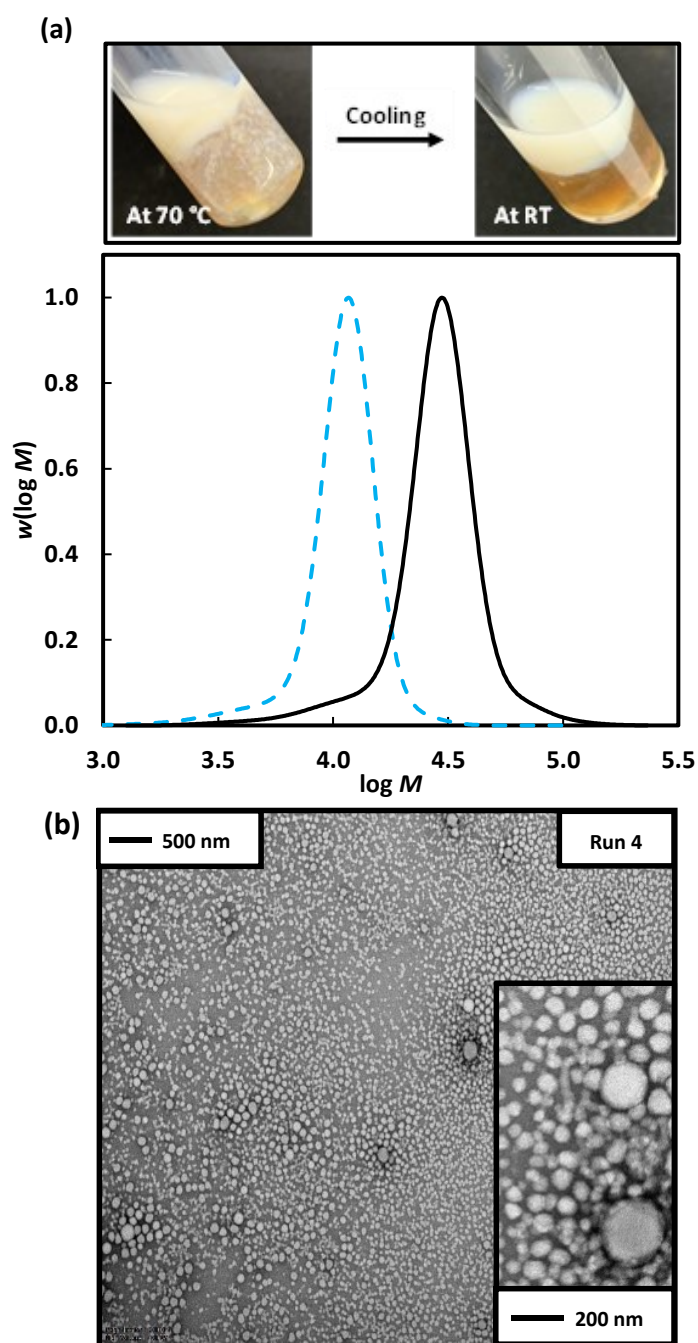


**Figure 3.8:** Poly(DMA)<sub>96</sub>, as macroRAFT agent (dashed blue line) in the 2 h dispersion polymerisations of 3-BAPhA (20 wt/vol%; full black line) in 3:1 Water/EtOH at 70 °C, where [poly(DMA)<sub>96</sub>]<sub>0</sub>/[VA-044]<sub>0</sub> = 40, and targeted degree of polymerisation,  $DP = 50$  (Run 4). (a) Visual appearance of polymerisation (with white stirrer bar within) before and after cooling to RT, and MWD (99% conv.) after pinacol protection (see ESI,<sup>68</sup> for additional images).

The MWD of the upper colloidal layer was superimposable with that of the lower brown coagulum (see ESI,<sup>68</sup> Fig. 3.9), indicating that boroxine formation had not affected control/livingness.

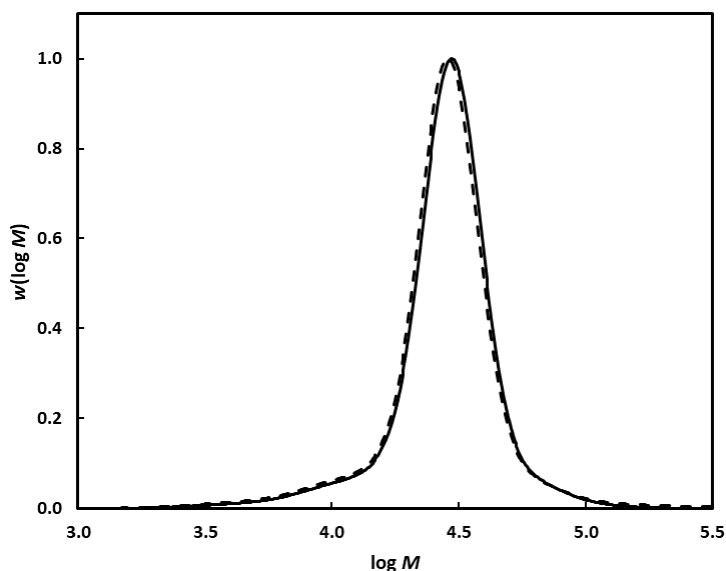


**Fig. 3.9:** MWDs (using GPC) of the separate layers for the dispersion polymerization in Fig. 3.8, with the lower boroxine layer dashed (Run 4).  $M_n = 24,500 \text{ gmol}^{-1}$ ,  $\mathcal{D} = 1.27$  (continuous) and  $M_n = 23,400 \text{ gmol}^{-1}$ ,  $\mathcal{D} = 1.37$  (dashed).

Given the distinct possibility of boroxine moieties (Scheme 3.7), colloidal stability was evaluated through 100-fold dilution with the dispersion solvent (3:1 Water/EtOH) at room temp. After 24 h, TEM analysis for the dilution showed the primary morphology was short rods and worms with some similar sized 50-100 nm diameters spheres remaining (Fig. 3.10, see ESI<sup>68</sup>).

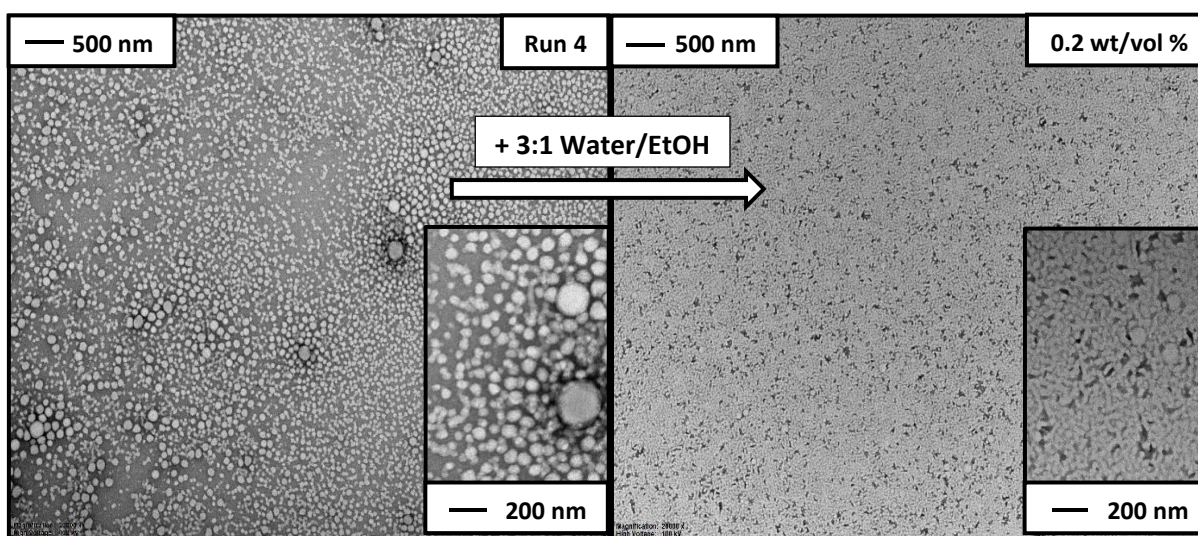


**Figure 3.10:** Poly(DMA)<sub>96</sub>, (100-fold) dilution of the upper layer with the dispersion solvent

A lesser (20-fold) dilution of the upper layer with the dispersion solvent, after 24 h, gave a greater abundance of spheres compared to rods, reflecting less boroxine hydrolysis (see ESI,<sup>68</sup> Fig. 3.11).

A decrease in polymer concentration would normally reduce the likelihood of transitions to higher order morphologies, since the number of polymer aggregates and thus collisions is less.<sup>72</sup> However, in this case, increased hydrolysis of boroxine at the core shifts the equilibrium from crosslinked polymer to linear poly(BA) chains, so affecting the interfacial energy and consequently self-assembly. This change in hydrophilic-hydrophobic block and polymer-solvent interactions is presumed to cause the observed sphere-to-rod (worm) transition.



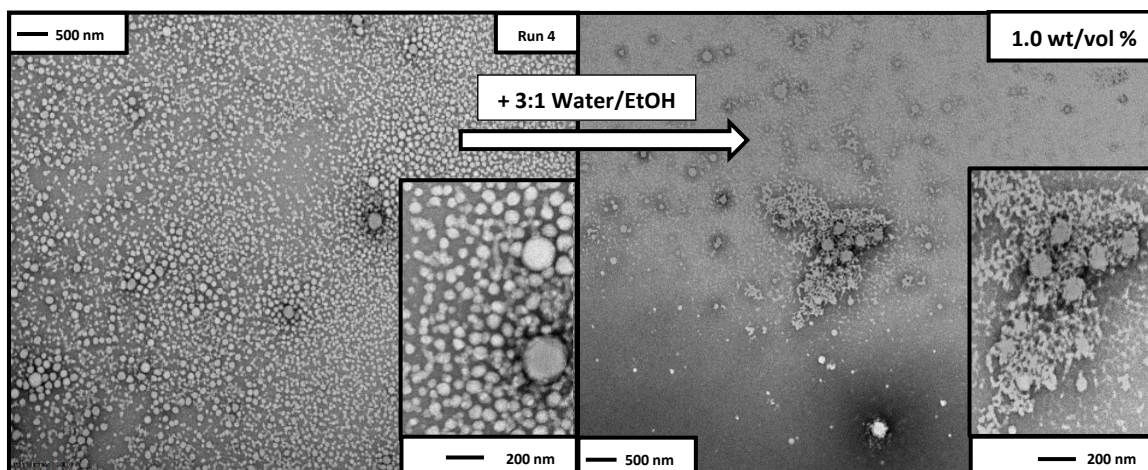


**Figure 3.11:** Poly(DMA)<sub>96</sub>, (20-fold) dilution of the upper layer with the dispersion solvent

### 3.4.5 Dispersion Polymerization of 3-BAEPhA using Poly(DMA)<sub>96</sub>

To circumvent boroxine, pinacol-protected BA (3-BAEPhA) was investigated. Given the similarities in monomer performance in solution (Fig. 2.10), the same conditions were employed for the dispersion polymerization of 3-BAEPhA (20 wt/vol%) as for 3-BAPhA (above), although the medium was different (1:2 Water/EtOH as opposed to 3:1 Water/EtOH). Since heterogeneous polymerizations of BBMA over longer polymerization times have been reported to give a slight coagulum,<sup>73</sup> the short polymerization time of 2 h was expected to minimise pinacol group hydrolysis and boroxine formation. Using the longer steric stabiliser poly(DMA)<sub>96</sub> macroRAFT agent with 3-BAEPhA (20 wt/vol%) for targeted degree of polymerizations ( $DP_s$ ) = 50, 150 and 200 (Fig. 3.12(a)) resulted in shifts in  $M_n$  to higher MWs of ( $M_n$ ) = 20,700, 39,000, and 44,500 g mol<sup>-1</sup> respectively, at near-full (99%) conversion (Run 5-7, Table 3.3). The low MW tail contributes to the high  $\bar{D}$  = 1.57-1.76, and is consistent with the carryover of dead chains from the preparation of the poly(DMA)<sub>96</sub> by chain extension of poly(DMA)<sub>39</sub>. However, dead chains (in Fig. 3.12 (a)) are also due to the increasing [VA-044]<sub>0</sub> used with higher targeted  $DP$ . The appearance of the resulting polymerization mixtures was gel-like, but importantly with no brown coagulum (Fig. 3.12).



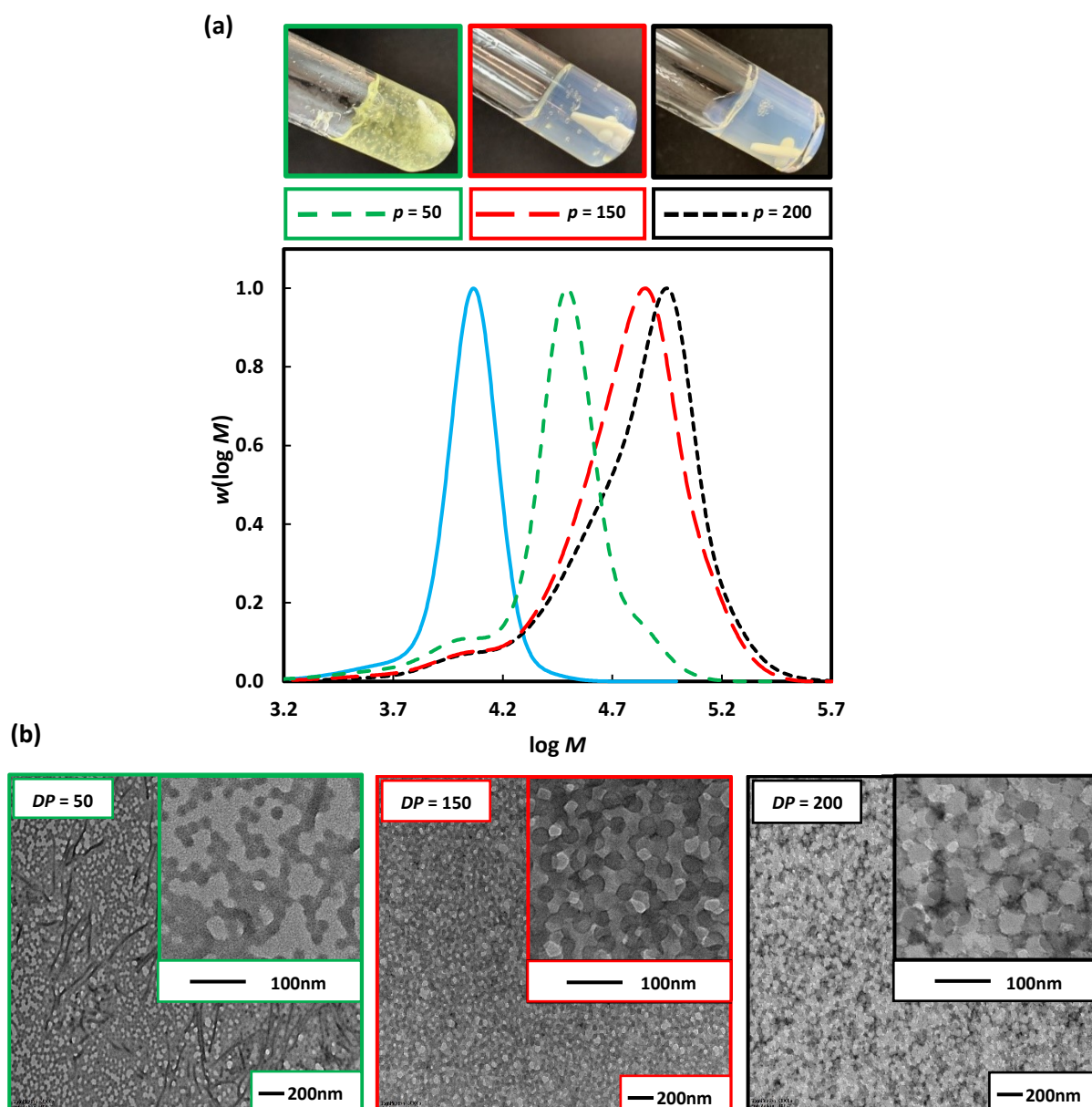


**Figure 3.12:** Poly(DMA)<sub>96</sub> as macroRAFT agent (solid blue line) in the 2 h dispersion polymerizations of 3-BAEPHA (20 wt/vol%) in 1:2 Water/EtOH at 70 °C, where  $[\text{poly}(\text{DMA})_{96}]_0/[\text{VA-044}]_0 = 50, 20, 14$  for targeted degree of polymerization,  $DP = 50$  (Run 5), 150 (Run 6) and 200 (Run 7) respectively. **(a)** MWDs (99% conv.); **(b)** Visual appearance of polymerizations (with white stirrer bar within) (see ESI,<sup>68</sup> for additional images).

The lowest  $DP$  sample gave the only non-cloudy gel, with viscosity appearing to decrease with increasing  $DP$ . In PISA, the formation of worm-like micelles is often the cause of increases in viscosity due to worm entanglement.<sup>81</sup> Long worms of up to 1  $\mu\text{m}$  in length are evident at the lowest targeted  $DP$  along with interconnected spherical particles (Run 5). Support for the decrease in viscosity is the replacement of the worm-like micelle phase at the lowest  $DP$  with about 20 nm solid NPs at  $DP = 150$  (Run 6) and 200 (Run 7) (Fig. 3.12(b)). From Run 6 to 7, the  $M_n(\text{GPC})$  increase of 5,500  $\text{g mol}^{-1}$  surprisingly resulted in little effect on morphology, other than rounder NPs (Table 3.2).

**Table 3.2.** Experimental results for dispersion PISA of 3-BAEPhA using poly(DMA)<sub>96</sub> macroRAFT agents.

Run <sup>a</sup>	[M] <sub>0</sub> /[poly(DMA)] <sub>0</sub>	Polymer <sup>b</sup>	Conv. (%) <sup>c</sup>	$M_{n,\text{th}}$ <sup>d</sup>	$M_n$ <sup>e</sup>	$\bar{D}$ <sup>e</sup>
5	50	poly(DMA) <sub>96</sub> - <i>b</i> -poly(3-BAEPhA) <sub>50</sub>	99	23,600	20,700 <sup>f</sup>	1.57 <sup>f</sup>
6	150	poly(DMA) <sub>96</sub> - <i>b</i> -poly(3-BAEPhA) <sub>149</sub>	99	50,600	39,000 <sup>f</sup>	1.76 <sup>f</sup>
7	200	poly(DMA) <sub>96</sub> - <i>b</i> -poly(3-BAEPhA) <sub>198</sub>	99	64,000	44,500 <sup>f</sup>	1.76 <sup>f</sup>

<sup>a</sup>See Fig. 3.12. for dispersion polymerization conditions and conversions. <sup>b</sup> $DP$  of the stabilizer block is calculated from  $M_n(\text{GPC})$  poly(DMA)<sub>96</sub> (9900  $\text{g mol}^{-1}$ ,  $\bar{D} = 1.17$ ) and the  $DP$  of the poly(3-BAPhA) block is based on conversion. <sup>c</sup>Measured by <sup>1</sup>H NMR see ESI<sup>68</sup>. <sup>d</sup>Theoretical ( $M_{n,\text{th}}$ ) is calculated from poly(3-BAEPhA)  $DP$  added to the poly(DMA)  $M_n(\text{GPC})$ . <sup>e</sup> $\text{g mol}^{-1}$  and determined by GPC/RI in DMF (0.01 M LiBr) <sup>f</sup>GPC for the polymerization of 3-BAPhA is after pinacol protection to poly(3-BAEPhA).

### 3.4.6 Dispersion Polymerization of 3-BAEPhA using Poly(DMA)<sub>36</sub>

The particle morphology in PISA is primarily dictated by the relative volume fractions of the two blocks as described by the packing parameter ( $P$ ).<sup>82</sup> Thus, extending a shorter stabilizer macroRAFT agent allows easier access to a wider range of morphologies. Poly(DMA)<sub>36</sub> (as opposed to poly(DMA)<sub>96</sub> above) was used for 2 h dispersion polymerization of 3-BAEPhA (20 wt/vol%) using targeted  $DP$  of 50 (Run 8), 100 (Run 9), 150 (Run 10), and 200 (Run 11) at 70 °C (Fig. 3.13).

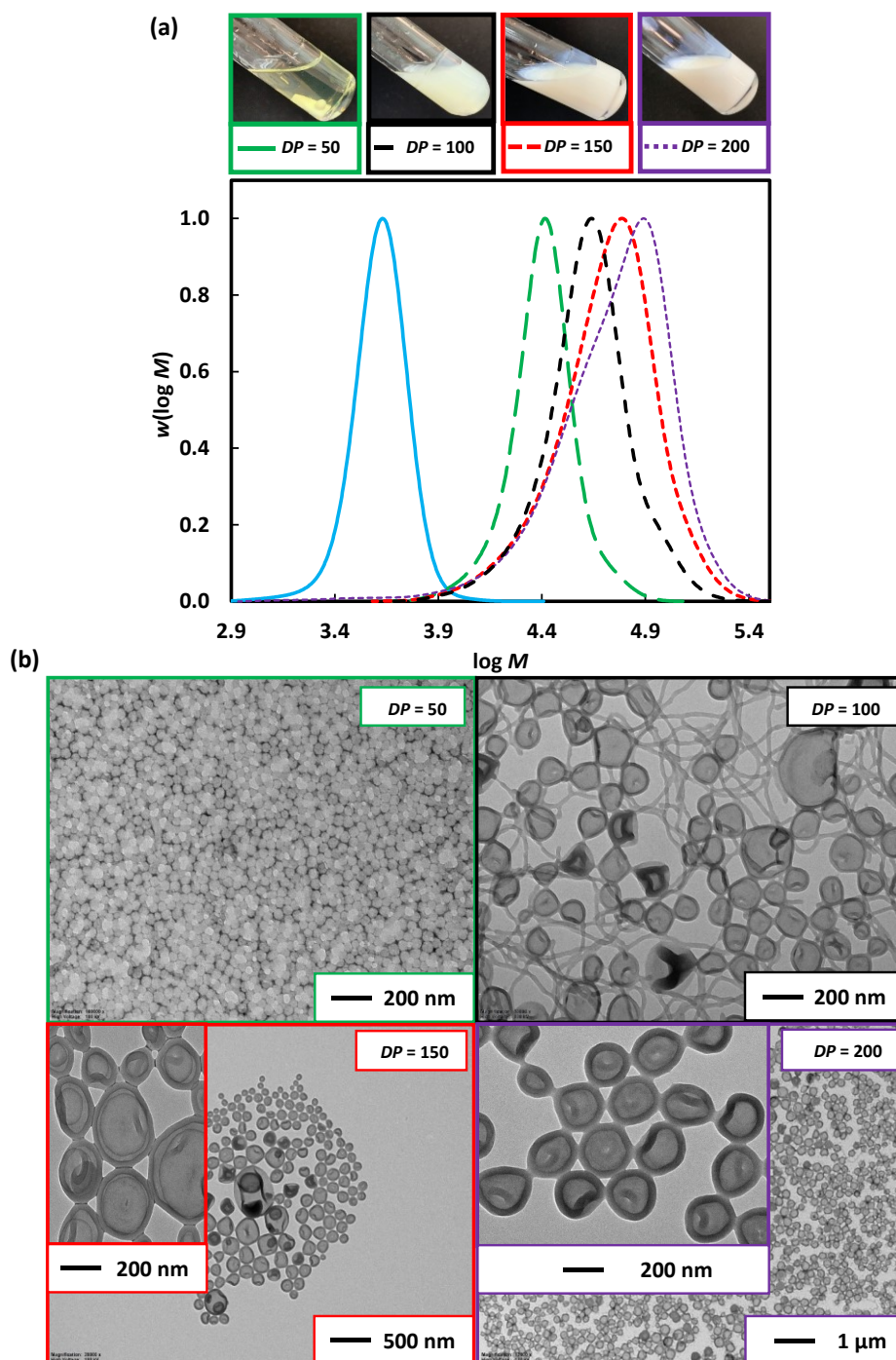


**Figure 3.13:** Poly(DMA)<sub>36</sub>, as macroRAFT agent (solid blue line) in the 2 h dispersion polymerizations of 3-BAEPHA (20 wt/vol%) in 1:2 Water/EtOH at 70 °C, where  $[\text{poly}(\text{DMA})_{36}]_0/[\text{VA-044}]_0 = 50, 25, 17$  and  $12$  for targeted degree of polymerization,  $DP = 50$  (Run 8), 100 (Run 9), 150 (Run 10) and 200 (Run 11) respectively. **(a)** Visual appearance of polymerizations (with white stirrer bar within) and MWDs (99% conv.) (see ESI,<sup>68</sup> for additional images).

Free-flowing white stable colloidal dispersions were formed for all polymerizations, apart from at the highest initial poly(DMA)<sub>36</sub> concentration ( $DP = 50$ ), which resulted in a clear gel. All polymerizations proceeded to completion (99%) in the case of  $DP = 50, 100,$  and  $150,$  with narrow MWDs ( $\mathcal{D} = 1.15-1.38$ ), with only the MWD at  $DP = 200$  ( $\mathcal{D} = 1.63$ , Table 3.3) broad.

**Table 3.3.** Experimental results for dispersion PISA of 3-BAEPHA using poly(DMA)<sub>36</sub> macroRAFT agents.

Run <sup>a</sup>	[M] <sub>0</sub> /[poly(DMA)] <sub>0</sub>	Polymer <sup>b</sup>	Conv. (%) <sup>c</sup>	$M_{n,th}$ <sup>d</sup>	$M_n$ <sup>e</sup>	$\mathcal{D}$ <sup>e</sup>
8	50	poly(DMA) <sub>36</sub> - <i>b</i> -poly(3-BAEPHA) <sub>50</sub>	99	17,600	23,600 <sup>f</sup>	1.15 <sup>f</sup>
9	100	poly(DMA) <sub>36</sub> - <i>b</i> -poly(3-BAEPHA) <sub>99</sub>	99	30,900	30,500 <sup>f</sup>	1.28 <sup>f</sup>
10	150	poly(DMA) <sub>36</sub> - <i>b</i> -poly(3-BAEPHA) <sub>149</sub>	99	44,600	43,100 <sup>f</sup>	1.38 <sup>f</sup>
11	200	poly(DMA) <sub>36</sub> - <i>b</i> -poly(3-BAEPHA) <sub>198</sub>	99	58,000	40,800 <sup>f</sup>	1.63 <sup>f</sup>

<sup>a</sup>See Fig. 3.13 for dispersion polymerization conditions and conversions. <sup>b</sup> $DP$  of the stabilizer block is calculated from  $M_n(\text{GPC})$  poly(DMA)<sub>36</sub> (3900 g mol<sup>-1</sup>,  $\mathcal{D} = 1.10$ ) and the  $DP$  of the poly(3-BAPHA) block is based on conversion. <sup>c</sup>Measured by <sup>1</sup>H NMR see SI. <sup>d</sup>Theoretical ( $M_{n,th}$ ) is calculated from poly(3-BAEPHA)  $DP$  added to the poly(DMA)  $M_n(\text{GPC})$ . <sup>e</sup>g mol<sup>-1</sup> and determined by GPC/RI in DMF (0.01 M LiBr) <sup>f</sup>GPC for the polymerization of 3-BAPHA is after pinacol protection to poly(3-BAEPHA).

High blocking efficiency was indicated by  $M_n$  of 23,600, 30,500, and 43,100 g mol<sup>-1</sup> in relatively close agreement with  $M_{n,th}$  of 17,600, 30,900, and 44,600 g mol<sup>-1</sup> for targeted  $DP = 50, 100,$  and  $150$  respectively. For  $DP = 50$  (Run 8), ~10 nm solid spherical particles of narrow size distribution were obtained (Fig. 3.13), with TEMs showing similar morphology to Runs 6 and 7 ( $DP = 150$  and  $200$  from poly(DMA)<sub>96</sub>), indicative of similar  $P$  or comparable ratios of solvophilic (poly(DMA)) to solvophobic (poly(3-BAEPHA)) chain lengths. The size of polymer objects significantly increases from  $DP = 50$  to  $DP = 100$ , with 50-200 nm diameter vesicles with filaments/worms within aggregates evident in the TEM images of Run 9. For  $DP = 150$  (Run 10), there are no worms, with 50-300 nm diameter spherical vesicles observed. Increasing  $DP$  further ( $DP = 200$ , Run 11) yields a narrower distribution of vesicles of mostly

200 nm in diameter. In TEM images for Run 9-11 encapsulation of NPs within vesicles is apparent, with at the highest *DP*, most particles appearing as yolk-shell type vesicles.<sup>83</sup>

### **3.5 Conclusions and Future Work**

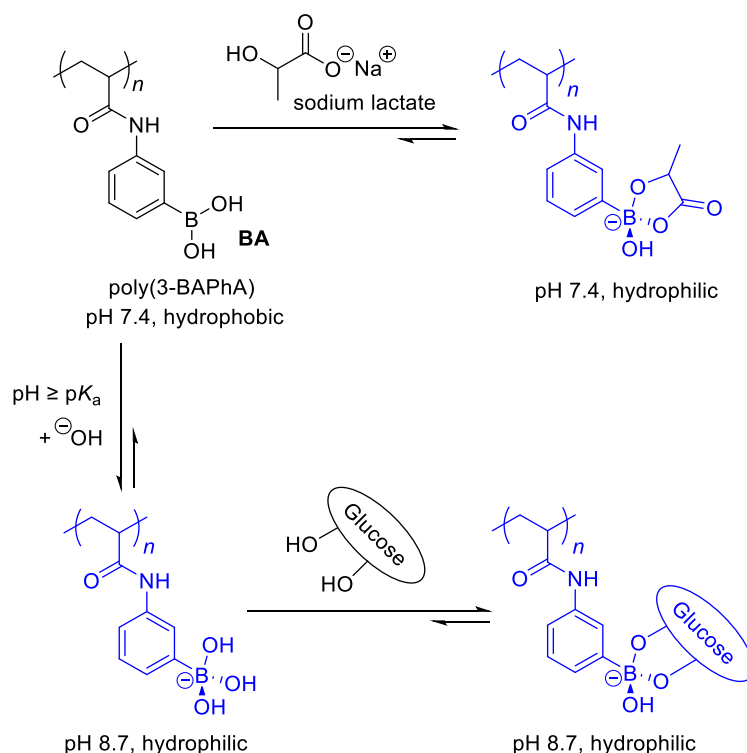
PISA is successful for the unprotected BA monomer (3-BAPhA) when using a longer stabilizer poly(DMA) block, yielding mainly spherical NPs. This polymerization appears to proceed in two phases giving boroxine agglomeration and a separable free-flowing dispersion. These suspended NPs undergo room temperature morphology transitions by aqueous dilution, where hydrolysis of the boroxine core to BA occurs. This new type of stimuli-responsive NP will be the subject of future investigations with the free BA moieties allowing sugar-sensing. Pinacol group protection (in 3-BAEPHA) prevents boroxine formation, with PISA giving core-shell spherical polyacrylamide NPs and an array of higher order objects, including worms and vesicles.

PISA of 3-BAPhA requires further investigation, where the dehydration of BA-moieties to boroxine is minimised. This would allow the preparation of high concentrations of sugar-responsive nanoparticles directly from PISA. Possible remedies could be to alter the dispersion phase or to add a diluent monomer or to carry out the dispersion polymerization using an alternative monomer with BA as part of the steric stabilizer block.

## Chapter 4: LACTATE and GLUCOSE-RESPONSIVE BLOCK COPOLYMER SPHERES and WORMS

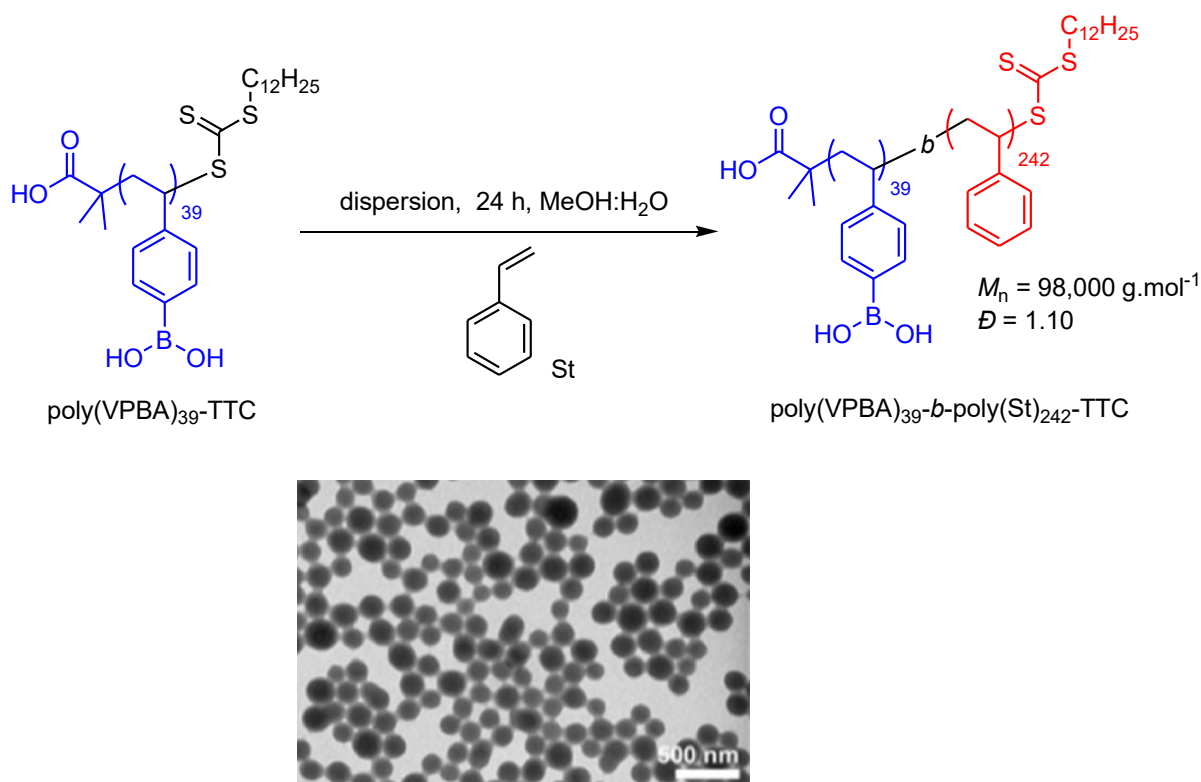
### 4.1 Introduction

Boronic acid (BA) reversibly binds to *cis*-diols, including sugars, to form anionic boronate esters.<sup>4,84</sup> The property is utilized in the regulation of blood glucose in insulin-deficient diabetic conditions.<sup>84,85</sup> Glucose binding to BA triggers disassembly and drug (including insulin) release from amphiphilic block copolymer nanoparticles.<sup>15,16,52,86-90</sup> The equilibrium for binding is however pH-dependent (Scheme 4.1), with the boronate ester of glucose most favoured at or above the pK<sub>a</sub> of boronic acid<sup>5,6,91</sup> of about pH 8.7.<sup>92</sup> Hydrophobic BA functionalized polymer thus becomes water-soluble under the basic conditions required for glucose binding. The trigonal planar BA moiety can however form tetrahedral boronate ester by binding with  $\alpha$ -hydroxy carboxylic acid salts, such as lactate, at neutral physiological pH 7.4.<sup>55,56</sup> Lactate binding of amphiphilic block copolymers remains unexplored, despite *L*-lactate production in anaerobic metabolism, with the reversible binding to BA offering an alternative to enzymatic monitoring useful to the fermentation industry,<sup>93</sup> clinical diagnostics,<sup>94</sup> and sports medicine.<sup>95</sup>



**Scheme 4.1:** The formation of charged boronate esters (in blue) from poly(3-BAPhA).

Most glucose-responsive amphiphilic block copolymers are prepared by reversible addition-fragmentation chain transfer (RAFT) polymerization of 3-(acrylamidophenyl)boronic acid (3-BAPhA).<sup>5,6,15,16,48,52,68</sup> Chapter 3 described spherical nanoparticles and sub-micron size rods by RAFT-mediated dispersion polymerization induced self-assembly (PISA) of 3-BAPhA.<sup>68</sup> However, the concentrated heterogeneous polymerization conditions (3-BAPhA loading = 20 wt/vol%) led to the cross-linking of polymer chains within the nanoparticle core by the reversible-formation of boroxine moieties. PISA implemented as dispersion polymerization directly gives higher order morphologies (worms and vesicles) only when the BA is protected as a pinacol ester.<sup>68,75</sup> Otherwise, PISA should be carried out with the BA-substituted sugar-binding functionality as part of the steric stabilizer block. In this case, RAFT-mediated PISA with styrene (St) gives nanospheres with the BA-substituent at the surface, although gelation due to boroxine formation is also observed.<sup>96</sup> Poly(4-vinylphenylboronic acid, VBA)<sub>39</sub>-TTC gave 135 nm spheres by dispersion polymerization of St (Scheme 4.2).



**Scheme 4.2:** Dispersion polymerization of St (TEM within).<sup>96</sup>

## 4.2 Chapter Aims and Objectives

Herein, 3-BAPhA in RAFT-mediated solution (homogeneous) polymerizations to give four all acrylamide amphiphilic block copolymers (Fig. 4.1). The effect of varying  $DP$  of the poly(DMA) and poly(3-BAPhA) blocks on morphology and stimuli-response (lactate and glucose) is examined. The effect of introducing a non-stimuli response hydrophobic block (*N*-*tert*-butylacrylamide; TBAM) on morphology was examined.

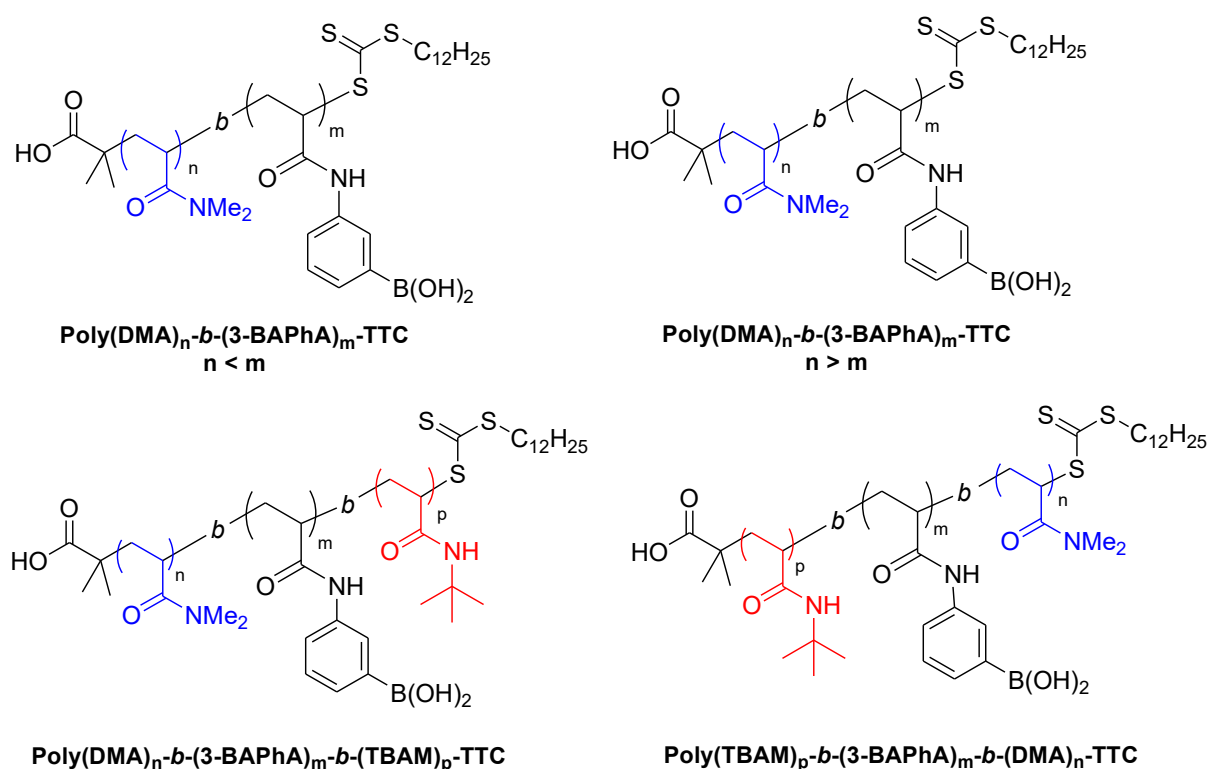


**Figure 4.1:** Amphiphilic block copolymers targets.

- To prepare amphiphilic diblock and triblock copolymers containing 3-BAPhA using RAFT solution polymerizations, which after dialysis give glucose-responsive nanoparticles. The dialysis allows high dilution conditions ( $\sim 0.2$  wt/vol%), which prevent agglomeration due to boroxine.<sup>68</sup>
- The preparation of the first worm-like morphologies of BA-block copolymers.
- To establish self-assembly using lactate at physiological pH for core-shell nanoparticles and compare with glucose response under basic conditions.



## 4.3 Experimental part

### 4.3.1 Materials

2-(Dodecylthiocarbonothioylthio)-2-methylpropionic acid (DMP; TCI, >98%) and 2,2'-azobis[2-(2-imidazolin-2-yl)propane]dihydrochloride (VA-044, Wako, 97%) were used as received. Milli-Q water, ethanol (EtOH, VWR, ≥99%), diethyl ether (Et<sub>2</sub>O; Fisher, >99.5%), dioxane (Fluorochem >99%), *N,N*-dimethylformamide (DMF; VWF, HPLC-grade ≥99.9%), and CHCl<sub>3</sub> (Fisher, >99.8%) were used directly as solvents. *N,N*-Dimethylacrylamide (DMA; TCI, 98%) was passed through a column of basic alumina (Acros Organics 40 – 300 μm, 60 Å) to remove the inhibitor prior to use.<sup>76</sup> *N-tert*-butylacrylamide (TBAM; TCI, >98%), anisole (TCI, >99%), and pinacol (TCI, >98%) were used as received. 3-(Acrylamidophenyl)boronic acid (3-BAPhA) was prepared according to the literature,<sup>11</sup> from 3-aminophenylboronic acid monohydrate (Fluorochem, 97%), acryloyl chloride (Alfa Aesar, 96%), and sodium bicarbonate (Fisher Scientific >99.7%) in 1:1 tetrahydrofuran (THF; Fisher, >99.8%):water. Molecular sieves (MS, Alfa Aesar, 3 Å, 0.800 g) were activated before use, by placing in a microwave (Toshiba ER-7620 650 W) three times for 2 min periods at medium power, with 30 s swirling aeration intervals. Sodium *L*-lactate (Alfa Aesar, >98%), NaOH (Alfa Aesar, 98%), and glucose (Alfa Aesar, 99%) were used as received.

### 4.3.2 Nuclear Magnetic Resonance (NMR) Spectroscopy

<sup>1</sup>H NMR spectra were recorded using a Bruker Avance II 400 MHz spectrometer. All spectra were recorded in *D*<sub>6</sub>-dimethyl sulfoxide (DMSO-*D*<sub>6</sub>, Goss Scientific, 99.9%), except for the final isolated block copolymers, which were recorded in methanol-*D*<sub>4</sub> (*D*<sub>4</sub>-MeOH, TCI, >99.8%).

### 4.3.3 Determination of monomer conversion

Please refer to section 2.2.2.2.1, with exception to the following: conversion is calculated by comparing the anisole peak integral (representing the standardized solution) at 3.75 ppm (Me, 3H) to the integral for the monomer (*cis*-vinyl, 1H) at 5.74 (3-BAPhA), 5.48 (TBAM) or 5.67 (DMA) ppm.

### 4.3.4 Calculation of the theoretical number fraction of living chains (*L*)

In RAFT, it is advantageous to use low initiator concentrations to improve *L*, since the number of chains that undergo bimolecular termination directly corresponds to the number of radicals generated from decomposition of the initiator during polymerization:

$$L = \frac{[RAFT]_0}{[RAFT]_0 + 2 \times f \times [VA-044]_0 \times (1 - e^{-k_d t}) \times \left(1 - \frac{f_c}{2}\right)} \quad (4.1)$$

Eq. (4.1) estimates  $L$ , where  $t$  is time in s,  $f$  is the initiator efficiency (assumed to be 0.5), and the decomposition rate constant  $k_d$  is taken as  $4.30 \times 10^{-4} \text{ s}^{-1}$  for VA-044 at 70 °C in 20% aq. DMF or dioxane (conditions employed in the present work).<sup>43,97</sup> The quantity  $\left(1 - \frac{f_c}{2}\right)$  accounts for the effect of the termination mechanism (combination or disproportionation). Combination would half the number of radicals, so  $f_c = 1$ , while disproportionation would not change the number of radicals, and herein this is assumed with  $f_c = 0$ .

#### 4.3.5 Gel Permeation Chromatography (GPC)

Please see section 2.2.2.3.

#### 4.3.6 Preparation of GPC Sample (GPC)

Molecular sieves (MS, Alfa Aesar, 3 Å, 0.800 g) were activated three times by microwave (Toshiba ER-7620 650 W) for 2 min periods at medium power, with 30 s swirling aeration intervals. Pinacol (TCl, >98%, 0.148 g, 1.250 mmol) in  $\text{CHCl}_3$  (Fisher, >99.8%, 5.00 mL) and the polymerization sample (20  $\mu\text{l}$ ) were added to the activated MS, and stirred for 24 h, at room temperature. MS were removed using gravity filtration, and the solution evaporated to a residue, which was dissolved in 1 mL of the GPC eluent. Herein, GPC is after pinacol protection of the BA block to poly(3-BAEPHA).

#### 4.4 General polymerization procedure

All polymerization solutions were added to borosilicate glass tubes sealed with septa and flushed with  $\text{N}_2$  for 30 min at 70 °C and heated for a further 1.5 h at 70 °C (total polymerization time = 2 h). An aluminium-heating block is used for heating and the temperature is maintained within  $\pm 0.2$  °C throughout.

##### 4.4.1 Preparation of poly(DMA)-TTC MacroRAFT agents

The preparation of poly(DMA)<sub>28</sub>-TTC (section 3.3.3.2), poly(DMA)<sub>36</sub>-TTC (section 3.3.3.3) and poly(DMA)<sub>96</sub>-TTC (section 3.3.3.4) is already described.<sup>68</sup> Poly(DMA)<sub>38</sub>-TTC is prepared as follows: A standardized solution of VA-044 ( $4.50 \times 10^{-4} \text{ molL}^{-1}$  using a volumetric flask) was prepared by serial dilution (250 times) of VA-044 (36 mg, 0.11 mmol) in 20% aq. dioxane. DMP

(0.163 g, 0.45 mmol), DMA (2.212 g, 22.32 mmol) and VA-044 ( $4.50 \times 10^{-4} \text{ molL}^{-1}$ ) in 20% aq. dioxane (5 mL) were heated at 70 °C for 2 h. The polymer was precipitated in Et<sub>2</sub>O, filtered, and dried at room temperature under vacuum for 24 h to give poly(DMA)<sub>38</sub>-TTC,  $M_n = 4,100 \text{ g.mol}^{-1}$ ,  $\bar{D} = 1.10$ , isolated = 2.30 g (97%).

#### 4.4.2 Chain extension of poly(DMA)<sub>38</sub>-TTC using [3-BAPhA]<sub>0</sub>/[poly(DMA)<sub>38</sub>-TTC]<sub>0</sub> = 100

A standardized solution of VA-044 ( $2.10 \times 10^{-4} \text{ molL}^{-1}$  using a volumetric flask) was prepared by serial dilution (625 times) of VA-044 (42 mg, 0.13 mmol) in 20% aq. DMF. Poly(DMA)<sub>38</sub>-TTC (0.123 g, 0.03 mmol), 3-BAPhA (0.573 g, 3.00 mmol) and VA-044 ( $2.10 \times 10^{-4} \text{ molL}^{-1}$ ) in 20% aq. DMF (1 mL) were heated at 70 °C for 2 h. The polymer was precipitated in Et<sub>2</sub>O, filtered, and dried at room temperature under vacuum for 24 h to give poly(DMA)<sub>38</sub>-(3-BAPhA)<sub>36</sub>-TTC, conv. = 36%,  $M_n = 14,300 \text{ g.mol}^{-1}$ ,  $\bar{D} = 1.36$ , isolated 0.48 = g (70%).

#### 4.4.3 One-pot iterative RAFT polymerization procedures

The synthesis begins with preparation (in volumetric flask) of a standardized initiator (VA-044) solution. E.g. poly(DMA)<sub>28-b</sub>-(3-BAPhA)<sub>84</sub>-TTC each polymerization cycle used 3-BAPhA]<sub>0</sub>/[MacroRAFT]<sub>0</sub> = 25 (Table 4.1): For the first block, VA-044 (64.6 mg, 0.20 mmol) is used to make a standardized  $8 \times 10^{-4} \text{ molL}^{-1}$  (M) solution by 250 dilution with 20% aq. DMF. Poly(DMA)<sub>28</sub>-TTC (368.6 mg, 0.12 mmol) and 3-BAPhA (561.5 mg, 2.94 mmol) were added to 1 mL of the standardized VA-044 solution. Before commencing each polymerization (20 μl) of the solution is sampled for conversion measurements by NMR (2.2.2.2.1).

**Table 4.1.** Experimental conditions for the preparation of poly(DMA)<sub>28</sub>-*b*-(3-BAPhA)<sub>84</sub>-TTC in 20% aq. DMF at 70 °C by one-pot 2 h iterative RAFT polymerizations from poly(DMA)<sub>28</sub>-TTC macroRAFT agent ( $M_n = 3,100$ ) with  $[3\text{-BAPhA}]_0/[MacroRAFT]_0 = 25$  for all four chain extensions.

Chain Extensions	1	2	3	4
Conversion (%)	84	66	92	92
3-BAPhA added (mg)	561.5	451.0 <sup>a</sup>	361.7 <sup>a</sup>	433.0 <sup>a</sup>
Poly(DMA) <sub>28</sub> added (mg)	362.7	-	-	-
VA-044 added (mg) <sup>b</sup>	0.2586	0.3904 <sup>c</sup>	0.7405 <sup>c</sup>	1.2357 <sup>c</sup>
Total Solvent (mL)	1.00	1.24	2.30	2.77
[3-BAPhA] <sub>0</sub> (molL <sup>-1</sup> )	2.94	2.24	1.26	0.88
[MacroRAFT] <sub>0</sub> (molL <sup>-1</sup> )	0.1170	0.0882 <sup>d</sup>	0.0498 <sup>d</sup>	0.0346 <sup>d</sup>
[VA-044] <sub>0</sub> (molL <sup>-1</sup> )	8.00 x 10 <sup>-4</sup>	9.74 x 10 <sup>-4</sup>	9.96 x 10 <sup>-4</sup>	1.38 x 10 <sup>-3</sup>
[MacroRAFT] <sub>0</sub> / [VA-044] <sub>0</sub>	146	91	50	25
Cumulative <i>L</i> (%) <sup>e</sup>	98.9	97.9	96.6	92.4

<sup>a</sup>Additions determined by conv. and 60 μl reaction sampling for conv. and GPC measurements. <sup>b</sup>After serial dilution. <sup>c</sup>Addition based on VA-044 remaining from the previous chain extension. <sup>d</sup>Estimated after reaction dilution and sampling. <sup>e</sup>Cumulative livingness (*L*) calculated using eq. (4.1) beginning from poly(DMA)<sub>28</sub>-TTC with *L* = 99.5%.

All polymerization cycles were heated at 70 °C in an aluminium-heating block for 2 h and stopped by quenching in an ice-water bath. At the end of the polymerization, samples are taken for GPC (20 µl, see 4.3.5) and conversion measurement (20 µl). Iterative chain extension reactions were performed directly on the macroRAFT agent polymerization solution (*i.e.* one-pot reaction) with the amount of initiator and monomer remaining after each cycle factored in. *E.g.* Table 4.1 shows that the first cycle proceeded in 84% conversion, thus ~16% monomer (considering sampling for conversion at  $t = 0$ ) is deducted from the amount of monomer added. The amount of initiator remaining, according to eq. 4.2 (considering sampling for conversion at  $t = 0$ ) is also factored in. Initiator decomposition eq. (4.2):

$$m_{\text{VA-044}_{\text{remaining}}} = m_{\text{VA-044}_{\text{Total}}} \times 2f e^{-k_d t} \times \left(1 - \frac{f_c}{2}\right) \quad (4.2)$$

Eq. 4.2 equation variables can be found in section 4.3.4. Thus, each cycle involved adding further monomer in VA-044 standardized solution to the *in situ* formed macroRAFT and agitating the reaction mixture by vortex (Stuart SA8) to ensure a homogenous solution prior to polymerization. The chain extensions were sampled before and after each cycle for NMR conversion (20 µl before and 20 µl after polymerization) and GPC analysis (20 µl after polymerization), as described above. The final block copolymers were precipitated from an excess of cold Et<sub>2</sub>O (500 mL). The latter solvent was removed by decanting from the precipitated polymer. The polymer was dried at room temperature under vacuum for 72 h.

#### 4.4.4 Self-assembly and stimuli-response

The amphiphilic block copolymers (1.2 µmol: poly(DMA)<sub>28</sub>-*b*-(3-BAPhA)<sub>84</sub>-TTC = 33.2 mg; poly(DMA)<sub>96</sub>-*b*-(3-BAPhA)<sub>62</sub>-TTC = 28.9 mg; poly(DMA)<sub>36</sub>-*b*-(3-BAPhA)<sub>49</sub>-*b*-(TBAM)<sub>46</sub>-TTC = 25.8 mg; poly(TBAM)<sub>74</sub>-*b*-(3-BAPhA)<sub>49</sub>-*b*-(DMA)<sub>79</sub>-TTC = 30.2 mg) were dissolved in MeOH/DMF (2.84 mL, 3/4) and water (~0.5 mL at pH 7.4) was added slowly with stirring (500 rpm) at a rate of ~1 drop every 10 s until turbidity (micellization) was observed. The resulting mixture was placed in a 20 cm dialysis bag (Thermo Scientific™ SnakeSkin™ dialysis tubing, molecular weight cut-off, MWCO = 3.5 KDa,) and exchanged with water (500 mL at pH 7.4) for 12 h to exclude the organic solvent and any unreacted monomer. The distilled water was replaced twice with distilled water (at pH 7.4) and dialyzed for a further 6 h each time.

**For *L*-lactate binding:** The same procedure as above was followed, except sodium *L*-lactate at pH 7.4 (0.1 M, ~0.5 mL) was added to the solvated block copolymers until turbidity (micellization) was observed. Further NaOH (0.05 M) dropwise additions were required to maintain the pH of 7.4 by monitoring with a pH meter (Mettler Toledo FP20). The resulting mixture was dialyzed against water (500 mL at pH 7.4), as described above.

**For the *D*-glucose response:** The same procedure as above was followed, except NaOH solution (at pH 8.7) was added to the solvated block copolymers until turbidity (micellization) was observed. The resulting mixture was dialyzed against NaOH solution (500 mL at pH 8.7), as described above. The dialyzed mixture (~10 mL) was sampled (1 mL) and *D*-glucose (0.1 mL, 0.5 M) added to the stirring (500 rpm) turbid sample, while maintaining pH 8.7 through further NaOH (0.05 M) dropwise additions.

#### **4.4.5 Transmission Electron Microscopy (TEM)**

Please refer to section 3.3.2.1. TEM analysis was conducted by Dr Fumi Ishizuka of The University of New South Wales, UNSW, Sydney, Australia.

## 4.5 Results and Discussion

### 4.5.1 Synthesis of Poly(DMA)<sub>n</sub>-*b*-(3-BAPhA)<sub>m</sub>

#### 4.5.1.1 Synthesis of Amphiphilic Diblock Copolymer using *DP* = 100

The one-pot iterative approach was preferred, since 2 h RAFT polymerization of 3-BAPhA (3.0 molL<sup>-1</sup>) with [3-BAPhA]<sub>0</sub>/[poly(DMA)<sub>38</sub>-TTC]<sub>0</sub>/[VA-044]<sub>0</sub> = 100/1/0.007, gave low conversion (36%) and a relatively broad molecular weight distribution (MWD) of the diblock copolymer ( $M_n = 14,300 \text{ gmol}^{-1}$ ,  $\bar{D} = 1.36$ ) (Fig. 4.2, Table 4.2). (TTC = trithiocarbonate end group)

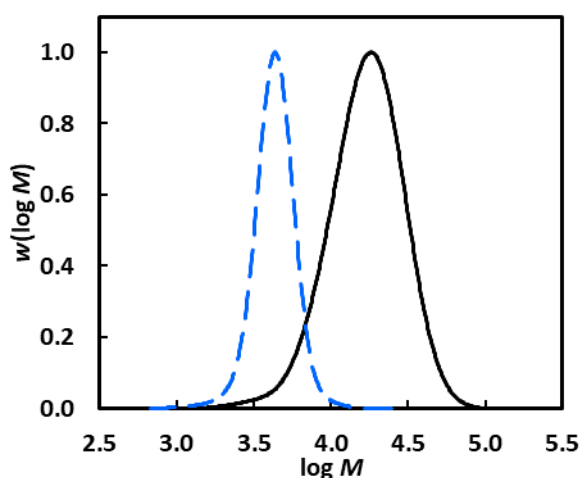


**Fig. 4.2:** GPC for the preparation of the *DP* = 100 diblock copolymer in 20% aq. DMF at 70 °C. RAFT polymerization of 3-BAPhA (3.0 M) from poly(DMA)<sub>38</sub>-TTC (blue dashed) using [3-BAPhA]<sub>0</sub>/[(poly(DMA)<sub>38</sub>-TTC)]<sub>0</sub>/[VA-044]<sub>0</sub> = 100/1/0.007

**Table 4.2:** Characterization of polymers.<sup>a</sup>

Fig.	Polymer <sup>b</sup>	% Conv. <sup>c</sup>	$M_{n,th}$ <sup>d</sup>	$M_n$ <sup>e</sup>	$\bar{D}$ <sup>e</sup>
<b>4.2</b>	poly(DMA) <sub>38</sub> -TTC	-	4,700	4,100	1.10
	poly(DMA) <sub>38</sub> - <i>b</i> -(3-BAPhA) <sub>36</sub> -TTC	36	13,900	14,300 <sup>f</sup>	1.36 <sup>f</sup>
<b>4.3</b>	poly(DMA) <sub>28</sub> -TTC	-	4,400	3,100	1.12
	poly(DMA) <sub>28</sub> - <i>b</i> -(3-BAPhA) <sub>21</sub> -TTC	84	8,800	8,300 <sup>f</sup>	1.26 <sup>f</sup>
	poly(DMA) <sub>28</sub> - <i>b</i> -(3-BAPhA) <sub>21</sub> - <i>b</i> -(3-BAPhA) <sub>17</sub> -TTC	66	13,000	15,600 <sup>f</sup>	1.27 <sup>f</sup>
	poly(DMA) <sub>28</sub> - <i>b</i> -(3-BAPhA) <sub>21</sub> - <i>b</i> -(3-BAPhA) <sub>17</sub> - <i>b</i> -(3-BAPhA) <sub>23</sub> -TTC	92	21,900	24,000 <sup>f</sup>	1.31 <sup>f</sup>
	poly(DMA) <sub>28</sub> - <i>b</i> -(3-BAPhA) <sub>84</sub> -TTC	92	30,300	27,700 <sup>f</sup>	1.32 <sup>f</sup>
	poly(DMA) <sub>96</sub> -TTC	-	9,400	9,900	1.17
<b>4.5</b>	poly(DMA) <sub>96</sub> - <i>b</i> -(3-BAPhA) <sub>14</sub> -TTC	57	13,700	14,000 <sup>f</sup>	1.24 <sup>f</sup>
	poly(DMA) <sub>96</sub> - <i>b</i> -(3-BAPhA) <sub>14</sub> - <i>b</i> -(3-BAPhA) <sub>24</sub> -TTC	95	20,600	19,900 <sup>f</sup>	1.34 <sup>f</sup>
	poly(DMA) <sub>96</sub> - <i>b</i> -(3-BAPhA) <sub>62</sub> -TTC	96	26,500	24,100 <sup>f</sup>	1.48 <sup>f</sup>
	poly(DMA) <sub>36</sub> -TTC	-	4,700	3,900	1.10
<b>4.6</b>	poly(DMA) <sub>36</sub> - <i>b</i> -(3-BAPhA) <sub>49</sub> -TTC	98	17,300	14,400 <sup>f</sup>	1.23 <sup>f</sup>
	poly(DMA) <sub>36</sub> - <i>b</i> -(3-BAPhA) <sub>49</sub> - <i>b</i> -(TBAM) <sub>46</sub> -TTC	91	20,300	21,500 <sup>f</sup>	1.31 <sup>f</sup>
	poly(TBAM) <sub>74</sub> -TTC	96	10,200	9,700	1.16
<b>4.8</b>	poly(TBAM) <sub>74</sub> - <i>b</i> -(3-BAPhA) <sub>49</sub> -TTC	97	23,100	20,100 <sup>f</sup>	1.37 <sup>f</sup>
	poly(TBAM) <sub>74</sub> - <i>b</i> -(3-BAPhA) <sub>49</sub> - <i>b</i> -(DMA) <sub>38</sub> -TTC	76	23,900	23,200 <sup>f</sup>	1.38 <sup>f</sup>
	poly(TBAM) <sub>74</sub> - <i>b</i> -(3-BAPhA) <sub>49</sub> - <i>b</i> -(DMA) <sub>79</sub> -TTC	82	27,300	25,200 <sup>f</sup>	1.43 <sup>f</sup>

<sup>a</sup>See Schemes 4.3, 4.4, 4.5 and 4.6 and Tables 4.1, 4.3-4.5 for polymerization conditions. <sup>b</sup> $\bar{D}P$  calculated from  $M_n$ (GPC) for the first block and conv. of subsequent iterative polymerization blocks. <sup>c</sup>Measured using <sup>1</sup>H NMR. <sup>d</sup>Theoretical ( $M_{n,th}$ ) is calculated using  $M_n$ (GPC) for the first block added to the  $M_n$  of subsequent iterative blocks calculated from conv., accounting for pinacol protection (see part<sup>f</sup>). <sup>e</sup>Determined by RI GPC in DMF (0.01 M LiBr) using commercial linear poly(styrene) as molecular weight standards. <sup>f</sup>GPC measurement after pinacol protection of the 3-BAPhA to 3-BAEPPhA block.

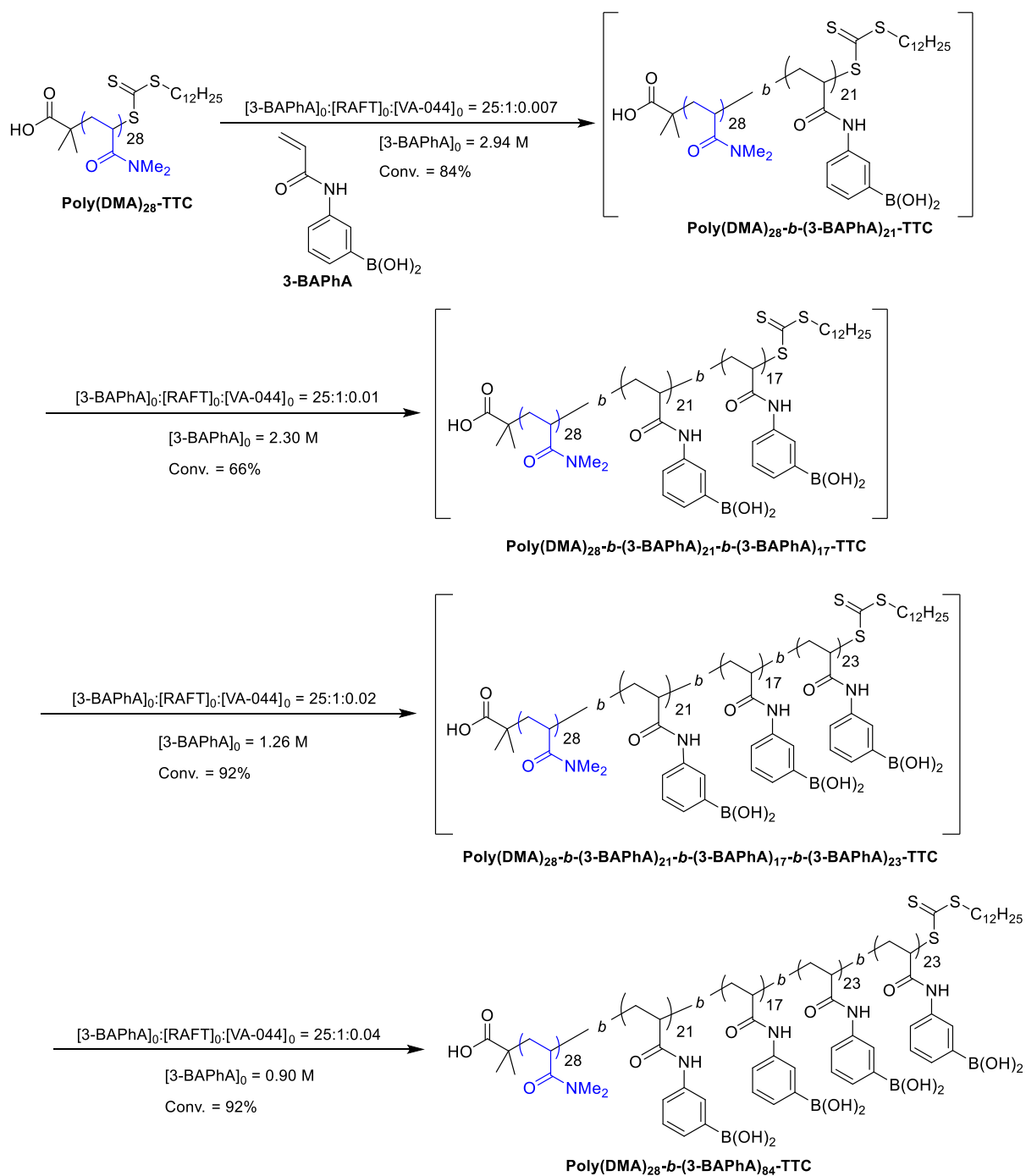
#### 4.5.1.2 Synthesis of Amphiphilic Diblock Copolymers using One-Pot Iterative

##### Polymerization Approach

##### 4.5.1.2.1 Preparation of poly(DMA)<sub>28</sub>-*b*-(3-BAPhA)<sub>84</sub>-TTC

Poly(DMA)<sub>28</sub>-*b*-(3-BAPhA)<sub>84</sub>-TTC was prepared using one-pot iterative RAFT-mediated solution polymerizations of 3-BAPhA, where each block is prepared in 2 h chain extension (cycles) without isolation (and purification) of intermediate blocks,<sup>43,63</sup> beginning from poly(DMA)<sub>28</sub>-TTC (Scheme 4.3), as macroRAFT agent.





**Scheme 4.3:** Preparation of poly(DMA)<sub>28</sub>-*b*-(3-BAPhA)<sub>84</sub>-TTC in 20% aq. DMF at 70 °C by one-pot 2 h iterative RAFT-mediated polymerizations of 3-BAPhA from poly(DMA)<sub>28</sub>-TTC.

The high RAFT agent-to-initiator (VA-044) ratio insures a high fraction of living chains ( $L = 98.8\%$ ) according to eq. 4.1. Beginning with the same initial monomer concentration ( $\sim 3.0 \text{ molL}^{-1}$ ) (as the  $DP = 100$  experiment, 4.5.1.1) and adjusting only  $DP$ , the four repetitive cycles at  $[3\text{-BAPhA}]_0/[\text{MacroRAFT}]_0 = 25$  gave the high MW diblock; poly(DMA)<sub>28</sub>-*b*-(3-BAPhA)<sub>84</sub>-TTC ( $27,700 \text{ gmol}^{-1}$ ) with  $M_n$  in close proximity to  $M_{n,\text{th}}$  ( $30,300 \text{ gmol}^{-1}$ ) and a narrower MWD ( $\mathcal{D} = 1.32$ ) (Fig. 4.3).

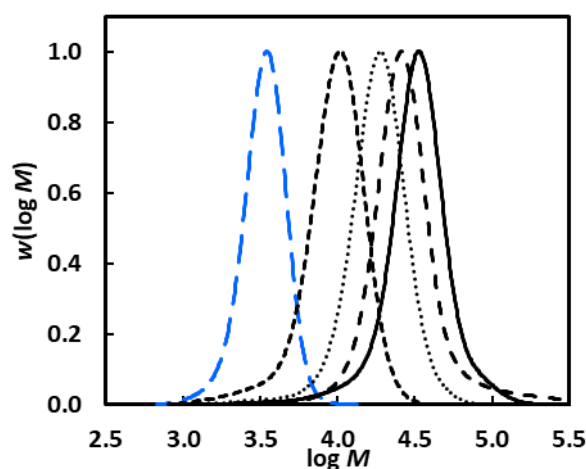


**Figure 4.3:** one-pot iterative RAFT polymerizations of 3-BAPhA from poly(DMA)<sub>28</sub>-TTC (blue long dashed) using  $[3\text{-BAPhA}]_0/[(\text{poly}(\text{DMA})_{28}\text{-TTC})]_0 = 25$  for each chain extension of 3-BAPhA (black lines), according to Scheme 4.3 and Table 4.1.

Thus, the increase in VA-044 ( $[\text{MacroRAFT}]_0/[\text{VA-044}]_0 = \sim 146$  to 25, Table 4.1) for successive cycles did not lead to a significant broadening of the final MWD. The successive dilution with 20% aq. DMF solubilizes added monomer and the increasingly hydrophobic *in situ* formed diblock copolymer macroRAFT agents with each 3-BAPhA addition contributing to the high overall (gram) polymer isolated yield; Poly(DMA)<sub>28</sub>-*b*-(3-BAPhA)<sub>84</sub>-TTC: 1.04 g (40%, if 100% conv. for each cycle). Note – an insurmountably (due to monomer solubility) high initial monomer concentration ( $\sim 2.3 \text{ g}$  ( $\sim 12 \text{ M}$ ) in 1 mL) for the single  $DP = 100$  chain extension would have been required to achieve a comparable isolated yield. Further the successive

dilutions contribute to the narrower MWDs, since lower ratio of [monomer]/[RAFT] at the locus of polymerization, the fewer are the monomer units added per RAFT activation/deactivation cycle.<sup>98</sup> Thus the dilution effect allowed 17-23 3-BAPhA monomer units to be added at each cycle and the amount of monomer (conversion) was not affected by the successive dilutions ( $[\text{Monomer}]_0 = 2.9 \text{ M to } 0.9 \text{ M}$ ). The polymer was isolated by precipitation from  $\text{Et}_2\text{O}$ .  $^1\text{H NMR}$  (30 mg in  $\sim 0.6 \text{ mL}$  recorded in methanol- $D_4$ ) (Fig. 4.4(c)).

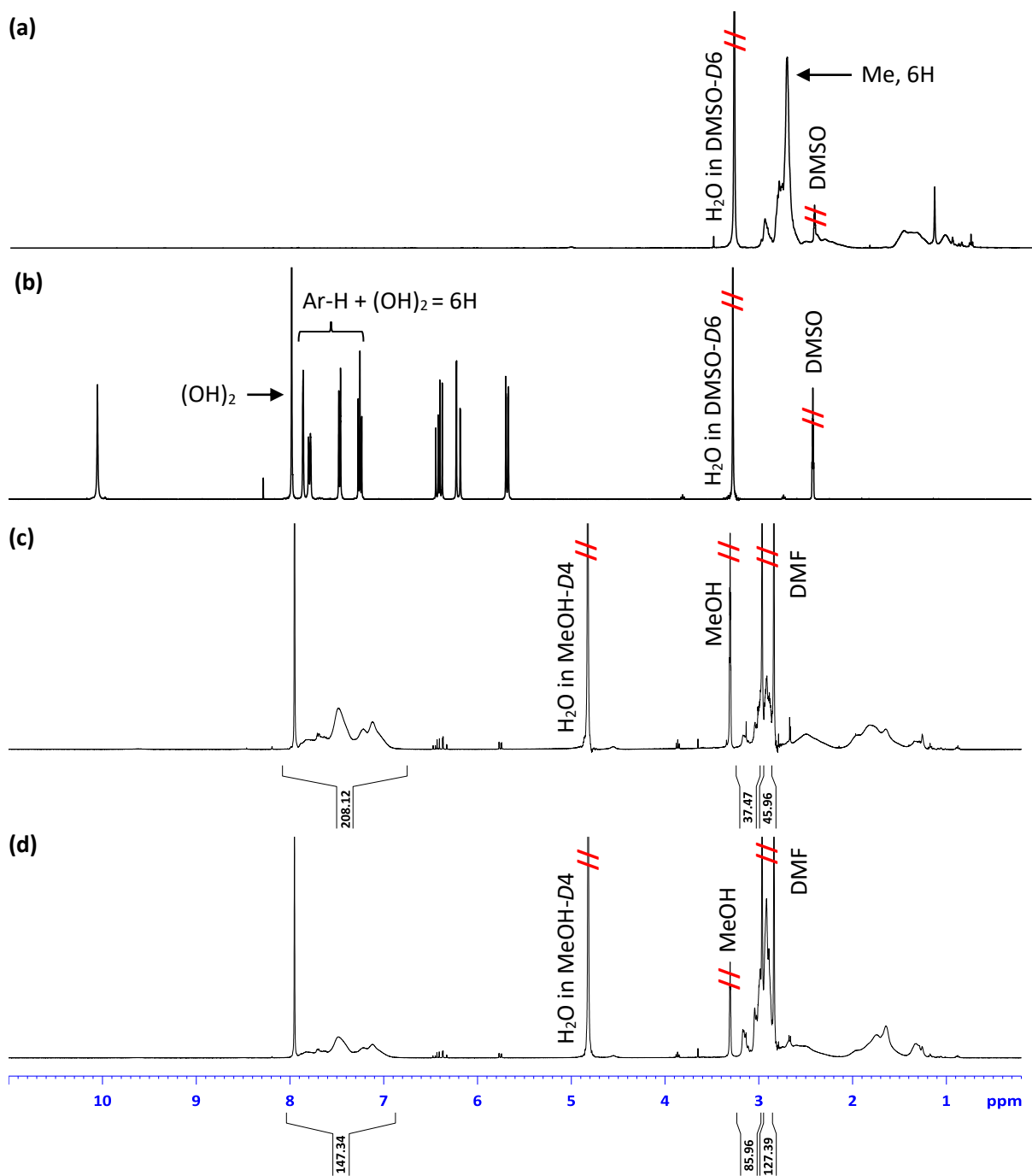
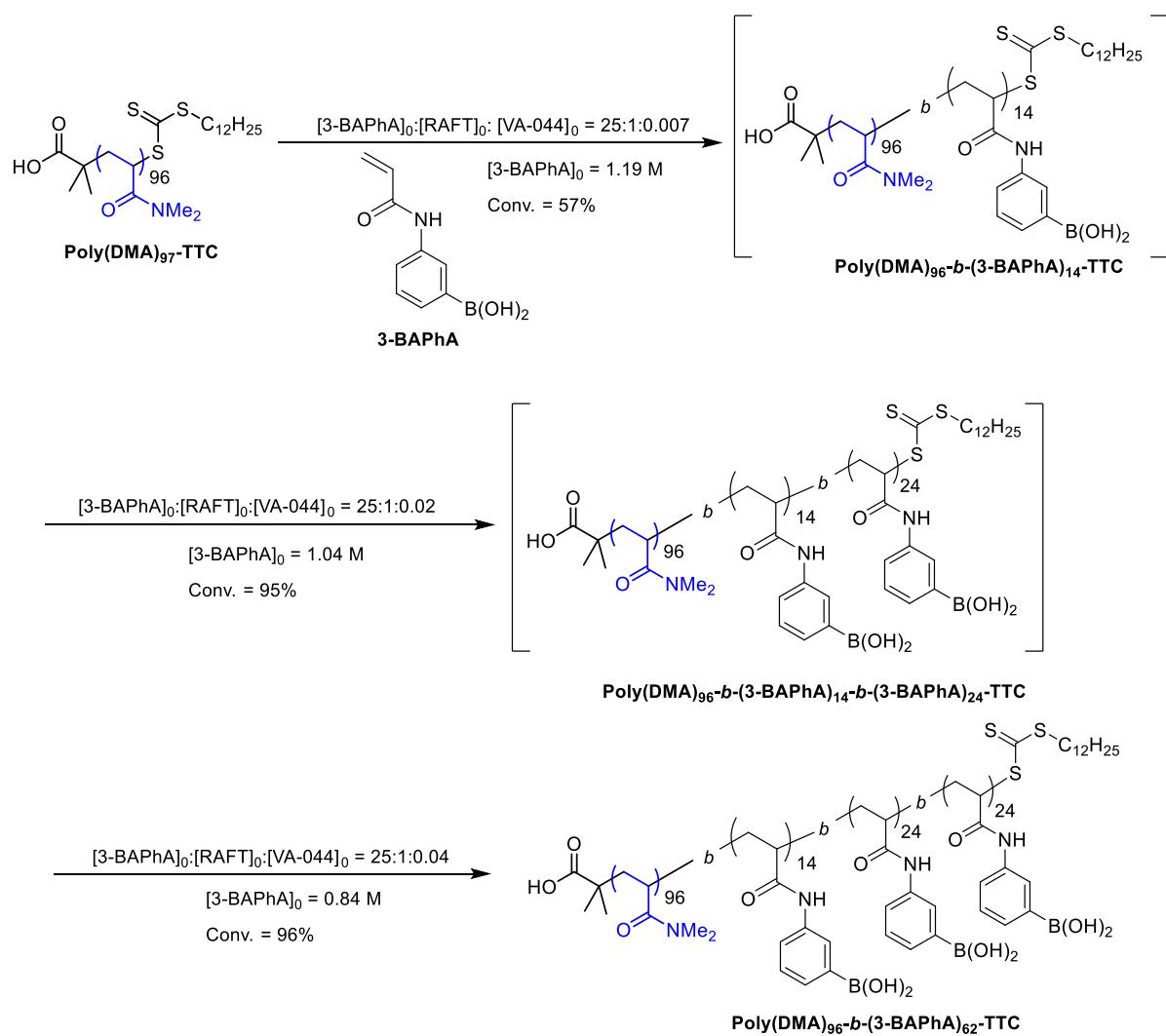


**Fig. 4.4:**  $^1\text{H}$  NMR spectra for the synthesis of diblock copolymers, (a) poly(DMA)-TTC in  $\text{DMSO-}D_6$ , (b) 3-BAPhA monomer in  $\text{DMSO-}D_6$ , (c) poly(DMA)<sub>28</sub>-b-(3-BAPhA)<sub>84</sub>-TTC in  $\text{MeOH-}D_4$ , and (d) poly(DMA)<sub>96</sub>-b-(3-BAPhA)<sub>62</sub>-TTC in  $\text{MeOH-}D_4$ .

The  $^1\text{H}$  NMR spectrum of isolated poly(DMA)<sub>28</sub>-*b*-(3-BAPhA)<sub>84</sub>-TTC gave a relative composition of 29% DMA and 71% (75% expected from relative *D*Ps) 3-BAPhA units, by comparing the polymer signal integrals at 2.86-3.24 (Me, 6H) and 6.75-8.08 (B(OH)<sub>2</sub> + Ar-H, 6H) ppm, respectively.

#### 4.5.1.2.2 Preparation of poly(DMA)<sub>96</sub>-*b*-(3-BAPhA)<sub>62</sub>-TTC

Poly(DMA)<sub>96</sub>-*b*-(3-BAPhA)<sub>62</sub>-TTC was also prepared using one-pot iterative RAFT-mediated solution polymerizations of 3-BAPhA, where each block is prepared in 2 h chain extension (cycles) without isolation (and purification) of intermediate blocks beginning from poly(DMA)<sub>96</sub>-TTC (Scheme 4.4, Table 4.3), as macroRAFT agents.



**Scheme 4.4:** Preparation of poly(DMA)<sub>96</sub>-*b*-(3-BAPhA)<sub>62</sub>-TTC in 20% aq. DMF at 70 °C by one-pot 2 h iterative RAFT polymerizations of 3-BAPhA from poly(DMA)<sub>96</sub>-TTC.

**Table 4.3:** Experimental conditions for the preparation of poly(DMA)<sub>96</sub>-*b*-(3-BAPhA)<sub>62</sub>-TTC in 20% aq. DMF at 70 °C by one-pot 2 h iterative RAFT polymerizations from poly(DMA)<sub>96</sub>-TTC macroRAFT agent ( $M_n = 9,900$ ) with  $[3\text{-BAPhA}]_0/[MacroRAFT]_0 = 25$  for all three chain extensions.

Chain Extensions	1	2	3
Conversion (%)	57	95	96
3-BAPhA added (mg)	563.7	313.8 <sup>a</sup>	500.1 <sup>a</sup>
Poly(DMA) <sub>96</sub> added (g)	1.1687	-	-
VA-044 added (mg) <sup>b</sup>	0.2598	0.7343 <sup>c</sup>	1.3783 <sup>c</sup>
Total Solvent (mL)	2.48	2.73	3.23
[3-BAPhA] <sub>0</sub> (molL <sup>-1</sup> )	1.19	1.04	0.84
[MacroRAFT] <sub>0</sub> (molL <sup>-1</sup> )	0.0476	0.0416 <sup>d</sup>	0.0337 <sup>d</sup>
[VA-044] <sub>0</sub> (molL <sup>-1</sup> )	3.24 x 10 <sup>-4</sup>	8.32 x 10 <sup>-4</sup>	1.32 x 10 <sup>-3</sup>
[MacroRAFT] <sub>0</sub> / [VA-044] <sub>0</sub>	147	50	26
Cumulative <i>L</i> (%) <sup>e</sup>	98.4	96.5	93.1

<sup>a</sup>Additions determined by conv. and 60 μl reaction sampling for conv. and GPC measurements. <sup>b</sup>After serial dilution. <sup>c</sup>Addition based on VA-044 remaining from the previous chain extension. <sup>d</sup>Estimated after reaction dilution and sampling. <sup>e</sup>Cumulative livingness (*L*) calculated using eq. (4.1) beginning from poly(DMA)<sub>96</sub>-TTC with *L* = 99.0%.

For the three iterative chain extensions at  $[3\text{-BAPhA}]_0/[MacroRAFT]_0 = 25$  from poly(DMA)<sub>96</sub>-TTC (Table 4.3), the MWD shift to higher MW is accompanied by a more significant low MW tail (Fig. 4.5) with the broader resultant MWD ( $\bar{D} = 1.48$ ) for poly(DMA)<sub>96</sub>-*b*-(3-BAPhA)<sub>62</sub>-TTC due mainly to a carryover of dead chains from the preparation of poly(DMA)<sub>96</sub>-TTC (3.4.4).<sup>68</sup> Nevertheless, the final diblock with longer hydrophilic block, poly(DMA)<sub>96</sub>-*b*-(3-BAPhA)<sub>62</sub>-TTC has  $M_n$  (= 24,100 gmol<sup>-1</sup>) in relatively close agreement with  $M_{n,th}$  (= 26,500 gmol<sup>-1</sup>). Determination of monomer incorporation by GPC and <sup>1</sup>H NMR conversion measurement agreed with the ratios of monomer units in the <sup>1</sup>H NMR spectra of the final isolated diblock copolymer (Fig. 4.4(d)). The <sup>1</sup>H NMR spectrum of isolated poly(DMA)<sub>96</sub>-*b*-(3-BAPhA)<sub>62</sub>-TTC gave a relative composition of 59% DMA and 41% (39% expected) 3-BAPhA units, by

comparing the polymer signal integrals at 2.85-3.23 (Me, 6H) and 6.87-8.04 (B(OH)<sub>2</sub> + Ar-H, 6H) ppm, respectively (Fig. 4.4(d)). The isolated yield: 1.26 g (44%, if 100% conv. for each cycle).

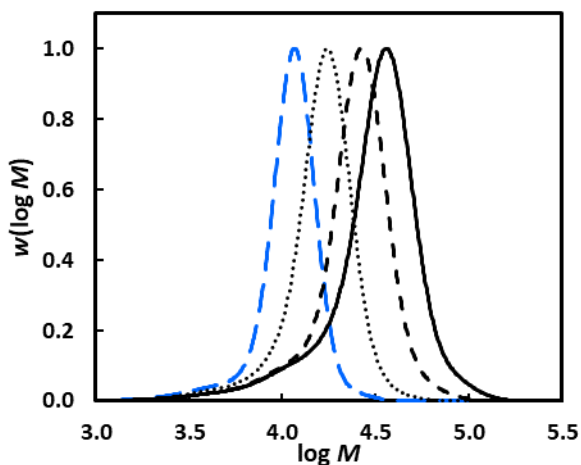


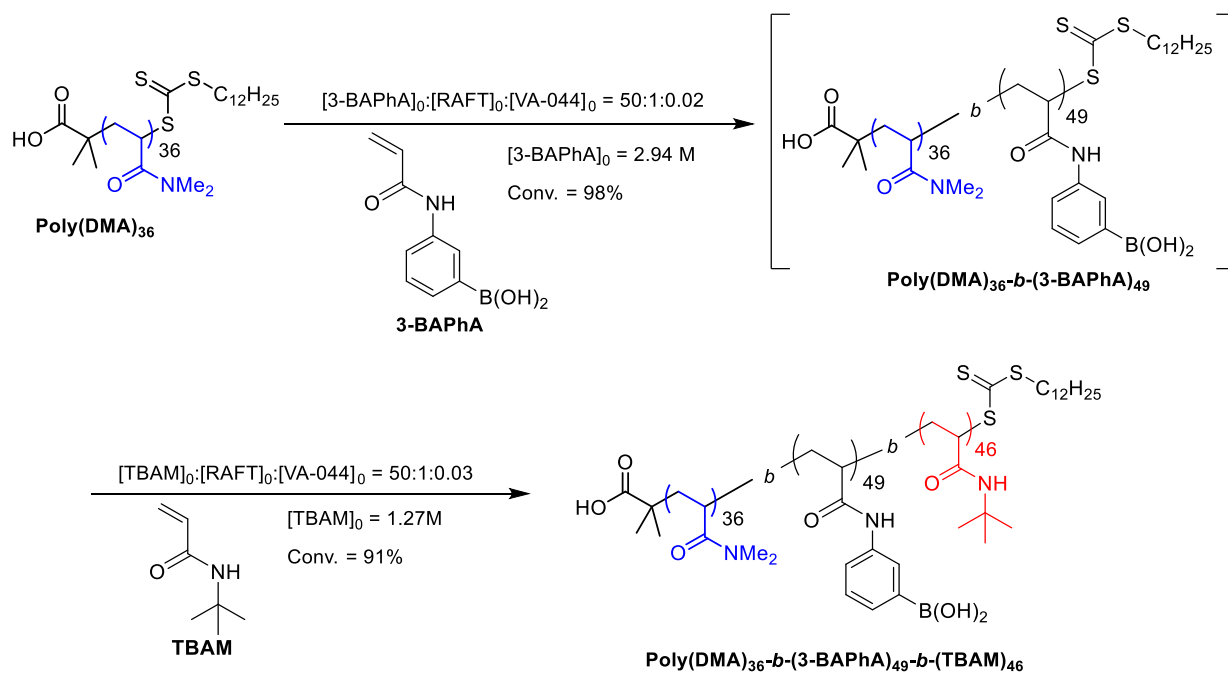
**Fig. 4.5:** GPC for the preparation of poly(DMA)<sub>96</sub>-*b*-(3-BAPhA)<sub>62</sub>-TTC (continuous line), using one-pot iterative RAFT polymerizations with 3-BAPhA (black lines) from poly(DMA)<sub>96</sub>-TTC (blue long dashed) using [3-BAPhA]<sub>0</sub>/[(poly(DMA)<sub>96</sub>-TTC)]<sub>0</sub> = 25 for each chain extension, according to Scheme 4.4 and Table 4.3.

## 4.5.2 Synthesis of TBAM-Containing Triblock Copolymers

### 4.5.2.1 Synthesis of Poly(DMA)<sub>36</sub>-*b*-(3-BAPhA)<sub>49</sub>-*b*-(TBAM)<sub>48</sub>-TTC

To assess the effect of a non-stimuli responsive hydrophobic block on self-assembled nanoparticle morphology, *tert*-butylacrylamide (TBAM) monomer was introduced, with triblock copolymers: poly(DMA)<sub>36</sub>-*b*-(3-BAPhA)<sub>49</sub>-*b*-(TBAM)<sub>46</sub>-TTC (Scheme 4.5, Table 4.4)





**Scheme 4.5:** Preparation of poly(DMA)<sub>36</sub>-*b*-(3-BAPhA)<sub>49</sub>-*b*-(TBAM)<sub>46</sub>-TTC in 20% aq. DMF at 70 °C by one-pot 2 h iterative RAFT polymerizations of 3-BAPhA and TBAM from poly(DMA)<sub>36</sub>-TTC.

**Table 4.4:** Experimental conditions for the preparation of Poly(DMA)<sub>36</sub>-*b*-(3-BAPhA)<sub>49</sub>-*b*-(TBAM)<sub>46</sub>-TTC in 20% aq. DMF at 70 °C by one-pot 2 h iterative RAFT polymerizations from poly(DMA)<sub>36</sub>-TTC macroRAFT agent ( $M_n = 3,900$ ) with  $[\text{Monomer}]_0/[\text{MacroRAFT}]_0 = 50$  for the two chain extensions.

Chain Extensions	1 (3-BAPhA)	2 (TBAM)
Conversion (%)	98	91
Monomer (mg)	561.5	352.1
Poly(DMA) <sub>36</sub> added (mg)	229.3	-
VA-044 added (mg) <sup>a</sup>	0.3815	0.5673 <sup>b</sup>
Total Solvent (mL)	1.00	2.18
$[\text{Monomer}]_0$ (molL <sup>-1</sup> )	2.94	1.27
$[\text{MacroRAFT}]_0$ (molL <sup>-1</sup> )	0.0588	0.0254 <sup>c</sup>
$[\text{VA-044}]_0$ (molL <sup>-1</sup> )	$1.18 \times 10^{-3}$	$8.05 \times 10^{-4}$
$[\text{MacroRAFT}]_0 / [\text{VA-044}]_0$	50	32
Cumulative $L$ (%) <sup>d</sup>	97.1	94.3

<sup>a</sup>After serial dilution. <sup>b</sup>Addition based on VA-044 remaining from the previous polymerization.

<sup>c</sup>Estimated after reaction dilution and 60  $\mu\text{l}$  reaction sampling. <sup>d</sup>Cumulative livingness ( $L$ ) calculated using eq. (4.1) beginning from poly(DMA)<sub>36</sub>-TTC with  $L = 99.0\%$ .

One-pot iterative polymerizations of 3-BAPhA and TBAM from poly(DMA)<sub>36</sub> using higher  $[\text{Monomer}]_0/[\text{MacroRAFT}]_0$  ratios (= 50, as opposed to 25 above), resulted in MWDs shifting perfectly to higher MWs (Fig. 4.6).

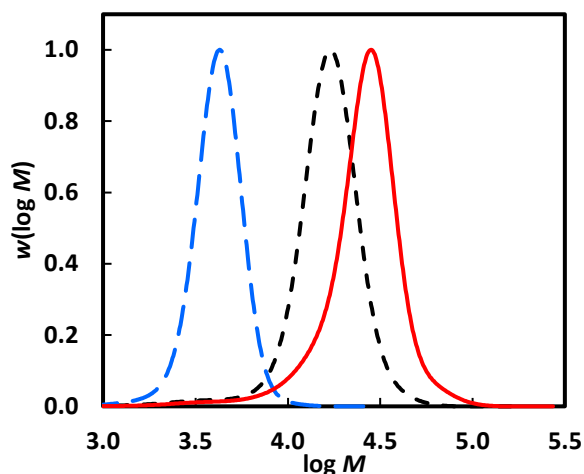


**Fig. 4.6.** GPC for the preparation poly(DMA)<sub>36</sub>-*b*-(3-BAPhA)<sub>49</sub>-*b*-(TBAM)<sub>46</sub>-TTC, using one-pot iterative RAFT polymerizations with 3-BAPhA (black short dashed) and TBAM (red continuous) from poly(DMA)<sub>36</sub>-TTC (blue long dashed) using [Monomer]<sub>0</sub>/[RAFT]<sub>0</sub> = 50 for each chain extension, according to Scheme 4.5 and Table 4.4.

In the case of the triblock copolymers, it is important that all the monomer is consumed before the introduction of a different monomer to avoid formation of impure blocks. Indeed near-complete conversion (98%) was obtained for chain extension of poly(DMA)<sub>36</sub>-TTC with 3-BAPhA. Chain extension with TBAM proceeded in 91% conversion (with  $M_n$  (= 21,500 g mol<sup>-1</sup>,  $D = 1.31$ ), in close agreement with  $M_{n,th}$  (= 20,300 g mol<sup>-1</sup>) (Table 4.2). The <sup>1</sup>H NMR spectrum of isolated poly(DMA)<sub>36</sub>-*b*-(3-BAPhA)<sub>49</sub>-*b*-(TBAM)<sub>46</sub>-TTC gave a relative composition of 26% (27% expected) DMA, 36% (37% expected) 3-BAPhA, and 38% (36% expected) TBAM units, by comparing the polymer signal integrals at 2.87-3.02 (Me, 6H), 6.38-8.10 (B(OH)<sub>2</sub> + Ar-H, 6H), and 1.26-1.39 (Me, 9H) ppm respectively, where the TBAM integral is divided by 1.5 (Fig. 4.7(c)). The isolated yield: 0.82 g (72%, if 100% conv. for each cycle).

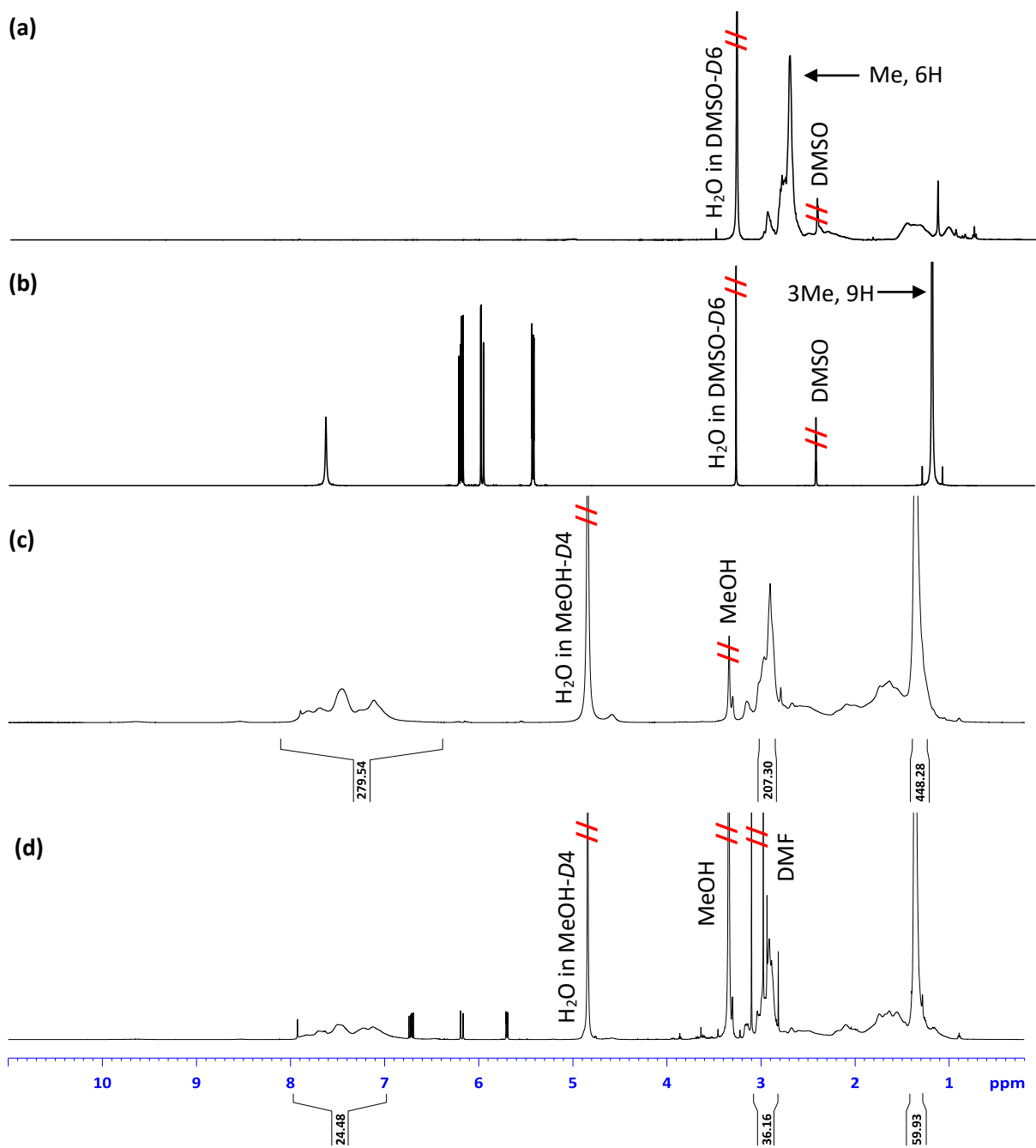
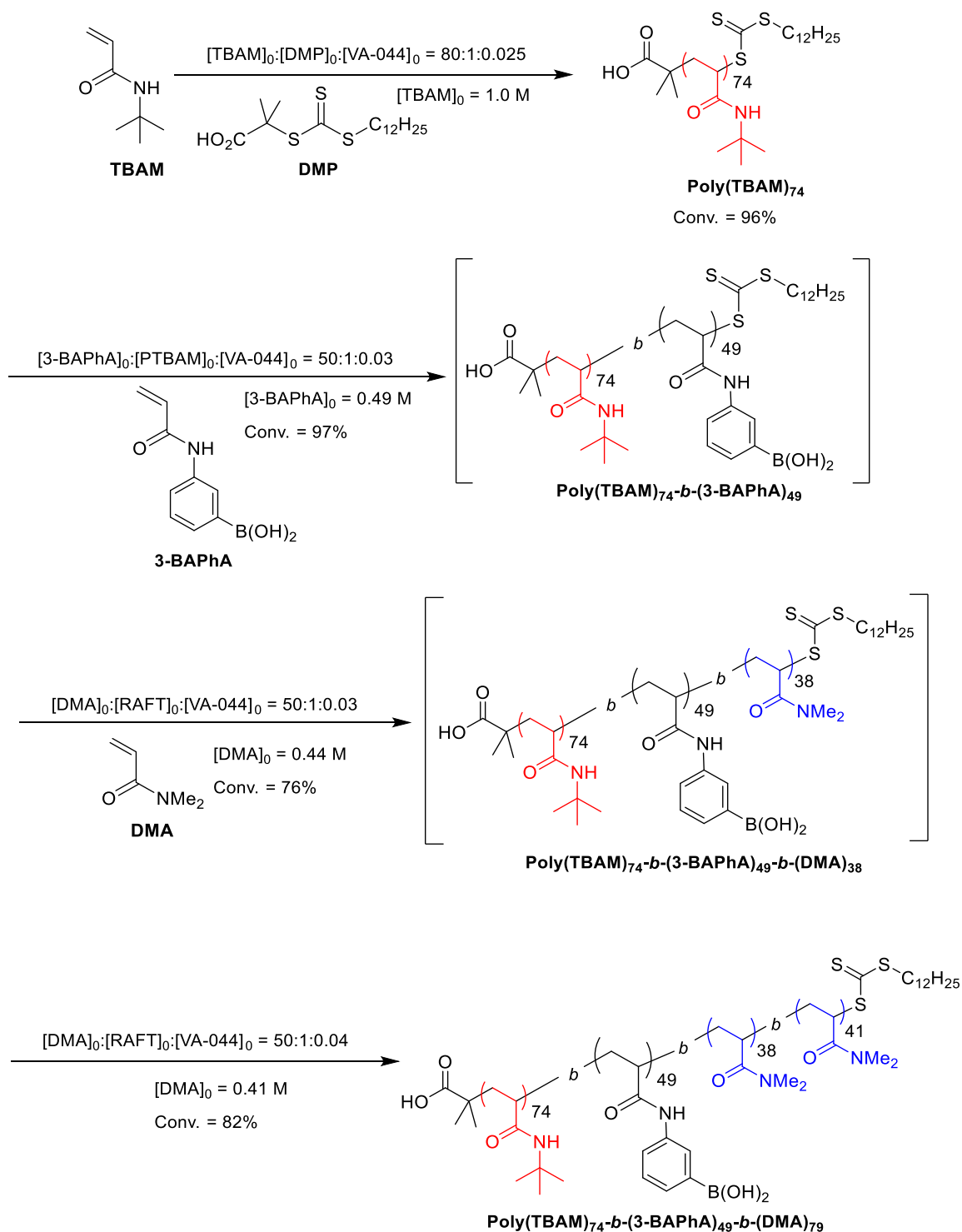


**Fig. 4.7.**  $^1\text{H}$  NMR spectra for the synthesis of triblock copolymers, **(a)** poly(DMA)-TTC in DMSO- $D_6$ , **(b)** TBAM monomer in DMSO- $D_6$ , **(c)** poly(DMA) $_{36}$ - $b$ -(3-BAPhA) $_{49}$ - $b$ -(TBAM) $_{46}$ -TTC in MeOH- $D_4$ , and **(d)** poly(TBAM) $_{74}$ - $b$ -(3-BAPhA) $_{49}$ - $b$ -(DMA) $_{79}$ -TTC in MeOH- $D_4$ .

### 4.5.3 Synthesis of Poly(TBAM)<sub>74</sub>-*b*-(3-BAPhA)<sub>49</sub>-*b*-(DMA)<sub>79</sub>-TTC

For the preparation of poly(TBAM)<sub>74</sub>-*b*-(3-BAPhA)<sub>49</sub>-*b*-(DMA)<sub>79</sub>-TTC (Scheme 4.6, Table 4.5) prepared. A different approach to the preceding three copolymers was taken. In this case, as previously reported,<sup>41</sup> no pre-prepared macroRAFT was introduced, and the one-pot approach began from TBAM monomer and 2-(dodecylthiocarbonothioylthio)-2-methylpropionic acid (DMP) in 20% aq. dioxane.



**Scheme 4.6:** Preparation of poly(TBAM)<sub>74</sub>-*b*-(3-BAPhA)<sub>49</sub>-*b*-(DMA)<sub>79</sub>-TTC in 20% aq. dioxane at 70 °C by one-pot 2 h iterative RAFT polymerizations of 3-BAPhA and DMA starting from TBAM and DMP, as monomer and RAFT agent respectively.

Poly(TBAM)<sub>74</sub>-TTC macroRAFT was prepared *in situ* using [TBAM]<sub>0</sub>/[DMP]<sub>0</sub> = 80 in 96% conversion. [Monomer]<sub>0</sub>/[MacroRAFT]<sub>0</sub> (= 50) was maintained for subsequent chain extensions. The MWDs are however noticeably wider for DMA polymerizations and shift less than for the initial chain extension with 3-BAPhA (Fig. 4.8). This can be attributed to the accumulation of initiator derived dead chains (synthesis of poly(TBAM)<sub>74</sub>-*b*-(3-BAPhA)<sub>49</sub>-*b*-(DMA)<sub>79</sub>-TTC has a cumulative *L* = 88.7% in comparison to *L* = 94.3% for poly(DMA)<sub>36</sub>-*b*-(3-BAPhA)<sub>49</sub>-*b*-(TBAM)<sub>46</sub>-TTC, according to eq. 4.1 and Tables 4.4 and 4.5), supplemented by some degradation of the RAFT end-group, which has been previously reported in acrylamide and methacrylamide polymerizations.<sup>46,59</sup>

**Table 4.5.** Experimental conditions for the preparation of poly(TBAM)<sub>74</sub>-*b*-(3-BAPhA)<sub>49</sub>-*b*-(DMA)<sub>79</sub>-TTC in 20% aq. dioxane at 70 °C by one-pot 2 h iterative RAFT polymerizations from TBAM monomer using DMP as RAFT agent with [TBAM]<sub>0</sub>/[DMP]<sub>0</sub> = 80 with subsequent chain extensions using [Monomer]<sub>0</sub>/[MacroRAFT]<sub>0</sub> = 50.

Chain Extensions	1 (TBAM)	2 (3-BAPhA)	3 (DMA)	4 (DMA)
Conversion (%)	96	97	76	82
Monomer (mg)	124.7	110.4	51.5	48.0 <sup>a</sup>
DMP added (mg) <sup>b</sup>	4.485	-	-	-
VA-044 added (mg) <sup>b</sup>	0.1012	0.1171 <sup>c</sup>	0.1179 <sup>c</sup>	0.1263 <sup>c</sup>
Total Solvent (mL)	1.00	1.18	1.18	1.18
[Monomer] <sub>0</sub> (molL <sup>-1</sup> )	0.98	0.49	0.44	0.41
[MacroRAFT] <sub>0</sub> (molL <sup>-1</sup> )	0.0123	0.0098 <sup>d</sup>	0.0089 <sup>d</sup>	0.0083 <sup>d</sup>
[VA-044] <sub>0</sub> (molL <sup>-1</sup> )	3.13 x 10 <sup>-4</sup>	3.07 x 10 <sup>-4</sup>	3.09 x 10 <sup>-4</sup>	3.31 x 10 <sup>-4</sup>
[MacroRAFT] <sub>0</sub> / [VA-044] <sub>0</sub>	39	32	29	25
Cumulative <i>L</i> (%) <sup>e</sup>	97.7	94.9	91.9	88.7

<sup>a</sup>Addition determined by conversion and 60 µl reaction sampling for conversion and GPC measurements. <sup>b</sup>After serial dilution. <sup>c</sup>Addition based on VA-044 remaining from the previous polymerization. <sup>d</sup>Estimated after reaction dilution and 60 µl reaction sampling. <sup>e</sup>Cumulative livingness (*L*) calculated using eq (4.1).

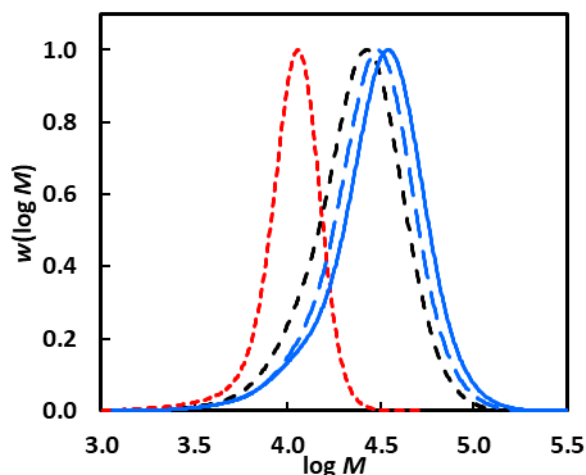


**Fig. 4.8:** GPC for the preparation of poly(TBAM)<sub>74</sub>-*b*-(3-BAPhA)<sub>49</sub>-*b*-(DMA)<sub>79</sub>-TTC (continuous line), using one-pot iterative RAFT polymerizations starting from TBAM and DMP, where [TBAM]<sub>0</sub>/[DMP]<sub>0</sub> = 80 (red short dashed), and subsequent chain extensions at *DP* = 50 with 3-BAPhA (black short dashed) and DMA (two blue lines), according to Scheme 4.6 and Table 4.5.

However, GPC error due to differences in the hydrodynamic volume between the triblock polyacrylamide and polystyrene calibration standards, and the lower MW of DMA compared to 3-BAEPHA (note – 3-BAEPHA is the pinacol ester of 3-BAPhA and GPC is taken after this protection, should be given due consideration). Nevertheless, despite the broader final MWD of the triblock copolymer ( $\mathcal{D} = 1.43$ ) than the poly(DMA)<sub>36</sub>-TTC derived triblock,  $M_n$  (= 25,200 g mol<sup>-1</sup>) remains close to  $M_{n,th}$  (= 27,300 g mol<sup>-1</sup>) (Table 4.2). For both isolated triblock copolymers, the <sup>1</sup>H NMR spectra (Fig. 4.7) gave ratios of the three monomers in relatively good agreement with GPC and NMR measurements. The <sup>1</sup>H NMR spectrum of isolated poly(TBAM)<sub>74</sub>-*b*-(3-BAPhA)<sub>49</sub>-*b*-(DMA)<sub>79</sub>-TTC gave a relative composition of 40% (37% expected) TBAM, 24% (24% expected) 3-BAPhA, and 36% (39% expected) DMA units, by comparing the polymer signal integrals at 1.32-1.42 (Me, 9H), 6.98-7.97 (B(OH)<sub>2</sub> + Ar-H, 6H), and 2.82-3.08 (Me, 6H) ppm respectively, where the TBAM integral is divided by 1.5 (Fig. 4.7(d)). The isolated yield: 0.12 g (35%, if each cycle proceeded to 100% conv.).



#### 4.5.4 Self-Assembly

A mixture of MeOH/DMF (3/4, 2.84 mL) was required to fully solvate block copolymers (1.2  $\mu\text{mol}$ ) prior to dialysis with water, which reduces the solvency of the hydrophobic blocks. Turbidity occurs due to colloidal aggregate formation in dilute aqueous solutions (0.2 wt/vol%) with micellar core and corona by association of the hydrophobic poly(3-BAPhA)-containing blocks, and solvation of the hydrophilic poly(DMA) blocks, respectively.

##### 4.5.4.1 Self-Assembly of poly(DMA)<sub>28</sub>-*b*-(3-BAPhA)<sub>84</sub>-TTC

Firstly, evaluated the influence of different relative block lengths on morphology at neutral pH 7.4. Poly(DMA)<sub>28</sub>-*b*-(3-BAPhA)<sub>84</sub>-TTC (with a long hydrophobic block) gave fused  $\sim$ 50-150 nm solid spheres with some bilayer shadowing evident in a significant fraction of spheres (Fig. 4.9).

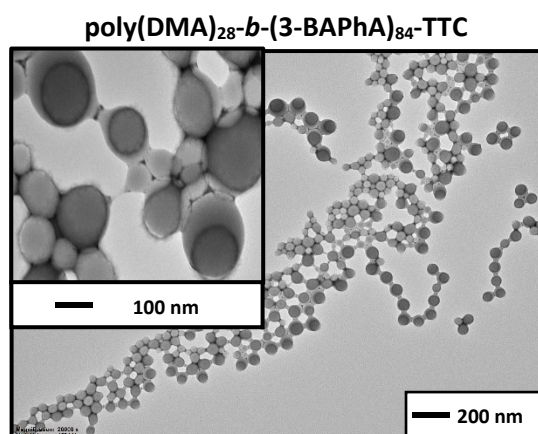


**Fig. 4.9:** TEM images of polymer aq. sol. (0.2 wt/vol%) at pH 7.4.

##### 4.5.4.2 Self-Assembly of poly(DMA)<sub>96</sub>-*b*-(3-BAPhA)<sub>62</sub>-TTC

Increasing the DMA corona block from  $DP = 28$  to 96 in poly(DMA)<sub>96</sub>-*b*-(3-BAPhA)<sub>62</sub>-TTC (whereby the hydrophilic block is significantly longer than the hydrophobic block) resulted in a mixture of small spheres and irregular rods, with a few large spherical particles of up to 200 nm in diameter (Fig 4.10). The observed heterogeneity of morphologies is presumably due to some boron centres existing as anionic species from the dynamic equilibrium of BA in water,<sup>4</sup>

thus at any one time, there is a range of block copolymers with different relative fractions of hydrophilic to hydrophobic block lengths.

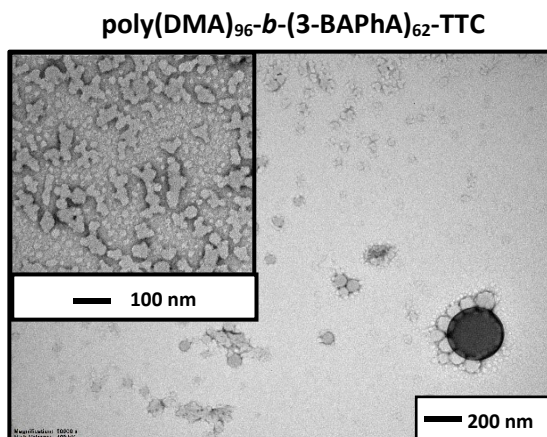


**Fig. 4.10:** TEM images of polymer aq. sol. (0.2 wt/vol%) at pH 7.4.

#### 4.5.4.3 Self-Assembly of poly(DMA)<sub>36</sub>-*b*-(3-BAPhA)<sub>49</sub>-*b*-(TBAM)<sub>46</sub>-TTC

Poly(DMA)<sub>36</sub>-*b*-(3-BAPhA)<sub>49</sub>-*b*-(TBAM)<sub>46</sub>-TTC gave large rodlike aggregates/worm-like morphologies (Fig. 4.11).

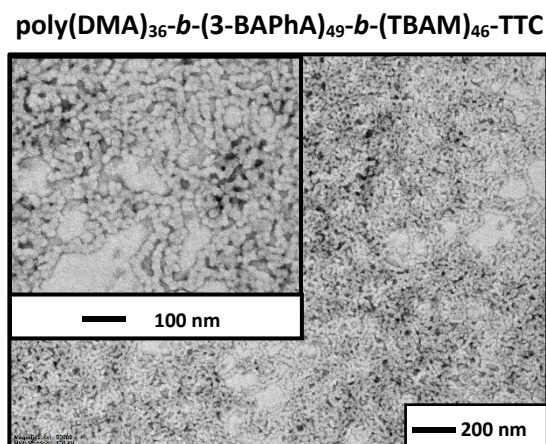


**Fig. 4.11:** TEM images of polymer aq. sol. (0.2 wt/vol%) at pH 7.4.

#### 4.5.4.4 Self-Assembly of poly(TBAM)<sub>74</sub>-*b*-(3-BAPhA)<sub>49</sub>-*b*-(TBAM)<sub>79</sub>-TTC

Poly(TBAM)<sub>74</sub>-*b*-(3-BAPhA)<sub>49</sub>-*b*-(DMA)<sub>79</sub>-TTC resulted in slender interconnected (filaments or) fibres (Fig. 4.12), thus the TBAM block leads to worm-like morphologies.

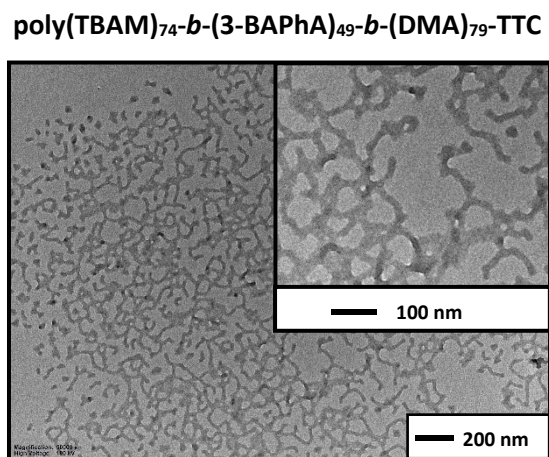


**Fig. 4.12:** TEM images of polymer aq. sol. (0.2 wt/vol%) at pH 7.4.

#### 4.5.5 Lactate and Glucose Response

TEM was further employed to investigate lactate and glucose-response of the amphiphilic block copolymers, where anionic boronate ester formation leads to changes in the packing parameter by increasing the overall mass of the hydrophilic stabilizer (now charged) blocks, while reducing the size of the hydrophobic core-component.

##### 4.5.5.1 Self-assembly of poly(DMA)<sub>28</sub>-*b*-(3-BAPhA)<sub>84</sub>-TTC

Upon addition of sodium lactate at pH 7.4, large spherical particle networks (diameter 50-150 nm) change to smaller interconnected spheres (diameter 10-50 nm, Fig. 4.13(ii)). For poly(DMA)<sub>28</sub>-*b*-(3-BAPhA)<sub>84</sub>-TTC, if all BA moieties convert to the charged pinacol ester, then effectively a hydrophilic diblock copolymer results. However, the RAFT end-group is a large hydrophobic trithiocarbonate dodecyl moiety that influences self-assembly,<sup>41,99,100</sup> thus upon BA-binding small micelles with long hydrophilic stabilizer chains result. Note that BA conversion to the boronate ester leads to acidification of the solution,<sup>101</sup> however in the TEM investigations herein, the pH was held at pH 7.4 and 8.7 for lactate and glucose response, respectively, through dropwise addition of further NaOH solution. The pH increase from 7.4

to 8.7 gives networks of smaller spheres of mostly <50 nm in diameter (Fig. 4.13(iii)), however subsequent glucose binding leads to more significant change with less well-defined networks of small interconnected spheres forming (Fig. 4.13(iv)). The trend in nanoparticle size reduction as a consequence of increased pH and glucose binding is in agreement with dynamic light scattering (DLS) studies on poly(DMA)-*b*-(3-BAPhA)-TTC copolymers reported by Sumerlin *et al.*<sup>5</sup> Moreover, the present work has shown that lactate binding at neutral (physiological-like) pH leads to comparable effects on morphology to that of glucose binding at moderately basic pH.

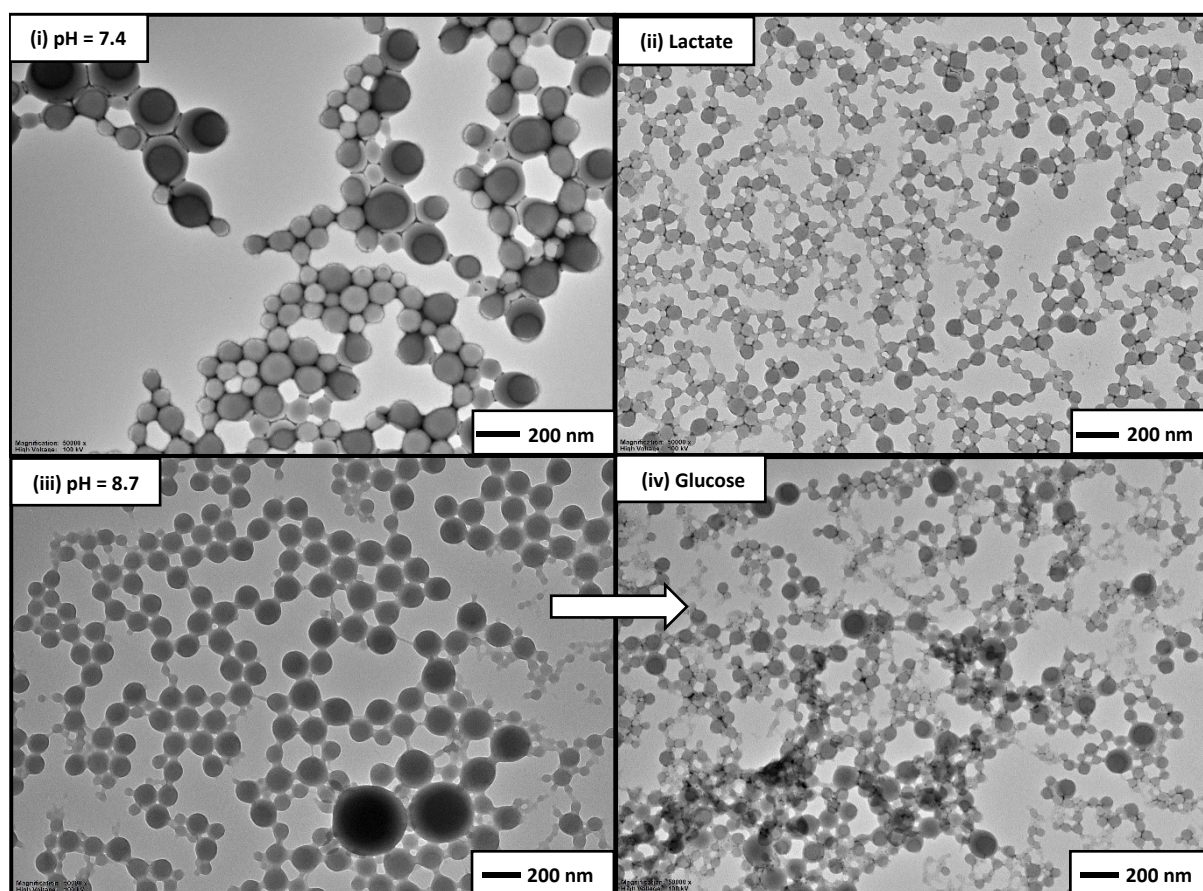


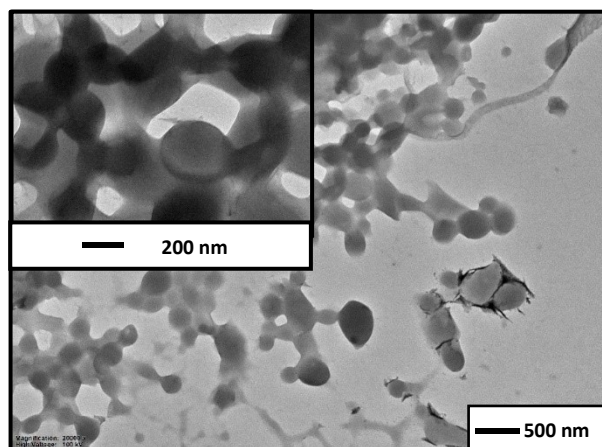
**Fig. 4.13:** TEM images for stimuli-response using aq. sol. (0.2 wt/vol%) of poly(DMA)<sub>28</sub>-*b*-(3-BAPhA)<sub>84</sub>-TTC at (i) pH 7.4, (ii) pH 7.4 with 0.1 M lactate aq. sol., (iii) pH 8.7, and (iv) pH 8.7 with 0.5 M glucose aq. sol.

#### 4.5.5.2 Response of Poly(DMA)<sub>96</sub>-*b*-(3-BAPhA)<sub>62</sub>-TTC

Lactate binding onto poly(DMA)<sub>96</sub>-*b*-(3-BAPhA)<sub>62</sub>-TTC at pH 7.4 gave less well-defined spherical morphologies, presumably due to increased dissolution (Fig. 4.14(i)). Disassembly was expected due to the formation of a significantly larger hydrophilic block (overall  $DP = 158$  for poly(DMA)<sub>96</sub>-*b*-(3-BAPhA)<sub>62</sub>-TTC compared to overall  $DP = 112$  for poly(DMA)<sub>28</sub>-*b*-(3-BAPhA)<sub>84</sub>-TTC, assuming lactate/glucose binding at all BA moieties). However, the RAFT end-group is a large hydrophobic trithiocarbonate (TTC) dodecyl moiety that influences self-assembly,<sup>41,100</sup> thus upon BA-binding small micelles with long hydrophilic stabilizer chains result. Elongation of the hydrophilic block at pH 8.7 led to a different outcome to that with lactate at pH 7.4 with a mixture of well-defined 500 nm long worms, lamellae, and 50-200 nm spherical particles formed (Fig. 4.14(ii)). Lamellae with rods extending from the edge are kinetically trapped intermediate structures, probably formed during rod-to-lamella transitions.<sup>72</sup> The formation of higher order morphologies with increases in the volume of coronal chains suggests interchain electrostatic repulsions of anionic hydroxyboronates are unimportant, otherwise spheres would predominate. The addition of glucose led to increases in the solubility of the poly(3-BAPhA) block with glucose binding transforming higher order morphologies (worms and lamella) to mostly irregular spherical particles (Fig. 4.14(iii)).



**Poly(DMA)<sub>96</sub>-*b*-(3-BAPhA)<sub>62</sub>-TTC**  
**(i) with Lactate at pH 7.4**



**(ii) at pH 8.7**

**(iii) with Glucose at pH 8.7**

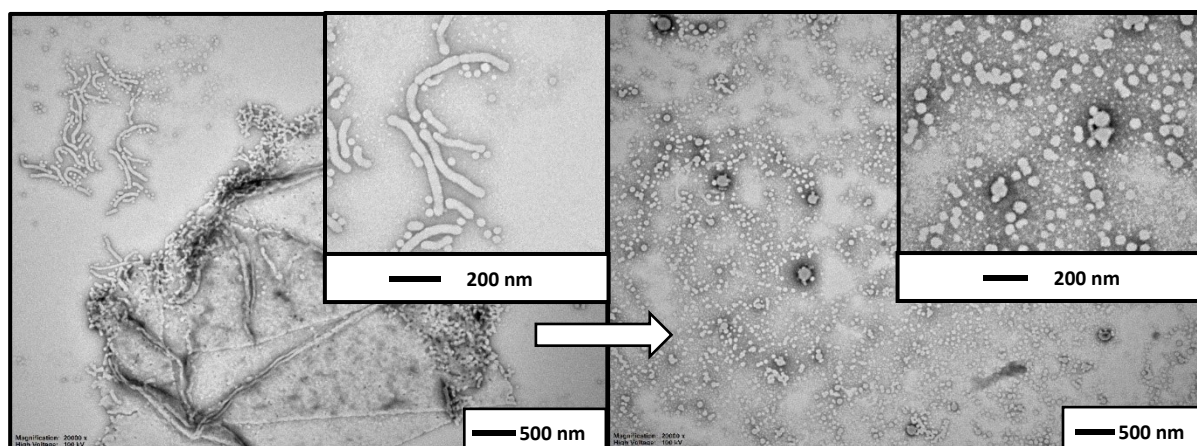


**Fig. 4.14.** TEM images of poly(DMA)<sub>96</sub>-*b*-(3-BAPhA)<sub>62</sub>-TTC aq. sol.

#### 4.5.5.3 Poly(DMA)<sub>36</sub>-*b*-(3-BAPhA)<sub>49</sub>-*b*-(TBAM)<sub>46</sub>-TTC

Like the diblock copolymers above, colloidal suspensions were obtained for this triblock copolymer upon boronate ester formation (Fig. 4.15).

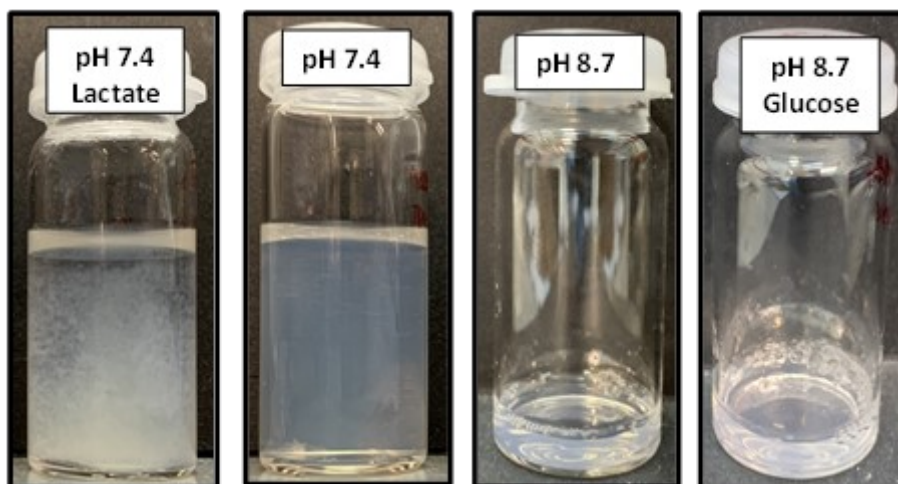


**Fig. 4.15.** Digital images of the vials containing poly(DMA)<sub>36</sub>-*b*-(3-BAPhA)<sub>49</sub>-*b*-(TBAM)<sub>46</sub>-TTC aq. sol. (0.2 wt/vol%).

The elongation of the hydrophilic block for poly(DMA)<sub>36</sub>-*b*-(3-BAPhA)<sub>49</sub>-*b*-(TBAM)<sub>46</sub>-TTC leads to a few solid spherical particles up to 200 nm in diameter when lactate is bound, although significant disassembly also occurs (Fig. 4.16). The addition of NaOH and glucose maintains the worm phase, although a greater fraction of dots are salt crystals or artefacts of staining (Fig. 4.17).

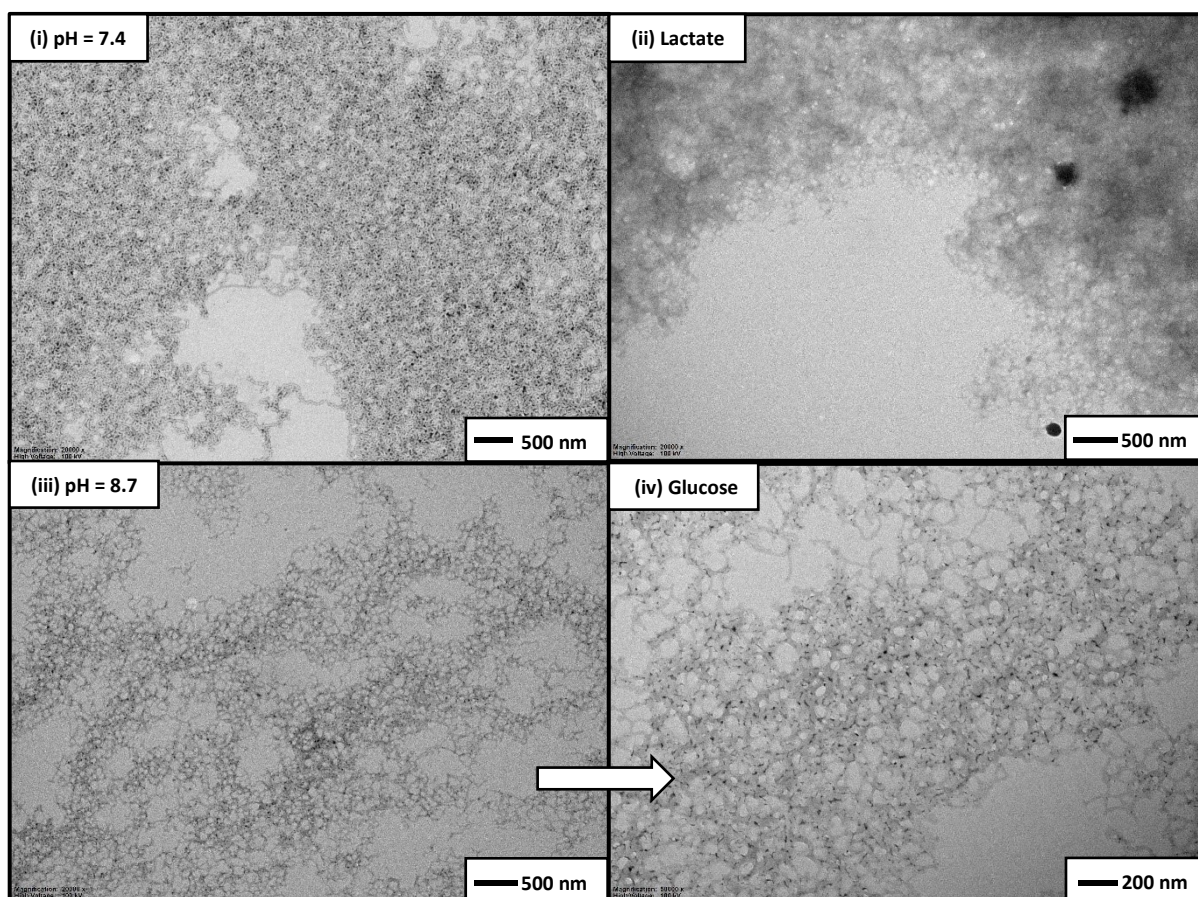


**Fig. 4.16:** TEM images for stimuli-response using aq. sol. (0.2 wt/vol%) of poly(DMA)<sub>36</sub>-*b*-(3-BAPhA)<sub>49</sub>-*b*-(TBAM)<sub>46</sub>-TTC at (i) pH 7.4, (ii) pH 7.4 with 0.1 M lactate aq. sol., (iii) pH 8.7, and (iv) pH 8.7 with 0.5 M glucose aq. sol.



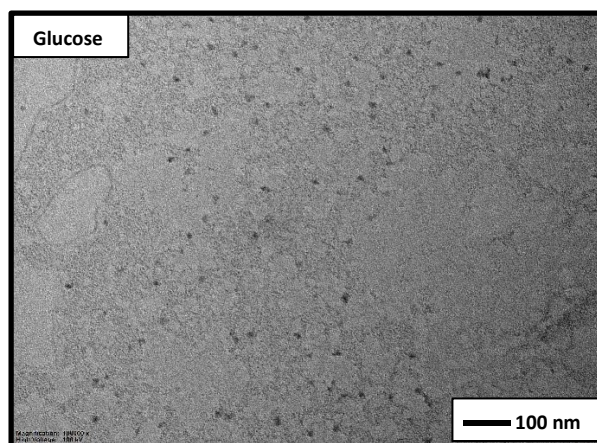


**Fig 4.17.** TEM image for glucose-response using aq. sol. (0.2 wt/vol%) of poly(DMA)<sub>36</sub>-*b*-(3-BAPhA)<sub>49</sub>-*b*-(TBAM)<sub>46</sub>-TTC at pH 8.7.

#### 4.5.5.4 Response of poly(TBAM)<sub>74</sub>-*b*-(3-BAPhA)<sub>49</sub>-*b*-(DMA)<sub>79</sub>-TTC

More complex self-assembly was expected when the large hydrophobic RAFT dodecyl moiety is attached to the hydrophilic block, as in ABA' type-triblock, poly(TBAM)<sub>74</sub>-*b*-(3-BAPhA)<sub>49</sub>-*b*-(DMA)<sub>79</sub>-TTC. The triblock copolymer fibres with addition of sodium *L*-lactate at pH 7.4 transformed to large worms or irregular rods, along with a minor fraction of spherical nanoparticles of up to 200 nm in diameter (Fig. 4.18(ii)). Increasing the pH led to a worm-to-spherical morphology transition with no worms remaining in the TEM images (Fig. 4.18(iii)). Boronate ester formation would increase the size of the central hydrophilic block and increased anionic charge density would increase repulsive forces between chains. The formation of higher order morphologies such as worms and vesicles require bringing hydrophilic chains in closer proximity due to the lower degree of curvature of the hydrophobic core-forming block.

Thus, in PISA, only spheres form when the charge density of the solvophilic block is high.<sup>102</sup> This rationalizes the morphology transitions of the poly(TBAM)<sub>74</sub>-*b*-(3-BAPhA)<sub>49</sub>-*b*-(DMA)<sub>79</sub>-TTC fibres (Fig. 4.18(i)) towards spherical morphologies upon treatment with lactate, base, and glucose. However, mostly worms in all TEMs lactate and base contain a minor amount of spherical particles (Fig. 4.18(iii)). At the latter basic pH (of 8.7), glucose binding gave a

spherical nanoparticle transition to irregular rods (worms) as part of a compound micelle arrangement, which is visible at 500 nm TEM magnification (Fig. 4.18(iv)).

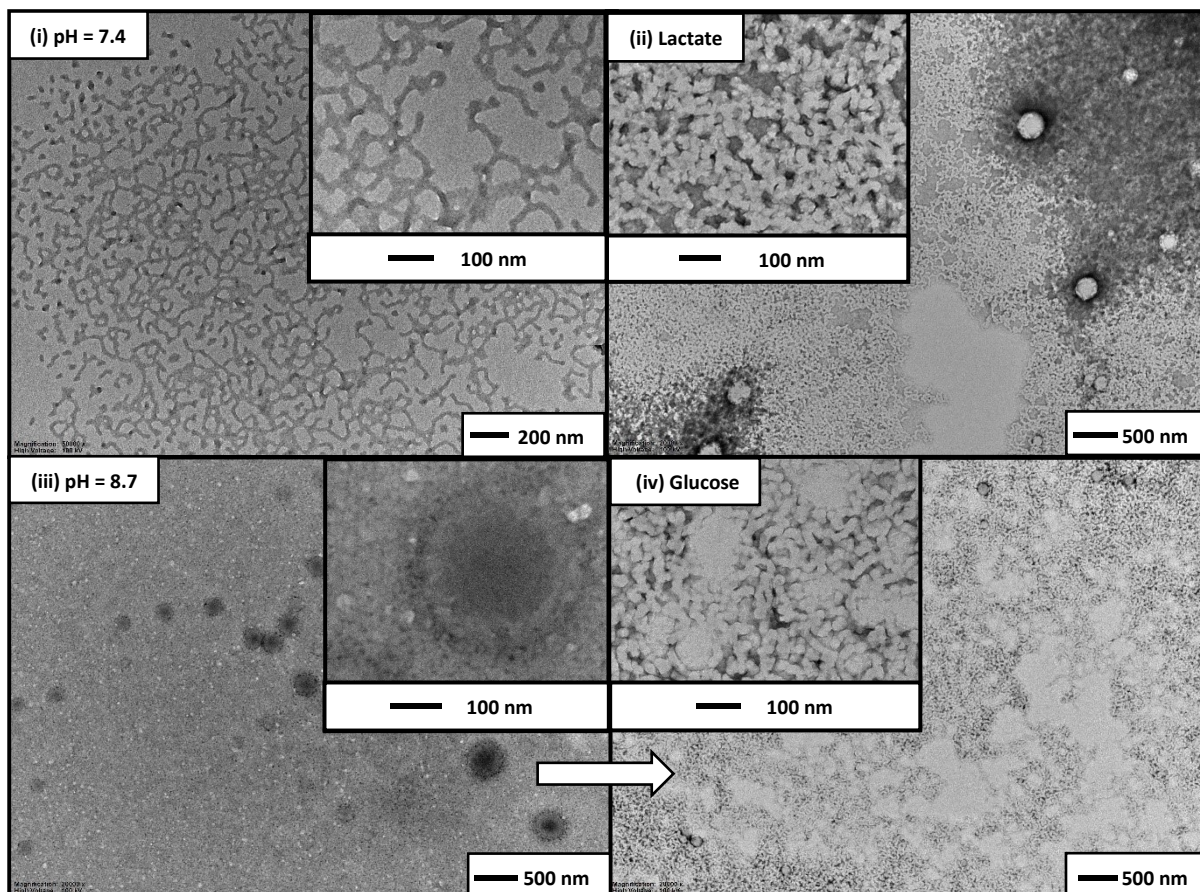


**Fig. 4.18:** TEM images for stimuli-response using aq. sol. (0.2 wt/vol%) of poly(TBAM)<sub>74</sub>-*b*-(3-BAPhA)<sub>49</sub>-*b*-(DMA)<sub>79</sub>-TTC at **(i)** pH 7.4, **(ii)** pH 7.4 with 0.1 M lactate aq. sol., **(iii)** pH 8.7, and **(iv)** pH 8.7 with 0.5 M glucose aq. sol.

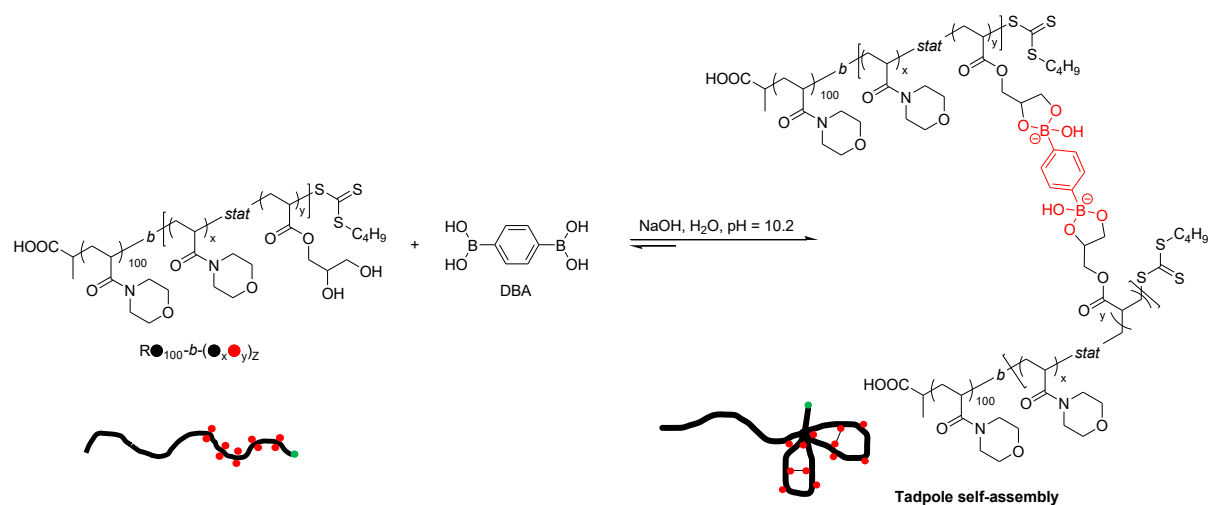
#### **4.6 Conclusions**

Lactate-response for amphiphilic block copolymer nanoparticles is established. Polyacrylamide morphology transitions caused by lactate binding at neutral pH (physiological pH = 7.4) are comparable to BA-glucose binding at basic pH (= 8.7). Incorporating non-stimuli responsive hydrophobic TBAM blocks gave triblocks that self-assembled to pure worm morphologies, unlike diblock copolymers that gave spheres and irregular rods. Worms undergo morphology transitions, as polymer solubility increases in response to lactate, base, and glucose binding. The morphology transitions caused by these three stimuli are explained by reactions at the BA moieties leading to blocks of boronic esters of different size and anionic charge density.

## Chapter 5: LACTATE and GLUCOSE-INDUCED SELF-ASSEMBLY of HYDROPHOBIC BORONIC ACID-SUBSTITUTED POLYMERS

### 5.1 Introduction

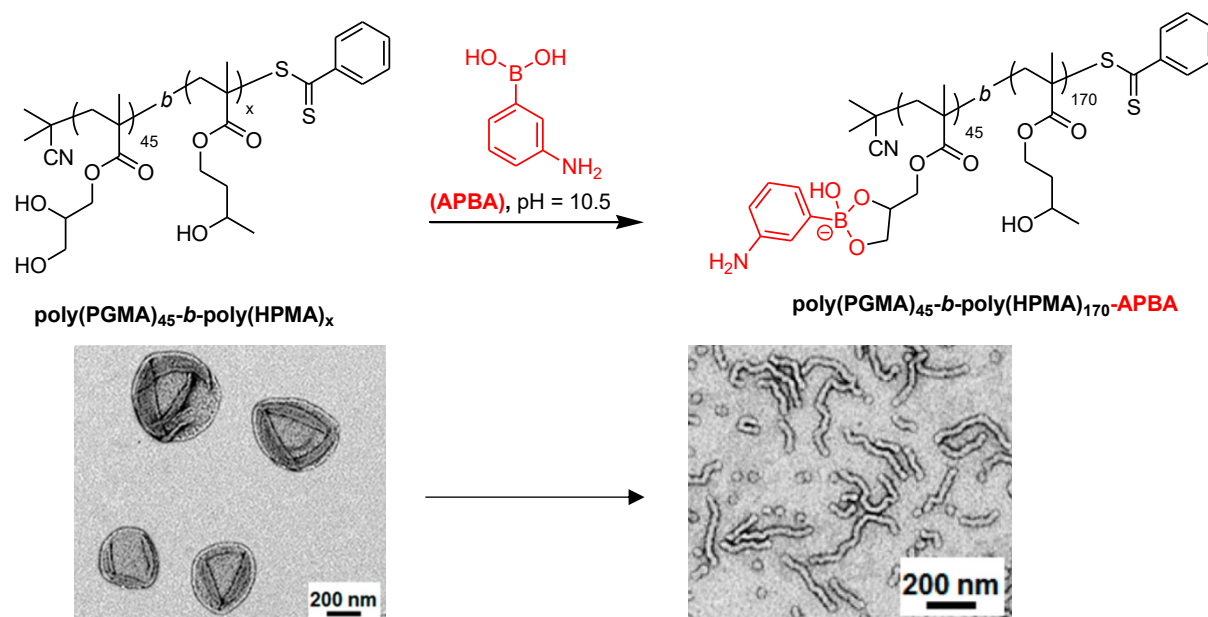
The literature overlooks that most amphiphilic block copolymer nanoparticles with BA-substituted blocks should be more selective towards binding of lactate than glucose under neutral physiological conditions. Chapter 4 describes lactate and glucose responsive BA-functionalized amphiphilic block copolymer nanoparticles, with lactate binding at pH = 7.4 leading to comparable effects on morphology to that of glucose binding at pH = 8.7. Morphology transitions occur in response to lactate, pH, and glucose, which change the packing parameter by increasing the overall mass of the stabilizer (now charged) blocks, while reducing the size of the hydrophobic core-component. Perrier *et al.* used the binding of di-BA (DBA) crosslinker onto diol-functionalized block copolymers to induce self-assembly into tadpole-like nanoparticles (Scheme 5.1).<sup>103</sup> Disassembly was triggered by varying environmental pH or by the addition of glucose.



**Scheme 5.1:** Self-assembly into tadpole-like nanoparticles using DBA.<sup>103</sup>

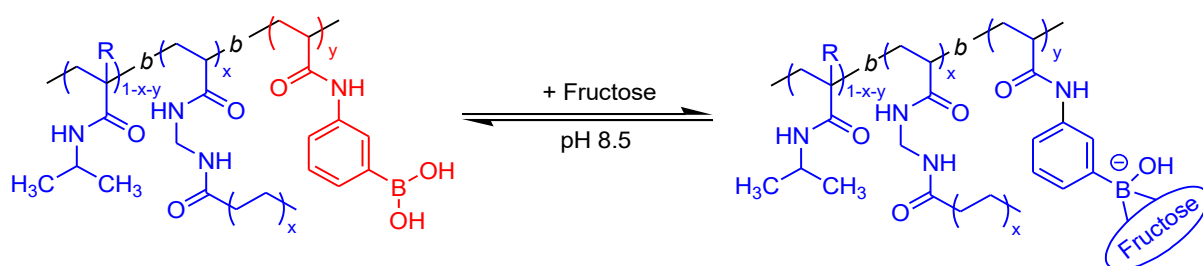
Armes *et al.* reported vesicle-to-worm transitions of block copolymers containing 1,2-diol groups, triggered through binding of water-soluble 3-aminophenylboronic acid (APBA,

Scheme 5.2).<sup>104</sup> The pH-sensitive equilibrium for boronate ester formation was manipulated to release encapsulated silica nanoparticles.



**Scheme 5.2:** APBA-induced morphology transitions (TEMs within).<sup>104</sup>

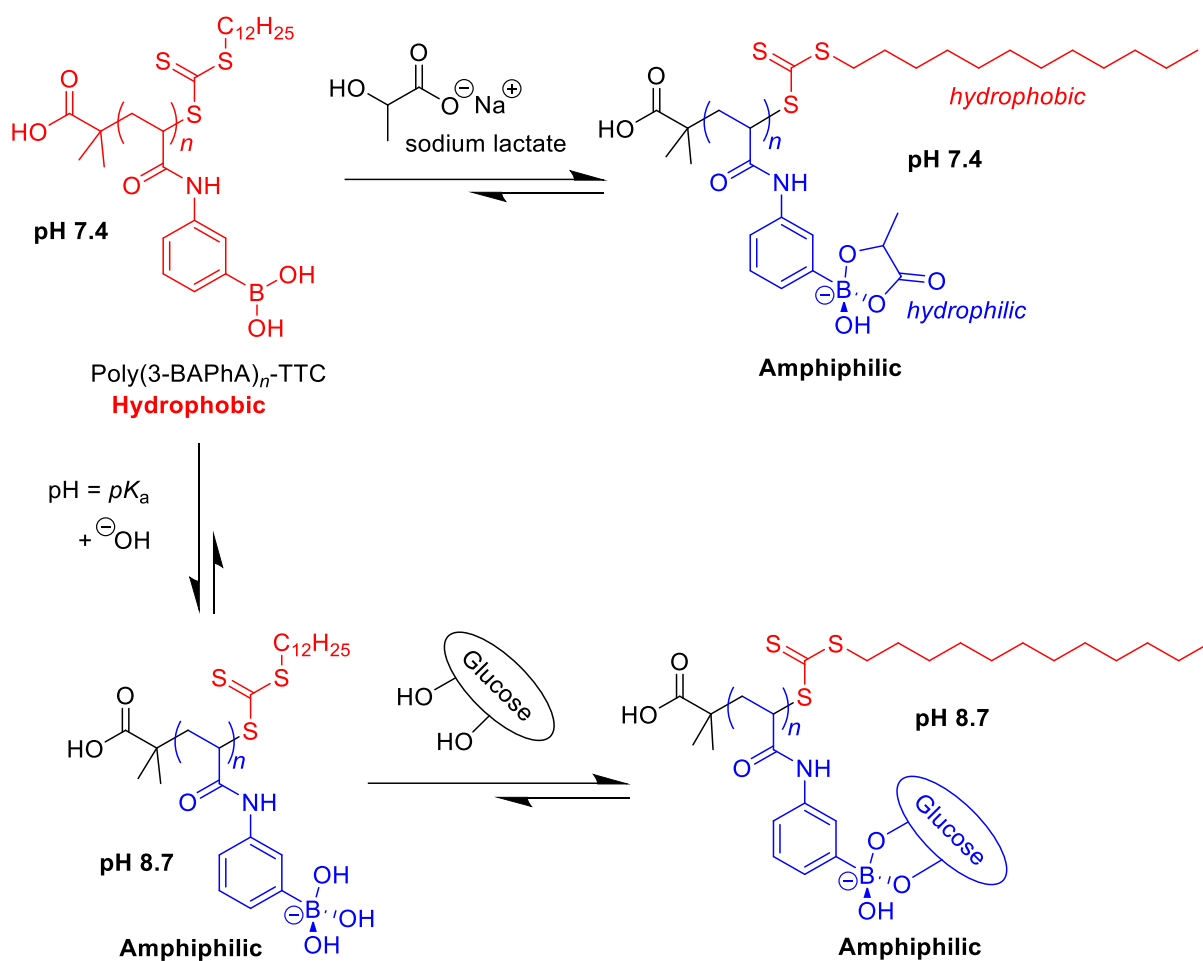
Schmitt and Ravaine et al. used fructose-binding onto BA-moieties to switch the hydrophobicity of microgels (Scheme 5.3).<sup>105</sup>



**Scheme 5.3:** Amphiphilic to hydrophilic using fructose binding.<sup>105</sup>

Nevertheless, although variation of pH and glucose-BA binding has been used to adjust polymer hydrophobicity and alter the morphology of nanoparticles, boronate ester formation has not been used to induce self-assembly of hydrophobic BA-substituted polymers. The large hydrophobic dodecyl group of the trithiocarbonate (TTC) reversible addition-fragmentation chain transfer (RAFT)-end group,<sup>41</sup> is expected to facilitate amphiphilic character for the

homopolymer (poly(3-BAPhA)-TTC) upon ionization to hydrophilic boronate residues (Scheme 5.4).



**Scheme 5.4.** Proposed lactate and glucose-induced self-assembly mechanism

## 5.2 Aims and Objectives

- To prepare high MW homopolymer of poly(3-BAPhA) of narrow MWD and high precision hydrophobic block copolymers derivatives (Fig. 5.1). This includes block copolymers with longer ( $n > m$ ) and shorter ( $n < m$ ) L-lactate and glucose binding blocks.

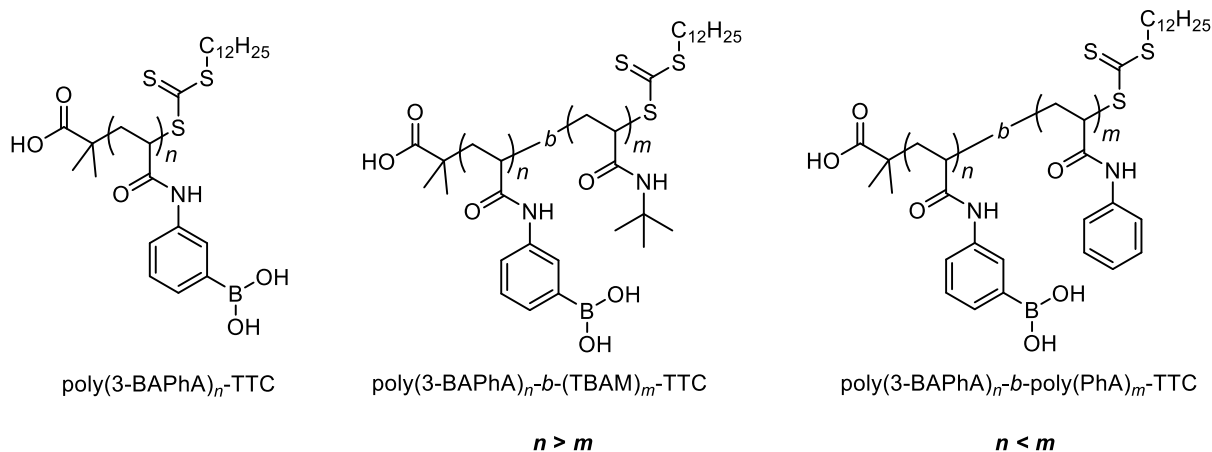


**Figure 5.1.** Synthetic target hydrophobic BA-functionalized polymers

- To induce self-assembly from the above hydrophobic polymers using lactate and glucose binding. Fig 5.2 shows the amphiphilic block copolymers produced upon binding to lactate.

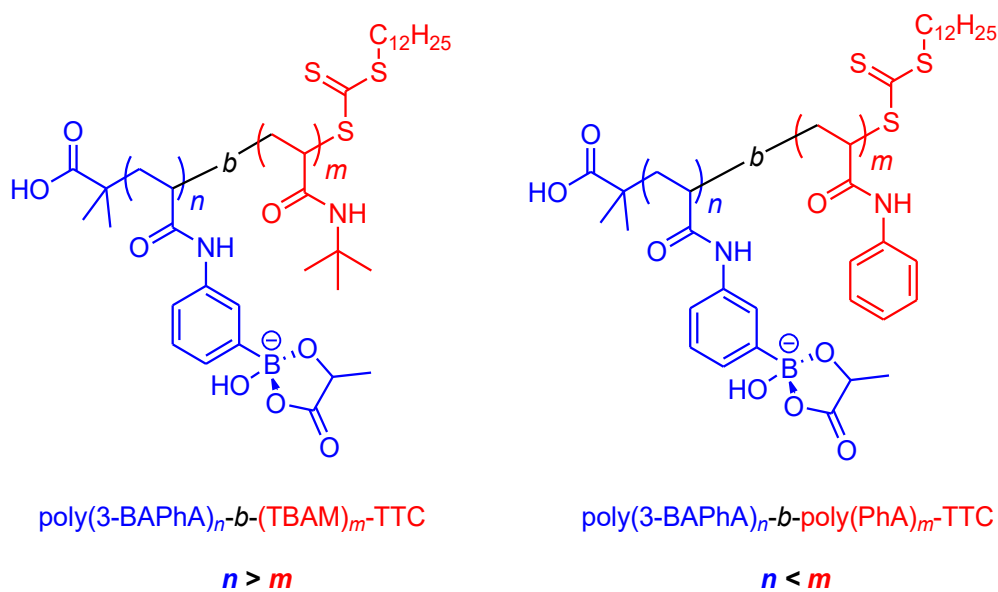


**Figure 5.2.** Induced self-assembly by lactate binding.



## 5.3 Experimental

### 5.3.1 Materials

2-(Dodecylthiocarbonothioylthio)-2-methylpropionic acid (DMP; TCI, >98%) and 2,2'-azobis[2-(2-imidazolin-2-yl)propane]dihydrochloride (VA-044, Wako, 97%) and 2,2'-azobis(2-methylpropionitrile) (AIBN; Sigma Aldrich, 98%) were used as received. Milli-Q water, methanol (MeOH, VWR,  $\geq 99\%$ ), diethyl ether (Et<sub>2</sub>O; Fisher, >99.5%), *N*-phenylacrylamide (PhA; Fluorochem >95%), *N,N*-dimethylformamide (DMF; VWF, HPLC-grade  $\geq 99.9\%$ ), and CHCl<sub>3</sub> (Fisher, >99.8%) were used directly as solvents. *N-tert*-butylacrylamide (TBAM; TCI, >98%), anisole (TCI, >99%), and pinacol (TCI, >98%) were used as received. Chapter 2 describes the synthesis of 3-(acrylamidophenyl)boronic acid (3-BAPhA) from 3-aminophenylboronic acid monohydrate (Fluorochem, 97%), acryloyl chloride (Alfa Aesar, 96%), and sodium bicarbonate (Fisher Scientific >99.7%) in 1:1 tetrahydrofuran (THF; Fisher, >99.8%):water. Molecular sieves (MS, Alfa Aesar, 3 Å, 0.800 g) were activated before use, by placing in a microwave (Toshiba ER-7620 650 W) three times for 2 min periods at medium power, with 30 s swirling aeration intervals. Sodium *L*-lactate (Alfa Aesar, >98%), NaOH (Alfa Aesar, 98%), and glucose (Alfa Aesar, 99%) were used as received.

### 5.3.2 Nuclear Magnetic Resonance (NMR) Spectroscopy

<sup>1</sup>H NMR spectra were recorded using a Bruker Avance II 400 MHz spectrometer. All conversion spectra were recorded in *D*<sub>6</sub>-dimethyl sulfoxide (DMSO-*D*<sub>6</sub>, Goss Scientific, 99.9%), and NMR of the final isolated block copolymers was carried out as following; poly(3-BAPhA)<sub>124</sub>-TTC in *D*<sub>4</sub>-MeOD, poly(3-BAPhA)<sub>91</sub>-*b*-(TBAM)<sub>35</sub>-TTC in *D*<sub>4</sub>-MeOD, and poly(3-BAPhA)<sub>34</sub>-*b*-(PhA)<sub>131</sub>-TTC in 1:3 MeOH:*D*<sub>6</sub>-DMSO.

### 5.3.3 Determination of monomer conversion

Conversion was measured using <sup>1</sup>H NMR spectroscopy by comparing the monomer content at 2 h to the monomer content before polymerization. An accurately weighed amount of anisole (~0.350 g) is dissolved in DMF (20% aq. 10 mL) to make standardized solution. A polymerization sample (20 μl), anisole standard (20 μl), and *D*<sub>6</sub>-DMSO (460 μl) are mixed in the NMR tube for conversion analysis. Conversion is calculated by comparing the anisole peak integral (representing the standardized solution) at 3.75 ppm (Me, 3H) to the integral for the monomer (*cis*-vinyl, 1H) at 5.74 (3-BAPhA),<sup>68</sup> 5.48 (TBAM, Fig. 5.3) or 5.76 (PhA, Fig. 5.4) ppm.



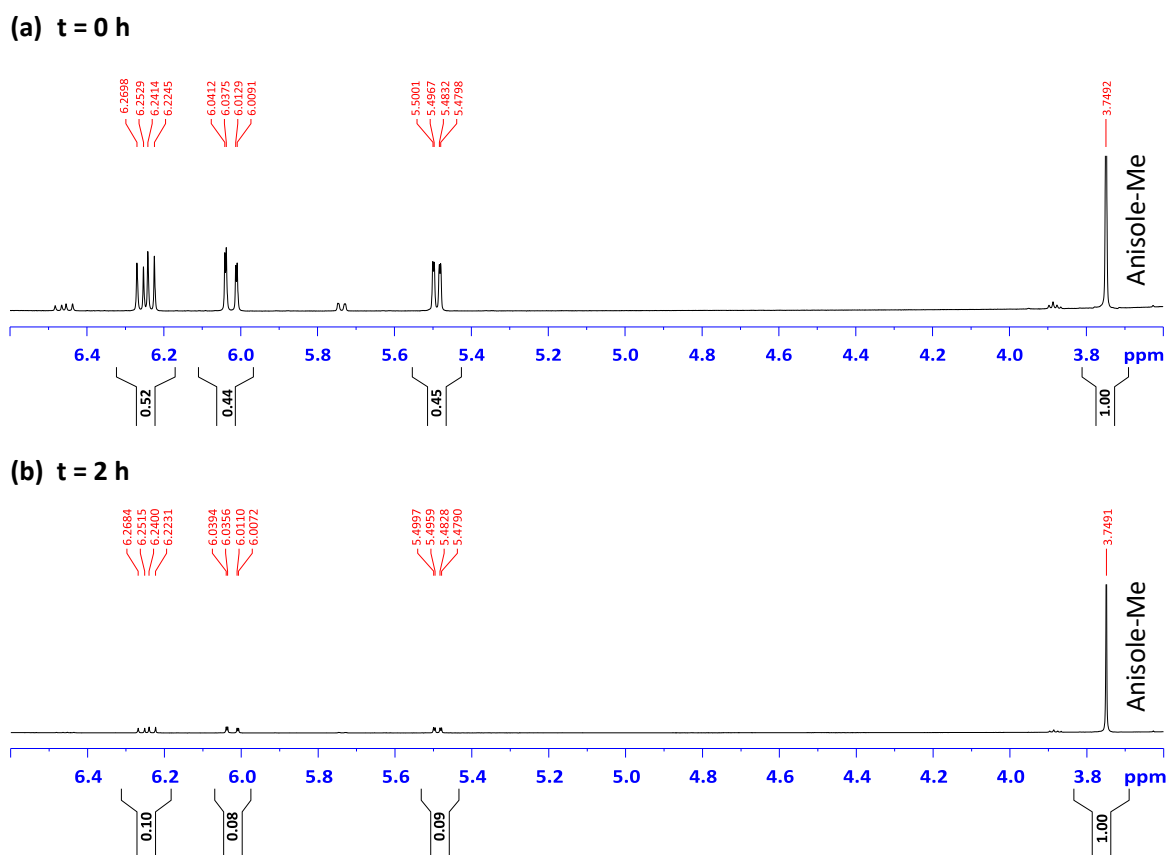


**Fig. 5.3.** Representative conversion measurement for the RAFT polymerization of TBAM (Scheme 5.6, fourth cycle):  $^1\text{H}$  NMR **(a)** before and **(b)** after polymerization (Conv. = 83%).

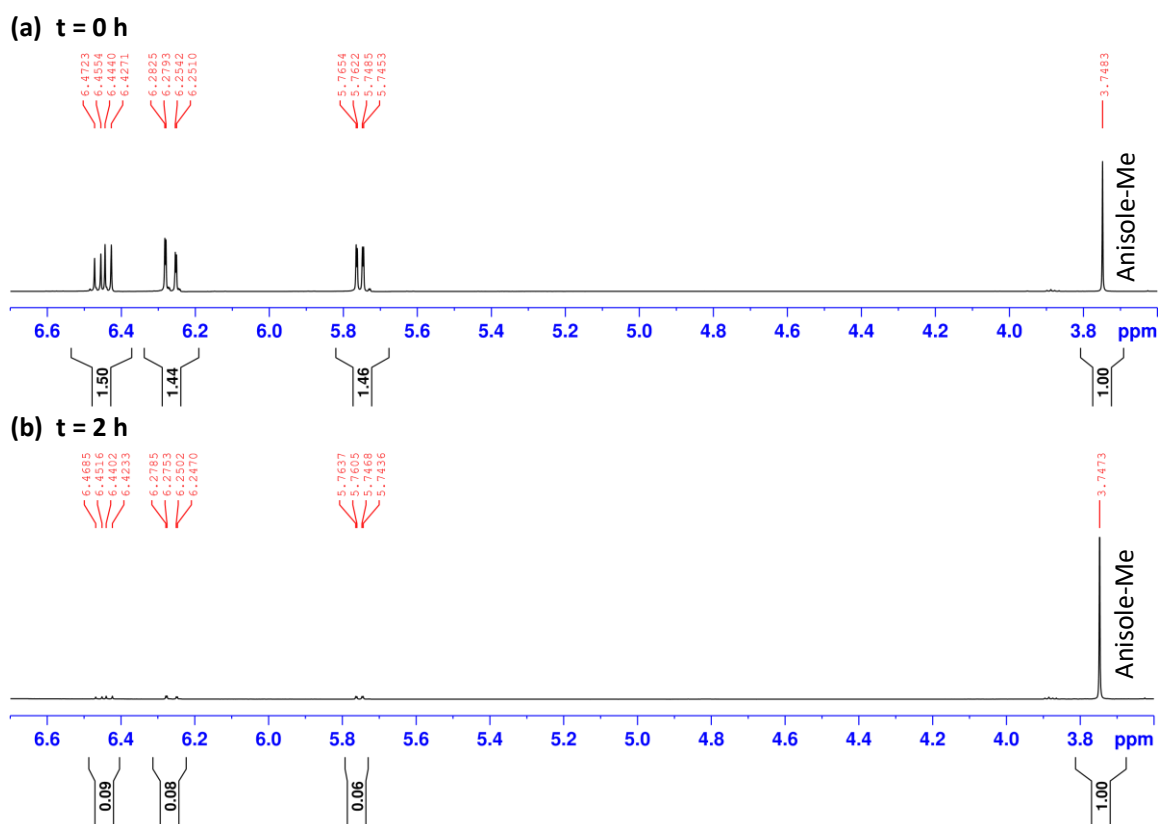
### 5.3.4 Calculation of the theoretical number fraction of living chains ( $L$ )

In RAFT, it is advantageous to use low initiator concentrations to improve  $L$ , since the number of chains that undergo bimolecular termination directly corresponds to the number of radicals generated from decomposition of the initiator during polymerization:

$$L = \frac{[\text{RAFT}]_0}{[\text{RAFT}]_0 + 2 \times f \times [\text{VA-044}]_0 \times (1 - e^{-k_d t}) \times \left(1 - \frac{f_c}{2}\right)} \quad (5.1)$$

Eq. (5.1) estimates  $L$ , where  $t$  is time in s,  $f$  is the initiator efficiency (assumed to be 0.5), and the decomposition rate constant  $k_d$  is taken as  $4.30 \times 10^{-4} \text{ s}^{-1}$  for VA-044 or  $4.34 \times 10^{-5} \text{ s}^{-1}$  for AIBN at 70 °C in 20% aq. DMF or dioxane (conditions employed in the present work).<sup>97</sup> The

quantity  $\left(1 - \frac{f_c}{2}\right)$  accounts for the effect of the termination mechanism (combination or disproportionation). Combination would half the number of radicals, so  $f_c = 1$ , while



disproportionation would not change the number of radicals, and herein this is assumed with  $f_c = 0$ .

**Fig. 5.4.** Representative conversion measurement for the RAFT polymerization of PhA (Scheme 5.7, second cycle):  $^1\text{H}$  NMR **(a)** before and **(b)** after polymerization (96%).

### 5.3.5 Gel Permeation Chromatography (GPC)

Molar mass distributions were measured using Agilent Technologies 1260 Infinity liquid chromatography system with Agilent GPC/SEC Software for Windows (version 1.2; Build 3182.29519) using a Polar Gel-M guard column (50 × 7.5 mm) and two Polar Gel-M columns (300 × 7.5 mm). DMF containing LiBr (0.01 molL<sup>-1</sup>) was used as eluent at 1.0 mL·min<sup>-1</sup> at 60 °C. Twelve narrow polydispersity poly(styrene, St) standards (Agilent, 580-301,600 gmol<sup>-1</sup>,  $\mathcal{D}$

= 1.05) were used to calibrate the GPC system. Samples were dissolved in the eluent and filtered through a PTFE membrane with 0.22  $\mu\text{m}$  pore size before injection (100  $\mu\text{L}$ ). Number average molecular weight ( $M_n$ ) values are not absolute, but relative to linear poly(St) standards.

### 5.3.6 Preparation of GPC Sample (GPC)

Molecular sieves (MS, Alfa Aesar, 3  $\text{\AA}$ , 0.800 g) were activated three times by microwave (Toshiba ER-7620 650 W) for 2 min periods at medium power, with 30 s swirling aeration intervals. Pinacol (TCI, >98%, 0.148 g, 1.250 mmol) in  $\text{CHCl}_3$  (Fisher, >99.8%, 5.00 mL) and the polymerization sample (20  $\mu\text{l}$ ) were added to the activated MS, and stirred for 24 h, at room temperature. MS were removed using gravity filtration, and the solution evaporated to a residue, which was dissolved in 1 mL of the GPC eluent. Herein, GPC is after pinacol protection of the BA block to poly(3-BAEPhA).

### 5.4 General polymerization procedure

All polymerization solutions were added to borosilicate glass tubes sealed with septa and flushed with  $\text{N}_2$  for 30 min at 70  $^\circ\text{C}$  and heated for a further 1.5 h at 70  $^\circ\text{C}$  (total polymerization time = 2 h). An aluminium-heating block is used for heating and the temperature is maintained within  $\pm 0.2$   $^\circ\text{C}$  throughout. With exception to AIBN macroRAFT (3 h) and chain extension (4 h) below.

#### 5.4.1 Polymerization of 3-BAPhA using $[\text{3-BAPhA}]_0/[\text{DMP}]_0/[\text{AIBN}]_0 = 100/1/0.15$

A stock solution (of AIBN  $1.48 \times 10^{-3} \text{ molL}^{-1}$  and DMP  $0.01 \text{ molL}^{-1}$ ) was prepared using AIBN (61 mg, 0.37 mmol) dissolved in DMF (5% aq., 25 mL) of which 1 mL was added to DMP (37 mg, 0.1 mmol) and topped up to 10 mL with 5% aq. DMF. The latter stock solution (1 mL) was added to 3-BAPhA (0.191 g, 1.00 mmol) and heated at 70  $^\circ\text{C}$  for 3 h (incl. 30 min with  $\text{N}_2$  flush). Conv. was determined by  $^1\text{H}$  NMR and GPC required pinacol protection, as described section 5.3.3.

#### 5.4.2 Chain extension using $[\text{3-BAPhA}]_0/[\text{DMP}]_0/[\text{AIBN}]_0 = 100/1/0.15$

A standardized solution (of AIBN  $1.19 \times 10^{-3} \text{ molL}^{-1}$ ) was prepared using AIBN (49 mg, 0.30 mmol) dissolved in DMF (5% aq., 250 mL). The AIBN stock solution (0.5 mL) and 3-BAPhA (0.177 g, 0.92 mmol) were added to the polymerization mixture (above, 1 mL, 3 h,  $M_n = 13,800 \text{ gmol}^{-1}$ ;  $\bar{D} = 1.35$ , Fig. 5.5) containing poly(3-BAPhA)<sub>49</sub>-TTC. The amount of 3-BAPhA and AIBN

added allowed for monomer (8% remaining) and initiator (62.6% remaining<sup>97</sup>) consumed in the initial 3 h polymerization. The polymerization solution thus contained, 3-BAPhA (0.67 molL<sup>-1</sup>), AIBN (1.0 x 10<sup>-3</sup> molL<sup>-1</sup>), and poly(3-BAPhA)<sub>49</sub>-TTC (6.67 x 10<sup>-3</sup> molL<sup>-1</sup>), which were heated at 70 °C for 4 h (incl. 30 min with N<sub>2</sub> flush). Conv. was determined by <sup>1</sup>H NMR and GPC required pinacol protection, as described section 5.3.2 and 5.3.6, respectively. The polymer was precipitated in Et<sub>2</sub>O, filtered, and dried at room temperature under vacuum for 24 h to give poly(3-BAPhA)<sub>79</sub>-TTC,  $M_n = 21,800 \text{ g}\cdot\text{mol}^{-1}$ ,  $\bar{D} = 1.44$ , isolated = 0.21 g (52%).

#### 5.4.3 Preparation of poly(3-BAPhA)-TTC using [3-BAPhA]<sub>0</sub>/[DMP]<sub>0</sub> = 250 with VA-044

Two VA-044 concentrations investigated: [3-BAPhA]<sub>0</sub>/[DMP]<sub>0</sub>/[VA-044]<sub>0</sub> = 250/1/0.02, where VA-044 (0.24 x 10<sup>-4</sup> molL<sup>-1</sup>) and DMP (0.012 molL<sup>-1</sup>) were added to 3-BAPhA (0.573 g, 0.003 mmol) in 1 mL of DMF (20% aq. solution), and [3-BAPhA]<sub>0</sub>/[DMP]<sub>0</sub>/[VA-044]<sub>0</sub> = 250/1/0.05, where VA-044 (0.61 x 10<sup>-4</sup> molL<sup>-1</sup>) and DMP (0.012 molL<sup>-1</sup>) were added to 3-BAPhA (0.573 g, 0.003 mmol) in 1 mL of DMF (20% aq.). The solutions were heated at 70 °C for 2 h. For the latter, the polymer was precipitated in Et<sub>2</sub>O, filtered, and dried at room temperature under vacuum for 24 h to give poly(3-BAPhA)<sub>96</sub>-TTC,  $M_n = 26,600 \text{ g}\cdot\text{mol}^{-1}$ ,  $\bar{D} = 1.42$ , isolated = 0.33 g (58%).

#### 5.4.4 One-pot iterative RAFT polymerizations using VA-044

The synthesis begins with preparation of a standardized initiator (VA-044) solution in DMF (20% aq.) to which DMP and 3-BAPhA are added. All chain extensions were heated at 70 °C in an aluminium-heating block for 2 h and stopped by quenching in an ice-water bath. Iterative chain extension reactions were performed directly on the macroRAFT agent polymerization solution (*i.e.* one-pot reaction) with the amount of initiator and monomer remaining after each cycle factored in (see Tables 5.1-5.3). Thus, each cycle involved adding further monomer in VA-044 standardized solution to the *in situ* formed macroRAFT and agitating the reaction mixture by vortex (Stuart SA8) to ensure a homogenous solution prior to polymerization. The chain extension was sampled before and after each cycle for NMR conversion (20 µl before and 20 µl after polymerization) and GPC analysis (20 µl after polymerization), as described above. The final polymers were precipitated from an excess of cold Et<sub>2</sub>O (500 mL) and dried at room temperature under vacuum for 72 h.

*E.g.* For the synthesis of poly(3-BAPhA)<sub>124</sub>-TTC each polymerization cycle used [3-BAPhA]<sub>0</sub>/[MacroRAFT]<sub>0</sub> = 50 (Scheme 5.6, Table 5.1).

For the first block, VA-044 (95.4 mg, 0.30 mmol) is used to make a standardized 1.18 x 10<sup>-3</sup> molL<sup>-1</sup> (M) solution by 250 dilution with 20% aq. DMF. DMP (21.4 mg, 0.06 mmol) and 3-BAPhA (561.5 mg, 2.94 mmol) were added to 1 mL of the standardized VA-044 solution.

For the synthesis of poly(3-BAPhA)<sub>91</sub>-*b*-(TBAM)<sub>35</sub>-TTC each polymerization cycle used [TBAM]<sub>0</sub>/[poly(3-BAPhA)<sub>91</sub>-TTC]<sub>0</sub> = 50 (Table 5.2): *E.g.* For the fourth block, VA-044 (66.9 mg, 0.21 mmol) is used to make a standardized 8.28 x 10<sup>-4</sup> molL<sup>-1</sup> (M) solution by 250 dilution with DMF (20% aq.). TBAM (273.8 mg, 2.15 mmol) was added to the *in situ* generated poly(3-BAPhA)<sub>91</sub>, and the polymerization solution (TBAM = 0.75 molL<sup>-1</sup>) was heated for 2 h at 70 °C.

For the synthesis of poly(3-BAPhA)<sub>34</sub>-*b*-(PhA)<sub>131</sub>-TTC each polymerization cycle used [PhA]<sub>0</sub>/[poly(3-BAPhA)<sub>34</sub>-TTC]<sub>0</sub> = 57 (Table 5.3): For the second block, VA-044 (33.6 mg, 0.104 mmol) is used to make a standardized 4.16 x 10<sup>-3</sup> molL<sup>-1</sup> (M) solution by 25 dilution with DMF (20% aq.). PhA (427.6 mg, 2.91 mmol) in the latter VA-044 standardized solution (0.28 mL) was added to the *in situ* generated poly(3-BAPhA)<sub>34</sub>, and the polymerization solution (PhA = 2.27 molL<sup>-1</sup>) was heated for 2 h at 70 °C.

**Table 5.1.** Experimental conditions for the preparation of poly(3-BAPhA)<sub>124</sub>-TTC in 20% aq. DMF at 70 °C by one-pot 2 h iterative RAFT polymerizations with [3-BAPhA]<sub>0</sub>/[RAFT]<sub>0</sub> = 50 for all five cycles (Scheme 5.5).

Chain Extensions	1	2	3	4	5
Conversion (%)	94	76	87	89	93
3-BAPhA added (mg)	561.5	500.3 <sup>a</sup>	456.0 <sup>a</sup>	426.9 <sup>a</sup>	410.5 <sup>a</sup>
DMP added (mg)	21.44	-	-	-	-
VA-044 added (mg) <sup>b</sup>	0.3815	0.3380 <sup>c</sup>	0.3853 <sup>c</sup>	0.4836 <sup>c</sup>	0.6459 <sup>c</sup>
Total Solvent (mL)	1.00	1.18	1.73	2.98	3.98
[3-BAPhA] <sub>0</sub> (molL <sup>-1</sup> )	2.94	2.22 <sup>d</sup>	1.38 <sup>d</sup>	0.75 <sup>d</sup>	0.54 <sup>d</sup>
[MacroRAFT] <sub>0</sub> (molL <sup>-1</sup> )	0.0588 <sup>e</sup>	0.0443 <sup>f</sup>	0.0276 <sup>f</sup>	0.0151 <sup>f</sup>	0.0109 <sup>f</sup>
[VA-044] <sub>0</sub> (molL <sup>-1</sup> )	1.18 x 10 <sup>-3</sup>	8.86 x 10 <sup>-4</sup>	6.89 x 10 <sup>-4</sup>	5.02 x 10 <sup>-4</sup>	5.02 x 10 <sup>-4</sup>
[MacroRAFT] <sub>0</sub> / [VA-044] <sub>0</sub>	50	50	40	30	22
Cumulative <i>L</i> (%) <sup>g</sup>	98.1	96.2	94.0	91.1	87.7

<sup>a</sup>Additions determined by conv. and 60 μl reaction sampling for conv. and GPC measurements, accounting for depreciation in [MacroRAFT] with sampling. <sup>b</sup>After serial dilution. <sup>c</sup>Addition based on VA-044 remaining from the previous chain extension. <sup>d</sup>monomer remaining after sampling and additions. <sup>e</sup>DMP. <sup>f</sup>Estimated after reaction dilution and sampling. <sup>g</sup>Cumulative livingness (*L*) calculated using eq. (5.1).

**Table 5.2:** Experimental conditions for the preparation of poly(3-BAPhA)<sub>91</sub>-*b*-(TBAM)<sub>35</sub>-TTC in 20% aq. DMF at 70 °C by one-pot 2 h iterative RAFT polymerizations: three chain extensions with [Monomer]<sub>0</sub>/[RAFT]<sub>0</sub> = 50 (Scheme 5.6).

Chain Extensions	1 (3-BAPhA)	2 (3-BAPhA)	3 (3-BAPhA)	4 (TBAM)
Conversion (%)	96	89	95	83
Monomer added (mg)	561.5	543.1 <sup>a</sup>	432.8 <sup>a</sup>	273.8 <sup>a</sup>
DMP added (mg)	21.44	-	-	-
VA-044 added (mg) <sup>b</sup>	0.3815	0.4578 <sup>c</sup>	0.4899 <sup>c</sup>	0.7682 <sup>c</sup>
Total Solvent (mL)	1.00	1.18	1.73	2.87
[Monomer] <sub>0</sub> (molL <sup>-1</sup> )	2.94	2.41 <sup>d</sup>	1.31 <sup>d</sup>	0.75 <sup>d</sup>
[MacroRAFT] <sub>0</sub> (molL <sup>-1</sup> )	0.0588 <sup>e</sup>	0.0481 <sup>f</sup>	0.0263 <sup>f</sup>	0.0149 <sup>f</sup>
[VA-044] <sub>0</sub> (molL <sup>-1</sup> )	1.18 x 10 <sup>-3</sup>	1.20 x 10 <sup>-3</sup>	8.76 x 10 <sup>-4</sup>	8.28 x 10 <sup>-4</sup>
[MacroRAFT] <sub>0</sub> / [VA-044] <sub>0</sub>	50	40	30	18
Cumulative <i>L</i> (%) <sup>g</sup>	98.1	95.8	92.8	88.2

<sup>a</sup>Additions determined by conv. and 60 μl reaction sampling for conv. and GPC measurements, accounting for depreciation in [MacroRAFT] with sampling. <sup>b</sup>After serial dilution. <sup>c</sup>Addition based on VA-044 remaining from the previous chain extension. <sup>d</sup>monomer remaining after sampling and additions. <sup>e</sup>DMP. <sup>f</sup>Estimated after reaction dilution and sampling. <sup>g</sup>Cumulative livingness (*L*) calculated using eq. (5.1).

**Table 5.3:** Experimental conditions for the preparation of poly(3-BAPhA)<sub>34</sub>-*b*-(PhA)<sub>131</sub>-TTC in 20% aq. DMF at 70 °C by one-pot 2 h iterative RAFT polymerizations: the first chain extension with [3-BAPhA]<sub>0</sub>/[RAFT]<sub>0</sub> = 50 and all other chain extensions with [PhA]<sub>0</sub>/[RAFT]<sub>0</sub> = 57 (Scheme 5.7).

Chain Extensions	1 (3-BAPhA)	2 (PhA)	3 (PhA)	4 (PhA)
Conversion (%)	96	96	94	91
Monomer added (mg)	561.5	427.6 <sup>a</sup>	395.6 <sup>a</sup>	372.8 <sup>a</sup>
DMP added (mg)	21.40	-	-	-
VA-044 added (mg) <sup>b</sup>	0.3879	0.4883 <sup>c</sup>	0.4477 <sup>c</sup>	0.5125 <sup>c</sup>
Total Solvent (mL)	1.00	1.28	1.78	2.98
[Monomer] <sub>0</sub> (molL <sup>-1</sup> )	2.94	2.27 <sup>d</sup>	1.51 <sup>d</sup>	0.85 <sup>d</sup>
[MacroRAFT] <sub>0</sub> (molL <sup>-1</sup> )	0.0587 <sup>e</sup>	0.0400 <sup>f</sup>	0.0265 <sup>f</sup>	0.0149 <sup>f</sup>
[VA-044] <sub>0</sub> (molL <sup>-1</sup> )	1.20 x 10 <sup>-3</sup>	1.18 x 10 <sup>-3</sup>	7.78 x 10 <sup>-4</sup>	5.32 x 10 <sup>-4</sup>
[MacroRAFT] <sub>0</sub> / [VA-044] <sub>0</sub>	49	34	34	28
Cumulative <i>L</i> (%) <sup>g</sup>	98.1	95.5	92.9	89.8

<sup>a</sup>Additions determined by conv. and 60 μl reaction sampling for conv. and GPC measurements, accounting for depreciation in [MacroRAFT] with sampling. <sup>b</sup>After serial dilution. <sup>c</sup>Addition based on VA-044 remaining from the previous chain extension. <sup>d</sup>monomer remaining after sampling and additions. <sup>e</sup>DMP. <sup>f</sup>Estimated after reaction dilution and sampling. <sup>g</sup>Cumulative livingness (*L*) calculated using eq. (5.1).

#### 5.4.5 Lactate and Glucose-Induced Self-Assembly

The hydrophobic polymers (41.0 mg of poly(3-BAPhA)<sub>124</sub>-TTC, 35.5 mg of poly(3-BAPhA)<sub>91</sub>-(TBAM)<sub>35</sub>-TTC; 34.6 mg of poly(3-BAPhA)<sub>34</sub>-(PhA)<sub>131</sub>-TTC) were dissolved in MeOH/DMF (2.84 mL, 3/4), while stirring (500 rpm) sodium *L*-lactate solution (0.1 molL<sup>-1</sup> at pH 7.4) was added, at a rate of ~1 drop every 10 s until turbidity (micellization) was observed. The aqueous lactate dispersion sample was monitored by a pH meter (Mettler Toledo FP20) and further



dropwise addition of NaOH (0.05 M) maintained pH 7.4. The resulting mixture was placed in a 20 cm dialysis bag (Thermo Scientific™ SnakeSkin™ dialysis tubing, molecular weight cut-off, MWCO = 3.5 KDa,) and exchanged with water (500 mL) for 12 h to exclude the organic solvent and any unreacted monomer. For *D*-glucose response, the same procedure as above was followed, except NaOH solution (at pH 8.7) was added to the solvated block copolymers until turbidity (micellization) was observed. The resulting mixture was dialyzed against NaOH solution (500 mL at pH 8.7), as described above. The dialyzed mixture (~10 mL) was sampled (1 mL) and *D*-glucose (0.1 mL, 0.5 M) added to the stirring (500 rpm) turbid sample, while maintaining pH 8.7 through further NaOH (0.05 M) dropwise additions.

#### 5.4.6 Transmission Electron Microscopy (TEM)

Please refer to section 3.3.2.1. TEM analysis was conducted by Dr Fumi Ishizuka of The University of New South Wales, UNSW, Sydney, Australia.

### 5.5 Results and Discussion

#### 5.5.1 Chain extension using AIBN to give poly(3-BAPhA)<sub>79</sub>-TTC

Initial RAFT polymerizations of 3-BAPhA were based on literature procedures,<sup>5,6</sup> using 2-(dodecylthiocarbonothioylthio)-2-methylpropionic acid (DMP) and 2,2'-azobis(2-methylpropionitrile) (AIBN), as RAFT agent and azo initiator respectively, in DMF (5% aq.) at 70 °C with  $[3\text{-BAPhA}]_0/[DMP]_0/[AIBN]_0 = 100/1/0.15$  (Fig. 5.5). The polymerization reached 92% conv. in 3 h, but the poly(3-BAPhA)<sub>49</sub>-TTC obtained had  $M_n$  (= 13,800 g mol<sup>-1</sup>) considerably lower than  $M_{n,\text{th}}$  (= 25,500 g mol<sup>-1</sup>) with a relatively broad molecular weight distribution (MWD,  $\bar{D} = 1.35$ , Table 5.4). Chain extension with 3-BAPhA, under the same conditions gave poly(3-BAPhA)<sub>79</sub>-TTC with  $M_n$  (= 21,800 g mol<sup>-1</sup>) also significantly lower than the (conv. based) theoretical value ( $M_{n,\text{th}} = 40,300$  g mol<sup>-1</sup>). The broadening in the MWD ( $\bar{D} = 1.44$ ) is indicative of a loss of livingness and a carryover of initiator-derived dead chains since according to eq. 5.1,  $L = 88.4\%$  for the two consecutive polymerizations. GPC calibration error is expected to have a less significant effect (note – 3-BAEPH is the pinacol ester of 3-BAPhA and GPC is taken after this protection).

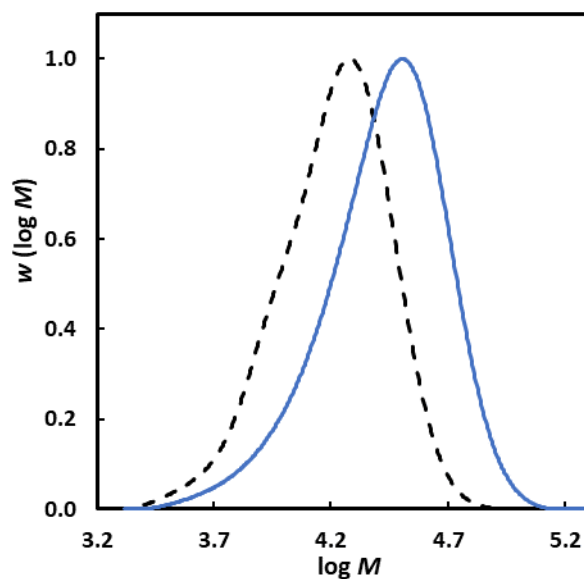


**Fig. 5.5:** Two consecutive RAFT-mediated polymerizations using  $[3\text{-BAPhA}]_0/[RAFT]_0/[AIBN]_0 = 100/1/0.15$  in DMF (5% aq.) at 70 °C: MWDs of  $[3\text{-BAPhA}]_0 = 1.0$  M, 3 h, to give poly(3-BAPhA)<sub>49</sub>-TTC, 92% conv. (dashed line), and one-pot chain extension of poly(3-BAPhA)<sub>49</sub>-TTC,  $[3\text{-BAPhA}]_0 = 0.67$  M, 4 h, 97% conv. to give poly(3-BAPhA)<sub>79</sub>-TTC.

### 5.5.2 Polymerization of 3-BAPhA using $[3\text{-BAPhA}]_0/[DMP]_0 = 250$

AIBN was replaced with 2,2'-azobis[2-(2-imidazolin-2-yl)propane]dihydrochloride (VA-044) due to its faster decomposition allowing very low initiator concentrations to be used, which achieve near-complete conversions of polyacrylamides within the 2 h polymerizations.<sup>43</sup> The aim was to achieve the highest possible *DP* BA-functionalized polymer, thus two polymerizations with  $[3\text{-BAPhA}]_0/[DMP]_0 = 250$  were carried out using  $[3\text{-BAPhA}]_0 = 3 \text{ molL}^{-1}$  at 70 °C and at two different VA-044 concentrations in DMF (20% aq.) at 70 °C (Fig. 5.6).

At the lower initiator concentration ( $[DMP]_0/[VA\text{-}044]_0 = 50$ ), conv. was low (18%) and the bimodality ( $M_n = 7,100 \text{ g mol}^{-1}$ ,  $\mathcal{D} = 1.56$ , Table 5.4) indicates some polymer chains remained in the pre-equilibrium stage. Increasing the VA-044 concentration ( $[DMP]_0/[VA\text{-}044]_0 = 20$ ) led to higher conversion (of 63%), but  $M_n = 26,600 \text{ g mol}^{-1}$  is well-below the theoretical value ( $M_{n,\text{th}} = 43,300 \text{ g mol}^{-1}$ ) with the relative broad MWD ( $\mathcal{D} = 1.42$ ) indicative of poor control/living character.

**Table 5.4:** GPC characterization of polymers.

Fig	Polymer <sup>b</sup>	% Conv. <sup>c</sup>	$M_{n,th}$ <sup>d</sup>	$M_n$ <sup>e</sup>	$\mathcal{D}$ <sup>e</sup>
<b>5.5</b>	poly(3-BAPhA) <sub>49</sub> -TTC	92	25,500	13,800	1.35
	poly(3-BAPhA) <sub>49</sub> - <i>b</i> -(3-BAPhA) <sub>30</sub> -TTC	97	40,300	21,800	1.44
<b>5.6</b>	poly(3-BAPhA) <sub>25</sub> -TTC	18	12,700	7,100	1.56
	poly(3-BAPhA) <sub>96</sub> -TTC	63	43,400	26,600	1.42
<b>5.8<sup>a</sup></b>	poly(3-BAPhA) <sub>33</sub> -TTC	94	13,200	9,400	1.16
	poly(3-BAPhA) <sub>33</sub> - <i>b</i> -(3-BAPhA) <sub>19</sub> -TTC	76	19,800	14,700	1.19
	poly(3-BAPhA) <sub>33</sub> - <i>b</i> -(3-BAPhA) <sub>19</sub> - <i>b</i> -(3-BAPhA) <sub>23</sub> -TTC	87	26,600	21,100	1.21
	poly(3-BAPhA) <sub>33</sub> - <i>b</i> -(3-BAPhA) <sub>19</sub> - <i>b</i> -(3-BAPhA) <sub>23</sub> - <i>b</i> -(3-BAPhA) <sub>36</sub> -TTC	89	33,300	30,800	1.22
<b>5.10<sup>a</sup></b>	poly(3-BAPhA) <sub>124</sub> -TTC	93	43,500	34,200	1.26
	poly(3-BAPhA) <sub>34</sub> -TTC	96	13,500	9,500	1.17
	poly(3-BAPhA) <sub>34</sub> - <i>b</i> -(3-BAPhA) <sub>27</sub> -TTC	89	21,700	16,900	1.18
	poly(3-BAPhA) <sub>34</sub> - <i>b</i> -(3-BAPhA) <sub>27</sub> - <i>b</i> -(3-BAPhA) <sub>30</sub> -TTC	95	29,900	25,200	1.23
<b>5.13<sup>a</sup></b>	poly(3-BAPhA) <sub>91</sub> - <i>b</i> -(TBAM) <sub>35</sub> -TTC	83	30,500	29,600	1.27
	poly(3-BAPhA) <sub>34</sub> -TTC	96	13,500	9,500	1.14
	poly(3-BAPhA) <sub>34</sub> - <i>b</i> -(PhA) <sub>56</sub> -TTC	96	17,600	17,800	1.16
	poly(3-BAPhA) <sub>34</sub> - <i>b</i> -(PhA) <sub>56</sub> - <i>b</i> -(PhA) <sub>42</sub> -TTC	94	25,700	23,800	1.20
	poly(3-BAPhA) <sub>34</sub> - <i>b</i> -(PhA) <sub>131</sub> -TTC	91	31,400	28,800	1.28

<sup>a</sup>See Scheme 5.5-5.7, and Tables 5.1-5.3 for polymerization conditions. <sup>b</sup> $DP$  calculated from  $M_n$ (GPC). <sup>c</sup>Measured using <sup>1</sup>H NMR. <sup>d</sup>Theoretical ( $M_{n,th}$ ) is calculated from conv. added to  $M_n$ (GPC) of the previous block, including pinacol protection (see part<sup>e</sup>). <sup>e</sup>Determined by GPC/RI in DMF (0.01 M LiBr) using commercial linear poly(styrene) as molecular weight standards with measurements in g mol<sup>-1</sup> after pinacol protection of the 3-BAPhA block.

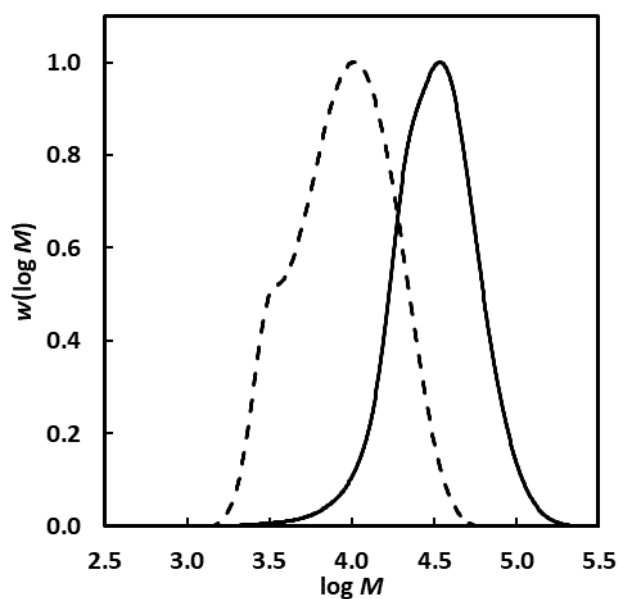


**Fig. 5.6:** RAFT polymerization of 3-BAPhA using  $[3\text{-BAPhA}]_0 = 3.0\text{ M}$  at two different VA-044 concentrations in DMF (20% aq.) at  $70\text{ }^\circ\text{C}$ : MWDs of  $[3\text{-BAPhA}]_0/[DMP]_0/[VA\text{-}044]_0 = 250/1/0.02$ , 18% conv. (dashed line) and  $[3\text{-BAPhA}]_0/[DMP]_0/[VA\text{-}044]_0 = 250:1:0.05$ , 63% conv. (continuous line) to give poly(3-BAPhA)<sub>25</sub>-TTC and poly(3-BAPhA)<sub>96</sub>-TTC, respectively.

### 5.5.3 Synthesis using one-pot iterative RAFT polymerizations

#### 5.5.3.1 Preparation of poly(3-BAPhA)<sub>124</sub>-TTC

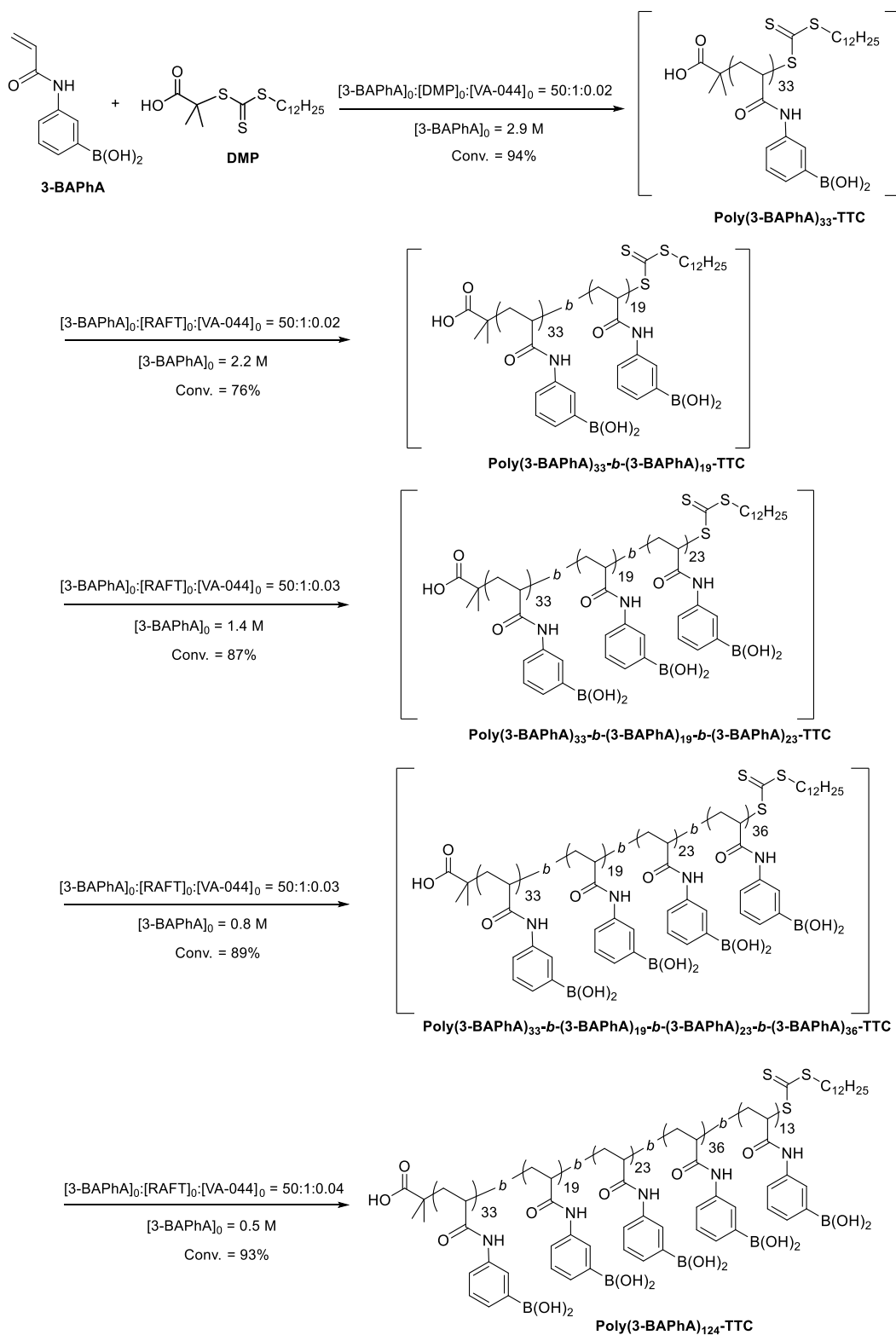
To maximize livingness, one-pot iterative RAFT polymerizations at high  $[RAFT]_0/[initiator]_0$  (= 50 to 22) ratios and lower targeted degree of polymerization ( $DP = 50$ ) for each block were pursued. Five 2 h cycles at  $70\text{ }^\circ\text{C}$  were performed with equivalent monomer ( $[3\text{-BAPhA}]_0 = 2.9\text{ M}$ ) and initiator concentrations at the first cycle to the  $DP = 250$  experiment (Fig. 5.6), with the successive addition of monomer and initiator in DMF (20% aq.) leading to progressive dilution at each cycle (leading to  $[3\text{-BAPhA}]_0 = 0.5\text{ molL}^{-1}$  at the final cycle, Scheme 5.6, Table 5.1). The dilutions are countered by a lowering in the  $[RAFT]_0/[VA\text{-}044]_0$  ratio to maintain high conversions (76-94%). MWDs shift to higher MW and remained narrow throughout (Fig. 5.7.  $\mathcal{D} = 1.16\text{-}1.26$ ).  $M_n$  remained close to  $M_{n,th}$  until the fifth cycle (Fig. 5.8), where deviation from the theoretical value (according to eq. 5.2) occurs because less monomer is added in the final

cycle than predicted by conv. measurement (Note -  $DP$  in Schemes 5.5-5.7 is calculated from  $M_n(\text{GPC})$ ). This is due to an accumulation of dead chains by loss of the RAFT end group with time (Scheme 2.1),<sup>46,59</sup> and the dilution of monomer. The relatively narrow final MWD is due to less 3-BAPhA units (13 as opposed 36 added in the previous cycle) added per RAFT activation-deactivation cycle due to the progressive dilution.<sup>98</sup>

$$M_{n,\text{th}} = \left( \frac{[\text{Monomer}]_0}{[\text{RAFT}]_0} \times MW_{\text{Monomer}} \times \text{Conv.} \right) + MW_{\text{RAFT}} \quad (5.2)$$

Where  $MW_{\text{RAFT}}$  is the MW of DMP or of the previous block using GPC.

Poly(3-BAPhA)<sub>124</sub>-TTC in DMF (in 20% aq. polymerization solvent) was precipitated from cold Et<sub>2</sub>O and dried under vacuum to give an isolated yield of 1.28 g (45%, based on every cycle going to 100% conv.).



**Scheme 5.5:** Preparation of poly(3-BAPhA)<sub>124</sub>-TTC in DMF (20% aq.) at 70 °C by one-pot 2 h iterative RAFT-mediated polymerizations of 3-BAPhA.

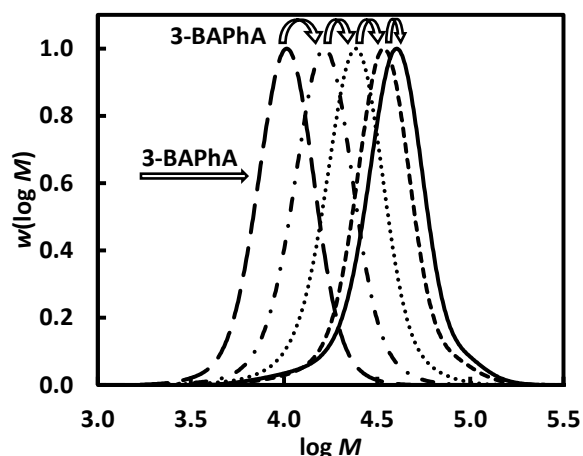


**Fig. 5.7:** MWD for the preparation of poly(3-BAPhA)<sub>124</sub>-TTC by one-pot iterative RAFT polymerizations of 3-BAPhA.

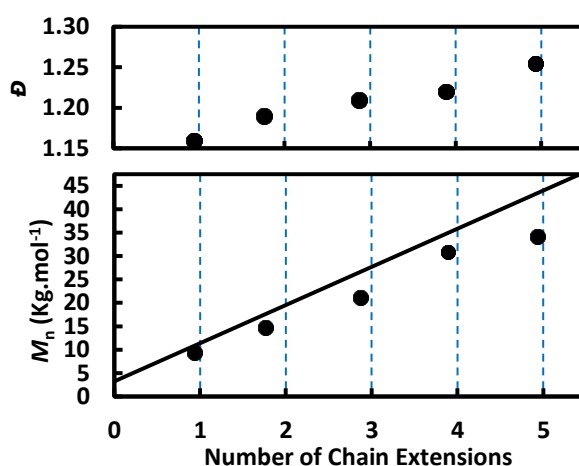
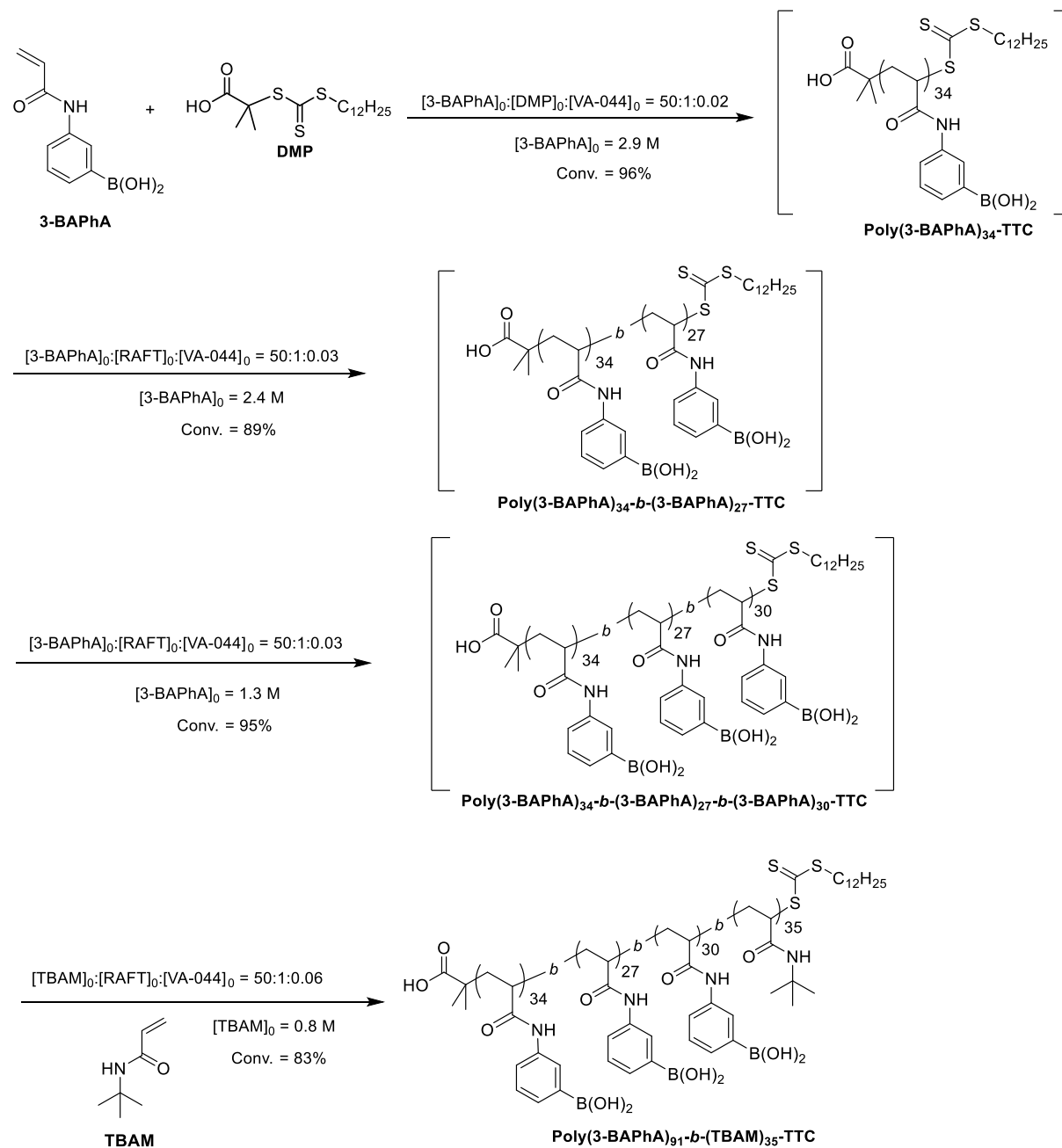


**Fig. 5.8**  $M_n$  and  $\bar{D}$  versus number of chain extensions (dashed vertical lines at 100% conv.) with targeted degree of polymerization ( $DP$ ) = 50, and  $M_{n,th}$  line calculated according to Eq (5.2).

### 5.5.3.2 Preparation of poly(3-BAPhA)<sub>91</sub>-*b*-(TBAM)<sub>35</sub>-TTC

Poly(3-BAPhA)<sub>91</sub>-*b*-(TBAM)<sub>35</sub>-TTC was prepared to assess the impact of a longer hydrophobic block (with TBAM) on self-assembly (Scheme 5.6). The same  $[3\text{-BAPhA}]_0/[RAFT]_0$  (= 50) and similar monomer concentrations were used as for the synthesis of poly(3-BAPhA)<sub>124</sub>-TTC, except for increased  $[VA\text{-}044]_0$  for the second and third cycle, to increase the rate of monomer consumption. The conv. increased from 76 to 89% and 87 to 95% for the two polymerization cycles of 3-BAPhA (Tables 5.1 and 5.2). It is important that the final polymerization of 3-BAPhA

goes to near-completion, otherwise the TBAM block would be impure, and 95% conv. was achieved. The RAFT of TBAM used a relatively high initiator concentration ( $[\text{MacroRAFT}]_0/[\text{VA-044}]_0 = 18$  at  $DP = 50$  to give 83% conv. for the final block.



**Scheme 5.6:** Preparation of poly(3-BAPhA)<sub>91</sub>-*b*-(TBAM)<sub>35</sub>-TTC in 20% aq. DMF at 70 °C by one-pot 2 h iterative RAFT polymerizations of 3-BAPhA and TBAM.



MWDs remained relatively narrow ( $\mathcal{D} = 1.17\text{-}1.25$ , Fig. 5.9), with a slight low MW tail apparent due to an accumulation of initiator derived dead chains ( $L = 88.2\%$  for the final polymer, Table 5.2).  $M_n$  increased linearly with conv. for the three 3-BAPhA polymerizations (Fig. 5.10), with the final  $M_n$  ( $= 29,600 \text{ gmol}^{-1}$ ) of poly(3-BAPhA)<sub>91</sub>-*b*-(TBAM)<sub>35</sub>-TTC remaining close to  $M_{n,\text{th}}$  ( $= 30,500 \text{ gmol}^{-1}$ ).

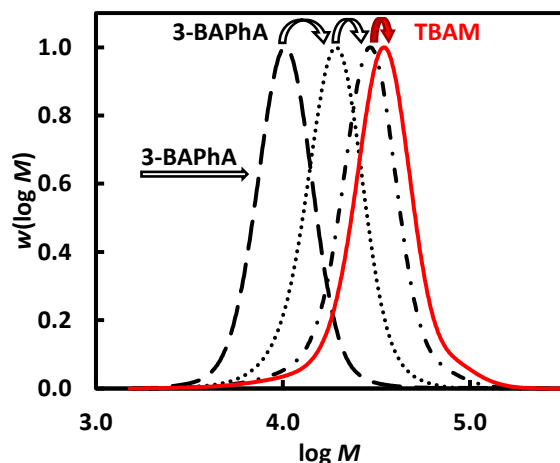


**Fig. 5.9.** MWD for the preparation of poly(3-BAPhA)<sub>91</sub>-*b*-(TBAM)<sub>35</sub>-TTC by one-pot iterative RAFT polymerizations of 3-BAPhA and TBAM.

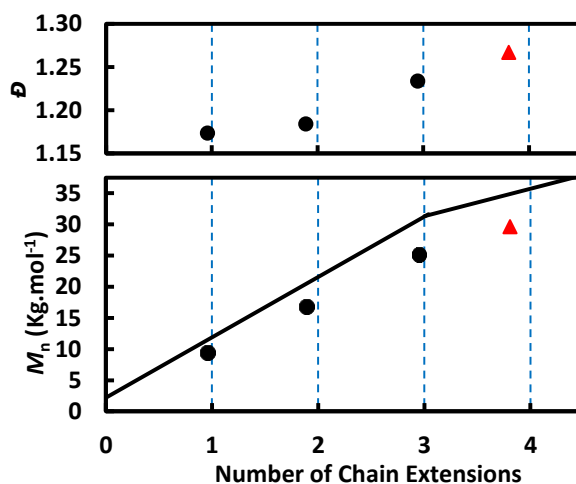


**Fig. 5.10:** Synthesis of poly(3-BAPhA)<sub>91</sub>-*b*-(TBAM)<sub>35</sub>-TTC by one-pot iterative RAFT polymerizations.  $M_n$  and  $\mathcal{D}$  versus number of chain extensions (dashed vertical lines at 100% conv.) with  $DP = 50$  for 3-BAPhA (black, circle) and TBAM (red, triangle), and  $M_{n,\text{th}}$  line calculated according to Eq (5.2)

The isolated block copolymer was isolated in 1.103 g (56%) yield. The isolated polymer has a relative monomer composition using  $^1\text{H}$  NMR spectrum of 73% (72% expected of) 3-BAPhA and 27% TBAM units, by comparing the polymer signal integrals at 6.87-8.02 (B(OH)<sub>2</sub> + Ar-H, 6H) ppm with 1.12-1.39 (Me, 9H) ppm, where the TBAM integral is divided by 1.5 (Fig. 5.11).

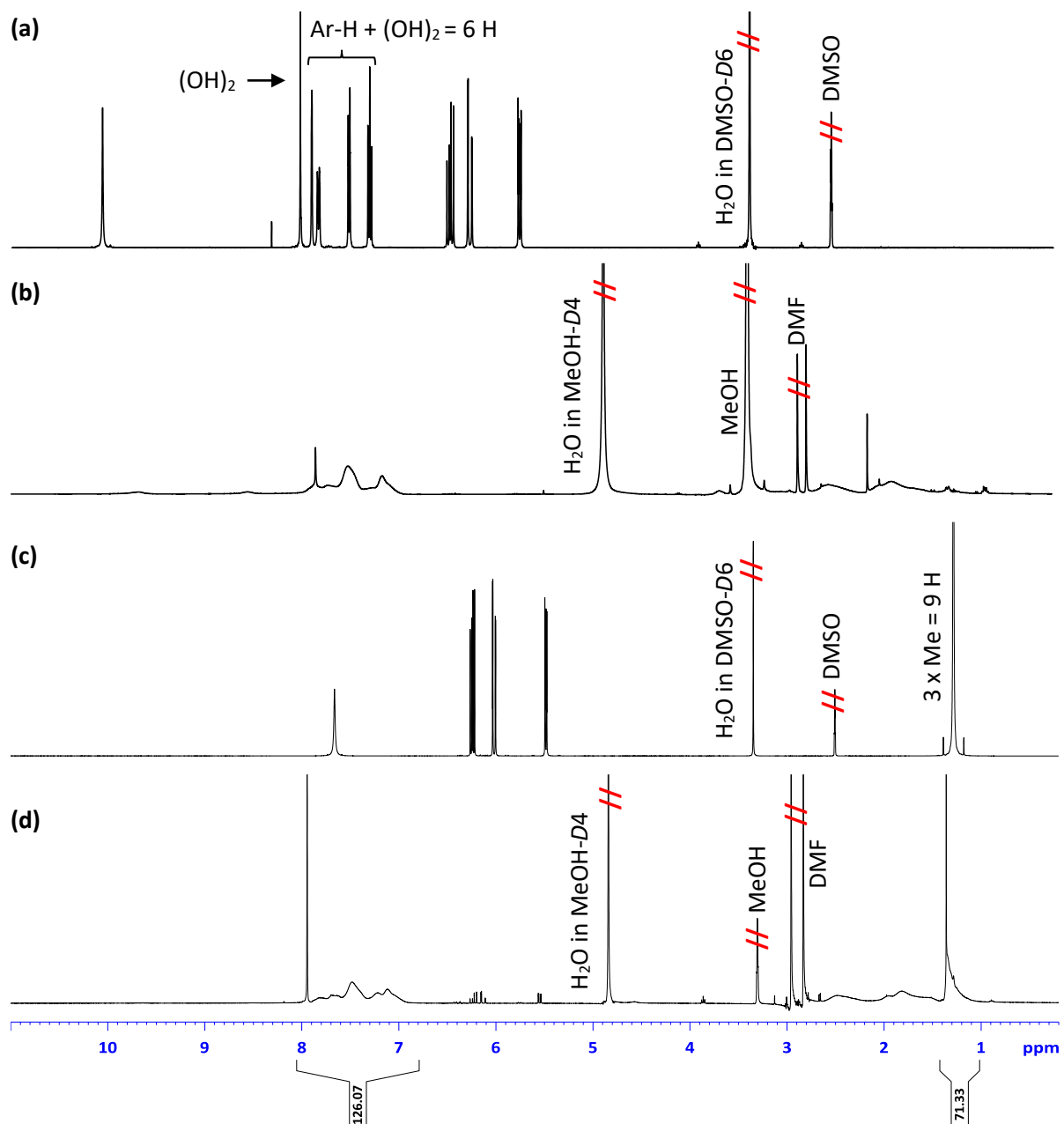
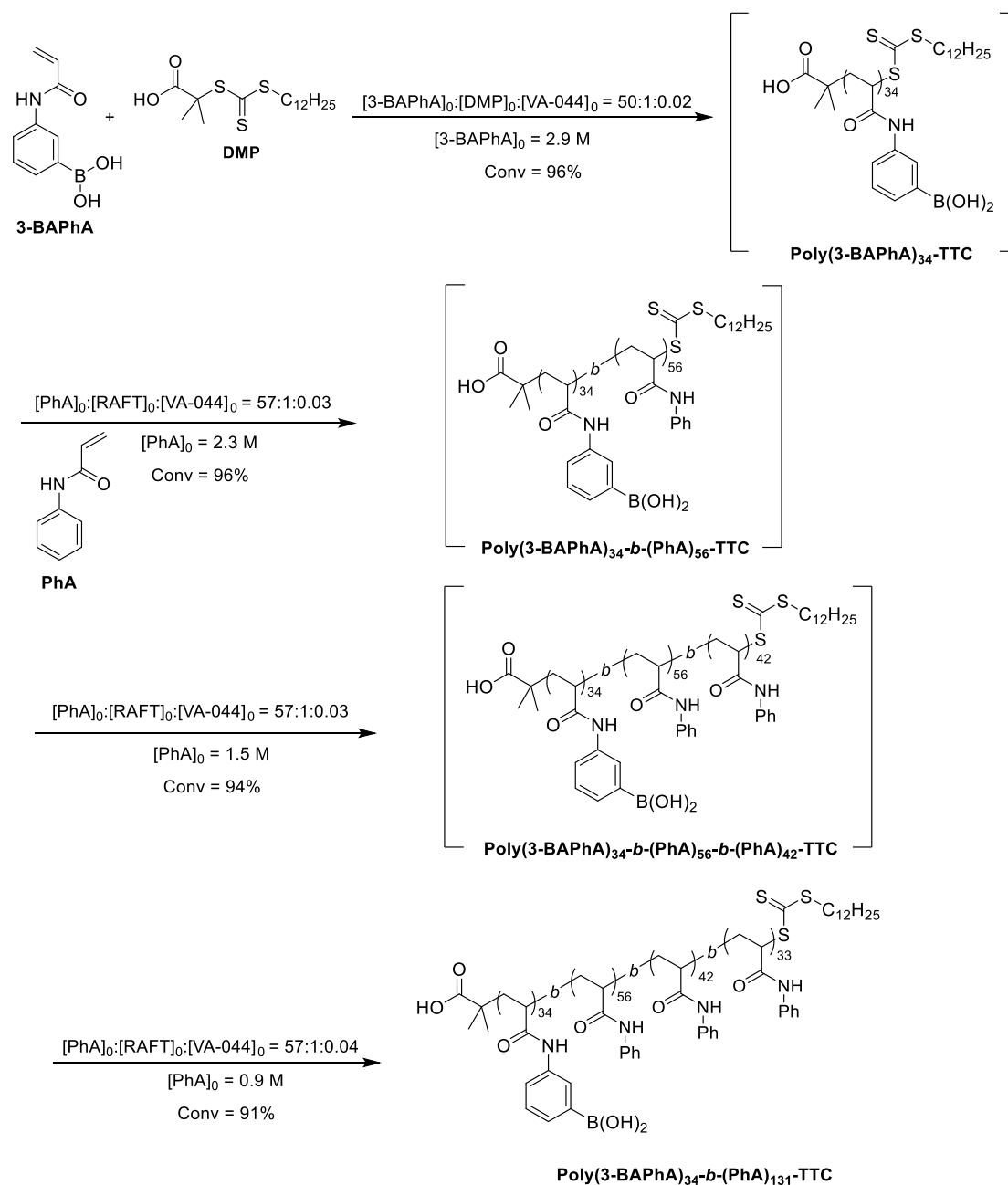


**Fig. 5.11:**  $^1\text{H}$  NMR spectra for the synthesis of block copolymer **(a)** 3-BAPhA in  $D_6$ -DMSO, **(b)** poly(3-BAPhA)<sub>124</sub>-TTC in  $D_4$ -MeOD, **(c)** TBAM in  $D_6$ -DMSO, and **(d)** poly(3-BAPhA)<sub>91</sub>-*b*-(TBAM)<sub>35</sub>-TTC in  $D_4$ -MeOD.

### 5.5.3.3 Preparation of poly(3-BAPhA)<sub>34</sub>-*b*-(PhA)<sub>131</sub>-TTC

A long hydrophobic block relative to hydrophilic (BA upon formation of the boronate ester) will allow high order morphologies upon self-assembly, thus the one-pot iterative approach was used to prepare poly(3-BAPhA)<sub>34</sub>-*b*-(PhA)<sub>131</sub>-TTC.



**Scheme 5.7:** Preparation of poly(3-BAPhA)<sub>34</sub>-*b*-(PhA)<sub>131</sub>-TTC in 20% aq. DMF at 70 °C by one-pot 2 h iterative RAFT polymerizations of 3-BAPhA and PhA.

The RAFT polymerization of 3-BAPhA at targeted  $DP = 50$ , was followed by three cycles of PhA at  $DP = 57$ . The MWDs remained narrow until the final cycle, where a low MW tail is apparent (Fig. 5.12), the  $M_n$  remained close to theoretical values for the polymerizations of PhA (Fig. 5.13). The final diblock copolymer was isolated with  $M_n (= 28,800 \text{ gmol}^{-1}, \mathcal{D} = 1.28)$ , in relatively good agreement with  $M_{n,\text{th}} (= 31,400 \text{ gmol}^{-1})$ .

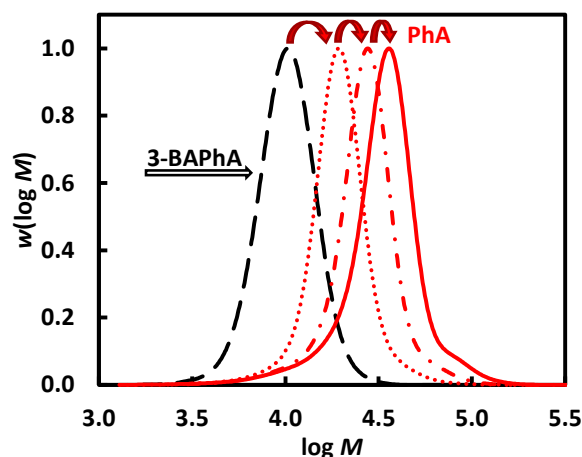


**Fig.5.12:** MWD of for the preparation of poly(3-BAPhA)<sub>34</sub>-*b*-(PhA)<sub>131</sub>-TTC by one-pot iterative RAFT polymerizations of 3-BAPhA and PhA.

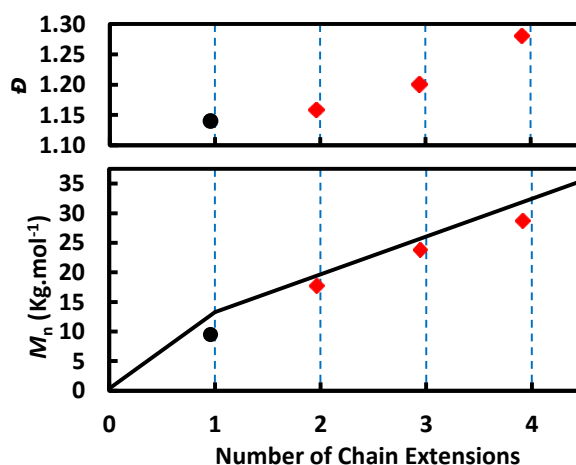


**Fig. 5.13:** Synthesis of poly(3-BAPhA)<sub>34</sub>-*b*-(PhA)<sub>131</sub>-TTC by one-pot iterative RAFT polymerizations of  $M_n$  and  $\mathcal{D}$  versus number of chain extensions (dashed vertical lines at 100% conv.).  $DP = 50$  and  $57$  for 3-BAPhA (black, circle) and PhA (red, diamonds) respectively, and  $M_{n,\text{th}}$  line calculated according to Eq. (5.2).

Poly(3-BAPhA)<sub>34</sub>-*b*-(PhA)<sub>131</sub>-TTC was isolated as 0.95 g (51% yield, based on 100% conv. for each cycle). The <sup>1</sup>H NMR spectrum of isolated poly(3-BAPhA)<sub>34</sub>-*b*-(PhA)<sub>131</sub>-TTC gave a relative composition of 18% (21% expected of) 3-BAPhA and 82% PhA units, by comparing the polymer signal integral at 7.88-8.19 for (B(OH)<sub>2</sub>, 2H), multiplied by 2.0 with the combined aromatic region for 3-BAPhA and PhA at 6.64-7.88 ppm, which contains 5H of PhA and 4H of 3-BAPhA (Fig. 5.14).

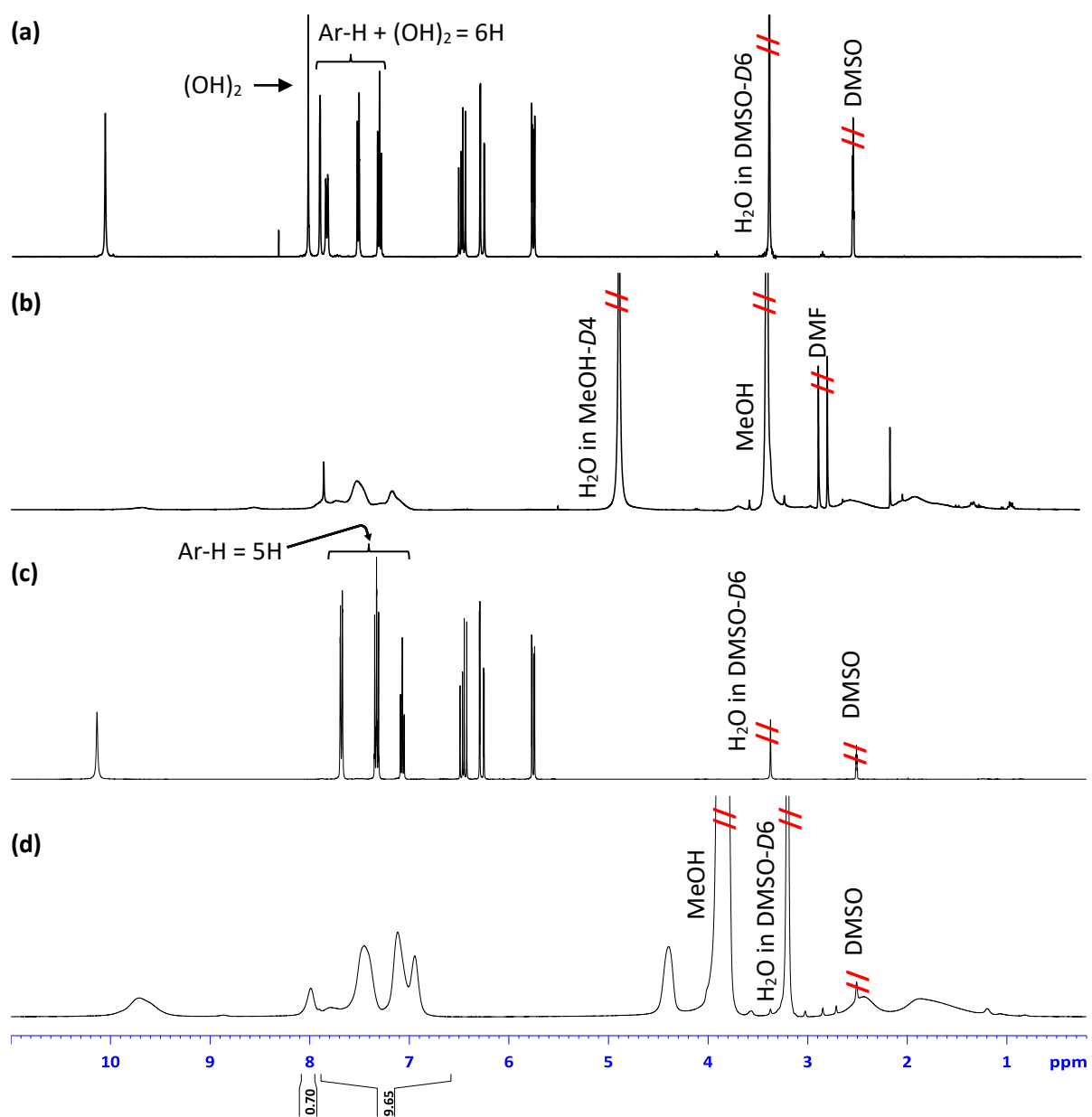


**Fig. 5.14:**  $^1H$  NMR spectra for the synthesis of block copolymer, **(a)** 3-BAPhA in  $D_6$ -DMSO, **(b)** poly(3-BAPhA)<sub>124</sub>-TTC in  $D_4$ -MeOD, **(c)** PhA in  $D_6$ -DMSO and **(d)** poly(3-BAPhA)<sub>34</sub>-*b*-(PhA)<sub>131</sub>-TTC in 1:3 MeOH: $D_6$ -DMSO.

## 5.6 Lactate and Glucose-Induced Self-Assembly

Low concentrations (aq. 5% w/w) of nanoparticles were generated through addition of lactate at pH 7.4 and base at pH 8.7 to the solvated polymers in 3/4 MeOH/DMF at room temp. After dialysis against pH 8.7 aq., glucose was added (see Experimental section). Upon lactate or glucose binding onto the poly(3-BAPhA), this block converts from hydrophobic to hydrophilic (becoming the stabilizer block) to give an amphiphilic core-shell polymer particle. The three hydrophobic polymers prepared provide different self-assembly opportunities due to differences in the relative lengths of the stabilizer block to the hydrophobic core-forming block.

### 5.6.1. Self-assembly of Poly(3-BAPhA)<sub>124</sub>-TTC

In the case of this homopolymer, self-assembly is expected upon boronate ester formation due to the presence of a relatively large hydrophobic RAFT end-group.<sup>41</sup> If all BA moieties convert to charged boronate esters then the corona (hydrophilic stabilizer block) would be much larger than the hydrophobic RAFT-end group at the core, such aggregates are referred to as “star-like”.<sup>106</sup> Dissolution is however possible based on observations in Chapter 4, when the hydrophilic block is relatively long compared to the hydrophobic block. Fig. 5.15 shows the generation of largely uniform spherical nanoparticles up to 50 nm in diameter upon treating poly(3-BAPhA)<sub>124</sub>-TTC with lactate at pH 7.4.



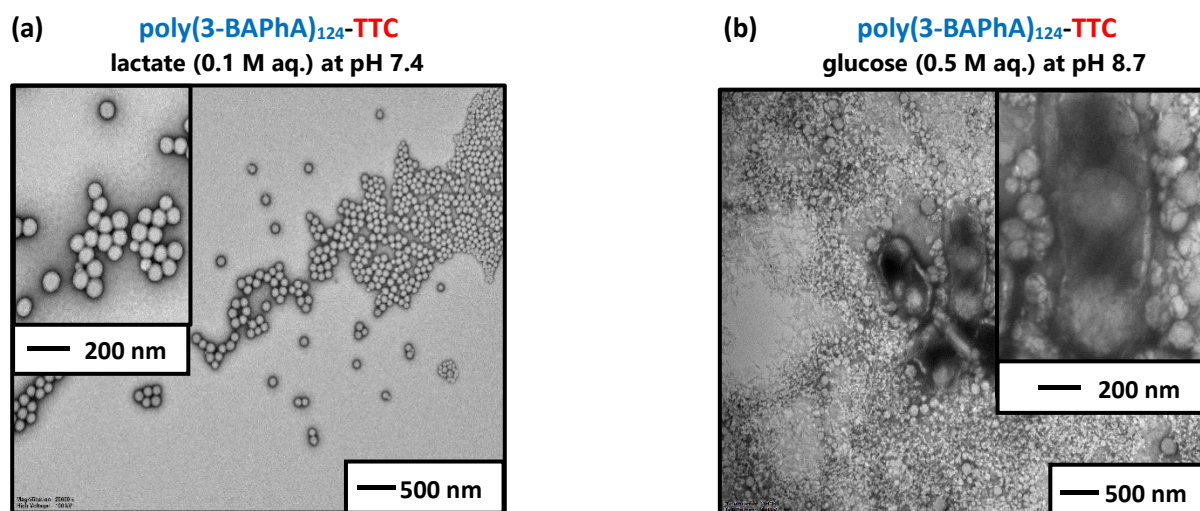


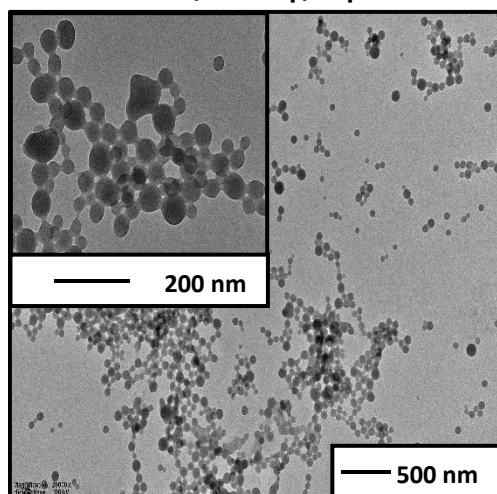
**Fig. 5.15.** TEM images of (a) lactate and (b) glucose-induced self-assembly (aq. 5% w/w).

Glucose induced-self-assembly led to the formation of spherical-like entities with patchy patterning on the surface, like the observation by Chalmers *et al.* for their diblock copolymer with the largest hydrophilic block.<sup>41</sup> Less well-defined spherical aggregates formed with base alone as a prelude to the patterned particles in Fig 5.15.

### 5.6.2. Self-assembly of Poly(3-BAPhA)<sub>91</sub>-*b*-(TBAM)<sub>35</sub>-TTC

For this diblock copolymer, BA ester formation would lead to self-assembly via hydrophobic and hydrophilic blocks of the AB copolymer of similar size. However, lactate and glucose induced very different morphologies, the former gave clusters of spherical nanoparticles of up to 50 nm in diameter, while the latter gave largely worm morphologies of about ~10 nm long with a minor phase of spherical particles of up to 30 nm in diameter. Less well-defined worms form with base alone.

(a) **poly(3-BAPhA)<sub>91</sub>-*b*-(TBAM)<sub>35</sub>-TTC**  
lactate (0.1 M aq.) at pH 7.4



(b) **poly(3-BAPhA)<sub>91</sub>-*b*-(TBAM)<sub>35</sub>-TTC**  
glucose (0.5 M aq.) at pH 8.7

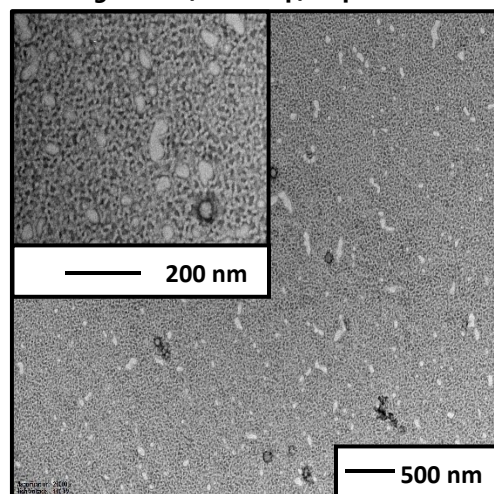


**Fig. 5.16.** TEM images of (a) lactate and (b) glucose-induced self-assembly (aq. 5% w/w).

### 5.6.3. Self-assembly of Poly(3-BAPhA)<sub>34</sub>-*b*-(PhA)<sub>131</sub>-TTC

“Crew-cut” aggregates occur when the hydrophobic blocks are much larger than the hydrophilic segment.<sup>106</sup> This can lead to a variety of morphologies, including higher order micelles related to the *DP* of the hydrophobic block (see Chapter 3).<sup>68</sup> Lactate binding onto poly(3-BAPhA)<sub>34</sub>-*b*-(PhA)<sub>131</sub>-TTC led to narrow long filaments/fibres (Fig. 5.17). Self-assembly was also observed by simply increasing pH, and the spherical/worm like morphologies did not change in appearance upon subsequent treatment with glucose, but slightly increased in size to about 20 nm in diameter.

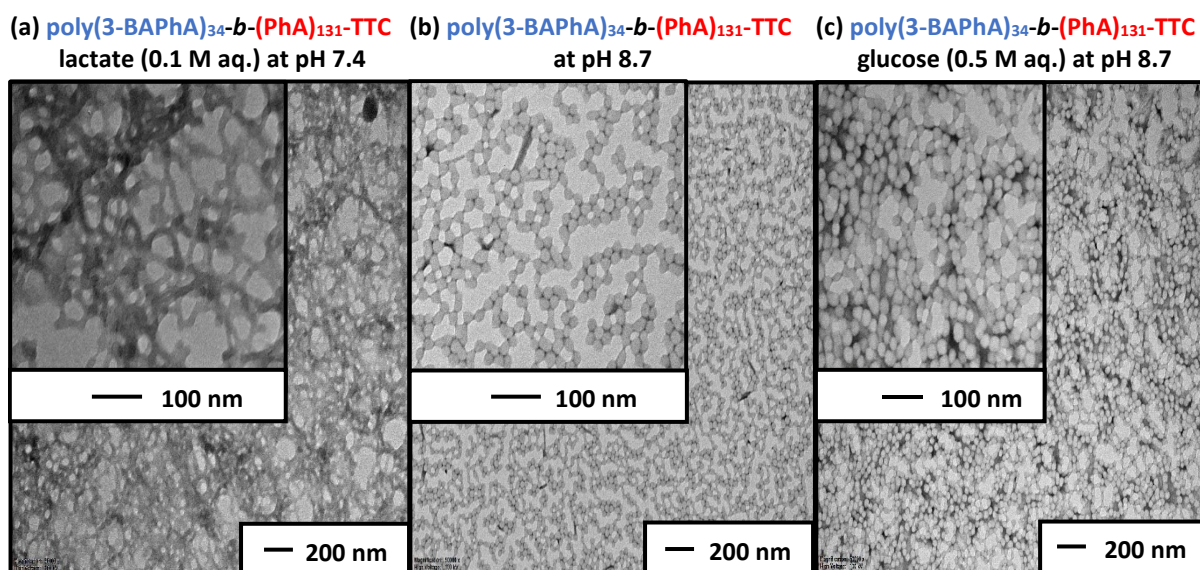


**Fig. 5.17.** TEM images of (a) lactate, (b) base and (c) glucose-induced self-assembly (aq. 5% w/w).

## 5.7. Conclusions

Lactate and glucose have been used for the first time to convert completely hydrophobic solvated polymers into self-assembled amphiphilic core-shell nanoparticles. A variety of morphologies are possible based upon the relative block size of the ionizable poly(3-BAPhA) to the other hydrophobic polymer component.

## 6.0 Overall Discussion/Conclusion and Future Work

At the start of this PhD, the polymerization induced self-assembly (PISA) of boronic acid (BA)-substituted monomers was unknown. PISA is important as it allows the preparation of high concentrations of nanoparticles, while also controlling microstructure via a controlled/living polymerization. During this PhD, there was two reports of PISA using pinacol ester protected BA-monomers.<sup>74,75</sup> In contrast, this PhD achieved the first successful PISA (dispersion polymerization) of a free BA monomer including higher order morphologies (worms and vesicles). These findings may have future applications in drug delivery, which traditionally uses spherical nanoparticles due to their straightforward synthesis, since morphology is known to play a crucial role in cellular uptake, with worms and rod-like structures more efficient in the delivery of therapeutics.<sup>107</sup> Due to boroxine formation upon particle nucleation in PISA, subsequent hydrolysis led to transitions to higher order morphology, thus new stimuli-response was also discovered.

This PhD is the first to demonstrate lactate response for core-shell nanoparticles, which is important given lactate is an essential anaerobic metabolite.<sup>53,54</sup> Response to glucose under basic conditions was shown to be comparable to lactate under physiologically neutral conditions for amphiphilic block copolymers. The binding to the BA-block by glucose and lactate allowed the first formation of nanoparticles from solvated hydrophobic polymers. These stimuli-responses due to the presence of BA-moieties also allowed access to higher order morphologies, such as worms and lamellae. It was expected that boronate ester formation would lead to a tendency towards spherical particles due to increased repulsive forces between charged chains, similar to PISA, where only spheres and not higher order morphologies (worms and vesicles) form when the charge density of the solvophilic block is high.<sup>102</sup> However, in contrast, this work has shown that increasing the volume fraction of the hydrophilic block of the amphiphilic block copolymers gives in most cases higher order morphologies, with worms predominating.

Future work could examine self-assembly using other chemically reactive entities towards BA (e.g. diols, other sugars or bases). The one-pot iterative RAFT polymerization approach

established in Chapters 4 and 5 could be used to prepare further core-shell nanoparticles, including hydrophobic triblocks, ABA' systems and longer hydrophobic to hydrophilic AB block copolymers, which are likely to give vesicles for biotechnology applications (e.g. in delivery of therapy in response to diabetes).

## 7.0 Thesis Reference

1. Zimmet, P. Z.; Magliano, D. J.; Herman, W. H.; Shaw, J. E. Diabetes: a 21st century challenge. *Lancet Diabetes Endocrinol.* **2014**, *2*, 56-64.  
[https://doi.org/10.1016/S2213-8587\(13\)70112-8](https://doi.org/10.1016/S2213-8587(13)70112-8)
1. Ward, W. C.; Lawrence, C. M. Ligand-induced activation of the insulin receptor: a multi-step process involving structural changes in both the ligand and the receptor. *BioEssays* **2009**, *31*(4), 422-434.  
<https://doi.org/10.1002/bies.200800210>
2. Sun, X.; James, T. D. Glucose sensing in supramolecular chemistry. *Chem. Rev.* **2015**, *115*, 8001-8037.  
<https://doi.org/10.1021/cr500562m>
3. Brooks, W. L. A.; Sumerlin, B. S. Synthesis and applications of boronic acid-containing polymers: from materials to medicine. *Chem. Rev.* **2016**, *116*, 1375-1397.  
<https://doi.org/10.1021/acs.chemrev.5b00300>
4. Roy, D.; Cambre, J. N.; Sumerlin, B. S. Sugar-responsive block copolymers by direct RAFT polymerization of unprotected boronic acid monomers. *Chem. Commun.* **2008**, 2477-2479.  
<https://doi.org/10.1039/B802293C>
5. Roy, D.; Cambre, J. N.; Sumerlin, B. S. Triply responsive boronic acid block copolymers: solution self-assembly induced by changes in temperature, pH, or sugar concentration. *Chem. Commun.* **2009**, 2106-2108.  
<https://doi.org/10.1039/B900374F>
6. Roy, D.; Sumerlin, B. S. Glucose-sensitivity of boronic acid block copolymers at physiological pH. *ACS Macro Lett.* **2012**, *1*, 529-532.  
<https://doi.org/10.1021/mz300047c>
7. Cambre, J. N.; Roy, D.; Sumerlin, B. S. Tuning the sugar-response of boronic acid block copolymers. *J. Polym. Sci. A: Polym. Chem.* **2012**, *50*, 3373-3382.  
<https://doi.org/10.1002/pola.26125>

8. Brooks, W.L.A.; Vancoillie, G.; Kabb, C.P.; Hoogenboom, R.; Sumerlin, B.S. Triple responsive block copolymers combining pH-responsive, thermoresponsive, and glucose-responsive behaviors. *J. Polym. Sci. Part A: Polym. Chem.* **2017**, *55*, 2309-2317.  
<https://doi.org/10.1002/pola.28615>
9. Kim, K. T.; Cornelissen, J. J. L. M.; Nolte, R. J. M.; Van Hest, J. C. M. Polymeric monosaccharide receptors responsive at neutral pH. *J. Am. Chem. Soc.* **2009**, *131*, 13908-13909.  
<https://doi.org/10.1021/ja905652w>
10. Zou, J.; Zhang, S.; Shrestha, R.; Seetho, K.; Donley, C. L.; Wooley, K. L. pH-Triggered reversible morphological inversion of orthogonally-addressable poly(3-acrylamidophenylboronic Acid)-*block*-poly(acrylamidoethylamine) micelles and their shell crosslinked nanoparticles. *Polym. Chem.* **2012**, *3*, 3146-3156.  
<https://doi.org/10.1039/C2PY20324C>
11. Guo, Q.; Zhang, T.; An, J.; Wu, Z.; Zhao, Y.; Dai, X.; Zhang, X.; Li, C. Block versus random amphiphilic glycopolymer nanoparticles as glucose-responsive vehicles. *Biomacromolecules* **2015**, *16*, 3345-3356.  
<https://doi.org/10.1021/acs.biomac.5b01020>
12. Cheng, C.; Zhang, X.; Wang, Y.; Sun, L.; Li, C. Phenylboronic acid-containing block copolymers: synthesis, self-assembly, and application for intracellular delivery of proteins. *New J. Chem.* **2012**, *36*, 1413-1421.  
<https://doi.org/10.1039/C2NJ20997G>
13. Sugnaux, C.; Klok, H. A. Glucose-sensitive QCM-sensors via direct surface RAFT polymerization. *Macromol. Rapid Commun.* **2014**, *35*, 1402-1407.  
<https://doi.org/10.1002/marc.201400217>
14. Yuan, W.; Shen, T.; Wang, J.; Zou, H. Formation–dissociation of glucose, pH and redox triply responsive micelles and controlled release of insulin. *Polym. Chem.* **2014**, *5*, 3968-3971.



<https://doi.org/10.1039/C4PY00463A>

15. Saleem, M.; Wang, L.; Yu, H.; Abdin, Z.; Akram, M.; Ullah, R.S. Synthesis of amphiphilic block copolymers containing ferrocene–boronic acid and their micellization, redox-responsive properties and glucose sensing. *Colloid Polym. Sci.* **2017**, 295, 995-1006.  
<https://doi.org/10.1007/s00396-017-4049-1>
16. Matsumoto, A.; Ikeda, S.; Harada, A.; Kataoka, K. Glucose-responsive polymer bearing a novel phenylborate derivative as a glucose-sensing moiety operating at physiological pH conditions. *Biomacromolecules* **2003**, 4, 1410-1416.  
<https://doi.org/10.1021/bm034139o>
17. Frohn, H. -J.; Adonin, N. Y.; Bardin, V. V.; Starichenko, V. F. Polyfluoroorganoboron-oxygen compounds. 2 [1] Base-catalysed hydrodeboration of polyfluorophenyl (dihydroxy) boranes. *Z. Anorg. Allg. Chem.* **2002**, 628, 2834-2838.  
[https://doi.org/10.1002/1521-3749\(200213\)628:13<2834::AID-ZAAC2834>3.0.CO;2-2](https://doi.org/10.1002/1521-3749(200213)628:13<2834::AID-ZAAC2834>3.0.CO;2-2)
18. Springsteen, G.; Wang, B. A detailed examination of boronic acid–diol complexation. *Tetrahedron* **2002**, 58, 5291-5300.  
[https://doi.org/10.1016/S0040-4020\(02\)00489-1](https://doi.org/10.1016/S0040-4020(02)00489-1)
19. Berson, J. A. What Is a Discovery? Carbon skeletal rearrangements as counter-examples to the rule of minimal structural change. *Angew. Chem. Int. Ed.* **2002**, 41, 4655-4660.  
<https://doi.org/10.1002/anie.200290007>
20. Fittig, R. ueber einige producte der trockenen destillation essigsaurer salze. *Justus Liebigs Ann. Chem.* **1859**, 110, 17-23.  
<https://doi.org/10.1002/jlac.18591100103>
21. Schmidt, P.; Stress, C.; Gillingham, D. Boronic acids facilitate rapid oxime condensations at neutral pH. *Chem. Sci.* **2015**, 6, 3329-3333.  
<https://doi.org/10.1039/C5SC00921A>



22. D'Hooge, F.; Rogalle, D.; Thatcher, M.J.; Perera, S.P.; van den Elsen, J. M. H.; Jenkins, A.T.A.; James, T.D.; Fossey, J.S. Polymerisation resistant synthesis of methacrylamido phenylboronic acids. *Polym.* **2008**, *49*, 3362-3365.  
<https://doi.org/10.1016/j.polymer.2008.05.039>
23. Wurster, B.; Hess, B. The reaction of hexokinase with equilibrated D-glucose. *Eur. J. Biochem.* **1973**, *36*, 68-71.  
<https://doi.org/10.1111/j.1432-1033.1973.tb02885.x>
24. Geacintov, C.; Smid, J.; Szwarc, M. Kinetics of anionic polymerization of styrene in tetrahydrofuran. *J. Am. Chem. Soc.* **1962**, *84*, 2508-2514.  
<https://pubs.acs.org/doi/pdf/10.1021/ja00872a012>
25. Laita, Z.; Szwarc, M. Mixed dimerization of living polymers having Li counterions. Kinetics of the addition of 1, 1-diphenylethylene to living lithium polystyrene in benzene. *Macromolecules* **1969**, *2*, 412-413.  
<https://pubs.acs.org/doi/pdf/10.1021/ma60010a017>
26. Fischer, H. The persistent radical effect: a principle for selective radical reactions and living radical polymerizations. *Chem. Rev.* **2001**, *101*, 3581-3610.  
<https://doi.org/10.1021/cr990124y>
27. Nicolas, J.; Guillaneuf, Y.; Lefay, C.; Bertin, D.; Gigmès, D.; Charleux, B. Nitroxide-mediated polymerization. *Prog. Polym. Sci.* **2013**, *38*, 63-235.  
<https://doi.org/10.1016/j.progpolymsci.2012.06.002>
28. Georges, M. K.; Veregin, R. P. N.; Kazmaier, P. M.; Hamer, G. K.; Saban, M. Narrow polydispersity polystyrene by a free-radical polymerization process-rate enhancement. *Macromolecules* **1994**, *27*, 7228-7229.  
<https://pubs.acs.org/doi/pdf/10.1021/ma00102a039>
29. Benoit, D.; Chaplinski, V.; Braslau, R.; Hawker, C. J. Development of a universal alkoxyamine for "living" free radical polymerizations. *J. Am. Chem. Soc.* **1999**, *121*, 3904-3920.  
<https://doi.org/10.1021/ja984013c>

30. Benoit, D.; Grimaldi, S.; Robin, S.; Finet, J.; Tordo, P.; Gnanou, Y. Kinetics and mechanism of controlled free-radical polymerization of styrene and *n*-butyl acrylate in the presence of an acyclic  $\beta$ -phosphonylated nitroxide. *J. Am. Chem. Soc.* **2000**, *122*, 5929-5939.  
<https://doi.org/10.1021/ja991735a>
31. Karky, K.; Billon, L.; Pouchan, C.; Desbrières, J. Amphiphilic gradient copolymers shape composition influence on the surface/bulk properties. *Macromolecules* **2007**, *40*, 458-464.  
<https://doi.org/10.1021/ma062456s>
32. Mchale, R.; Aldabbagh, F.; Zetterlund, P. B. The role of excess nitroxide in the SG1 (*N*-*tert*-butyl-*N*-[1-diethylphosphono-(2, 2-dimethylpropyl)] nitroxide)-mediated polymerization of methyl methacrylate. *J. Polym. Sci., Part A: Polym. Chem.* **2007**, *45*, 2194-2203.  
<https://doi.org/10.1002/pola.21986>
33. Mchale, R.; Aldabbagh, F.; Carroll, W. M.; Yamada, B. Polymerization of *N*-isopropylacrylamide in the presence of poly(acrylic acid) and poly(methacrylic acid) containing  $\omega$ -unsaturated end-groups. *J. Polym. Sci., Part A: Polym. Chem.* **2007**, *45*, 4394-4400.  
<https://doi.org/10.1002/pola.22232>
34. Wang, J.; Matyjaszewski, K. Controlled/" living" radical polymerization. atom transfer radical polymerization in the presence of transition-metal complexes. *J. Am. Chem. Soc.* **1995**, *117*, 5614-5615.  
<https://doi.org/10.1021/ja00125a035>
35. Kato, M.; Kamigaito, M.; Sawamoto, M.; Higashimura, T. Polymerization of methyl methacrylate with the carbon tetrachloride/dichlorotris-(triphenylphosphine) ruthenium (II)/methylaluminum bis(2, 6-di-*tert*-butylphenoxide) initiating system: possibility of living radical polymerization. *Macromolecules* **1995**, *28*, 1721-1723.  
<https://doi.org/10.1021/ma00109a056>
36. Alzahrani, A.; Zhou, D.; Kuchel, R. P.; Zetterlund, P. B.; Aldabbagh, F. Polymerization-induced self-assembly based on ATRP in supercritical carbon dioxide. *Polym. Chem.* **2019**, *10*, 2658-2665.

<https://doi.org/10.1039/C9PY00498J>

37. Perrier, S. 50th Anniversary Perspective: RAFT Polymerization. A User Guide. *Macromolecules* **2017**, *50*, 7433-7447.  
<https://doi.org/10.1021/acs.macromol.7b00767>
38. Chiefari, J.; Chong, Y. K.; Ercole, F.; Krstina, J.; Jerry, J.; Le, T. P. T.; Mayadunne, R. T. A.; Meijs, G. F.; Moad, C. L.; Moad, G.; Rizzardo, E.; Thang, S. H. Living free-radical polymerization by reversible addition– fragmentation chain transfer: the RAFT process. *Macromolecules* **1998**, *31*, 5559-5562.  
<https://doi.org/10.1021/ma9804951>
39. Moad, G. RAFT polymerization to form stimuli-responsive polymers. *Polym. Chem.* **2017**, *8*, 177-219.  
<https://doi.org/10.1039/C6PY01849A>
40. Chalmers, B. A.; Magee, C.; Cheung, D. L.; Zetterlund, P. B.; Aldabbagh, F. CO<sub>2</sub>-responsive polyacrylamide copolymer vesicles with acid-sensitive morpholine moieties and large hydrophobic RAFT end-group. *Eur. Polym. J.* **2017**, *97*, 129-137.  
<https://doi.org/10.1016/j.eurpolymj.2017.10.004>
41. Moad, G.; Rizzardo, E.; Thang, S. H. Living radical polymerization by the RAFT process. *Aust. J. Chem.* **2005**, *58*, 379-410.  
<https://doi.org/10.1071/CH05072>
42. Gody, G.; Maschmeyer, T.; Zetterlund, P. B.; Perrier, S. Pushing the limit of the RAFT process: multiblock copolymers by one-pot rapid multiple chain extensions at full monomer conversion. *Macromolecules* **2014**, *47*, 3451-3460.  
<https://doi.org/10.1021/ma402435n>
43. Gody, G.; Maschmeyer, T.; Zetterlund, P. B.; Perrier, S. Exploitation of the degenerative transfer mechanism in RAFT polymerization for synthesis of polymer of high livingness at full monomer conversion. *Macromolecules* **2014**, *47*, 639-649.  
<https://doi.org/10.1021/ma402286e>
44. Li, K.; Stöver, H. D. H. Synthesis of monodisperse poly (divinylbenzene) microspheres. *J. Polym. Sci., Part A: Polym. Chem.* **1993**, *31*, 3257-3263.  
<https://doi.org/10.1002/pola.1993.080311313>

45. Chalmers, B. A.; Alzahrani, A.; Hawkins, G.; Aldabbagh, F. Efficient synthesis and RAFT polymerization of the previously elusive *N*-[(cycloalkylamino) methyl] acrylamide monomer class. *J. Polym. Sci., Part A: Polym. Chem.* **2017**, *55*, 2123-2128.  
<https://doi.org/10.1002/pola.28607>
46. Cambre, J. N.; Roy, D.; Gondi, S. R.; Sumerlin, B. S. Facile strategy to well-defined water-soluble boronic acid (co) polymers. *J. Am. Chem. Soc.* **2007**, *129*, 10348-10349.  
<https://doi.org/10.1021/ja074239s>
47. Bapat, A. P.; Roy, D.; Ray, J. G.; Savin, D. A.; Sumerlin, B. S. Dynamic-covalent macromolecular stars with boronic ester linkages. *J. Am. Chem. Soc.* **2011**, *133*, 19832-19838.  
<https://doi.org/10.1021/ja207005z>
48. Chen, Q.; Hill, M. R.; Brooks, W. L.; Zhu, A.; Sumerlin, B. S.; An, Z. Boronic acid linear homopolymers as effective emulsifiers and gelators. *ACS Appl. Mater. Interfaces* **2015**, *7*, 21668-21672.  
<https://doi.org/10.1021/acsami.5b07456>
49. Crespy, D.; Rossi, R. M. Temperature-responsive polymers with LCST in the physiological range and their applications in textiles. *Polym. Int.* **2007**, *56*, 1461-1468.  
<https://doi.org/10.1002/pi.2277>
50. De, P.; Gondi, S. R.; Roy, D.; Sumerlin, B. S. Boronic acid-terminated polymers: synthesis by RAFT and subsequent supramolecular and dynamic covalent self-assembly. *Macromolecules* **2009**, *42*, 5614-5621.  
<https://doi.org/10.1021/ma900835y>
51. Prossnitz, A. N.; Pun, S. H. Modulating boronic ester stability in block copolymer micelles via the neighbor effect of copolymerized tertiary amines for controlled release of polyphenolic drugs. *ACS Macro Lett.* **2022**, *11*, 276-283.  
<https://doi.org/10.1021/acsmacrolett.1c00751>
52. Adeva-Andany, M.; López-Ojén, M.; Funcasta-Calderón, R.; Ameneiros-Rodríguez, E.; Donapetry-García, C.; Vila-Altesor, M.; Rodríguez-Seijas, J. Comprehensive review on lactate metabolism in human health. *Mitochondrion* **2014**, *17*, 76-100.  
<https://doi.org/10.1016/j.mito.2014.05.007>

53. Adeva, M.; González-Lucán, M.; Seco, M.; Donapetry, C. Enzymes involved in L-lactate metabolism in humans. *Mitochondrion* **2013**, *13*, 615-629.  
<https://doi.org/10.1016/j.mito.2013.08.011>
54. Sartain, F. K.; Yang, X.; Lowe, C. R. Holographic lactate sensor. *Anal. Chem.* **2006**, *78*, 5664-5670.  
<https://doi.org/10.1021/ac060416g>
55. Sartain, F. K.; Yang, X.; Lowe, C. R. Complexation of L-lactate with boronic acids: a solution and holographic analysis. *Chem. Eur. J.* **2008**, *14*, 4060-4067.  
<https://doi.org/10.1002/chem.200701911>
56. Pizer, R. D.; Tihal, C. A. Mechanism of boron acid/polyol complex formation. Comments on the trigonal/tetrahedral interconversion on boron. *Polyhedron* **1996**, *15*, 3411-3416.  
[https://doi.org/10.1016/0277-5387\(96\)00042-3](https://doi.org/10.1016/0277-5387(96)00042-3)
57. Deng, C. C.; Brooks, W. L.; Abboud, K. A.; Sumerlin, B. S. Boronic acid-based hydrogels undergo self-healing at neutral and acidic pH. *ACS Macro Lett.* **2015**, *4*, 220-224.  
<https://doi.org/10.1021/acsmacrolett.5b00018>
58. Abel, B. A.; McCormick, C. L. Mechanistic insights into temperature-dependent trithiocarbonate chain-end degradation during the RAFT polymerization of *N*-arylmethacrylamides. *Macromolecules* **2016**, *49*, 465-474.  
<https://doi.org/10.1021/acs.macromol.5b02463>
59. Villemin, D.; Thibault-Starzyk, F. Domestic microwave ovens in the laboratory. *J. Chem. Educ.* **1991**, *68*, 346.  
<https://pubs.acs.org/doi/pdf/10.1021/ed068p346>
60. De Geest, B.G.; Jonas, A.M.; Demeester, J.; De Smedt, S.C. Glucose-responsive polyelectrolyte capsules. *Langmuir* **2006**, *22*, 5070-5074.  
<https://doi.org/10.1021/la053368o>
61. Smith, T. A. D.; Trembleau, L. A. C.; McLaughlin, A. C.; Simpson, M. Materials and methods for medical imaging. WO2009056837. May 7, 2009.

62. Gody, G.; Maschmeyer, T.; Zetterlund, P. B.; Perrier, S. Rapid and quantitative one-pot synthesis of sequence-controlled polymers by radical polymerization. *Nat. Commun.* **2013**, *4*, 1-9.  
<https://doi.org/10.1038/ncomms3505>
63. Keddie, D. J. A guide to the synthesis of block copolymers using reversible-addition fragmentation chain transfer (RAFT) polymerization. *Chem. Soc. Rev.* **2014**, *43*, 496-505.  
<https://doi.org/10.1039/C3CS60290G>
64. Thickett, S. C.; Teo, G. H. Recent advances in colloidal nanocomposite design via heterogeneous polymerization techniques. *Polym. Chem.* **2019**, *10*, 2906-2924.  
<https://doi.org/10.1039/C9PY00097F>
65. Qiu, J.; Charleux, B.; Matyjaszewski, K. Controlled/living radical polymerization in aqueous media: homogeneous and heterogeneous systems. *Prog. Polym. Sci.* **2001**, *26*, 2083-2134.  
[https://doi.org/10.1016/S0079-6700\(01\)00033-8](https://doi.org/10.1016/S0079-6700(01)00033-8)
66. Qiao, X. G.; Lansalot, M.; Bourgeat-Lami, E.; Charleux, B. Nitroxide-mediated polymerization-induced self-assembly of poly(poly(ethylene oxide) methyl ether methacrylate-co-styrene)-*b*-poly(*n*-butyl methacrylate-co-styrene) Amphiphilic Block Copolymers. *Macromolecules* **2013**, *46*, 4285-4295.  
<https://doi.org/10.1021/ma4003159>
67. Dhiraj, H. S.; Ishizuka, F.; ElShaer, A.; Zetterlund, P. B.; Aldabbagh, F. RAFT dispersion polymerization induced self-assembly (PISA) of boronic acid-substituted acrylamides. *Polym. Chem.* **2022**, *13*, 3750-3755.  
<https://doi.org/10.1039/D2PY00530A>
68. O'Connor, P.; Zetterlund, P. B.; Aldabbagh, F. Effect of monomer loading and pressure on particle formation in nitroxide-mediated precipitation polymerization in supercritical carbon dioxide. *Macromolecules* **2010**, *43*, 914-919.  
<https://doi.org/10.1021/ma9022179>
69. Blanazs, A.; Armes, S. P.; Ryan, A. J. Self-assembled block copolymer aggregates: from micelles to vesicles and their biological applications. *Macromol. Rapid Commun.* **2009**, *30*, 267-277.

<https://doi.org/10.1002/marc.200800713>

70. Byard, S. J.; Williams, M.; McKenzie, B. E.; Blanz, A.; Armes, S. P. Preparation and cross-linking of all-acrylamide diblock copolymer nano-objects via polymerization-induced self-assembly in aqueous solution. *Macromolecules* **2017**, *50*, 1482-1493.

<https://doi.org/10.1021/acs.macromol.6b02643>

71. Zhang, L.; Eisenberg, A. Multiple morphologies of "crew-cut" aggregates of polystyrene-*b*-poly (acrylic acid) block copolymers. *Science* **1995**, *268*, 1728-1731.

<https://doi.org/10.1126/science.268.5218.1728>

72. Huang, L. S.; Le, D.; Hsiao, I.; Fritsch-Decker, S.; Hald, C.; Huang, S.; Chen, J.; Hwu, J. R.; Weiss, C.; Hsu, M.; Delaitre, G. Boron-rich, cytocompatible block copolymer nanoparticles by polymerization-induced self-assembly. *Polym. Chem.* **2021**, *12*, 50-56.

<https://doi.org/10.1039/D0PY00710B>

73. Pitto-Barry, A. Polymers and boron neutron capture therapy (BNCT): a potent combination. *Polym. Chem.* **2021**, *12*, 2035-2044.

<https://doi.org/10.1039/D0PY01392G>

74. Fan, B.; Wan, J.; Zhai, J.; Chen, X.; Thang, S. H. Triggered degradable colloidal particles with ordered inverse bicontinuous cubic and hexagonal mesophases. *ACS nano* **2021**, *15*, 4688-4698.

<https://doi.org/10.1021/acsnano.0c09166>

75. Ree, L.; Kelland, M. A.; Haddleton, D.; Alsubaie, F. Comparison of the kinetic hydrate inhibition performance of block and statistical *N*-acrylamide copolymers. *Energy Fuels* **2017**, *31*, 1355-1361.

<https://doi.org/10.1021/acs.energyfuels.6b02785>

76. Zetterlund, P. B.; Kagawa, Y.; Okubo, M. Controlled/living radical polymerization in dispersed systems. *Chem. Rev.* **2008**, *108*, 3747-3794.

<https://doi.org/10.1021/cr800242x>

77. Blanz, A.; Madsen, J.; Battaglia, G.; Ryan, A. J.; Armes, S. P. Mechanistic insights for block copolymer morphologies: how do worms form vesicles? *J. Am. Chem. Soc.* **2011**, *133*, 16581-16587.

<https://doi.org/10.1021/ja206301a>

78. Korich, A. L.; Iovine, P. M. Boroxine chemistry and applications: A perspective. *Dalton Transactions* 2010, 39, 1423-1431.  
<https://doi.org/10.1039/B917043J>
79. Li, S.; Lv, X.; Sun, X.; Wan, W.; Bao, H. Well-controlled polymerization of tri-vinyl dynamic covalent boroxine monomer: One dynamic covalent boroxine moiety toward a tunable penta-responsive polymer. *Polym. Chem.* **2020**, *11*, 2914-2922.  
<https://doi.org/10.1039/D0PY00401D>
80. Fielding, L. A.; Lane, J. A.; Derry, M. J.; Mykhaylyk, O. O.; Armes, S. P. Thermo-responsive diblock copolymer worm gels in non-polar solvents. *J. Am. Chem. Soc.* **2014**, *136*, 5790-5798.  
<https://doi.org/10.1021/ja501756h>
81. Warren, N. J.; Armes, S. P. Polymerization-induced self-assembly of block copolymer nano-objects via RAFT aqueous dispersion polymerization. *J. Am. Chem. Soc.* **2014**, *136*, 10174-10185.  
<https://doi.org/10.1021/ja502843f>
82. He, W.; Sun, X.; Wan, W.; Pan, C. Multiple morphologies of PAA-*b*-PSt assemblies throughout RAFT dispersion polymerization of styrene with PAA macro-CTA. *Macromolecules* **2011**, *44*, 3358-3365.  
<https://doi.org/10.1021/ma2000674>
83. Banach, Ł; Williams, G. T.; Fossey, J. S. Insulin delivery using dynamic covalent boronic acid/ester-controlled release. *Adv. Therap.* **2021**, *4*, 2100118.  
<https://doi.org/10.1002/adtp.202100118>
84. Yu, J.; Wang, J.; Zhang, Y.; Chen, G.; Mao, W.; Ye, Y.; Kahkoska, A. R.; Buse, J. B.; Langer, R.; Gu, Z. Glucose-responsive insulin patch for the regulation of blood glucose in mice and minipigs. *Nat. Biomed. Eng.* **2020**, *4*, 499-506.  
<https://doi.org/10.1038/s41551-019-0508-y>
85. Yang, H.; Zhang, C.; Li, C.; Liu, Y.; An, Y.; Ma, R.; Shi, L. Glucose-responsive polymer vesicles templated by  $\alpha$ -CD/PEG inclusion complex. *Biomacromolecules* **2015**, *16*, 1372-1381.  
<https://doi.org/10.1021/acs.biomac.5b00155>



86. Zhao, L.; Ding, J.; Xiao, C.; He, P.; Tang, Z.; Pang, X.; Zhuang, X.; Chen, X. Glucose-sensitive polypeptide micelles for self-regulated insulin release at physiological pH. *J. of Mater. Chem.* **2012**, *22*, 12319-12328.  
<https://doi.org/10.1039/C2JM31040F>
87. Jiang, G.; Jiang, T.; Chen, H.; Li, L.; Liu, Y.; Zhou, H.; Feng, Y.; Zhou, J. Preparation of multi-responsive micelles for controlled release of insulin. *Colloid Polym. Sci.* **2015**, *293*, 209-215.  
<https://doi.org/10.1007/s00396-014-3394-6>
88. Gaballa, H.; Theato, P. Glucose-responsive polymeric micelles via boronic acid–diol complexation for insulin delivery at neutral pH. *Biomacromolecules* **2019**, *20*, 871-881.  
<https://doi.org/10.1021/acs.biomac.8b01508>
89. Kim, W. J.; Kwon, Y.; Cho, C.; Ye, S.; Kim, K. O. Insulin smart drug delivery nanoparticles of aminophenylboronic acid–POSS molecule at neutral pH. *Sci. Rep.* **2021**, *11*, 1-13.  
<https://doi.org/10.1038/s41598-021-01216-3>
90. Shiomori, K.; Ivanov, A. E.; Galaev, I. Y.; Kawano, Y.; Mattiasson, B. Thermoresponsive properties of sugar sensitive copolymer of *N*-Isopropylacrylamide and 3-(acrylamido) phenylboronic acid. *Macromol. Chem. Phys.* **2004**, *205*, 27-34.  
<https://doi.org/10.1002/macp.200300019>
91. Edwards, J. O.; Sederstrom, R. J. The thermodynamics of ionization of benzeneboronic acid. *J. Phys. Chem.* **1961**, *65*, 862-863.  
<https://doi.org/10.1021/j100823a035>
92. Giménez-Gómez, P.; Gutiérrez-Capitán, M.; Capdevila, F.; Puig-Pujol, A.; Fernández-Sánchez, C.; Jiménez-Jorquera, C. Monitoring of malolactic fermentation in wine using an electrochemical bienzymatic biosensor for *l*-lactate with long term stability. *Anal. Chim. Acta* **2016**, *905*, 126-133.  
<https://doi.org/10.1016/j.aca.2015.11.032>
93. Nakamura, H.; Murakami, Y.; Yokoyama, K.; Tamiya, E.; Karube, I.; Suda, M.; Uchiyama, S. A compactly integrated flow cell with a chemiluminescent FIA system for determining lactate concentration in serum. *Anal. Chem.* **2001**, *73*, 373-378.  
<https://doi.org/10.1021/ac000855u>

94. Spehar-Délèze, A.; Anastasova, S.; Vadgama, P. Monitoring of lactate in interstitial fluid, saliva and sweat by electrochemical biosensor: the uncertainties of biological interpretation. *Chemosensors* **2021**, *9*, 195.  
<https://doi.org/10.3390/chemosensors9080195>
95. Li, T.; Liu, J.; Sun, X.; Wan, W.; Xiao, L.; Qian, Q. Boronic acid-containing polymeric nanomaterials via polymerization induced self-assembly as fructose sensor. *Polymer* **2022**, 125005.  
<https://doi.org/10.1016/j.polymer.2022.125005>
96. Dixon, K. W.; Decomposition rates of organic free radical initiators, In: J. Brandrup, E.H. Immergut, E.A. Grulke (Eds.), *Polymer Handbook* (4th ed.). Wiley, New York 1999, p. 1–76.
97. Clothier, G. K.; Guimarães, T. R.; Moad, G.; Zetterlund, P. B. Multiblock copolymer synthesis via reversible addition–fragmentation chain transfer emulsion polymerization: effects of chain mobility within particles on control over molecular weight distribution. *Macromolecules* **2021**, *54*, 3647–3658.  
<https://doi.org/10.1021/acs.macromol.1c00345>
98. Rieger, J.; Gazon, C.; Charleux, B.; Alaimo, D.; Jérôme, C. Pegylated thermally responsive block copolymer micelles and nanogels via in situ RAFT aqueous dispersion polymerization. *J. Polym. Sci. Part A: Polym. Chem.* **2009**, *47*, 2373–2390.  
<https://doi.org/10.1002/pola.23329>
99. Du, J.; Willcock, H.; Patterson, J. P.; Portman, I.; O'Reilly, R. K. Self-assembly of hydrophilic homopolymers: a matter of RAFT end groups. *Small* **2011**, *7*, 2070–2080.  
<https://doi.org/10.1002/sml.201100382>
100. Bosch, L. I.; Fyles, T. M.; James, T. D. Binary and ternary phenylboronic acid complexes with saccharides and Lewis bases. *Tetrahedron* **2004**, *60*, 11175–11190.  
<https://doi.org/10.1016/j.tet.2004.08.046>
101. Zhou, D.; Dong, S.; Kuchel, R. P.; Perrier, S.; Zetterlund, P. B. Polymerization induced self-assembly: tuning of morphology using ionic strength and pH. *Polym. Chem.* **2017**, *8*, 3082–3089.  
<https://doi.org/10.1039/C7PY00552K>

102. Zhang, J.; Tanaka, J.; Gurnani, P.; Wilson, P.; Hartlieb, M.; Perrier, S. Self-assembly and disassembly of stimuli responsive tadpole-like single chain nanoparticles using a switchable hydrophilic/hydrophobic boronic acid cross-linker. *Polym. Chem.* **2017**, *8*, 4079-4087.  
<https://doi.org/10.1039/C7PY00828G>
103. Deng, R.; Derry, M. J.; Mable, C. J.; Ning, Y.; Armes, S. P. Using dynamic covalent chemistry to drive morphological transitions: controlled release of encapsulated nanoparticles from block copolymer vesicles. *J. Am. Chem. Soc.* **2017**, *139*, 7616-7623.  
<https://doi.org/10.1021/jacs.7b02642>
104. Tatry, M.; Qiu, Y.; Lapeyre, V.; Garrigue, P.; Schmitt, V.; Ravaine, V. Sugar-responsive Pickering emulsions mediated by switching hydrophobicity in microgels. *J. Colloid Interface Sci.* **2020**, *561*, 481-493.  
<https://doi.org/10.1016/j.jcis.2019.11.023>
105. Mai, Y.; Eisenberg, A. Self-Assembly of Block Copolymers. *Chem. Soc. Rev.* **2012**, *41*, 5969-5985.  
<https://doi.org/10.1039/C2CS35115C>
106. Karagoz, B.; Esser, L.; Duong, H. T.; Basuki, J. S.; Boyer, C.; Davis, T. P. Polymerization-Induced Self-Assembly (PISA) – control over the morphology of nanoparticles for drug delivery applications. *Polym. Chem.* **2014**, *5*, 350-355.  
<https://doi.org/10.1039/C3PY01306E>

# Appendix



Cite this: *Polym. Chem.*, 2022, **13**, 3750

Received 25th April 2022,  
Accepted 6th June 2022

DOI: 10.1039/d2py00530a

rsc.li/polymers

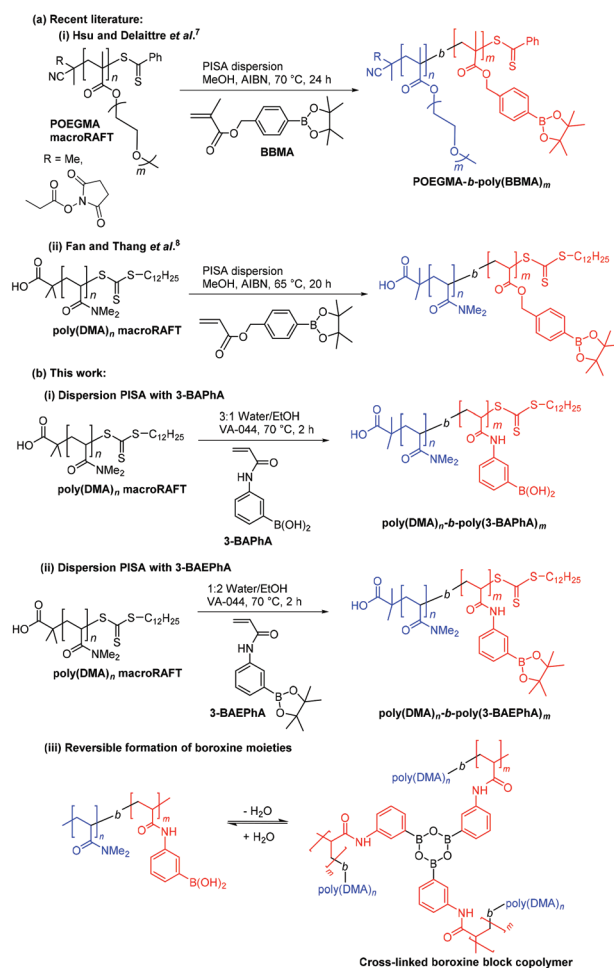
## RAFT dispersion polymerization induced self-assembly (PISA) of boronic acid-substituted acrylamides†

Harpal S. Dhiraj,<sup>a</sup> Fumi Ishizuka,<sup>b</sup> Amr Elshaer,<sup>a</sup> Per B. Zetterlund<sup>\*b</sup> and Fawaz Aldabbagh<sup>\*a</sup>

Reversible addition–fragmentation chain transfer (RAFT)-mediated dispersion polymerization induced self-assembly (PISA) of boronic acid (BA)-substituted acrylamides is established. The first PISA on unprotected BA-substituted monomer yields spherical nanoparticles (NPs) that undergo room-temperature transitions to higher order morphologies upon dilution with the dispersion solvent. PISA with the BA pinacol ester-derivative yields spherical NPs, worms, and vesicles.

Boronic acid (BA) is a Lewis acid moiety utilized in analytical and biomedical applications, most notably sugar sensing.<sup>1,2</sup> Polymerization induced self-assembly (PISA) allows direct access to high concentrations of block copolymer core–shell nanoparticles (NPs) without polymer processing.<sup>3–6</sup> The most widely used reversible deactivation radical polymerization (RDRP) or controlled/living technique for PISA is reversible addition–fragmentation chain transfer (RAFT) polymerization.<sup>6</sup> For PISA of BA-substituted monomers, only a pinacol ester-protected BA acrylate and methacrylate are reported (Scheme 1(a)(i and ii)).<sup>7,8</sup> RAFT-mediated PISA of 4-pinacolboronylbenzyl methacrylate (BBMA) was implemented as an emulsion polymerization in water/EtOH and dispersion polymerization in methanol (MeOH).<sup>7</sup> The dispersion polymerization involved chain extension of poly(oligo(ethylene glycol) methacrylate) (POEGMA) macroRAFT agents with BBMA to give sub-100 nm spheres at high conversion. Hsu and Delaittre *et al.* proposed applications in boron-neutron capture therapy<sup>9</sup> for BA pinacol-ester derivative NPs.<sup>7</sup> Fan and Thang *et al.* reported the dispersion polymerization of the acrylate analogue also in

MeOH, using poly(DMA, *N,N*-dimethylacrylamide) macroRAFT agents as the steric stabilizer block.<sup>8</sup> In this case, a range of higher order polymer objects were achieved, including with



**Scheme 1** PISA of BA, BA-pinacol ester protected monomers and equilibrium for boroxine formation.

<sup>a</sup>Department of Pharmacy, School of Life Sciences, Pharmacy and Chemistry, Kingston University, Penrhyn Road, Kingston upon Thames, KT1 2EE, UK. E-mail: f.aldabbagh@kingston.ac.uk

<sup>b</sup>Cluster for Advanced Macromolecular Design (CAMD), School of Chemical Engineering, The University of New South Wales, Sydney, NSW 2052, Australia. E-mail: p.zetterlund@unsw.edu.au

† Electronic supplementary information (ESI) available: Experimental section, additional figs, including TEMs and NMR spectra. See DOI: <https://doi.org/10.1039/d2py00530a>



cubic and hexagonal mesophases, and oxidative removal of the BA group led to disassembly.

Sumerlin *et al.* pioneered controlled/living homogeneous polymerizations of BA-substituted phenylacrylamides (PhAs).<sup>2,10–12</sup> Polymerization of (3-acrylamidophenyl)boronic acid (3-BAPhA) in DMF-5% water at 70 °C used 2-(dodecylthiocarbonothioylthio)-2-methylpropionic acid (DMP) and 2,2'-azobisisobutyronitrile (AIBN) as the RAFT agent and azo initiator, respectively.<sup>10</sup> The polymerizations displayed controlled/living characteristics with  $M_n$  of 37 800 g mol<sup>-1</sup> and  $\bar{D}$  of 1.16 at [3-BAPhA]<sub>0</sub>/[DMP]<sub>0</sub> = 200. The polymerization of BA-substituted monomers can however be challenging due to dehydration giving boroxine cross-linked chains.<sup>13,14</sup> There is also the requirement for pinacol protection of the BA moieties prior to GPC analysis.<sup>10,11,13</sup> This led to RAFT-mediated polymerization using the pinacol ester protected (3-acrylamidophenyl)boronic acid (3-BAEPhA) monomer in DMF at 70 °C.<sup>12</sup> Control was demonstrated by linear increases in  $M_n$  up to 68–74% conversion in accordance with reaction stoichiometry for [3-BAEPhA]<sub>0</sub>/[DMP]<sub>0</sub> = 100 and [3-BAEPhA]<sub>0</sub>/[DMP]<sub>0</sub> = 200. Chain extension with hydrophilic DMA or *N*-isopropylacrylamide (NIPAM) gave sugar and thermally-responsive block copolymer micelles after dialysis of the block copolymer solutions with water.<sup>10–12</sup> This traditional block copolymer self-assembly method is however time-consuming and results in low concentrations of NPs (<1% wt/vol%).<sup>15</sup> Dialysis involves the reduction in the solvency of the hydrophobic poly(3-BAPhA) block by slow exchange of the organic solvent with water.

In the present study, we use dispersion polymerizations of 3-BAPhA or 3-BAEPhA monomer (20 wt/vol%) from hydrophilic poly(DMA) macroRAFT agents to establish high concentrations of BA-functionalized amphiphilic (all) polyacrylamide core-shell NPs (Scheme 1(b)(i and ii)). We have thus carried out the first PISA on an unprotected BA-substituted monomer, and PISA with the pinacol ester derivative allowed the attainment of higher order macro-objects.

The water-soluble azo initiator 2,2'-azobis[2-(2-imidazolyl)propane]dihydrochloride (VA-044) was chosen due to its high decomposition rate coefficient ( $k_d$ ) allowing completion of each polymerization in 2 h at 70 °C while maximizing livingness.<sup>16</sup> Solution homopolymerizations using VA-044 and the RAFT agent DMP and the monomers DMA and 3-BAPhA gave solvophilic poly(DMA) macroRAFT agents,<sup>17</sup> (for subsequent chain extensions) and poly(3-BAPhA) for solubility studies (see ESI†), respectively. 3-BAPhA and the derived homopolymer are soluble in hot water, but to meet the requirements for dispersion polymerization, the polymer needs to be insoluble. This was achieved through the addition of ethanol with 3 : 1 water/EtOH, providing soluble monomer and insoluble poly(3-BAPhA) at 70 °C.

Initial studies involved optimizing the initiator concentration ([VA-044]<sub>0</sub>) for the 2 h dispersion polymerization of 3-BAPhA (20 wt/vol%) using poly(DMA)<sub>28</sub> as macroRAFT agent at 70 °C. Three different initiator concentrations at [poly(DMA)<sub>28</sub>]<sub>0</sub>/[VA-044]<sub>0</sub> = 70, 57 and 45 were investigated, at a targeted degree of polymerization of [3-BAPhA]<sub>0</sub>/[poly(DMA)<sub>28</sub>]<sub>0</sub> =

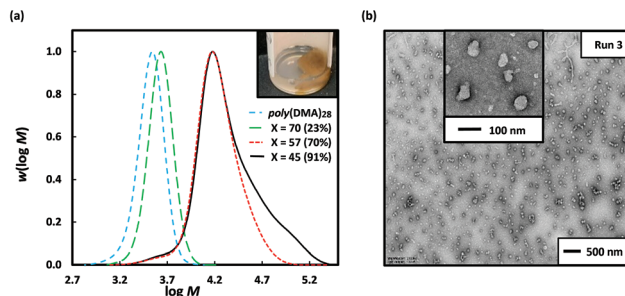


**Fig. 1** Varying the initiator concentration [VA-044]<sub>0</sub> for the 2 h RAFT dispersion polymerization of 3-BAPhA (20 wt/vol%) in 3 : 1 water/EtOH at 70 °C using [3-BAPhA]<sub>0</sub>/[poly(DMA)<sub>28</sub>]<sub>0</sub> = 50, with [poly(DMA)<sub>28</sub>]<sub>0</sub>/[VA-044]<sub>0</sub> = X (Run 1–3). (a) MWDs after pinacol protection (with conv.) and visual appearance of polymerization for X = 45; (b) TEM images for PISA at X = 45 (additional images in Fig. S1†).

50 (Fig. 1). For the lowest [VA-044]<sub>0</sub>, the solution remained transparent and conversion was low (23%, Run 1; Table 1), with the low rate of polymerization ( $R_p$ ) attributed to the absence of particle nucleation. After nucleation, monomer swell the formed micelles, leading to a relatively high local monomer concentration, and thus rate enhancement.<sup>18,19</sup>

Considerably higher conversion (70%) was obtained for [poly(DMA)<sub>28</sub>]<sub>0</sub>/[VA-044]<sub>0</sub> = 57, with relatively good control/livingness ( $M_n$  = 14 600 g mol<sup>-1</sup>;  $M_{n,th}$  = 12 700 g mol<sup>-1</sup>;  $\bar{D}$  = 1.35) (Run 2, Table 1). Note that the GPC data are recorded after the pinacol-protection of BA moieties to give poly(3-BAEPhA) and is subject to calibration error against linear polystyrene standards. Near-complete conversion (91%, Run 3) was obtained at the highest VA-044 concentration, but with a broad molecular weight distribution (MWD,  $\bar{D}$  = 1.80), with  $M_n$  (19 500 g mol<sup>-1</sup>) higher than  $M_{n,th}$  (15 700 g mol<sup>-1</sup>). The two polymerizations of 3-BAPhA at high conversions led to significant agglomeration, which visibly increases upon cooling. This brown coagulum is assumed to be boroxine, which is the anhydride of BA formed in the solid state,<sup>20</sup> and is in equilibrium in solution (Scheme 1(b)(iii)).<sup>14</sup> Boroxine is favored at the locus of polymerization (within the monomer-rich particles), where the concentration of water is low, in contrast to the dispersion medium. Part of the highest conversion sample (Run 3) could however be re-suspended on shaking, with TEM analysis indicating irregularly shaped near-spherical sub-100 nm solid particles (Fig. 1).

Attempts to circumvent the formation of coagulum by carrying out the dispersion polymerization of 3-BAPhA using poly(DMA)<sub>28</sub> macroRAFT at lower monomer loadings resulted in low  $R_p$ , agglomeration and inferior control/living character. The use of a longer hydrophilic macroRAFT agent was investigated – this would lead to a significant delay in the on-set of particle nucleation, but the longer stabiliser block may improve colloidal stability. Thus dispersion polymerization of 3-BAPhA (20 wt/vol%) was carried out using poly(DMA)<sub>96</sub> macroRAFT agent (as opposed to poly(DMA)<sub>28</sub>); a free-flowing colloidal dispersion formed, as indicated by a cloudy-white





**Table 1** Experimental results for dispersion PISA of 3-BAPhA and 3-BAEPPhA using poly(DMA) macroRAFT agents (Scheme 1b(i and ii))

Run <sup>a</sup>	[M] <sub>0</sub> /[poly(DMA)] <sub>0</sub>	Polymer <sup>b</sup>	Conv. <sup>c</sup> (%)	M <sub>n,th</sub> <sup>d</sup>	M <sub>n</sub> <sup>e</sup>	D	Vis. <sup>g</sup>	TEM <sup>h</sup>
1	50	Poly(DMA) <sub>28</sub> - <i>b</i> -poly(3-BAPhA) <sub>12</sub>	23	6400	4000 <sup>f</sup>	1.10 <sup>f</sup>	sol	—
2	50	Poly(DMA) <sub>28</sub> - <i>b</i> -poly(3-BAPhA) <sub>35</sub>	70	12 700	14 600 <sup>f</sup>	1.35 <sup>f</sup>	cg	—
3	50	Poly(DMA) <sub>28</sub> - <i>b</i> -poly(3-BAPhA) <sub>46</sub>	91	15 700	19 500 <sup>f</sup>	1.80 <sup>f</sup>	cg&dis	s
4	50	Poly(DMA) <sub>96</sub> - <i>b</i> -poly(3-BAPhA) <sub>50</sub>	99	23 600	24 500 <sup>f</sup>	1.27 <sup>f</sup>	cg&dis	s
5	50	Poly(DMA) <sub>96</sub> - <i>b</i> -poly(3-BAEPPhA) <sub>50</sub>	99	23 600	20 700	1.57	gel	w
6	150	Poly(DMA) <sub>96</sub> - <i>b</i> -poly(3-BAEPPhA) <sub>149</sub>	99	50 600	39 000	1.76	gel	s
7	200	Poly(DMA) <sub>96</sub> - <i>b</i> -poly(3-BAEPPhA) <sub>198</sub>	99	64 000	44 500	1.76	gel	s
8	50	Poly(DMA) <sub>36</sub> - <i>b</i> -poly(3-BAEPPhA) <sub>50</sub>	99	17 600	23 600	1.15	gel	s
9	100	Poly(DMA) <sub>36</sub> - <i>b</i> -poly(3-BAEPPhA) <sub>99</sub>	99	30 900	30 500	1.28	dis	v
10	150	Poly(DMA) <sub>36</sub> - <i>b</i> -poly(3-BAEPPhA) <sub>149</sub>	99	44 600	43 100	1.38	dis	v
11	200	Poly(DMA) <sub>36</sub> - <i>b</i> -poly(3-BAEPPhA) <sub>198</sub>	99	58 000	40 800	1.63	dis	v

<sup>a</sup> See Fig. 1–4 for dispersion polymerization conditions and conversions. <sup>b</sup> DP of the stabilizer block is calculated from M<sub>n</sub>(GPC) poly(DMA)<sub>28</sub> (3100 g mol<sup>-1</sup>, D = 1.12), poly(DMA)<sub>96</sub> (9900 g mol<sup>-1</sup>, D = 1.17) and poly(DMA)<sub>36</sub> (3900 g mol<sup>-1</sup>, D = 1.10), and the DP of the poly(3-BAPhA) and poly(3-BAEPPhA) block is based on conversion. <sup>c</sup> Measured by <sup>1</sup>H NMR, see ESI†. <sup>d</sup> Theoretical (M<sub>n,th</sub>) is calculated from poly(3-BAEPPhA) DP added to the poly(DMA) M<sub>n</sub>(GPC). <sup>e</sup> g mol<sup>-1</sup> and determined by GPC/RI in DMF (0.01 M LiBr). <sup>f</sup> GPC for the polymerization of 3-BAPhA is after pinacol protection to poly(3-BAEPPhA) (see ESI†). <sup>g</sup> Visual appearance, where sol, cg, and dis are solution, coagulum, and dispersion respectively. <sup>h</sup> Major morphology, where s, w, and v are spheres, worms, and vesicles respectively.

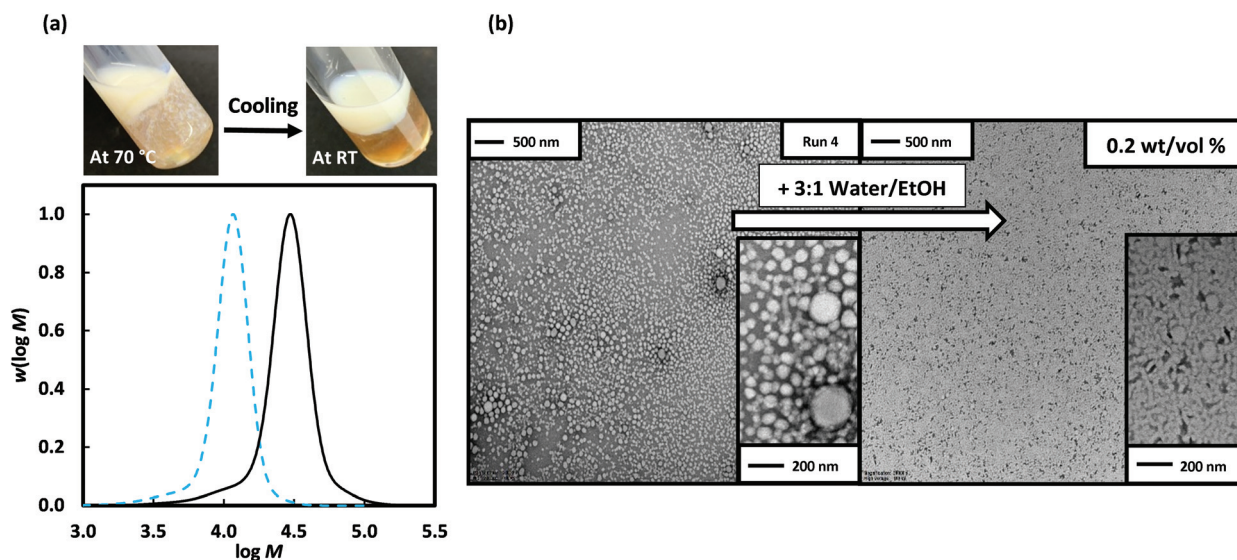


**Fig. 2** Poly(DMA)<sub>96</sub> as macroRAFT agent (dashed blue line) in the 2 h dispersion polymerizations of 3-BAPhA (20 wt/vol%; full black line) in 3:1 water/EtOH at 70 °C, where [poly(DMA)<sub>96</sub>]<sub>0</sub>/[VA-044]<sub>0</sub> = 40, and targeted degree of polymerization, DP = 50 (Run 4). (a) Visual appearance of polymerization (with white stirrer bar within) before and after cooling to RT, and MWD (99% conv.) after pinacol protection; (b) TEM images for PISA after separation of the cooled cloudy dispersion (upper layer) and room temp (RT) dilution 100-fold with 3:1 water/EtOH (same as polymerization medium, TEM after 24 h) (additional images in Fig. S3 and S4,† respectively).

layer, which separated from the lower brown agglomeration upon cooling (Fig. 2). The polymerization reached completion (99% conv., Run 4), with excellent control/living character demonstrated by M<sub>n</sub> (24 500 g mol<sup>-1</sup>) in close agreement with M<sub>n,th</sub> (23 600 g mol<sup>-1</sup>), and a narrow MWD (D = 1.27) (Table 1). The MWD of the upper colloidal layer was superimposable with that of the lower brown coagulum (Fig. S2†), indicating that boroxine formation had not affected control/livingness. TEM analysis of the white dispersion layer showed mainly small spherical NPs (Fig. 2(b)), but with some short rods, and large well-defined up to 200 nm spherical particles. Given the distinct possibility of boroxine moieties (Scheme 1(b)(iii)), col-

loidal stability was evaluated through 100-fold dilution with the dispersion solvent (3:1 water/EtOH) at room temp. After 24 h, TEM analysis for the dilution showed the primary morphology was short rods and worms with some similar sized 50–100 nm diameters spheres remaining (Fig. 2). A lesser (20-fold) dilution of the upper layer with the dispersion solvent (at room temp.), after 24 h, gave a greater abundance of spheres compared to rods, reflecting less boroxine hydrolysis (Fig. S5†). A decrease in polymer concentration would normally reduce the likelihood of transitions to higher order morphologies, since the number of polymer aggregates and thus collisions is less.<sup>21</sup> However, in this case, increased hydrolysis



of boroxine at the core shifts the equilibrium from crosslinked polymer to linear poly(BA) chains, so affecting the interfacial energy and consequently self-assembly. This change in hydrophilic–hydrophobic block and polymer–solvent interactions is presumed to cause the observed sphere-to-rod (worm) transition.

To circumvent boroxine, pinacol-protected BA (3-BAEPHA) was investigated. Homogeneous (solution) RAFT-mediated polymerizations of 3-BAPhA and 3-BAEPHA (1 M) using AIBN and DMP at 70 °C proceeded with almost identical  $R_p$  and similar control/living character indicated by overlapping points on the conversion *vs.* time and  $M_n$  *versus* conversion plots (Fig. S6†). However, the 3-BAPhA polymerization MWDs were consistently broader ( $D = 1.48$ – $1.61$ ) than for the pinacol derivative ( $D = 1.31$ – $1.45$ ), possibly due to the presence of boroxine despite 5% water in DMF (polymerization solvent). Given the similarities in monomer performance in solution, the same conditions were employed for the dispersion polymerization of 3-BAEPHA (20 wt/vol%) as for 3-BAPhA (above), although the medium was different (1 : 2 water/EtOH as opposed to 3 : 1 water/EtOH). The greater proportion of ethanol allowed solvation of the more hydrophobic monomer 3-BAEPHA, while maintaining insolubility of the derived polymer. Since heterogeneous polymerizations of BBMA over longer polymerization times have been reported to give a slight coagulum,<sup>7</sup> the short polymerization time of 2 h was

expected to minimise pinacol group hydrolysis and boroxine formation. Using the longer steric stabiliser poly(DMA)<sub>96</sub> macroRAFT agent with 3-BAEPHA (20 wt/vol%) for targeted degree of polymerizations (DPs) = 50, 150 and 200 (Fig. 3) resulted in shifts in  $M_n$  to higher MWs of ( $M_n$ ) 20 700, 39 000, and 44 500 g mol<sup>-1</sup> respectively, at near-full (99%) conversion (Run 5–7, Table 1). The low MW tail contributes to the high  $D = 1.57$ – $1.76$ , and is consistent with the carryover of dead chains from the preparation of the poly(DMA)<sub>96</sub> ( $M_n = 9900$  g mol<sup>-1</sup>,  $D = 1.17$ ) by chain extension of poly(DMA)<sub>39</sub> ( $M_n = 4200$  g mol<sup>-1</sup>,  $D = 1.10$ ) (Fig. S10,† thus poly(DMA)<sub>96</sub> is equiv. to poly(DMA)<sub>39</sub>-*b*-poly(DMA)<sub>57</sub>). Note attempted preparation of this longer stabilizer block in a single RAFT polymerization of DMA at 70 °C with  $[DMA]_0/[DMP]_0 = 100$ , resulted in lower conversion (72%) and thus shorter stabilizer, poly(DMA)<sub>65</sub> ( $M_n = 6800$  g mol<sup>-1</sup>,  $D = 1.15$ ) (Fig. S11†). However, dead chains (in Fig. 3(a)) are also due to the increasing  $[VA-044]_0$  used with higher targeted DP. The appearance of the resulting polymerization mixtures was gel-like, but importantly with no brown coagulum (Fig. 3). The lowest DP sample gave the only non-cloudy gel, with viscosity appearing to decrease with increasing DP. In PISA, the formation of worm-like micelles is often the cause of increases in viscosity due to worm entanglement.<sup>22</sup> Long worms of up to 1 μm in length are evident at the lowest targeted DP along with interconnected spherical particles (Run 5). Support for the decrease in

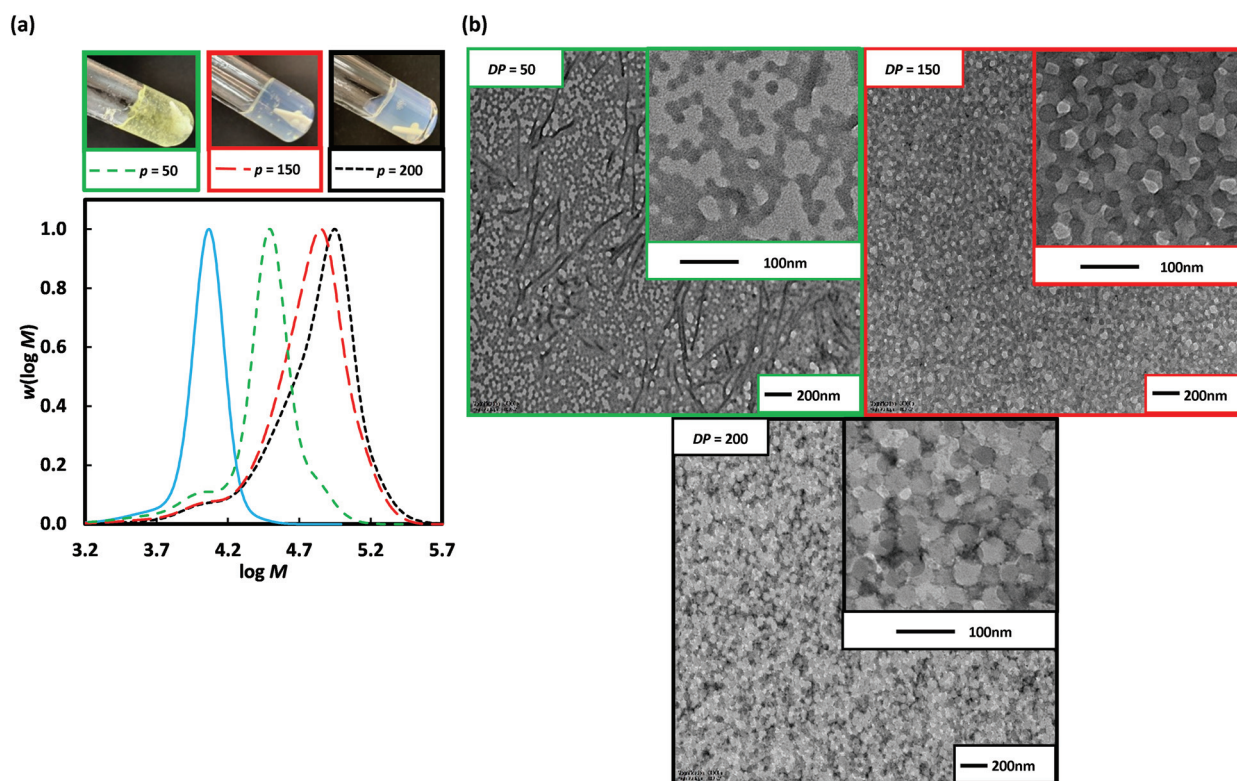


**Fig. 3** Poly(DMA)<sub>96</sub> as macroRAFT agent (solid blue line) in the 2 h dispersion polymerizations of 3-BAEPHA (20 wt/vol%) in 1 : 2 water/EtOH at 70 °C, where  $[poly(DMA)_{96}]_0/[VA-044]_0 = 50, 20, 14$  for targeted degree of polymerization, DP = 50 (Run 5), 150 (Run 6) and 200 (Run 7) respectively. (a) Visual appearance of polymerizations (with white stirrer bar within) and MWDs (99% conv.); (b) TEM images for PISA (additional images in Fig. S7–S9,† respectively).





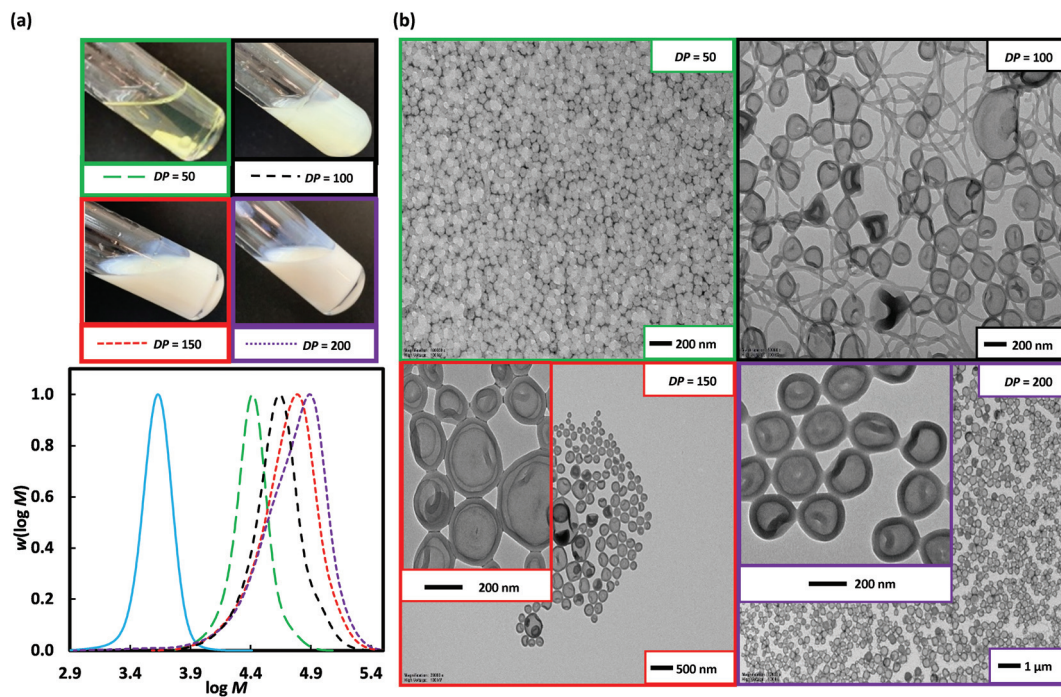


**Fig. 4** Poly(DMA)<sub>36</sub> as macroRAFT agent (solid blue line) in the 2 h dispersion polymerizations of 3-BAEPHA (20 wt/vol%) in 1 : 2 water/EtOH at 70 °C, where [poly(DMA)<sub>36</sub>]<sub>0</sub>/[VA-044]<sub>0</sub> = 50, 25, 17 and 12 for targeted degree of polymerization, DP = 50 (Run 8), 100 (Run 9), 150 (Run 10) and 200 (Run 11) respectively. (a) Visual appearance of polymerizations (with white stirrer bar within) and MWDs (99% conv.); (b) TEM images for PISA (additional images in Fig. S12–S15,† respectively).

viscosity is the replacement of the worm-like micelle phase at the lowest DP with about 20 nm solid NPs at DP = 150 (Run 6) and 200 (Run 7) (Fig. 3). From Run 6 to 7, the  $M_n(\text{GPC})$  increase of 5,500 g mol<sup>-1</sup> surprisingly resulted in little effect on morphology, other than rounder NPs.

The particle morphology in PISA is primarily dictated by the relative volume fractions of the two blocks as described by the packing parameter ( $P$ ).<sup>5</sup> Thus, extending a shorter stabiliser macroRAFT agent allows easier access to a wider range of morphologies. Poly(DMA)<sub>36</sub> (as opposed to poly(DMA)<sub>96</sub> above) was used for 2 h dispersion polymerization of 3-BAEPHA (20 wt/vol%) using targeted DP of 50 (Run 8), 100 (Run 9), 150 (Run 10), and 200 (Run 11) at 70 °C (Fig. 4). Free-flowing white stable colloidal dispersions were formed for all polymerizations, apart from at the highest initial poly(DMA)<sub>36</sub> concentration (DP = 50), which resulted in a clear gel. All polymerizations proceeded to completion (99%) in the case of DP = 50, 100, and 150, with narrow MWDs ( $D = 1.15$ – $1.38$ ), with only the MWD at DP = 200 ( $D = 1.63$ , Table 1) broad. High blocking efficiency was indicated by  $M_n$  of 23 600, 30 500, and 43 100 g mol<sup>-1</sup> in relatively close agreement with  $M_{n,\text{th}}$  of 17 600, 30 900, and 44 600 g mol<sup>-1</sup> for targeted DP = 50, 100, and 150 respectively. For DP = 50 (Run 8), ~10 nm solid spherical particles of narrow size distribution were obtained (Fig. 4), with TEMs showing similar morphology to Runs 6 and 7 (DP = 150 and 200 from poly(DMA)<sub>96</sub>), indicative of similar  $P$  or comparable ratios of solvophilic (poly(DMA)) to solvophobic (poly(3-BAEPHA)) chain lengths. The size of polymer objects signifi-

cantly increases from DP = 50 to DP = 100, with 50–200 nm diameter vesicles with filaments/worms within aggregates evident in the TEM images of Run 9. For DP = 150 (Run 10), there are no worms, with 50–300 nm diameter spherical vesicles observed. Increasing DP further (DP = 200, Run 11) yields a narrower distribution of vesicles of mostly 200 nm in diameter. In TEM images for Run 9–11 encapsulation of NPs within vesicles is apparent, with at the highest DP, most particles appearing as yolk-shell type vesicles.<sup>23</sup>

In summary, PISA is successful for the unprotected BA monomer (3-BAPHA) when using a longer stabilizer poly(DMA) block, yielding mainly spherical NPs. This polymerization appears to proceed in two phases giving boroxine agglomeration and a separable free-flowing dispersion. These suspended NPs undergo room temperature morphology transitions by aqueous dilution, where hydrolysis of the boroxine core to BA occurs. This new type of stimuli-responsive NP will be the subject of future investigations with the free BA moieties allowing sugar-sensing. Pinacol group protection (in 3-BAEPHA) prevents boroxine formation, with PISA giving core-shell spherical polyacrylamide NPs and an array of higher order objects, including worms and vesicles.

## Author contributions

H.S.D. experimentation, methodology and writing; F.I. experimentation and methodology (TEM); A.E. supervision; P.B.Z.



and F.A. conceptualization, supervision, writing-review, and editing. All authors have given approval to the final version of the manuscript.

## Conflicts of interest

The authors declare no competing financial interest.

## Notes and references

- X. Sun and T. D. James, *Chem. Rev.*, 2015, **115**, 8001–8037.
- W. L. A. Brooks and B. S. Sumerlin, *Chem. Rev.*, 2016, **116**, 1375–1397.
- N. J. Penfold, W. J. Yeow, C. Boyer and S. P. Armes, *ACS Macro Lett.*, 2019, **8**, 1029–1054.
- D. Le, D. Keller and G. Delaître, *Macromol. Rapid Commun.*, 2019, **40**, 1800551.
- N. J. Warren and S. P. Armes, *J. Am. Chem. Soc.*, 2014, **136**, 10174–10185.
- F. D'Agosto, J. Rieger and M. Lansalot, *Angew. Chem., Int. Ed.*, 2020, **59**, 8368–8392.
- L.-C. S. Huang, D. Le, I.-L. Hsiao, S. Fritsch-Decker, C. Hald, S.-C. Huang, J.-K. Chen, J. R. Hwu, C. Weiss, M.-H. Hsu and G. Delaître, *Polym. Chem.*, 2021, **12**, 50–56.
- B. Fan, J. Wan, J. Zhai, X. Chen and S. H. Thang, *ACS Nano*, 2021, **15**, 4688–4698.
- A. Pitto-Barry, *Polym. Chem.*, 2021, **12**, 2035–2044.
- D. Roy, J. N. Cambre and B. S. Sumerlin, *Chem. Commun.*, 2008, 2477–2479.
- D. Roy, J. N. Cambre and B. S. Sumerlin, *Chem. Commun.*, 2009, 2106–2108.
- J. N. Cambre, D. Roy and B. S. Sumerlin, *J. Polym. Sci., Part A: Polym. Chem.*, 2012, **50**, 3373–3382.
- J. Zou, S. Zhang, R. Shrestha, K. Seetho, C. L. Donley and K. L. Wooley, *Polym. Chem.*, 2012, **3**, 3146–3156.
- S.-S. Li, X.-H. Lv, X.-L. Sun, W.-M. Wan and H. Bao, *Polym. Chem.*, 2020, **11**, 2914–2922.
- L. Zhang and A. Eisenberg, *Science*, 1995, **268**, 1728–1731.
- G. Gody, T. Maschmeyer, P. B. Zetterlund and S. Perrier, *Macromolecules*, 2014, **47**, 3451–3460.
- B. A. Chalmers, A. Alzahrani, G. Hawkins and F. Aldabbagh, *J. Polym. Sci., Part A: Polym. Chem.*, 2017, **55**, 2123–2128.
- P. B. Zetterlund, Y. Kagawa and M. Okubo, *Chem. Rev.*, 2008, **108**, 3747–3794.
- A. Blanz, J. Madsen, G. Battaglia, A. J. Ryan and S. P. Armes, *J. Am. Chem. Soc.*, 2011, **133**, 16581–16587.
- A. L. Korich and P. M. Iovine, *Dalton Trans.*, 2010, **39**, 1423–1431.
- S. E. Burke and A. Eisenberg, *Langmuir*, 2001, **17**, 6705–6714.
- L. A. Fielding, J. A. Lane, M. J. Derry, O. O. Mykhaylyk and S. P. Armes, *J. Am. Chem. Soc.*, 2014, **136**, 5790–5798.
- W.-M. Wan and C.-Y. Pan, *Macromolecules*, 2010, **43**, 2672–2675.

